LEABHARLANN CHOLÁISTE NA TRÍONÓIDE, BAILE ÁTHA CLIATH | TRINITY COLLEGE LIBRARY DUBLIN
Ollscoil Átha Cliath | The University of Dublin

Terms and Conditions of Use of Digitised Theses from Trinity College Library Dublin

Copyright statement

All material supplied by Trinity College Library is protected by copyright (under the Copyright and Related Rights Act, 2000 as amended) and other relevant Intellectual Property Rights. By accessing and using a Digitised Thesis from Trinity College Library you acknowledge that all Intellectual Property Rights in any Works supplied are the sole and exclusive property of the copyright and/or other IPR holder. Specific copyright holders may not be explicitly identified. Use of materials from other sources within a thesis should not be construed as a claim over them.

A non-exclusive, non-transferable licence is hereby granted to those using or reproducing, in whole or in part, the material for valid purposes, providing the copyright owners are acknowledged using the normal conventions. Where specific permission to use material is required, this is identified and such permission must be sought from the copyright holder or agency cited.

Liability statement

By using a Digitised Thesis, I accept that Trinity College Dublin bears no legal responsibility for the accuracy, legality or comprehensiveness of materials contained within the thesis, and that Trinity College Dublin accepts no liability for indirect, consequential, or incidental, damages or losses arising from use of the thesis for whatever reason. Information located in a thesis may be subject to specific use constraints, details of which may not be explicitly described. It is the responsibility of potential and actual users to be aware of such constraints and to abide by them. By making use of material from a digitised thesis, you accept these copyright and disclaimer provisions. Where it is brought to the attention of Trinity College Library that there may be a breach of copyright or other restraint, it is the policy to withdraw or take down access to a thesis while the issue is being resolved.

Access Agreement

By using a Digitised Thesis from Trinity College Library you are bound by the following Terms & Conditions. Please read them carefully.

I have read and I understand the following statement: All material supplied via a Digitised Thesis from Trinity College Library is protected by copyright and other intellectual property rights, and duplication or sale of all or part of any of a thesis is not permitted, except that material may be duplicated by you for your research use or for educational purposes in electronic or print form providing the copyright owners are acknowledged using the normal conventions. You must obtain permission for any other use. Electronic or print copies may not be offered, whether for sale or otherwise to anyone. This copy has been supplied on the understanding that it is copyright material and that no quotation from the thesis may be published without proper acknowledgement.

Towards the Development of a Novel Electro-Pneumatic Hybrid Robot Morphology

---

Conor L. McGinn

Department of Mechanical & Manufacturing Engineering

Parsons Building

Trinity College

Dublin 2

Ireland

July 2015

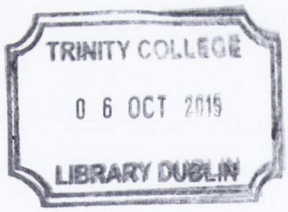
A thesis submitted to the University of Dublin in partial fulfilment of the requirements for the degree of Ph.D.

TRINITY COLLEGE DUBLIN
23 SEP 2015
ACADEMIC REGISTRY

50564175

PhD in Engineer

THESIS
10908

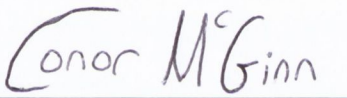


Thesis 10902

Declaration

I declare that this thesis has not been submitted as an exercise for a degree at this or any other university and it is entirely my own work.

I agree to deposit this thesis in the University's open access institutional repository or allow the library to do so on my behalf, subject to Irish Copyright Legislation and Trinity College Library conditions of use and acknowledgement.



Conor L. McGinn, July 2015

Abstract

Existing robot morphologies have typically failed to demonstrate the full range of terrain adaptability, physical practicality and behavioural diversity needed for general-purpose use, as the most suitable morphologies for certain tasks are highly unsuitable for others. Legged robot morphologies offer increased terrain adaptability at a cost of high energy consumption and poor stability, while infinite rotational mechanisms (e.g.wheels, tracks) possess high stability and energy efficiency but low terrain adaptability. This work presents a hybrid robot morphology that has the terrain adaptability needed to traverse a diverse range of civilian environments, the physical traits required to exploit ergonomically designed spaces and user interfaces which enable practical usage.

The core hypothesis that underlies this work is that the successful design of a complex, multi-functional system capable of general-purpose usage can be facilitated by adopting an embodied design approach and through detailed integration at the design stage of:

(a) mechanical design

(b) robotic system architecture (low/high level sensing and control)

(c) human-robot interface

(d) detailed consideration of the range of task environments

A full-scale embodiment of the proposed morphology has been built, and subjected to a broad range of performance tests and physical assessments in order to support the hypothesis. The forward kinematics of the morphology are given. This is followed by a description of how inverse kinematics is achieved using the pseudo-Inverse of the Jacobian method. The static stability criteria is outlined and the various gait patterns

needed to realise advanced terrain adaptability are described. To determine the joint forces and torques, a static inverse dynamics study is undertaken using the joint segment method. The embodied design is detailed - including information on how the limb geometry was optimised for civilian environments. The hybrid electro-pneumatic actuation scheme is described in detail. Details of how the pneumatic air muscles (PAMs) were characterised and integrated into the robot's design are provided. In addition to the proposed morphology, a novel control architecture is demonstrated, along with a novel method of semi-autonomous control. The capability of the robot embodiment is demonstrated through adherence with a broad range of physical and performance-based design targets. It is shown that the robot possesses terrain adaptability and environmental suitability comparable with legged biped robots and stability and energy efficiency comparable with wheeled/tracked robots. Furthermore with the integration of a dedicated social interface and semi-autonomous controller, the morphology is among the few systems that have simultaneously demonstrated the capability for both high behavioural diversity and complex social interaction.

Acknowledgements

Over the period of a PhD research project, one learns many new things. More often than not this new acquisition of knowledge is technical in nature and closely related to the particular discipline or field of research. However I have found that every now and again this learning takes a higher, more philosophical form. There were occasions when I learnt things about myself that I hadn't previously recognised (both good and bad!) and times also when I gained new perspectives on various things in my life. Now, looking back over the years; since beginning school, secondary school, college and then my PhD research, I am confronted with the realisation that I simply would not be here without the help, guidance, advice and support of many people. While I will only proceed to specifically thank a relatively small subset of these people, I am incredibly grateful to them all.

First and foremost, I would like to thank my family and those people that have been closest to me. In particular I would like to thank my parents, John and Kathryn, and my brother David. I know that without the support, love and encouragement they have given me, my life would be very different and I would simply not be where I am today.

Secondly I would like to thank the teachers that have made a big difference to me, both in Belvedere and Trinity College. Not only have great teachers helped me gain important knowledge, but they have taught me to enjoy the process of learning. Furthermore it has been their example that has inspired the development of my own passion for teaching. In particular I would like to thank Mr. Phil Conway, Mr. Oliver Murphy, Dr. Liam Boland, Dr. Steven Collins, Prof. Henry Rice and Dr. Ciaran Simms.

Within the Department of Mechanical and Manufacturing Engineering where I completed my PhD research, I would like to acknowledge Prof. David Taylor, Dr. Gareth Bennett

and Prof. Darnina Murray for their roles in guiding and assisting my work. I would also like to extend a special gratitude to Dr. Garret O'Donnell for his dedicated support and tutelage. I have avoided many certain pitfalls from following his advice (note to any PhD students reading this thesis - listen to what he tells you!).
For the continued help, time and interest that they have shown in me and my work, I would like to take the opportunity to thank Mr. Michael Reilly and the whole technical staff. In particular I would like to extend gratitude to Mr. Alex Kearns, Mr. JJ Ryan, Mr. Sean Doonan, Mr. Gabriel Nicholson and Mr. Daniel Boardman.
Within the College community, a special thank you also must go to Prof. Garry Lyons and Prof. Dermot McAleese for their continued friendship, guidance and encouragement.

A highlight of the past four years has been getting the opportunity to work with passionate, talented and ambitious final-year and Masters students. Much of the work presented in this thesis could not have been done with the help, time and commitment that they have displayed. In this regard, a special acknowledgement is given to Ben Woods, Aran Sena, Phil Wardlaw, Mark Culleton, Dave MacManus, Michael Cullinan, Rob MacDowell, George Walsh, Adam Jordan, Adam McCreevey and Romulo Marques.
Since starting my PhD research, I have been lucky to meet many new people who share my interest and passion for engineering. I am extremely grateful to these people not only for the technical help they have given me but for there role in making my work feel more like a pastime than a job. A special thank you goes to Cian Donovan, Donal MacCarthy, Brian Byrne, Filip Florek, Eamon Bourke, Andrew Anderson and Kevin Mahon.

Finally I would like to take the opportunity to unreservedly thank those people who have ever taken a chance in me. In repaying your faith and loyalty, I have found my single biggest source of motivation over the years. You have taught me to look beyond appearances and inspired me to take chances on people. I hope that I can continue to follow the example you have shown. In this regard I would like to firstly thank my first year rugby coaches. How you could have picked a kid who couldn't see and didn't know the rules of the sport in a team that went on to have five elite professional athletes is a mystery to me! I would also like to extend my thanks and appreciation to Mr. Pat

Stakem whom for reasons completely unknown, has on many occasions gone out of his way to help me and provide me with unique opportunities.

Lastly and most importantly, I want to thank my supervisor and mentor Professor Kevin Kelly for the tremendous support, friendship, loyalty, trust and guidance he has given me over the past few years. It's difficult to express in words how thankful I am for all that he has done to help me - both in my studies and in the many opportunities that he has helped open up for me.

Contents

Declaration iii

Acknowledgements vii

List of Figures xvii

List of Tables xxv

Nomenclature xxvii

1 Introduction 1

1.1 Motivation and Challenges . . . 2

1.2 Research Objectives . . . 4

1.3 Overview . . . 5

1.4 Contribution of Thesis . . . 7

2 Literature review 9

2.1 Embodied Intelligence . . . 9

2.2 Robot Morphology . . . 11

2.2.1 Infinite Rotational Mechanisms . . . 12

2.2.1.1 Steered Mechanisms . . . 13

2.2.1.2 Differentially Driven . . . 16

2.2.1.3 Skid-Steered Mechanisms . . . 17

2.2.2 Legged Robots . . . 18

2.3 Actuation . . . 21

2.3.1 Passive Dynamics and Decoupled Actuation . . . 21

2.3.2 Electric Actuation . . . 23

2.3.3 Hydraulic Actuation . . . 26

2.3.4 Pneumatic Actuation . . . 27

2.4 Design Guidelines and Standards 33
2.4.1 Existing with People: The Human Environment 33
2.4.1.1 Human-Robot Interaction 34
2.4.1.2 Review of ISO 13482 38
2.4.2 Operating in Human Spaces: The Built Environment 39
2.4.2.1 Human Factors and Building Regulations 39
2.5 Review of Existing Service Robot Technology 45
2.5.1 Honda Asimo 45
2.5.2 Care-O-Bot III 46
2.5.3 PR-2 48
2.5.4 Other Robots 49
2.5.5 Robot Stair-Climbing 52
2.5.5.1 Tracked/Wheeled Solutions 53
2.6 High-level Comparison of Morphologies 62
2.7 Summary/Conclusions 67

3 Description of Morphology **71**

3.1 Design Process 71
3.2 High Level Description 74
3.2.1 Locomotion 75
3.2.2 Actuation and Articulation 76
3.2.3 Embodied Intelligence Philosophy 77
3.3 Mathematical Description 77
3.3.1 Forward Kinematics 78
3.3.2 Relating the Shank and Stabiliser Angles 79
3.3.3 Inverse Kinematics 80
3.4 Stability 83
3.4.1 Control through Self-Balancing 85
3.4.2 Control through Inverse Kinematics 86
3.4.3 Stability on Uneven Surfaces 87
3.5 Stair/Obstacle Climbing 87

3.5.1 Traversing an Obstacle . . . 89
3.5.2 Ascending Stairs . . . 90
3.5.3 Descending Stairs . . . 94
3.5.4 Bridging Crevices . . . 97

4 Embodiment Design **99**

4.1 Prior Work . . . 99
4.2 Physical/Performance metrics as Design targets . . . 99
4.3 Dynamic Analysis . . . 101
4.3.1 Inverse Dynamic Analysis . . . 101
4.3.2 Dynamic Analysis: Stair Climbing . . . 103
4.4 Leg Design . . . 105
4.4.1 The Shank . . . 106
4.4.2 The Stabiliser . . . 107
4.4.3 The Thigh . . . 107
4.4.4 Leg Geometry . . . 107
4.5 Design of Torso and Lower Hip Mechanism . . . 110
4.6 Design of Arms . . . 112
4.7 Actuation . . . 113
4.7.1 Characterisation of McKibben Air Muscle . . . 113
4.7.2 Actuation of Stabiliser Joint . . . 115
4.7.3 Actuation of Knee . . . 117
4.7.4 Actuation of the Hip Joint . . . 118

5 Sensing and Control **125**

5.1 Robot Control Architecture . . . 125
5.1.1 Overview of Architecture . . . 127
5.1.2 Low Level System Design . . . 129
5.1.3 High Level System Design . . . 131
5.1.4 Embodiment Design . . . 133
5.1.5 Actuation Control . . . 137
5.2 Sensing . . . 140

5.2.1 Sensor Overview . . . 140
5.2.2 Proprioception . . . 142
5.2.3 Safety . . . 144
5.3 Human-Robot Interaction and Control . . . 145
5.3.1 Design of Social Interface . . . 145
5.3.2 Human-in-the-Loop Control . . . 147
5.3.3 Semi-Autonomous Control Schema and Embodiment Design . . . 149
5.3.3.1 Hardware Controller Implementation . . . 151
5.3.3.2 Software App Control Implementation . . . 152

6 Results **155**
6.1 Physical Metrics . . . 156
6.1.1 Robot dimensions and inertial properties . . . 156
6.1.2 System modularity . . . 158
6.1.3 Actuation and Safety . . . 158
6.2 Performance Metrics . . . 161
6.2.1 Locomotion . . . 161
6.2.1.1 Zero-point turn . . . 163
6.2.2 Pick-and-Place . . . 164
6.2.3 Crevice Crossing . . . 167
6.2.4 Traversing Obstacles . . . 168
6.2.5 Stairclimbing - Ascent . . . 170
6.2.6 Stairclimbing - Descent . . . 173
6.3 Human control of service robots . . . 175
6.3.1 Experimental Procedure . . . 175
6.3.2 Results from Simulation study . . . 182
6.3.3 Findings from Simulation study . . . 184
6.4 Summary . . . 186

7 Conclusions **189**
7.1 Future Work . . . 193

Bibliography **197**

A V1.0 Robot 213

B V2.0 Robot 215

C Awards/Publicity 219

D Inverse Kinematics Matlab Code 223

List of Figures

2.1 The most common wheeled/tracked configurations used on mobile robots. Circular shapes represent omni-directional wheels and rectangular shapes represent regular wheels. Circular arrows identify actively steered wheels. . 13

2.2 Common steered configurations used on mobile robots (a) Ackermann steering used on the Google car (b) Omni-steering on the Care-O-Bot III (c) Synro-drive on the Denning B-12 15

2.3 Several popular robots that have a differential drive configuration (a) Willow Garage Turtlebot (b) Khepera robot (c) Adapt Technology Pioneer 3-DX robot 16

2.4 Several popular differentially-driven self-balancing robots (a) Segway RMP 220 (b) IHMC T-Bot robot (c) Anybots QB Tele-presence robot 17

2.5 Several notable skid-steered service robots (a) Battlefield Extraction-Assist Robot (BEAR) (b) CMU Highly Intelligent Mobile Platform (CHIMP) (c) iRobot ATRV 18

2.6 Robosimian using limbs for locomotion (left) and manipulation (right) . . . 20

2.7 Notable passive dynamic walkers (a) McGeer's original passive dynamic platform (b) Cornell Ranger hybrid passive dynamic platform 22

2.8 Legged robots with harmonic gear drives (a) 2006 Honda Asimo (b) HRP-3 (c) HUBO (d) Johnnie (e) WABIAN-2 (f) iCub 25

2.9 Legged robots with compliant series elastic actuators (a) Flame (b) Roboy (c) COMAN 26

2.10 Notable mobile robots with pneumatic cylinder drives (a) DIEES (b) CB2 (c) Wheeleg 28

2.11 Principle of operation of an antagonistic joint using a pair of McKibben muscles. The controlled contraction of one muscle creates a tensile force which causes the opposing muscle to extend. Joint control can be thus achieved by regulating the pressure in each muscle. 30
2.12 Popular types of pneumatic air muscle(PAM) (a) McKibben Actuator (b) FESTO Fluidic muscle (c) Pleated air muscle 31
2.13 Lifelike robots and the uncanny valley (a) graph describing Mori's uncanny valley (b) Philip K. Dick robot by Hanson robotics (c) Gemenoid F robot by Hiroshi Ishiguro 37
2.14 Robots retaining basic anthropomorphic social interfaces (a) Kismet (b) Pearl (c) Sparky 38
2.15 Several state-of-the-art personal service robot research platforms (a) Honda Asimo serving coffee (b) Care-O-Bot serving a drink (c) Willow Garage PR-2 attending a table 49
2.16 Wheeled service robots designed for civilian environments (a) Cero mounted on top of a Nomad Scout (b) ARMAR-III (c) uBot (d) Home Exploring Robotic Butler (HERB) (e) Golem Krang (f) NASA Centaur platform . . 52
2.17 Stair-climbing tracked wheelchairs (a) Tankchair mobility platform (b) Unimo wheelchair by Nano Optonics Energy 53
2.18 Stair-climbing tracked robots (a) PackBot by iRobot (b) double articulated Silver robot (c) MACbot robot (d) Double articulated Aladdin robot (e) LMA robot (f) powder-filled track-belt configuration by Yoneda et al. (g) Reconfigurable VIPeR robot by Elbit systems 56
2.19 Wheeled stair-climbing robots (a) NASA Soujourner with rocker-bogey mechanism (b) Helios-V 6-wheeled robot (c) iBot mobility platform 58
2.20 Legged stair-climbing robots (a) BARt-UH robot (b) DARPA Atlas robot climbing steps (c) HRP-2 robot climbing steps (d) Boston Dynamics RHex robot (e) Titan-VI quadruped robot (f) Quadruped stair-climbing robot developed at the Univ. of Maryland 60
2.21 Hybrid stair-climbing robots (a) Zero-carrier robot (b) Matsumoto hybrid wheel-biped robot (c) hybrid stair-climbing wheelchair 62

2.22 Terrain adaptability of existing morphologies. The number of asterisks indicates the number of manipulators the robot possesses. 64

2.23 Behavioural Diversity Vs. Interface Complexity. The number of asterisks indicates the number of manipulators the robot possesses. 67

3.1 Graphical illustration of three-constituent principle as applied to the design of a personal service robot 73

3.2 Graphical description of the proposed morphology (a) labelled image of primary components (b) visualisation of robot's controllable joints 74

3.3 Primary modes of locomotion for the proposed morphology (left) the robot in default differential drive mode (right) the robot in high stability 4WD mode 76

3.4 Sequence of actions for picking up object from the ground (left) pick-up stance with arm contracted (right) pick-up stance with arm elongated . . . 77

3.5 Robot Segment Parameters 78

3.6 Geometrical relationship between shank and stabiliser mechanisims 80

3.7 Inverse kinematics MATLAB simulation demonstrating the action of placing the end effector on a raised surface (a) wireframe model of the robot's links and joints plotted as a function of the number of solver iterations (b) change in joint angles with respect to the number of solver iterations . . . 83

3.8 Modifying the static stability margin through actuation of the stabiliser linkage 84

3.9 Simplifying the stability of the morphology to approximate that of a single degree of freedom wheeled self-balancing platform 86

3.10 The relative joint angles of the robot in positions of varying stability: (left) high stability (right) low stability 87

3.11 The lower hip mechanism providing additional stability during navigation on broken/uneven terrain. 88

3.12 Sequence of actions required for traversing an obstacle 89

3.13 Sequence of actions describing the approach stage of stair climbing 90

3.14 The repeated sequence of actions for stair ascent 92

3.15 Pattern of actions that enable the robot to return to a standing position after climbing the last stair 93
3.16 The repeated sequence of actions for stair descent 95
3.17 Pattern of actions that enable the robot to return to a standing position after climbing the last stair. 96
3.18 Sequence of actions required for crossing a crevice 98

4.1 Free body diagram of the major limbs for standing poses 102
4.2 Static stability criteria for proposed morphology during stair-climbing . . . 103
4.3 Free body diagram of the major limbs during stair climbing (Robot at rest on stair) 104
4.4 Free body diagram of the major limbs during stair climbing (Robot ascending nosing) 105
4.5 Design of the lower body assemblies (a)shank assembly (b) stabiliser assembly (c) thigh assembly (pneumatic air muscles omitted) 106
4.6 Geometry of stairs with respect to the robot during stair climbing 108
4.7 Geometry of legs during stair climbing 109
4.8 Geometric constraints on leg angles during stair climbing 110
4.9 Design of the upper body (a) torso (b) lower hip mechanism (LHM) (c) torso with LHM attached (pneumatic air muscles omitted) 111
4.10 Design of the arm (a) arm extended when muscle is contracted (b) arm retracted when muscle is at environmental pressure (note: image not drawn to scale) 112
4.11 Muscle Contraction data for various muscle lengths 115
4.12 Design of the stabiliser actuation system (a) labelled cross section of assembly (b) action of stabiliser muscle assembly (note: image not drawn to scale) 116
4.13 Design of the knee actuation system (a) labelled cross section of assembly (b) action of knee muscle assembly (note: image not drawn to scale) 118
4.14 Antagonistic muscle configuration in the Hip 119
4.15 Design variables for antagonistic hip muscle configuration 120

4.16 Variability of pneumatic muscle length over the range of hip rotation for hip muscles 122

4.17 Design variables for additional hip muscle configuration 123

4.18 Variability of pneumatic muscle length over the range of hip rotation for additional hip muscle 124

5.1 High-level description of the two-tiered architecture. Direction of arrows indicate the direction of information/data exchange. The thickness of arrows indicates the relative data bandwidth of the communication channel. . 129

5.2 Graphical description the of architecture focusing on the low-level tier. Blue lines indicate actuator control commands. Red lines indicate sensor information. The directions of the arrows indicate the direction of information/data exchange. The thickness of the arrows indicates the relative bandwidth of the communication channel. 130

5.3 Graphical description the of architecture focusing on the higher-level tier. Blue lines indicate actuator control commands. Red lines indicate sensor information. The directions of the arrows indicate the direction of information/data exchange. The thickness of the arrows indicates the relative bandwidth of the communication channel. 132

5.4 Graphical description of prototype architecture. Blue lines indicate actuator control commands. Red lines indicate sensor information. The direction of the arrows indicates the direction of information/data exchange. The thickness of arrows indicates the relative bandwidth of the communication channel. 133

5.5 The design of the GPIO module v1.0 printed circuit board 134

5.6 The BeagleBone Black SBC used as the 'master' module on the v2.0 demonstrator embodiment 135

5.7 The distribution of the GPIO modules and 'master' module throughout the robot 136

5.8 Hardware for controlling actuators: (a) Sabertooth 2x25 motor driver (b) Stc 5/2 valves with manifold (c) MOSFET board to control solenoids (d) Adafruit PWM Breakout board 138
5.9 Low-level actuator control topology 139
5.10 Physical layout of the electronics and pneumatics control hardware in the *v2.0* demonstrator embodiment 140
5.11 Distribution of low-level sensors throughout the demonstrator embodiment 141
5.12 Determining joint angles from IMU readings 143
5.13 Embodiment of the social interface on *v2.0* demonstrator 146
5.14 Core functionalities of social interface (a) interactive customisable face (b) programming interface (c) sensor visualisation 147
5.15 The two controller embodiments designed for use in the proposed control schema (a) Hardware embodiment (b) Android application installed on tablet computer 150
5.16 Semi-autonomous control mode using the touchpad (a) low confidence (b) medium confidence (c) high confidence 152
5.17 Manual control using the control app (a) low speed in the forward-left direction (b) medium speed in the forward-right direction (c) fast speed in the forward direction 153
5.18 Performing a zero-point turn. Actions (a)-(d) finger dragged clockwise within the joystick area 154

6.1 Several views of the demonstrator embodiment 156
6.2 Implementation of interactive social interface on *v2.0* demonstrator 159
6.3 The demonstrator embodiment demonstrating indoor locomotion capability and the physical ability to comfortably pass through a gap equivalent to a typical residential doorway. 161
6.4 Indoor locomotion and traversal over a large door sill 162
6.5 Outdoor locomotion on grass 162
6.6 Outdoor locomotion on cobblestone 163
6.7 Demonstrator embodiment performing a zero point turn 163

6.8 Demonstrator embodiment picking up a small object from the floor 165
6.9 Demonstrator embodiment leaning forward to increase task space or to engage in a hand-over 166
6.10 Demonstrator embodiment performing vertical height adjustment through modification of static stability margin 167
6.11 Demonstrator embodiment crossing a 100mm crevice 168
6.12 Demonstrator embodiment traversing a 110mm obstacle 169
6.13 Simulations using MSC Adams 170
6.14 The process of stair ascent on the *v2.0* demonstrator (a)-(c) stair approach (d)-(f),(j-l) action #1 (g)-(i),(m)-(o) action #2 (p)-(t) stair recovery 172
6.15 The process of stair descent on the *v2.0* demonstrator (a)-(g) stair approach (h-i) action #1 (j) action #2 (k-o) stair recovery 174
6.16 A walk-through of the 3D simulation where the user is challenged to guide a personal service robot as it performs some useful tasks 178
6.17 The control embodiments used during the simulation testing (a) Xbox game controller (b) custom built tablet control application 180
6.18 Practical testing of the control schema and custom control embodiment (a) user testing in lab in Trinity (b) field testing with personal service robot user 182
6.19 Overall performance of each controller (time penalties not included) (a) bar chart (b) cumulative frequency plot 183
6.20 Overall performance of each controller (time penalties included) (a) bar chart (b) cumulative frequency plot 183
6.21 Number of collisions recorded for each controller 184
6.22 Average time recorded per stage 184

A.1 Leg assembly on the v1.0 robot 213
A.2 The upper body structure (left) v1.0 protype upper body in the lab (b) CAD model showing upper body structure integrated with leg assembly . . 213
A.3 v1.0 robot moving around the lab 214
A.4 v1.0 robot interacting with a wheelchair user 214

A.5 v1.0 robot (left) the v1.0 social interface (right) the engineering team behind the design/construction of the v1.0 robot 214

B.1 Leg assembly on the v2.0 robot 215
B.2 Range of motion of the v2.0 leg assembly 216
B.3 Action of the lower hip mechanism (LHM) 216
B.4 Assembly of the torso, lower hip mechanism (LHM) and arm structures on the v2.0 embodiment 216
B.5 Assembly of the torso, lower hip mechanism (LHM) and arm structures on the v2.0 embodiment 217
B.6 Images of the v2.0 robot assembly with interactive social interface 217

C.1 Press coverage of the v1.0 embodiment (a) Miscellaneous press articles on the robot (b) headline on RTE main evening news (c) front page of the Irish Times weekend edition. March 2014 219
C.2 At the press launch of Robbie v1.0 (l-r): Dr. Hamadoun Tour, Secretary General ITU; Conor McGinn, lead engineer; Prof. Kevin Kelly, project lead. March 2014 220
C.3 Presenting the design of the robot morphology at the 'Universal Design Grand Challenge'(UDGC) finals. May 2014 220
C.4 Conor McGinn accepting the 'Smart World, Full Life'award with Dean of Research, Prof. Vinnie Cahill, at the Discover Research Dublin event. September 2014 221
C.5 The TCD Engineering team accepting the Engineers Ireland Excellence Award for Innovation. November 2014 221

D.1 Flowchart describing the how (a) the forward kinematic model is implemented (b) the joint trajectories are generated for the inverse kinematic model 224

List of Tables

3.1 DH Parameters for robot morphology 79

4.1 Mechanical properties of pneumatic air muscles used on robot 114

5.1 Hardware specifications of the GPIO module v1.0 135

6.1 Physical parameters of the demonstrator 157

6.2 Comparison of existing platforms 187

Abbreviations

ADA	Americans with Disabilities Act (1990)
AR	Aspect Ratio
BPAM	Braided Pneumatic Air Muscle
CAN	Controller Area Network
CDOF	Controllable Degrees Of Freedom
COM	Centre Of Mass
DOF	Degrees Of Freedom
DH	Denavit-Hartenberg convention
FK	Forward Kinematics
FOV	Field Of View
GPIO	General Purpose Input Output
HRI	Human-Robot Interaction

ID	Inner Diameter
IMU	Inertial Measurement Unit
ID	Inverse Dynamics
IK	Inverse Kinematics
IFR	International Federation of Robotics
JSM	Joint Segment Method
LHM	Lower Hip Mechanism
OD	Outer Diameter
PAM	Pneumatic Air Muscle
$PPAM$	Pleated Pneumatic Air Muscle
ROS	Robot Operating System
RTS	Real Time
SEA	Series Elastic Actuator
SBC	Single Board Computer
SSM	Static Stability Margin

SSH	Secure SHell
UCD	User-Centred Design

Operators

a_i	link length - DH Parameter
α_i	link twist - DH Parameter
d_i	link offset - DH Parameter
θ_i	joint angle - DH Parameter
J	Jacobian matrix
J^{-1}	Inverse of Jacobian matrix
J^{+}	Pseudo-inverse of Jacobian matrix
δe	Unit vector corresponding to the change in end-effector coordinates
$\delta\theta$	Unit vector corresponding to the change in joint angles.
$c\theta$	Cosine theta
$s\theta$	Sine theta
x_{COM}	x-coordinate of the centre of mass

y_{COM}	y-coordinate of the centre of mass
m_i	mass of i^{th} component
l_i	length of i^{th} component
l_0	default uninflated length of air muscle
l_1	contracted inflated length of air muscle
l_2	stretched uninflated length of air muscle
$\ddot{\theta}$	angular acceleration of angle theta
$\ddot{x}$	linear acceleration in the x-direction
g	acceleration due to gravity $\{(-9.81\frac{m}{s^2}\})$
T_n^{n-1}	Transformation matrix between reference frames 'n' and 'n-1'
$\theta_{0123..n}$	Sum from θ_0 to θ_n
T_n	Torque acting at joint 'n'
R_n	Reaction force at point 'n'

Glossary

Aspect ratio A robot's height-to-width ratio in the saggital plane.

Antagonistic muscle configuration A configuration compromising of two opposing, linearly contracting muscles. Contraction in one muscle causes relaxation/stretching in the other and vise versa. An example of such configuration in the human body is the arm where the bicep contracts and the tricep relaxes when the arm is bent.

Behavioural diversity The behaviour an agent refers to the manner in which it complies/interacts with the environment. Behaviour is an emergent property that depends on the agent's morphology, its underlying control structure and the surrounding environment. Behavioural diversity refers multitude of different types of behaviour that an agent can exhibit. In accordance with the theory of embodied cognition/intelligence, the overall intelligence of an agent is best conveyed through its behavioural diversity and the complexity of its interaction with the environmental.

Bottom-up design The bottom-up design philosophy promotes developing robots through detailed consideration of the design, function, behaviour and coordination of the robot's subsystems (as opposed to top-down design which focuses mainly on the robot's end function). By prioritising high adaptability over specific functionality, the approach aspires to produce systems that will ultimately be capable of increased behavioural diversity across varying environmental conditions.

Centre of mass (COM) The centre of mass of a rigid body is the unique point where the weighted relative position of the distributed mass sums to zero. When supported at this point, there is no net torque and (unless disturbed), the body will remain in static equilibrium.

Configuration space The space contained within all of the available positions and orientations (called poses) of a robot's linkages. The configuration space is determined from the length of the robot's linkages and the type/configuration of its joints.

Dead reckoning Dead-reckoning is the process of estimating the current position of a system from a previously determined position and a known/estimated subsequent motion.

Degrees of freedom (DOF) The degrees of freedom (DOF) of a system are the number of independent parameters that describe its configuration. The degrees of freedom of a robot typically corresponds with the number of actuated joints or controllable degrees of freedom (CDOF) it possesses.

Deliberative control paradigm A paradigm in robot control that couples sensing and planning with action. Also referred to as the 'Hierarchical'or 'Sense-Plan-Act'paradigm.

Differentially-driven locomotion Robots that are differentially driven possess two (typically concentric) independently driven wheels located on either side of the robot. Locomotion (both forward motion and steering) is achieved through individual control of each wheel. For stability reasons, the majority of differentially driven robot's utilise a third passive caster wheel for support.

Denavit-Hartenberg Convention The Denavit-Hartenberg (DH) convention is a standardised methodology used for describing the forward kinematics of robot chain mechanisms through the specification of four link parameters (link length, link twist, link offset, joint angle).

Dynamic Stability Systems that are dynamically stable require active stability control in order to maintain balance. In other words, dynamically stable systems require continuous close-loop feedback and actuation for stability. Examples of dynamically stable systems found in nature include; humans, insect flight and horses during galloping gait.

Embodied design Embodied design is derived from the philosophy of embodied cognition, a field which which explores the interdependent relationship between the mind and body in biologically intelligent agents. The embodied design approach is a bottom-up approach which was developed to guide the design of artificially intelligent agents. The embodied design philosophy promotes the holistic design of intelligent systems through detailed consideration of the task environment, the agent morphology and the governing control structure. The design process involves incorporating design considerations from across three time perspectives; the here-and-now, the lifespan of the agent (ontogenetic perspective) and the lifespan of several generations of agent (phylogenetic perspective).

Ergonomics See 'human factors'.

Exeroceptive sensing Exeroceptive sensors transmit data about the external local environment and allow the robot to interact with people or objects in its vicinity.

Forward kinematics The process of computing the position/orientation of a robot's end-effector from the its associated joint and link parameters.

Going (stair geometry) The horizontal distance from the edge of a stair nosing to the projection of the adjacent stair nosing.

GPIO module In the proposed system architecture, the GPIO module represents a general purpose development board that can be configured for either low-level sensing or actuation. Multiple GPIO modules are distributed throughout the robot and are connected to one another through a communication bus. It is the job of the Master Module (presently embodied using a SBC) to coordinate the functionality of the system's low-level GPIO modules as well as to interface with computer modules in the high-level tier of the proposed architecture.

Grousers A grouser/cleat is a protrusion on the surface of a wheel/track segment, intended to increase traction with the terrain.

High-level tasks A high-level goal is one that possesses several layers of abstraction. To reach the goal, the high-level task must be decomposed into more applied, interconnected lower-level subtasks (this process can be recursive) which can then be solved directly. Achieving high-level goals typically requires advanced levels of perception as well as the coordination of both deliberation and planning processes. To achieve advanced perception, high level tasks typically require the use of high bandwidth, exeroceptive sensors (optical vision systems, 3D depth cameras etc.). Additionally to achieve the required processing, high-powered computers are typically needed.

Human factors Human factors is the scientific discipline concerned with the understanding of interactions among humans and other elements of the system. It directly concerns the practice of designing products, systems or processes to take proper account of the interaction between them and the people that use them.

Human-robot interaction (HRI) The field of HRI studies the interactions between humans and robots. HRI is a multidisciplinary field with contributions from areas including humancomputer interaction, artificial intelligence, robotics, natural language understanding, design, and social sciences.

Hybrid control paradigm A paradigm in robot control that using an architecture possessing both deliberative and reactive/reflex-based mechanisms.

Inertial measurement unit (IMU) A sensor typically consisting of a combination accelerometers, gyroscopes and magnetometers which are used to determine 3D orientation and movement.

Inverse dynamics (ID) The procedure of computing forces and/or torques based on the kinematics of a rigid body and its inertial properties.

Inverse kinematics (IK) The procedure of computing the necessary joint variable parameters needed in order to move an end-effector into a desired position/orientation. Depending on the type of joint (rotary/ prismatic), joint variable parameters can either be angles or lengths.

Joint segment method (JSM) A technique used to predict the joint torques and reaction forces in an open-chain mechanism. It is a directionally dependent methodology which operates through progressive application of the Newton-Euler equations between between the links in the kinematic chain.

Low-level task A low-level goal is one that can be accomplished without abstract deliberation and through the utilisation of locally available resources/data. In robotics, low-level tasks typically involve either addressing direct reflex-based real-time performance targets or contributing towards finding the solution to a decomposed deliberative high-level task. Sensors used for low-level tasks are often low bandwidth, high frequency proprioceptive sensors (rotary encoder, IMU etc.). A notable exception to this are tactile sensors which measure touch. Computers performing low-level tasks are typically low-power embedded platforms capable of robust real-time performance .

Lower-hip mechanism (LHM) A novel aspect of the proposed morphology. The LHM is a mechanism located below the hip and connected to the torso through a prismatic joint running parallel to the vertical axis of the robot's torso. The mechanism consists of two independently controlled driven wheels and plays an active role in tasks including outdoor locomotion, crevice crossing, obstacle traversal and stair climbing.

Mechanical complexity A qualitative measure of the overall physical complexity of a system. It is determined primarily by the system's overall controllable degrees of freedom however it can be affected by other factors including the number or moving/unique/generic parts.

Odometry Odometry is the process of using data from motion sensors (wheel encoders etc.) to estimate the change in position over time.

Omni-wheels Wheels that can move freely in any planar direction. Using rollers mounted along the circumference of the wheel to overcome lateral resistance, omni-wheels can roll like a normal wheel or move laterally using the rollers. The 'mecanum wheel'is a popular variation of the conventional omni-wheel and is characterised by the circumferential rollers being mounted at a 45deg angle to the wheel circumference. Passive omnidirectional wheeled motion can also be achieved using caster and/or ball-wheel configurations.

Personal Service Robot A service robot is a robot that performs useful tasks for humans or equipment (excluding industrial automation applications). If the robot is being used for a non-commercial task (i.e. domestic servant, automated wheelchair) then the robot is termed a 'personal service robot'.

Professional Service Robot A service robot is a robot that performs useful tasks for humans or equipment (excluding industrial automation applications). If the robot is being used for a commercial task (i.e. mail delivery robot, fire-fighting robot) then the robot is called a 'professional service robot'.

Proprioceptive sensing Proprioceptive sensors measure data relating to the robot's internal states (joint orientation, battery level, wheel angular velocity etc.). Using proprioceptive sensors, a robot is able to infer its own system states.

Reactive control paradigm A paradigm in robot control that directly couples sensing with action (planning phase omitted).

Rise height (stair geometry) Vertical distance from the top of one tread to the next.

Robot morphology The physical form/structure that a robot possesses is defined by its morphology. A robots morphology can be classified through examination of its forward kinematics and of how it interacts with the task environment (i.e. how it achieves locomotion, manipulation, social interaction).

Robot Operating System (ROS) The Robot Operating System (ROS) is a popular middleware used on autonomous mobile robots. It consists of a collection of software frameworks for robot software development. It provides operating system-like functionality on a heterogeneous computer cluster. ROS provides many standard operating system services (hardware abstraction, low-level device control, implementation of commonly used functionality, package management etc.) as well as separate robotics-specific functionalities.

Segmental method A commonly used method of determining the overall centre of mass of a rigid body.

Self-balancing Self-balancing or wheeled self-balancing, is the process whereby a statically unstable, diff-driven/skid-steered robot maintains balance through active control of its drive wheels. Once sensors (typically a combination of gyros and accelerometers) located in the robot detect the onset of tipping, a real-time reactive controller commands the wheels to rotate in a manner which equalises the system.

Static stability A robot is statically stable if it does not require continuous actuation and sensory feedback to remain in equilibrium. The static stability of a system can be quantified through measurement of its static stability margin (SSM).

Static stability margin (SSM) The Static Stability Margin (SSM) is a measure of a systems static stability based on the geometry of its ground support polygon. The support polygon for a ground-based robot is the polygon created by connecting the vertices of each of its ground contact points. The SSM is defined by the distance from the ground projection of the robot's centre of mass to the nearest edge of the support polygon.

Service Robot According to the International Federation of Robotics (IFR), robots that perform useful tasks for people (excluding industrial applications) are broadly known as 'service robots'. Service robots can be sub-categorised into personal or professional service robots.

Simultaneous localisation & mapping (SLAM) Simultaneous Localisation And Mapping (SLAM) is the process of constructing/updating a map of an unknown environment while simultaneously keeping track of an agent's position/orientation within it.

Task space The task space is the space of all positions and orientations (called poses) of a robot's endeffector.

Tele-operated control Tele-robotics or tele-operated robotics is concerned with the control of robots from a distance. Human operators located at a distance from the robot transmit control commands which the robot interprets and executes. It is noted that many robots controlled under tele-operation have autonomous capabilities and are therefore semi-autonomous in nature. Noteable exammples of semi-autonomous tele-operated robots include; surgical robotic manipulators, bomb disposal robots and the Canada arm on-board the International Space Station.

Top-down design Also known as 'functional design', the top-down philosophy focuses primarily on the designing robots that perform a specific function (range of functions). With this more product-orientated approach, factors such as reliability, robustness and accuracy play a central role in influencing the system design.

Tread depth Horizontal distance from the edge of one stair nosing to the corresponding vertical riser.

Chapter 1

Introduction

Mankind has long since dreamed of developing robots, cyborgs and various other forms of automata capable of performing tasks that are currently being undertaken by people. As early as 350 B.C., Aristotle predicted the advent of autonomous machinery when he wrote in his treatise 'Politics':

> *"if every instrument could accomplish its own work, obeying or anticipating the will of others, like the statues of Daedalus, or the tripods of Hephaestus, which, says the poet, "of their own accord entered the assembly of the Gods;" if, in like manner, the shuttle would weave and the plectrum touch the lyre without a hand to guide them, chief workmen would not want servants, nor masters slaves."* [1]

For many of the centuries that followed, these Aristotelian prophecies remained firmly rooted within the realms of science fiction. However in the advent of the modern machine age and with increasing political and societal factors driving the progression of robotics, both mankind's ability and the societal need to develop useful robots has grown substantially. While robots have yet to gain ubiquity within our society, we are moving ever closer to the day when it is possible to equip machines with the intelligence and practical capabilities needed to perform many of the tasks that are currently being done by people. Such tasks typically take place in unstructured, ergonomically designed environments that are continuously occupied by people.

According to the International Federation of Robotics (IFR), robots that perform useful tasks for people (excluding industrial applications) are broadly known as 'service robots' [2] [3]. Depending on the nature of usage, a further classification can be made. If the robot

is being used for a non-commercial task (i.e. domestic servant, automated wheelchair) then the robot is termed a 'personal service robot'. On the other hand, if the robot is being used for a commercial task (i.e. mail delivery robot, fire-fighting robot) then the robot is called a 'professional service robot'. It is observed that in the former case the operator is likely a lay person while in the latter case they are assumed to be a trained professional.

1.1 Motivation and Challenges

In a article published in the Scientific American in 2006, Bill Gates famously remarked on the current state of the service robotics industry [4]. Based on the many similarities he observed between the service robot industry in 2006 and that of the computer industry in the 1970s, he predicted a time in the not too distant future when robots (like the computer in the 1990s) will be capable of practical, general-purpose use. Even the title of the article, 'A Robot in Every Home' promoted this bold vision.

Personal service robots that can reliably operate in human environments (public buildings, houses, hospitals etc.) have the potential to provide unprecedented independence to people with a wide range of disabilities, the elderly and any other interest group that presently requires human assistance in order to perform everyday tasks. In addition to performing tedious and repetitive household chores (cleaning, ironing etc.), service robots have the potential to significantly reduce the risk of injuries occurring in the home. In addition to reducing common work-related accidents (poisoning due to inhalation of toxic fumes from cleaning agents, back problems due to overexertion etc.) [5], assistive robots are likely to cut down the number of accidental falls that take place in the home. This latter offering is particularly significant considering falls consistently account for the single largest cause of injury in the home [6]. As the ageing population in the Western world continues to grow, it is especially worrying that the risk of falling increases dramatically with age [7]. However robots that can perform useful tasks and can better regulate the activity levels of high-risk elderly people will serve a secondary function of helping extend people's independence. In so doing they will help reduce the burden on the hospitals and care homes where they may otherwise be forced to reside. It is interesting to note that

since architectural features (stairways in particular) are leading causes of falls [8] [9], a robot that simply reduces the number of times a person needs to go up/down the stairs may play a tangible role in reducing the risk of falling and thus enabling people to live more independently. Finally, in addition to performing useful jobs and reducing their users risk of falling/injury, personal service robots offer the potential for a portable, cost effective and relatively unobtrusive means of health monitoring that would not otherwise be achieved without a high-degree of direct human supervision.

There are many challenges associated with the design, construction and programming of service robots that are capable of general-purpose use (i.e. capable of performing multiple, distinct tasks). Among the most significant challenge that designers face in developing a practical general-purpose robot is a morphological one. While legged robots possessing many degrees of freedom are capable of high behavioural diversity, they are generally impractical due to high control complexity, poor reliability, high mass, large power consumption, poor stability and high cost. On the other hand, wheeled/tracked robots offer increased levels of reliability, stability and efficiency but they possess drawbacks of their own. Due to their low centre of mass, large wheelbase and the high level of ground deformation, tracked robots are unsuited for use in indoor civilian environments. Similarly wheeled systems often possess a low centre of mass, a large wheelbase and poor terrain adaptability.

Control of multi-purpose robots also presents a significant challenge. While significant progress has been made in field of artificial intelligence in recent decades, both the performance robustness and range of tasks that service robots can reliably carry out autonomously is extremely limited. Robots capable of high levels of behavioural diversity typically possess many degrees of freedom and their control requires complex coupling between low and high level control systems. Although efforts have been made in recent years to standardise software used on robots through the development of specialised middleware [10] [11], the scope of these solutions are limited as they require increased levels of hardware support as well as improved real-time performance.

Another important control related challenge that must be overcome pertains to the human control of robots. The first of these problems relates to balance and stability. When human

operators control robots through manual remote control (tele-operation), they heavily rely on visual feedback to guide the control process. Since the robot's on-board sensing has a limited effect on its real-time control actions, in these instances it is very difficult for human operators to issue appropriate actuator instructions during instances when visual feedback is limited (i.e. robot is visually obscured) or vision alone is insufficient to maintain control (i.e. maintaining stability of bipedal robot).

A second associated problem relates to performing inverse kinematics. As the state-space for simple robots possessing only a few degrees of freedom is low, unique solutions are possible and performing inverse kinematics is typically a computationally inexpensive process. However as the state-space grows with mechanical complexity, so too does the computational complexity needed to find suitable solutions. As a unique solution is seldom possible, the performance of the system to generate/execute suitable motion plans is often heavily dependent on the algorithm chosen.

For example, a two degree of freedom robot vehicle can be controlled in the open-loop through adjustment of its forward wheel speed and its steering angle where as a more complex bipedal robot may require the precise close-loop coordinated movement of as many as fifty degrees of freedom. Therefore if personal service robots are to possess reasonably high mechanical complexity, novel control embodiments and schema are needed to ensure efficient and effective control by human users.

1.2 Research Objectives

The overall objective of this work was to develop a robot morphology that simultaneously possessed high practical feasibility (low system complexity, high stability, good controllability etc.) and was capable of demonstrating high levels of behavioural diversity within typical human-centred environments. The core hypothesis of this work was that the successful design of such a complex system can be achieved through the adoption of an embodied design approach whereby detailed consideration is given to the mechanical design (kinematics, dynamics, actuation etc.), the robotic system architecture (low/high level sensing and control), the human-robot interface and the coupling between each of these subsystems. This approach also stipulates that detailed consideration of the range

of task environments should also play a tangible role in shaping the design of the robot. To validate the hypothesis, an embodiment of the proposed morphology was designed and built. An in-depth kinematic and dynamic analysis was undertaken to guide the design of a full scale embodiment of the proposed morphology. The development of this physical demonstrator involved the integrated design of the mechanical robotic system (optimised to suit human domestic environments), a hybrid electro-pneumatic actuation scheme, a dynamically interactive social interface, a distributed robot system architecture and an integrated schema for semi-autonomous tele-operated control. The performance and multi-purpose capability of this robot was evaluated against both physical and performance based design metrics. The embodiment's capability was then compared against existing state-of-the-art robots built for multi-purpose use.

1.3 Overview

Chapter 2 presents a detailed review of the literature pertaining to the design and development of general-purpose type service robots. The embodied intelligence/cognition approach, a design philosophy that closely couples the physical design of a system with that which controls it, is discussed. A review of existing robot morphologies is given followed by the a discussion on the various actuation schemes available to mobile robots. Attention is given to the architectural barriers and environmental constraints that service robots must overcome in buildings, both residential and utility. Relevant background pertaining to human-robot interaction (HRI) and the design of social interfaces is given. The chapter concludes with a high level overview of physical properties and practical capabilities of over 100 robots developed to date. From the information presented, it is evident that no single morphology developed to date simultaneously possesses the capability for high behavioural diversity and terrain adaptability yet retains high levels of static stability, low system complexity and integrated HRI capabilities.

In chapter 3, a high level description of the proposed robot morphology is presented and the core features of the proposed robot morphology are described. The forward kinematics of the system are defined through a system of heterogeneous transformations between the robot's joint co-ordinate systems. The Jacobian for the robot's end effector is defined and

the process of how the inverse kinematics problem is solved through the pseudo-inverse Jacobian approach is outlined. The criteria for maintaining static stability is described. As the robot's static stability margin is variable and can be small at times, two approaches for maintaining dynamic stability are outlined. The first describes how dynamic stability is achieved through wheeled self-balancing (i.e. similar to a Segway mobility platform [12]) and the second alludes to the use of inverse kinematics to augment the robot's overall centre of mass such that the system returns to a state of static stability. The chapter concludes with a description of how the morphology can be adapted to traverse small obstacles, ascend/descend stairs and bridge small crevices.

The mechanical design of the embodiment is described in chapter 4. Firstly an inverse dynamics analysis of the system is performed for various postural configurations to determine the reaction forces and joint torques needed to maintain system equilibrium. A detailed overview of the mechanical design of the embodiment is presented. Specific attention is given to the design of the legs, torso, lower-hip mechanism (LHM) and the arms. The unique electro-pneumatic actuation system used on the robot is outlined and special attention given to the custom design, in-house fabrication and morphological optimisation of the network of pneumatic air muscles used on the robot.

The low-level control and sensing system used on the robot is presented in chapter 5. The design of a highly modular distributed control architecture is described and its embodiment presented in detail. This is followed by a discussion detailing how the morphology's low-level sensing requirements can be integrated within the proposed system architecture. A mathematical description of how proprioception is achieved in real-time using on-board sensors is given. A summary of the robot's safety features is presented. The chapter concludes with an overview of both the proposed semi-autonomous control schema and associated physical controller embodiments.

In chapter 6, a practical performance evaluation is conducted. The ability of the robot to meet relevant physical and performance-based design targets is evaluated. Details describing the development of a realistic 3D simulator which is used to evaluate the ability of a human user to control a personal service robot in a interactive virtual environment are provided. Experiments were conducted using the simulator to test the hypothesis that semi-autonomous control offers improved overall performance over manual control in cer-

tain navigation based tasks. A second hypothesis investigating whether semi-autonomous control schema that facilitate increased levels of operator interaction perform statistically better than less interactive equivalent systems is examined. Through assessment of the robot's overall physical traits, practical capabilities and controllability, the overall utility of the system is benchmarked against existing state-of-the-art robotic systems.
Chapter 7 presents the conclusions of the research followed by suggestions for future work. The remainder of the thesis is comprised of both the references and attached appendices.

1.4 Contribution of Thesis

The work contained in this thesis addresses several important issues relating to the design and control of service robots operating in civilian environments. Through consideration of the environments that the robot will be used in, the nature of the tasks that the robot will be required to carry out and the practical requirements of the human user, it was possible to develop a novel robot morphology that offers very high performance capability while simultaneously achieving relatively low mechanical and control complexity. In so doing, the following distinct contributions were made:

1. The design, analysis and practical embodiment of a novel robot morphology capable of high behavioural diversity including the ability to pick-up objects from the ground, traverse a wide range of civilian environments and overcome several significant architectural barriers including small vertical obstacles, crevices and stairways.
2. A robot morphology capable of pose adjustment through active control of its static stability margin.
3. A novel electro-pneumatic actuation schema that utilises electric motors for accurate wheeled locomotion and pneumatics for actions requiring high compliance and the generation of large forces.
4. A robust, modular and distributed robot control architecture capable of integrating low-level proprioceptive sensing and reactive actuation with high-level perception and control. In addition to providing autonomous capability, this control architecture facilitates integration with a range of manual and semi-autonomous control schemes.

5. A novel embodiment of a semi-autonomous control schema which when integrated with the proposed control architecture, offers increased levels of performance over conventional manual or semi-autonomous control mechanisms.

Chapter 2

Literature review

One of the biggest practical challenges in the field of robotics is to develop robots with the capability of navigating and performing useful tasks in unstructured civilian environments. In 2012, the US Defence Advanced Research Projects Agency (DARPA) announced the 'DARPA Robotics Challenge (DRC)', a competition that would take place over two years (2014-2015) whereby research teams from around the world would be tasked with making a single robot perform a range of tasks that are commonly required during disaster-response efforts [13]. The design of such robust, general-purpose machines is a complex process that requires many detailed considerations - both practical and philosophical. In this chapter the embodied intelligence design philosophy is described. The standard mobile robot morphologies are described with specific reference to their respective actuation and control requirements. A review of mobile robot actuation schemes is presented and their relative strengths and weaknesses are outlined. Pertinent human factors and environmental considerations relevant to the implementation and operation of robots in human centred environments is presented. The chapter concludes with a review of several existing general-purpose platforms and a comparison of their respective performance capabilities.

2.1 Embodied Intelligence

For a robot to successfully undertake tasks in a previously unknown environment, high levels of cognition, terrain adaptability and physical dexterity are required. For this reason a very close coupling must exist between the robot's software, hardware and the physical environment in which it operates.

The interdependence and couplings that exist between the robot's hardware, its underlying control software and operating environment was first fully explored in the early 1990s. Prior to this point, artificial intelligence was treated as a disembodied process and the dominant control paradigm involved the robot sequentially sensing the environment, using this data to construct/update a global model and then explicitly planning/executing its next action [14]. According to this paradigm (known as the 'Hierarchical' or 'Deliberative' paradigm), this process of 'sense-plan-act' is carried out iteratively until the desired goal is achieved. The first core flaw with this scheme arises from the fact that the effectiveness of the robot's performance is heavily dependent on the accuracy of its model of the world. Problems in generating an accurate model quickly arise when the world is unstructured and the only available environmental readings are noisy and only contain information about the robot's immediate local environment. As actions are taken as a consequence of a planning stage and not directly as a consequence of sensing, it is also observed an additional problem with this approach is that sensing is somewhat decoupled from actuation. These issues and several others were first formally observed by Brooks in his landmark papers 'Intelligence without Representation' [15] and 'Intelligence without Reason' [16]. In the former work, Brooks stresses that control should be decentralised where possible and argues that control based on internal modelling alone is inherently flawed. Following from this, in [16] Brooks proposes a bottom-up design methodology for the realisation of intelligent, highly embodied robots. According to Brooks, the intelligence of a robot is not exclusively a property of the computer controlling the robot but it is also derived from *"the situation in the world, the signal transformations within the sensors, and the physical couplings within the world"*.

Brooks therefore hypothesises that intelligence is not some centralised binary quantity that exists in a distinct location within a system but instead it is a inherently decentralised property that is manifested as an emergent behaviour that is itself a consequence of the interaction of the system with its own components and with the physical environment around it. Owing to the means through which control is obtained using Brooks's approach - mainly that actuation is directly coupled with environmental sensing and the planning stage is omitted - became known as 'Reactive paradigm'. While this approach enjoyed popularity during the early 1990s, it was soon surpassed by architectures contain-

ing both deliberative/hierarchical and reactive elements. These architectures, also known as 'hybrid architectures', were advantageous as they enabled both deliberative planning and reflex-based sensory-motor coupling to take place on the same physical system.

As the embodied design methodology gained in popularity over time, the original design principles proposed by Brooks were expanded and refined. In a ground breaking book published in 2006, authors Rolf Pfeifer and Josh Bongard argue that the principles of embodied intelligence form a coherent basis for a general theory of intelligence [17]. In their book, the authors present the theory of embodied intelligence through a series of generalised design principles that span three time scales; the here-and-now perspective, the ontogenetic perspective and the phylogenetic perspective. The contention of the authors is that the function of the design principles is to form a general theory of how intelligence is manifested in embodied agents and to explore the important role that the agent's physical body plays in that process. Therefore while the design principles provide an excellent insight into the nature of intelligence and how it might be realised on a machine, they remain (mostly) philosophical in nature as they provide little direct technical instruction of how they may be practically integrated onto robots.

In accordance with the embodied design principles proposed by Pfeifer and Bongard, the design guideline that best encapsulates the relationship between the robot's design and the task environment in which it operates is the 'Three-Constituent Principle'. This principle states that three core considerations are required in order to optimally design an autonomous robot. These considerations are (1) the environment in which the robot is to operate (2) the desired behaviour/capabilities of the robot (3) the physical design of the robot. According to this principle, once any two constituents are defined, it is possible to engineer the remaining constituent. It follows then that prior to the commencement of the robot's design, it is first necessary to define the desired behaviour of the robot and to study the environment where it is expected to operate.

2.2 Robot Morphology

The diversity of behaviour that will emerge from a robots interaction with the environment will be fundamentally dependent on the physical form that the robot possesses. In

general the more controllable degrees of freedom that a robot has, the richer the diversity of behaviour it has the ability to exhibit. However as the complexity of the robot increases so too does the robot's weight, power consumption and control requirements. Therefore the engineer is tasked with the multifaceted problem of designing a robot such that an acceptable compromise is found between a system that is physically simple but functionally limited and one that is functionally complex but physically impractical.

There are three different fundamental locomotive configurations that can be employed on ground-based mobile robots [18]. These include (1) wheeled/tracked vehicles (known generically as infinite rotational mechanisms) (2) legged systems (3) articulated body mechanisms (i.e. snake-like robots). Each type of mechanism possesses different and often unique characteristics that defines how it achieves locomotion. Since articulated body mechanisms possess an aspect ratio and kinematic morphology that is poorly suited for exploiting human ergonomics, detailed discussion of their locomotive design principles have been omitted from consideration in this section.

2.2.1 Infinite Rotational Mechanisms

Wheeled/tracked locomotion remains the single most popular configuration for mobile robots [19]. Wheeled or tracked/crawler motion is referred to as infinite rotational as movement is achieved through continuous rotation of mechanisms that are in continuous contact with the ground surface.

Relative to the other mechanisms of locomotion, wheeled systems are generally the simplest and most lightweight configurations to implement. Wheeled vehicles are highly effective over flat, firm ground however they perform poorly over soft, uneven or broken terrain [20]. Many wheeled configurations can be implemented on mobile robots however the most common ones include differential drive, skid-steered and active steered. A graph illustrating the most popular wheeled/tracked configurations is given in figure 2.1.

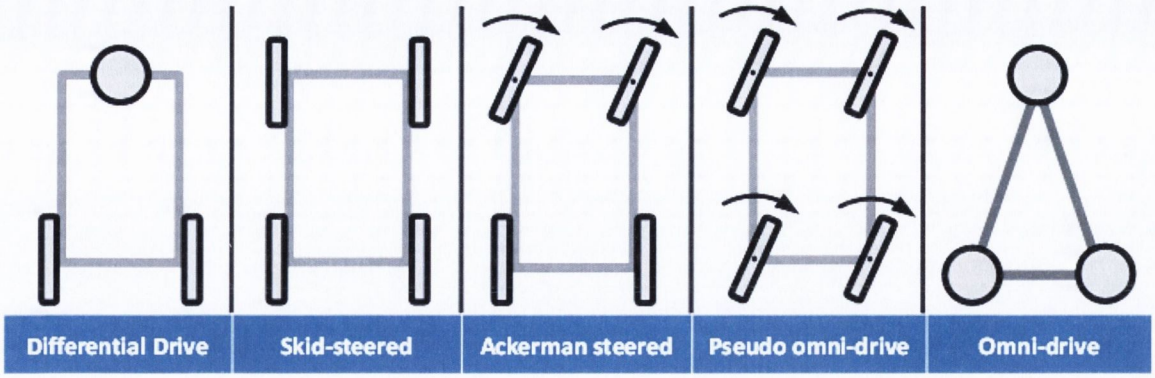


Figure 2.1: The most common wheeled/tracked configurations used on mobile robots. Circular shapes represent omni-directional wheels and rectangular shapes represent regular wheels. Circular arrows identify actively steered wheels.

2.2.1.1 Steered Mechanisms

Robots that manoeuvre using active steering do so by actuation of the wheel's steering axis. This axis can be actuated independently (i.e. pneudo omni-directional configuration) or in a coupled fashion using a mechanical steering mechanism/linkage (i.e. Ackermann steering, syncro-drive). The majority of steered vehicles possess some combination of steered and fixed orientation wheels. The most popular configuration of this type is known as 'Ackermann steering'. Vehicles using Ackerman steering possess two fixed rear wheels and two steered front wheels. The two front wheels are coupled through a steering mechanism which ensures that the steering angles for both front wheels are suitably orientated during a cornering manoeuvre.

An important measure of a robot's manoeuvrability is its 'degree of mobility'This metric takes account of the constraints imposed on a vehicle by its own kinematics. An interesting kinematic property of a steered wheel is that it instantaneously only possesses a single degree of freedom (lateral motion resisted). Since Ackermann vehicles have fixed rear wheels and mechanically coupled steered front wheels, this configuration instantaneously possess only a single degree of freedom, resulting in an overall degree of mobility of one. However when the effect of steering over time is considered, an additional degree of freedom is effectively added. A robot's manoeuvrability due to steering can be quantified through its 'degree of steerability' which is defined by the number of independently controlled steering parameters that the robot possesses [19]. Thus the overall manoeu-

vrability of a wheeled vehicle is given by the sum of its overall 'degree of mobility' and 'degree of steerability'This value, known as the 'degree of manoeuvrability' provides insight into the cumulative overall effect of a system's instantaneous mobility and steering characteristics. Some significant examples of mobile robot systems which use conventional steered configurations include self-driving vehicles such as the *Google car* [21] (Fig. 3.7a) and NASA's *Centaur* platform [22] which uses a steered vehicle base to provide mobility to a humanoid upper body.

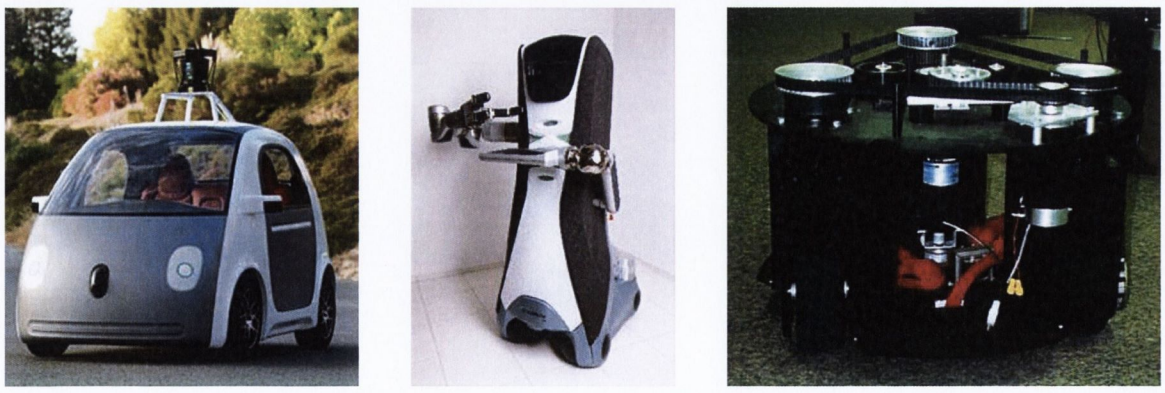
Despite their utility on road vehicles and field robots, conventional steered mechanisms possess several significant limitations. Firstly as Ackermann vehicles have both a 'degree of mobility' and 'degree of steerability' of one , they are kinematically unable to follow any path in its workspace. For example consider how a car using Ackermann steering can only move into certain parking spaces through the process of 'parallel parking'. This poor overall manoeuvrability makes Ackermann steered systems poorly suited for use in cramped, cluttered environments commonly found in indoor residential buildings. Secondly performing dead-reckoning through the process of odometry becomes more complex. Skidding induced in the front steered wheels during turning can add significant noise to the motion sensor readings since the actual wheel rotation does not map accurately to the actual distance travelled by the wheel. Furthermore using active steering is likely to add at least one new control variable into the odometry calculations thus increasing the overall computational complexity. For efficient cornering, the rotational velocity of the wheels on the left and right side of the vehicle must be different. Therefore the third practical requirement is that all wheels should be capable of rotating independently. This implies that for driven wheels, either separate actuators or a form of differential coupling is required.

An interesting steered configuration that is commonly utilised by service-type mobile robotics is the pseudo-omnidirectional form. Robots with pseudo-omnidirectional configurations possess no fixed wheels and are characterised by each driven wheel possessing an independently actuated steering axis. While such systems do not utilise kinematically omnidirectional wheels (i.e. Mecanum/Swedish wheel or omni-wheels), the behaviour of the system is said to approximate that of one that does. While such configurations

are instantaneously limited to a single 'degree of mobilityrq they possess two 'degree of steerability' and an overall 'degree of manoeuvrability' of three. This degree of manoeuvrability allows the robot to move in any direction thus achieving behaviour similar to fully omni-directional systems. The major difference between pseudo omnidirectional and and fully omnidirectional systems as that while the both are capable of following any path in the workspace, only fully omni-directional systems are capable of following any trajectory.

Two widely used robots which uses a pseudo omnidirectional configuration are the *Care-O-Bot* developed at the Fraunhofer Institute [23] (Fig. 3.7b) and the *PR-2* robot developed by Willow Garage [24].

An interesting variation of the pseudo omnidirectional form is the syncro-drive. The syncro-drive possesses three/four wheels which are steered and driven just just two motors. A belt-drive which is connected to the steering axis of each wheel is typically used to orientate the wheels while their forward/reverse drive is provided by the remaining motor. This system does not full achieve omnidirectional-like behaviour as it is not possible to instantaneously modify the robots pose. In an effort to maintain symmetry during locomotion, many robots that utilise this configuration adopt cylindrical body shapes [25] [26] (Fig.2.2c).



(a) (b) (c)

Figure 2.2: Common steered configurations used on mobile robots (a) Ackermann steering used on the Google car (b) Omni-steering on the Care-O-Bot III (c) Synro-drive on the Denning B-12

2.2.1.2 Differentially Driven

Differentially driven robots utilise two independently controlled drive wheels located on either side of the vehicle and achieve turning by varying the relative velocities of each wheel. Conventional differentially-driven robots are statically stable machines. This means that the horizontal ground projection of the robot's centre of mass lies within the support polygon formed by connecting its ground contact points. To achieve static stability, the majority of differentially driven robots utilise additional passive omni-directional wheels which provide additional ground-contact points while also ensuring no additional motion constraints are added. The exact location of the COM ground projection point is proportional to both the vertical height at which the COM resides and the robot's pitch/roll angle. Therefore to maximise stability, differentially driven vehicles typically possess low centres of mass and large longitudinal/lateral wheelbases. Such dynamic properties are disadvantageous for practical use in human-centred environments that are ergonomically designed to be used by embodied agents possessing a human-like form factor and task-space. Amongst the most notable of the many robots built with this configuration include Willow Garage's *turtlebot* [27] (Fig. 2.3a), the K-Team corporation's *Khepra* robot [28] (Fig. 2.3b) and the *Pioneer 3DX* robot by Adept Mobilerobots [29] (Fig. 2.3c).

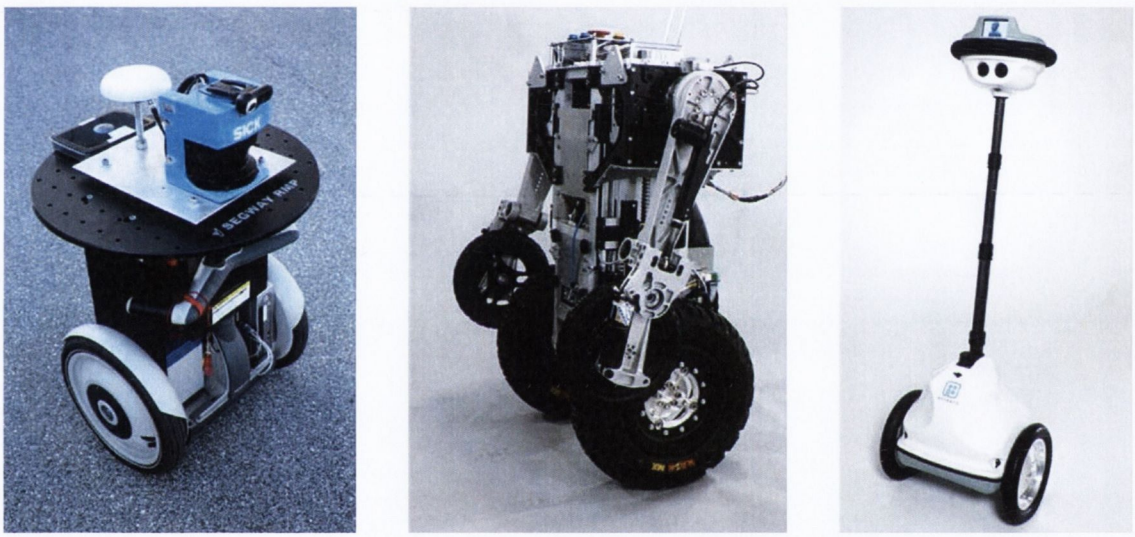


(a) (b) (c)

Figure 2.3: Several popular robots that have a differential drive configuration (a) Willow Garage Turtlebot (b) Khepera robot (c) Adapt Technology Pioneer 3-DX robot

An important class of differentially driven robots exist which do not possess additional passive wheels and lack the ability to naturally maintain static stability. These type of configurations, popularised by the Segway mobility platform [12] (Fig. 2.4a), are known

as self-balancing robots. Maintaining upright stability requires the robot to adjust its wheel velocities in response to the displacement of the robot's centre of mass from the vertical. Since the angular acceleration of a point on a rigid body is inversely proportional to its distance from the point of rotation, maintaining control becomes easier as the centre of mass on the robot becomes higher. Several notable examples of self-balancing robots designed to perform useful tasks in civilian environments include *Golem Krang* developed at Georgia Tech [30], *T-Bot* developed at IHMC [31](Fig. 2.4b), *UBot* [32] [33] and the *Anybots QB* telepresence robot [34](Fig. 2.4c).



(a) (b) (c)

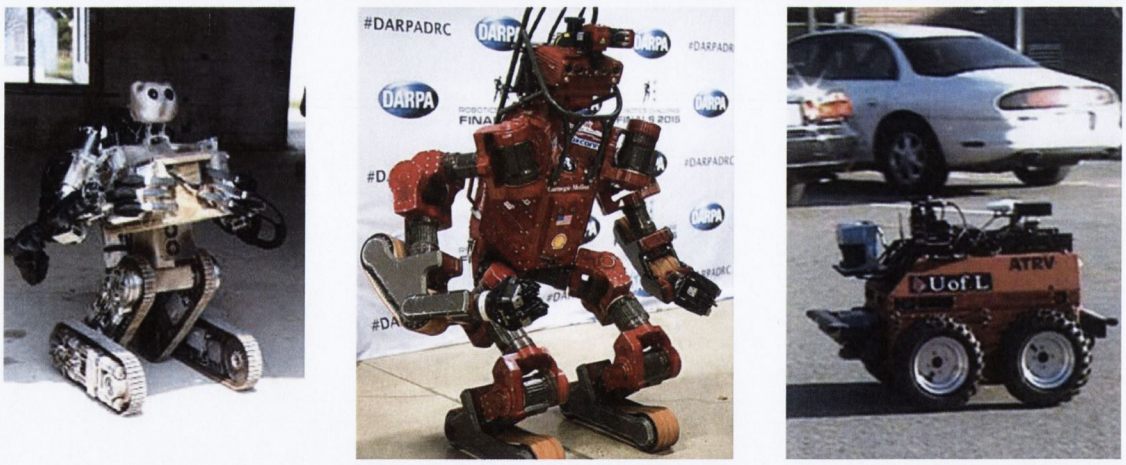
Figure 2.4: Several popular differentially-driven self-balancing robots (a) Segway RMP 220 (b) IHMC T-Bot robot (c) Anybots QB Tele-presence robot

2.2.1.3 Skid-Steered Mechanisms

A skid-steered configuration refers to vehicles that possess either a fixed caterpillar track or several fixed wheels on either side of the vehicle. Skid-steered systems operate in a manner almost identical to differentially driven systems in that steering is achieved by controlling the relative speed of the wheels/tracks on either side of the vehicle. As the lateral resistance to motion of a fixed wheel/track is is extremely high, skid-steered vehicles experience large lateral resistance during turning. Due to these large resistive forces during turning, skid-steered vehicles are generally power inefficient and prone to

vibration and noise. Additionally as the motor torque required to overcome this lateral resistance can be high, in certain cases skid-steered set-ups may be practically unable to execute trajectories that are otherwise kinematically feasible (i.e. a zero point turn). An additional problem for tracked vehicles is that when lateral forces build up, they can cause the track to slip and misalign with the guide wheels.

A notable benefit of skid-steered vehicles over differentially driven vehicles is that, due to their longer wheelbase, they are able to move on soft terrain and traverse obstacles (such as stairs) that would normally impede a differentially driven robot. Other benefits of skid-steered vehicles typically include high static stability, simple control requirements and robust mechanical construction. Several skid-steered robots have been developed for applications in civilian environments including the *Battlefield Extraction-Assist Robot(BEAR)*[35](Fig. 2.5a), the *CMU Highly Intelligent Mobile Platform (CHIMP)* developed for the DARPA Robotics Challenge [36](Fig. 2.5b), iRobot's *ATRV* series[37](Fig. 2.5c) and *Packbot* robot [38].



(a) (b) (c)

Figure 2.5: Several notable skid-steered service robots (a) Battlefield Extraction-Assist Robot (BEAR) (b) CMU Highly Intelligent Mobile Platform (CHIMP) (c) iRobot ATRV

2.2.2 Legged Robots

Over the past two decades, legged locomotion has become a very active area of research and a wide range of legged robots have been developed. Unlike infinite rotational mechanisms where locomotion requires sustained physical contact between the tyre/track and

the ground, legged locomotion requires the coordinated movement of two or more leg linkages which make contact with the ground at discrete locations. Since the ground contact points (or footholds) can be chosen somewhat arbitrarily, legged morphologies are especially well suited for use in civilian environments where climbing stairs, bridging crevices and stepping over obstacles are common requirements. In addition to being suitable for locomotion on uneven and broken terrain, legged robots possess the potential for high levels of manoeuvrability. By pivoting the legs at the hip joint, it is possible for legged robots to adjust their orientation independent of the ground surface. This allows them to change their direction of motion without slipping or skidding.

Legged systems are also well suited for use on soft surfaces (i.e. sand). Since legged robots make contact with the ground at discrete points, ground deformation is minimised during locomotion. This is in contrast to infinite rotation vehicles that make continuous contact with the ground and waste energy obtaining traction on surfaces that deform significantly under the stress of the terrain interaction [18].

Legged robots can also be adopted to have benefits aside from locomotion. Firstly legged robots can serve as an active platform. For example, elongation of the legs may allow a robot to orientate itself so that it can grasp an object that was otherwise out of its reach. Another advantage of using legs is that they can serve a secondary purpose as a manipulator. The *RoboSimian* robot developed at NASA JPL to compete at the DARPA Robotics Challenge (DRC) provides an excellent example of this philosophy in action [39] (Fig. 2.6).

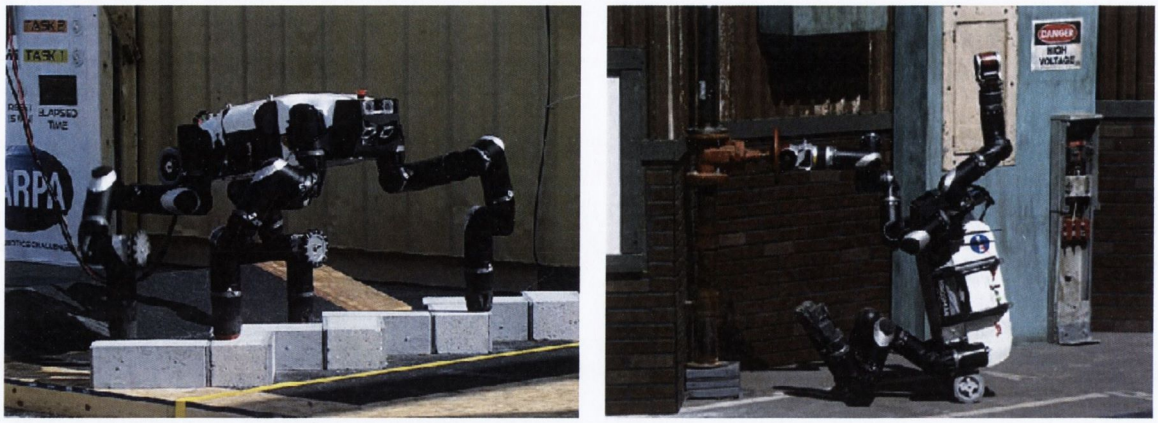


Figure 2.6: Robosimian using limbs for locomotion (left) and manipulation (right)

Despite some impressive capabilities, legged systems suffer several significant practical limitations. The first issue concerning walking robots is stability. Depending on the number of legs and the gait pattern, walking robots are either statically stable or statically unstable. Statically stable robots continuously maintain static equilibrium (even during locomotion) while statically unstable robots do not. Static stability is achieved mathematically if the projection of the robot's centre of mass lies within the support polygon formed by connecting the robot-ground contact points [40]. The minimum number of legs needed for a system to possess static stability is four. However statically stable walking gaits on four legged robots only allow for one leg to be lifted at a time. To improve the speed and overall stability of the system, most statically stable legged robots possess more than four legs (typically six). Since bipedal robots possess just two legs, in the absence of dedicated mechanisms for static stability (i.e. foot suction cups), they are categorised as statically unstable robots. Statically unstable robots are inherently unstable systems that require both sensing and actuation to remain upright. In comparison with equivalent statically unstable systems, statically stable morphologies have significantly fewer real-time control requirements as stability can theoretically be obtained in the open loop. Furthermore since statically stable systems do not require actuation to maintain balance, significant power/energy savings can be made.

The problem of static instability, often likened to that of maintaining the upright position of an inverted pendulum, requires the system to continuously sense falling motion and to then apply counteracting responses through actuation. Owing to the complexity of

modern walking robots and the unstructured environments in which they are typically required to operate, reliably maintaining dynamic stability is a computationally expensive and a technically complex control problem. Furthermore, unless the robot is capable of forming statically stable resting poses, the system will have high energy consumption as power is continuously required to stop the robot from falling over. To date the most widely used and best established method for maintaining dynamic stability for bipedal robots is the 'Zero Moment Point (ZMP)' method. The ZMP is defined as the point on the ground which the sum of all the moments of the active forces equals zero. Similar to the static stability margin, if the ZMP lies within the convex hull of all the contact points between the foot and the ground, the biped can walk [41]. This method has been used on Honda's *P2* and *Asimo* robots [42] [43], the *H6* and *H7* robots developed at Japan's JSK lab [44] [45], the biped *Johnnie* developed at the TUM [46], the *Wabian-2* robot developed at Waseda University [47]. Derivatives of this method have also been adopted for use on the *HRP-2* platform [48] and also on Boston Dynamics's *Petman* system [49].

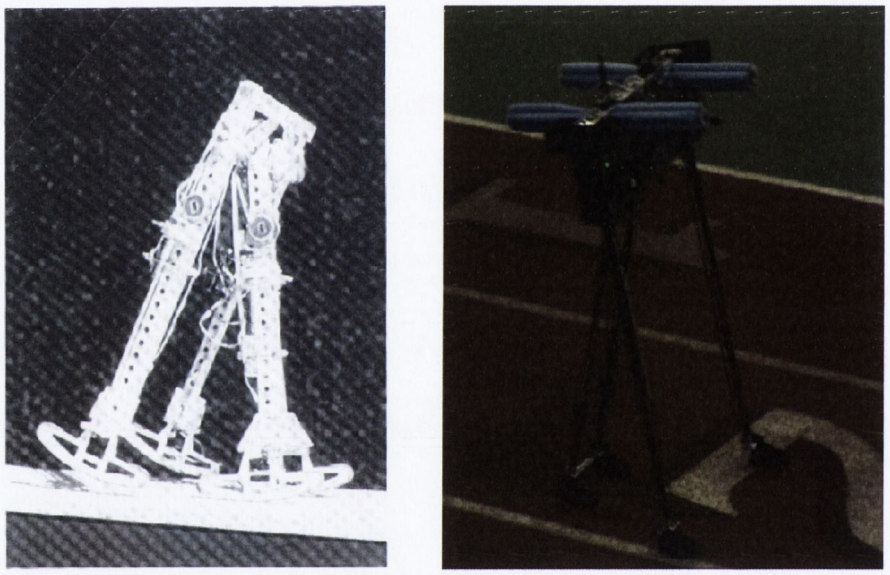
2.3 Actuation

2.3.1 Passive Dynamics and Decoupled Actuation

As legged systems accomplish locomotion through the coordinated movement of several linkages, legged robots usually require many more actuators than mechanically simpler wheeled/tracked morphologies. This typically results in increased complexity (control and mechanical), inertia and energy consumption. Furthermore the speed of limb movement in legged systems is often limited in order to minimise to the inertial effects caused by cyclic accelerations induced during walking.

One approach that has been used to overcome these practical issues has involved the utilisation of passive dynamics in designing the robot and its walking gait. Unlike traditional legged robots that move under active control, passive dynamic walkers possess no actuators and generate motion from gravity and inertia alone. Through the research of McGeer and others it has been shown that passive dynamic machines can possess an extremely high energy efficiency while retaining low mechanical and control complexity

[50](Fig. 2.7a). Due to their limited controllability (owing to their few controllable degrees of freedom) conventional passive dynamic walkers are not a practical configuration for general-purpose use. However through the addition of motors that provide actuation in the absence of gravity, it is possible to achieve substantially improved performance while still retaining high levels of energy efficiency and mechanical simplicity. For example, the longest distance walked by an untethered legged robot was officially recorded by the *Cornell Ranger*, a passive dynamic hybrid, when it was found to be capable of walking over sixty five kilometres on a single battery charge [51](Fig. 2.7b).



(a) (b)

Figure 2.7: Notable passive dynamic walkers (a) McGeer's original passive dynamic platform (b) Cornell Ranger hybrid passive dynamic platform

A basic and very popular method of reducing motor torque requirements is through decoupling the actuator from the joint. Since it is usually advantageous for legged robots to possess lightweight legs, designers often choose to position leg actuators in the body of the robot and use chain/belt drives to remotely drive the joint. In this way, the inertia from the drive system does not significantly add to the actuation torque needed to control the joint. Decoupled actuation has the added effect of isolating the actuator from vibration and impacts such that should the joint be damaged, the damage is not transferred to the actuator also. Another approach that has been proposed in the literature to improve the suitability of conventional electric motors in legged applications is to design the legs and

gait such that negative power (power supplied from the output side of actuator i.e. motor breaking) is minimised. This approach termed ' Gravity Decoupled Actuation (GDA) ', requires careful design of both the leg structure itself and the gait adopted by the robot [52]. Some examples of robots that use this approach include *TITAN III* and *TITAN VIII* [53].

Another method, known as 'coupled drive', hypothesises that low actuator power-to-weight ratios can be overcome through actuator coupling. It proposes that the morphology should be designed such that it maximises the use of installed actuators (i.e. actuators located on the robot should have overlapping functionality and be utilised in many different required movements). This approach has been embodied on the *NINJA-I*[54] and *NINJA-II*[55] platform.

A third novel approach involves using springs to reduce the power requirements of the actuators at joints where large torques build up (such as the knees in bipedal robots). Using this technique, known as 'gravity compensation', force produced by the stretched spring will reduce torque requirements of the actuator when the limb moving in opposition to its own inertia as it returns to its equilibrium position. Similarly the effect of the robot's inertia on the joint reduces the force that the actuator would otherwise need to overcome in order to stretch the spring and rotate the joint. Use of this method can be observed in the *Saika-4* robot, developed at Tohoku University [56].

2.3.2 Electric Actuation

Owning to their control simplicity, mechanical reliability, relative low-cost and flexibility of use, electric actuators remain the most popular type of actuator used on mobile robots. They have proven an especially effective form of actuation on infinite rotational robots as they can be used not only as a means of locomotion but through the integration of rotary encoders, they can provide odometric feedback which can be subsequently used for localisation through a process known as dead-reckoning. The utilisation of rotary encoders is often desirable in closed-loop joint control applications where it is required that joint positions/velocities are closely monitored.

Due to the large number of controllable degrees of freedom required for legged locomo-

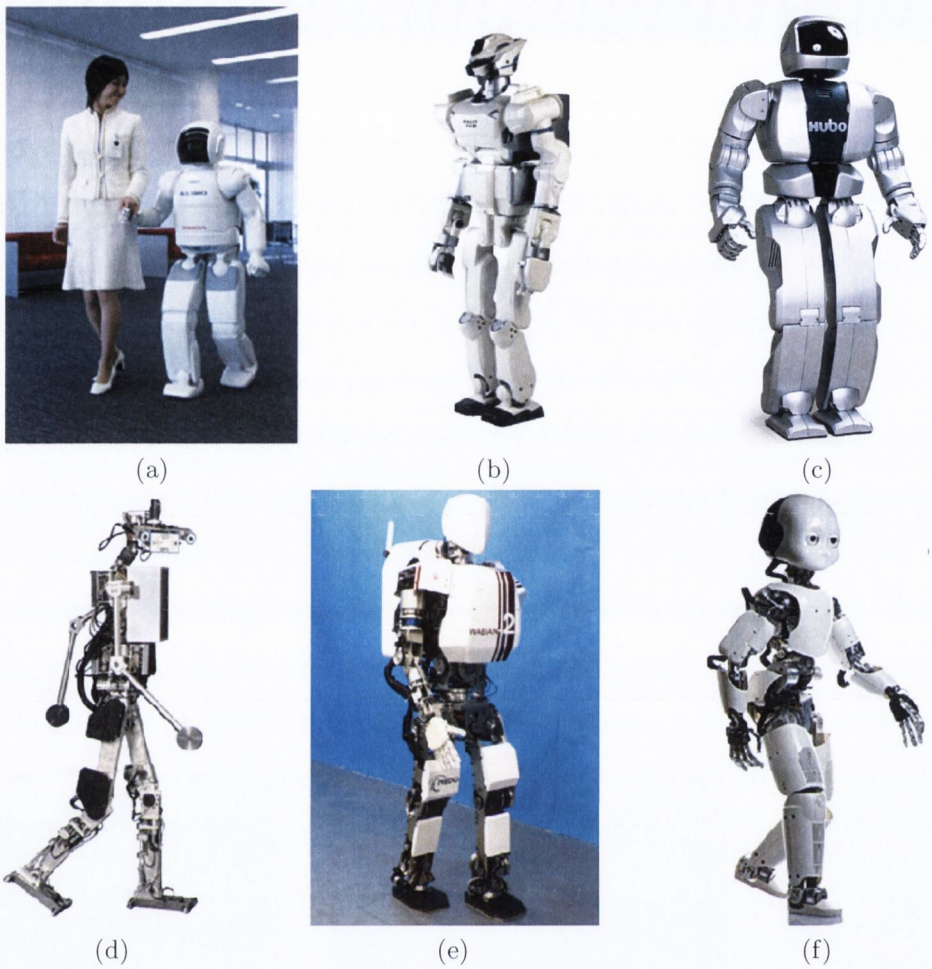
tion, legged robots tend to require many actuators. Using multiple electric motor drive units adds significantly to the robot's overall mass, thus serving to increase the torque requirements of the joints. Furthermore due to factors such as backlash, high stiffness, low power-to-weight ratios and energy efficiency, modern geared electric motor drive units in the most conventional form are highly impractical for usage on legged robots.

The power of a motor drive unit can be described in terms of its torque and rotational velocity (Eqn. 2.1). As electric motors naturally produce low torque, they are usually implemented in conjunction with a reduction gearbox which increases torque at a cost of lowering rotational speed.

$$P = T\omega \tag{2.1}$$

Gearboxes which achieve increased torque through the mechanical coupling of multiple cog gears (i.e. planetary, spur gears) suffer from backlash, the effect of the slack caused due to the clearance between the mated gear teeth. While backlash negatively affects statically stable wheeled robots by causing odometry errors, it is a much bigger problem for statically unstable robots that require smooth output from the actuators to maintain balance. The most common method of overcoming backlash is to utilise a non-backlash gearbox such as a harmonic drive. Robots possessing such drive systems include the Honda *P2* and *Asimo* robots [42] [43] (Fig. 2.8a), *Wabian-2* [47](Fig. 2.8e), *H6* [44], *Saika-4* [56], *Hubo* [57](Fig. 2.8c), *Johnnie* [46](Fig. 2.8d), *iCub* [58] (Fig. 2.8f) and *HRP-3* [59](Fig. 2.8b).

As harmonic gearboxes are non-backdrivable, robots that utilise them possess a high inherent joint stiffness. This makes them excellently suited for highly accurate positioning however the high mechanical impedance of the system imposes limitations on the robot's ability to adapt to uncertain terrain conditions. Furthermore in the absence of dedicated shock absorbing mechanisms, both vibration and impact forces induced when the feet contact the ground are transmitted throughout the body. The stiffness of these robots also makes them potentially unsuitable for use around people. Since the joints are not naturally backdrivable, the robot will act as a rigid body should it come into physical contact with a person/object. It is noted that compliance can be added to the system through the utilisation of impedance-based control. Through utilisation of joint torque sensor data,



(a) (b) (c)

(d) (e) (f)

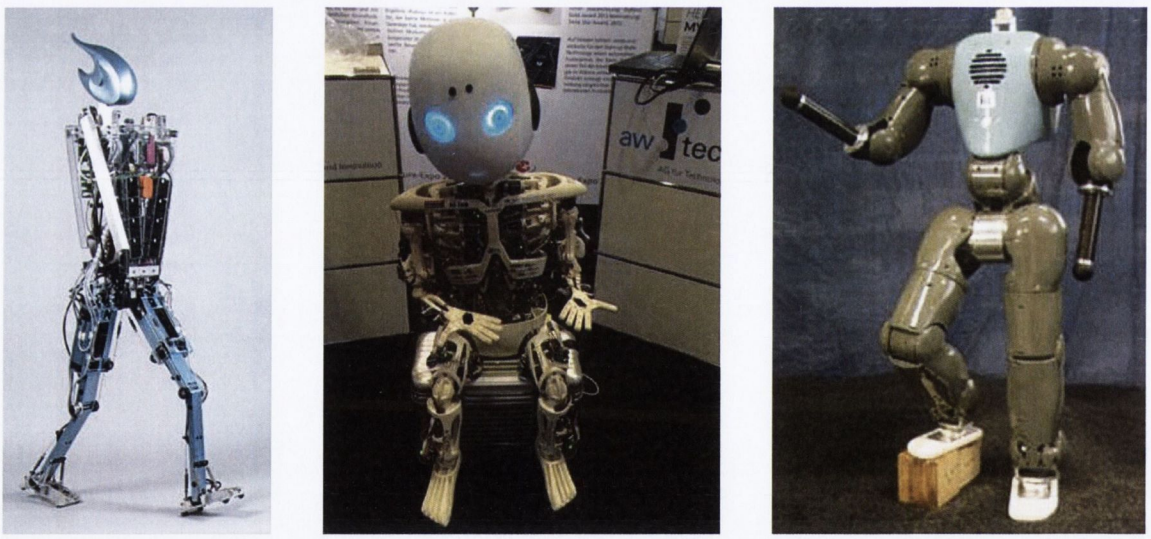
Figure 2.8: Legged robots with harmonic gear drives (a) 2006 Honda Asimo (b) HRP-3 (c) HUBO (d) Johnnie (e) WABIAN-2 (f) iCub

an impedance-driven controller can be tuned to minimise additionally experienced joint torques through direct motor control. For example, if an impedance-driven manipulator made contact with a rigid object, the manipulator would experience an immediate increase in joint torque arising from the reaction force caused from the collision. To minimise the impedance, the controller would likely stop/backdrive the motors until the collision induced loading was removed.

Naturally compliant actuators offer an attractive alternative to conventional stiff actuation systems. It is observed that biological systems which possess high degrees of natural compliance adapt naturally to the environment, are capable of dampening low frequency vibrations/shocks, are extremely efficient at storing/releasing energy and possess a versatility not possible with conventional fixed-stiffness actuators. For example, a human arm

muscle is stiff when it needs to perform an accurate task such as pouring a drink in a glass while it is loose during walking [60].

An effective and proven method of overcoming many of the limitations imposed by by electric drives to connect a mechanical spring in series with the motor drive. These actuators, known as 'Series Elastic Actuators (SEA)' [61], are then capable of effectively filtering out high frequency noise and absorbing impacts. This configuration also enables improved force control to be achieved. Since position is easy to control on motor drives and the spring stiffness can be easily ascertained, accurate force inferences can be made. Another interesting advantage of using SEAs is that through their in-built elasticity, they possess the capability for energy storage. It has been shown that for legged systems, the utilisation of such energy storage capabilities enables significant efficiency improvements [62]. Several robots of note that have implemented such actuation systems include *Flame/TuLip* [63] (Fig. 2.9a), *Roboy* [64] (Fig. 2.9b) and *COMAN* [65] (Fig. 2.9c).



(a)) (b) (c)

Figure 2.9: Legged robots with compliant series elastic actuators (a) Flame (b) Roboy (c) COMAN

2.3.3 Hydraulic Actuation

Due to their high controllability and power generation capabilities, hydraulic actuators have a long history in robot development. While traditionally hydraulic actuators were used in industrial applications, they have increasingly found usage in mobile robotics,

especially in applications where large joint torques are required (i.e. biped robots) or where large payloads are required (i.e. robot mules). Unlike SEAs that typically utilse non-adjustable springs, hydraulically driven robots can vary the stiffness of the joints through control of the fluid pressure in the actuators. This makes them highly adaptable and capable of performing tasks where variable joint stiffness is required.

Despite their suitability in certain applications, hydraulic systems suffer two significant practical limitations. In order to operate untethered, they must use a high-powered on-board pump to generate the fluid flow required for movement. These pumps generate vibration and noise and often occupy significant volume in the body. Furthermore hydraulics consume significant electric power and often depend upon dedicated power generator to achieve practical run times. For example, *Bigdog*, a hydraulically driven quadruped developed by Boston Dynamics uses a 15hp two-stroke internal combustion engine to drive its on-board electric pump [66]. A second major disadvantage of hydraulic systems is mass. Hydraulically driven robots are typically heavy because in addition to the reservoir of liquid they are required to carry, they also need on-board pumps, heat exchangers and large power supplies. Both Boston Dynamic's *Petman/Atlas* [49] and Carnegie Mellon's *Sarcos Primus* robots [67] have demonstrated impressive practical performance capabilities using this actuation scheme.

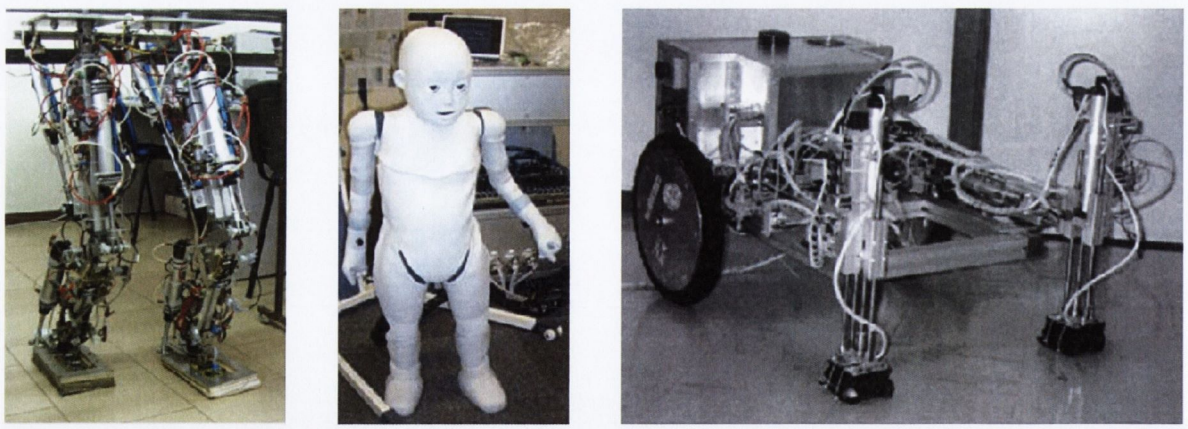
2.3.4 Pneumatic Actuation

A second alternative to electric actuation are pneumatic drive systems. Like hydraulic actuators, pneumatic air systems are capable of generating significantly higher actuation forces than equivalent electric drives. However since the pumping requirements are less demanding and air weighs much less than liquid, they tend to possess a higher overall power-to-weight ratio for use on robots. Additionally since the air used in the actuators is not recycled, active cooling is usually not required. Since pneumatic systems can also vary the pressure in the actuator, another trait that they share with hydraulics is the ability to vary the stiffness of the joint. It is noted that since air is compressible, pneumatic actuator configurations typically exhibit spring-like behaviour if disturbed from equilibrium. On the other hand, as the fluid medium in oil-based hydraulic actuators is incompressible,

spring-like behaviour is only realised through the integration of additional passive springs or [66] [68] or through an impedance-based control system.

Another key advantage of pneumatic systems over hydraulics is that they possess the capability of using a stable stored energy supply (i.e. compressed air tank) rather than relying on continuous operation of an on-board pump. This reduces the energy consumption and overall mass of the robot. Furthermore in comparison to hydraulic systems, pneumatic configurations tend to be less expensive and pose a smaller environmental risk should leakage occur.

Since the earliest walking robots, conventional pneumatic cylinders have been used for actuation on mobile robots. The statically stable *EP-WAR I, II* and *III* robots used pneumatic cylinders to actuate pantograph inspired legs [69] [70] [71]. *DIEES* used an arrangement of pneumatic cylinders in realising an anthropomorphic bipedal design [72](Fig. 2.10a). The *CB2* robot developed by Minato et al. also adopted pneumatic cylinders to create a childlike, biomimetic humanoid robot [73] (Fig. 2.10b). The *Wheeleg* robot used a hybrid morphology where two driven wheels at the rear were coupled by two pneumatically driven legs at the front [74] (Fig. 2.10c).



(a) (b) (c)

Figure 2.10: Notable mobile robots with pneumatic cylinder drives (a) DIEES (b) CB2 (c) Wheeleg

A well documented control problem of conventional pneumatic cylinders the ability to achieve and maintain positional accuracy. Conventional double acting pneumatic cylinders, driven by the difference in pressure across the drive piston, possess an innate compliance due to the compressibility of air. Not only does this springlike property affect the

ability for the system to reach an equilibrium but it also results in a delayed response time [75].

A popular alternative to the pneumatic cylinder is the pneumatic artificial muscle (PAM). These actuators are so-called because like human muscle they contract linearly when activated. The PAM was first patented in 1958 by R.H. Gaylord [76]. In his disclosure, Gaylord described the muscle as "*an elongated expansible tubular means surrounded by a woven sheath forming an expansible chamber which contracts in length when expanded circumferentially*".

In more practical terms, the pneumatic air muscle can be describes as: "*contractile and linear motion engines operated by gas pressure. Their core element is a flexible reinforced closed membrane attached at both ends to fittings along which mechanical power is transferred to a load. As the membrane is inflated or gas is sucked out of it, it bulges outward or is squeezed, respectively. Together with this radial expansion or contraction, the membrane contracts axially and thereby exerts a pulling force on its load. The force and motion thus generated by this type of actuator are linear and unidirectional. This contractile operation distinguishes the PAM from bellows, which extend upon inflation.*" [77].

The practical potential of 'artificial muscles' was first realised by Dr. Joseph McKibben who applied this technology to develop advanced orthotics for polio patients. McKibben, a renowned physicist, made the device practical through utilisation of a compressed gas canister connected to the PAM through a controllable valve. Contraction of the muscle was achieved through opening of the valve [78]. This specific embodiment has become known as the 'McKibben actuator' and remains arguably the most popular design utilised on mobile robots.

Pneumatic artificial muscles possess several interesting properties. As their composition is simple and they use air for actuation, PAMs are cheap, lightweight and easily customised. Since they can support similar pressures to pneumatic cylinders, they possess a very high power-to-weight ratio. Due to their soft form, air muscles are a highly compliant actuator. They do not occupy a fixed volume on the robot and can adopt to fit in

spaces where equivalent rigid actuators cannot be mounted. Unlike conventional two-way pneumatic cylinders which can supply controllable forces in two directions, PAMs only supply force in one direction during contraction. To enable bilateral actuation, two muscles are installed on opposite sides of a joint. Therefore the torque developed by one muscle during contraction applies a tensile force on the other (Fig. 2.11). Accurate control of the air pressure in the PAM is achieved through utilisation of throttling valves and using PWM control of the solenoid valve regulating flow of compressed air to the muscles.

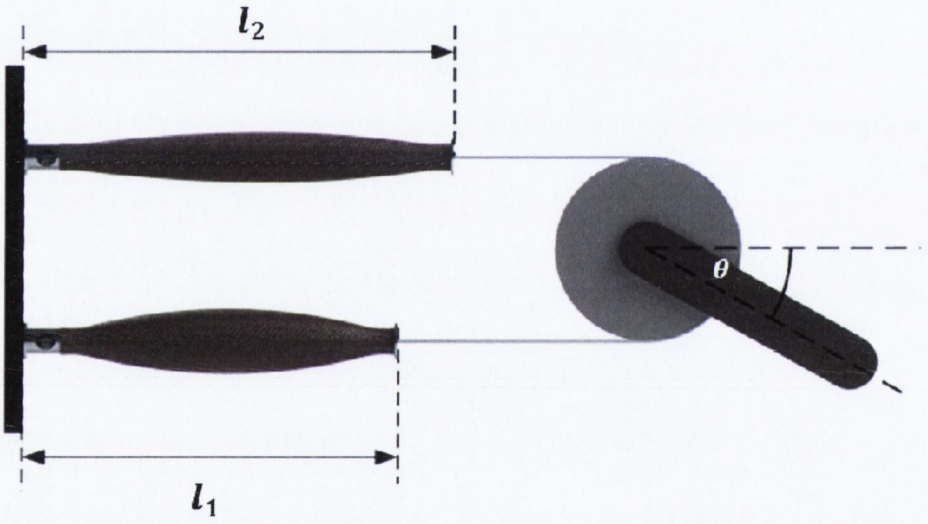
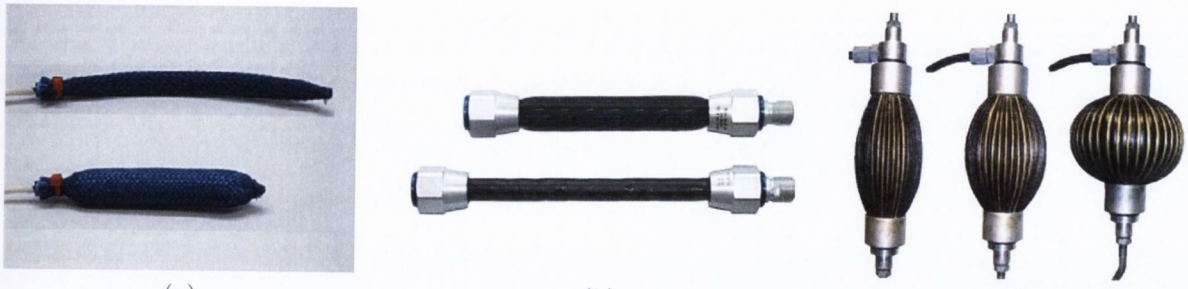


Figure 2.11: Principle of operation of an antagonistic joint using a pair of McKibben muscles. The controlled contraction of one muscle creates a tensile force which causes the opposing muscle to extend. Joint control can be thus achieved by regulating the pressure in each muscle.

To achieve controlled actuation, the pressure of the air in the PAM is regulated by valves linking the muscle to a compressed air source. For reasons of cost and practicality, solenoid valves with extremely fast response times (typically less than 10ms) are often deployed [79] [80]. Commercialisation of this technology was undertaken in the 1980s by Bridgestone [81] [82] and then again in the early 2000s by the Shadow Robotics Company [83] and FESTO [84](Fig. 2.12b).

To date several designs of PAM have been proposed and subjected to varying degrees of development [77]. The most successful categories of PAM have been the braided PAM (BPAM)(Fig. 2.12a) and the pleated PAM (PPAM) (Fig. 2.12c).



(a) (b) (c)

Figure 2.12: Popular types of pneumatic air muscle(PAM) (a) McKibben Actuator (b) FESTO Fluidic muscle (c) Pleated air muscle

Braided PAMs (BPAM) consist of an air-tight rubber tube enclosed by a sleeve of helically braided fibres. Increasing the pressure in the tube (typically achieved by opening a valve connecting the muscle to a compressed air source) causes the tube to expand against the braided sleeve. The helical pattern of the braid causes an anisotropic expansion where the muscle expands radially and contracts longitudinally. As the internal pressure in the tube increases, so too does the tension developed in the braid fibres which integrate at the extreme ends of the muscle where they act on the applied load. The muscle originally popularised by McKibben (now often referred to as the 'McKibben actuator') remains the most commonly used muscle of this type. Despite its non-linear characteristics, the McKibben muscle is generally well understood and has been subject to successful characterisation [85] [86] [87]. Additionally due to the simplicity and availability of the required components, BPAMs are simple to build and custom fit on a robot. Despite its advantages, the McKibben muscle has several drawbacks. Degradation of the braid fibre at the clamping points is a leading cause of failure [77]. In addition to the conventional challenges of controlling pneumatic systems, the hysteresis caused by the dry friction between the tube and sleeve during expansion further increases the control complexity and energy consumption. Furthermore it has been reported that this friction relationship is affected by the temperature of the braid fibres which rise during the cyclic compression and elongation of the muscle [87] [88]. The 'Fluidic Muscle' currently under development by Festo [89] overcomes some of these issues by integrating the braided sleeve with the

rubber membrane. This design boasts a substantially longer operational life than the conventional McKibben actuator however it is only rated for 15% contraction of its nominal length.

The pleated PAM (PPAM) consists of a single membrane that is arranged into folds along the longitudinal direction. When the pressure inside the muscle increases, the membrane expands radially and the pleats open out. When the pressure is reduced, the pleats will elastically return to their default state. Like BPAMs, PPAMs can operate at high pressure. However since PPAMs do not experience friction during expansion, hysteresis is virtually avoided. Not only does this make the configuration more energy efficient but it enables more accurate control to be achieved. The max contraction that a PPAM can undergo is dependent on its geometry however contraction rates as high as 45% are practically achievable [77]. This is substantially higher than BPAMs which typically have contraction rates of approx 30%. Several notable works have been done on the modelling and characterisation of PPAMs [90] [91].

Despite possessing numerous advantages over conventional actuation technology, the PAM has never gained widespread use in robotics. While numerous attempts have been made to utilise PAMs on legged robots, few have succeeded in achieving dynamically stable locomotion using PAMs alone. Possibly the most impressive robot to achieve walking motion using PAMs is the *Lucy* robot developed at the Vrije University in Brussels [90]. Using pleated air muscles, Lucy demonstrated dynamic walking. Weighing only 30kg (not including mass of pump and computers), the system demonstrated that adopting pneumatic actuation could significantly reduce the overall mass of the robot. Another PAM driven robot that successfully achieved a stable dynamic bipedal gait was *Dexter* prototype by the Anybots robotics company [92]. Caldwell et al. demonstrated that high controllability of robotic legs could be achieved with PAMs through adaptive pole-placement controllers [87]. However despite achieving standing stability, the research did not lead to an unassisted walking gait. It is noted that despite the relative successes of these robots, no system of this type has yet to demonstrate untethered locomotion using PAMs.

While few projects have succeeded in utilizing PAMs for locomotion, several groups have

adopted PAMs for use on robotic subsystems or on fixed platforms. The Bridgestone Corporation and Hitachi developed the *Bridgestone-Hitachi Arm* in the 1980s in an effort to improve the tactile ability of industrial manipulators [93]. The Shadow Robotics Company have a rich history of incorporating pneumatic air muscles into their robot designs. In the 1980s Shadow Robotics developed a biped platform, the *Shadow Biped Walker* which relied on BPAMs for actuation [94]. More recently they have developed advanced robotic limbs capable of high levels of articulation [95] [96]. Other people who have developed PAM actuated robotic limbs include Colbrunn et al. at the Case Western Reserve University [97] and Caldwell et al. at Salford University [87]. The Festo company have developed an advanced anthropomorphic robotic torso which makes use of their own proprietary fluidic actuators [84].

2.4 Design Guidelines and Standards

Having discussed the morphological considerations necessary to build practical robotic systems, it is now appropriate to consider the environment in which the robot is required to operate. When developing robots that will operate in human-centred spaces, it's important that the robot is designed such that it can physically exploit the built environment as well as be capable of operating safely/reliably in the proximity of and in co-operation with people, at least some of whom may be untrained users.

2.4.1 Existing with People: The Human Environment

As service robots are required to perform tasks in human environments and coexist with humans, it is important that they are designed such that they are both capable of performing useful tasks and working comfortably alongside people. One philosophy which is particularly attractive in developing such systems is User-Centred Design (UCD). In accordance with this practise, the design should pay particular focus on the needs, wants and limitations of the end-user throughout the whole design process. A formal description for UCD is given in ISO 9241-210:2010 [98]. According to this standard, there are six key principles that must be followed to ensure that a design is user-centred:

1. The design is based upon an explicit understanding of users, tasks and environments
2. Users are involved throughout design and development
3. The design is driven and refined by user-centred evaluation
4. The process is iterative
5. The design addresses the whole user experience
6. The design team includes multidisciplinary skills and perspectives

While many engineers have integrated human factors into the design of robots, few have attempted to apply it to the design of the system as a whole. In section 2.5, the design of several such platforms is discussed in detail.

2.4.1.1 Human-Robot Interaction

The ability to communicate efficiently with people and technology is among the most fundamental functional requirements of service robots. The importance of this function is magnified when the robot is required to work with untrained civilian users and/or with people from vulnerable demographics such as the elderly or the disabled. Research has shown that robots operating in the vicinity of people aught to possess an easily identifiable feature which both serves as a 'focal point' for interaction and provides continuous feedback to users. In comparing the robotic museum-tour guide *Minerva* with its predecessor *Rhino*, two virtually identical robots but with the former possessing a basic social interface, it was reported that *Minerva* achieved substantially greater success in attracting people's interest and performing the task of leading visitors thorough a museum [99]. In a project by Green et al. to develop a user-centred designed robot for an office environment, researchers discovered that during interactions between a customised *Nomadic Scout* robot and an untrained user, the lack of continuous feedback elicited confusion in the user which caused them to closely monitor the movement of the robot. Additionally they found that usability of the robot improved when the social interface served a secondary purpose of identifying the front-facing direction of the robot [100]. Similar research by Kiesler and Goetz found that the willingness of visitors at a museum to complete a long

questionnaire was substantially increased if they were approached by a humanoid-type robot rather than from a vehicle-type robot with no distinguishable social interface [101]. The specific form that a social interface on a robot should take remains an active area of research. In the cases where the functionality of the robot is limited (i.e. a robotic vacuum cleaner) or the environment is heavily constrained (i.e. a virtual avatar), functionally designed user interfaces (UIs) typically work best. As the level of user interaction is typically low in such circumstances, such interfaces can be made simple, intuitive, robust and less resource intensive. For example, the Dyson *360 Eye* vacuum cleaner can be set up and easily programmed using an application on a smartphone/tablet [102]. Similarly by pressing a button and asking a question on an connected Apple device, the virtual assistant *Siri*, can receive, interpret and respond to the query [103].

As the functionality and the degree to which the robot is required to interact with people increases, so too must the complexity of the interface. While a study of the psychological requirements for bio-inspired social interfaces is outside the scope of this study, reference should be made to how the 'intentional stance', proposed by Daniel Dennett [104], influences our understanding of social interaction in humans. The intentional stance postulates that through abstraction, it is possible to rationalise and consequently predict human behaviour as a consequence of the beliefs and desires held by a person who is held to be a rational agent. While machines are not biological agents and therefore do not share the same internal/external states as people, it is still common for people to apply the intentional stance to better understand their observed behaviour. The human brain is innately adaptable and constantly applies the intentional stance to help it understand and interpret the actions and behaviours of agents in the world around it, human or otherwise. Indeed 'anthropomorphism', the human tendency of rationalising non-human behaviour through superimposing aspects of the human observer, is something that humans experience in everyday life. The degree to which humans anthromorphise objects in the world is especially evident when one considers the many websites which depict animals-as-people and how companies such as Disney have achieved repeated success from producing animations which consistently anthropomorphise both animals and objects [105].

The 'Life-like Agents Hypothesis' also suggests that interfaces that interact with humans are most effectively designed by imitating natural life. This can be achieved both su-

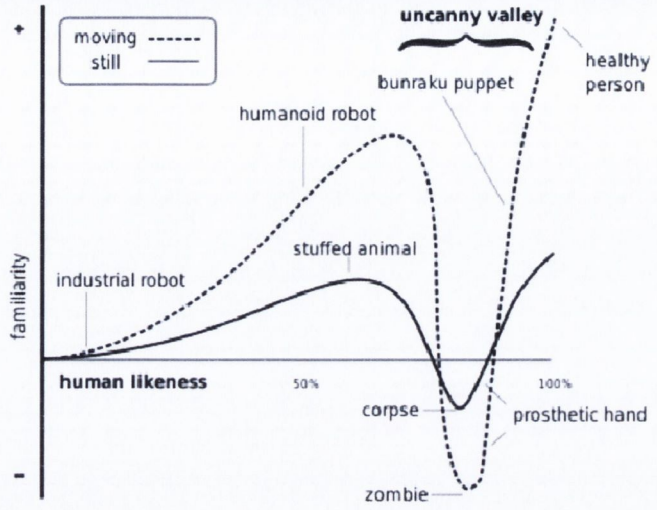
perficially through adopting lifelike appearance/behaviour but also through development of deep bio-inspired cognitive architectures [106]. It is proposed that such systems are advantageous for the following key reasons:

1. Since they are required to fulfil roles normally done by humans, they benefit from human-like forms of social intelligence

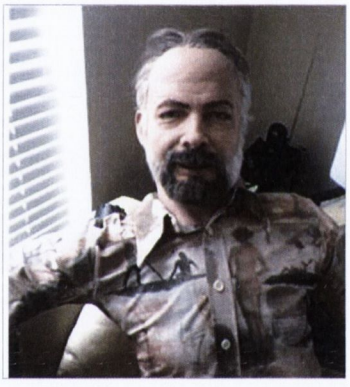
2. Humans prefer to interact with other humans and not less ideally with human-like agents

3. Replicating life can serve to increase understanding and promote the study of animal behaviour and cognition

Despite evidence that would appear to suggest that optimally designed robot interfaces should approximate human likeness in both form and behaviour, this is not necessarily the case. While researchers such as David Hanson [107] and Hiroshi Ishiguro [108] continue to develop remarkably lifelike robots, considerable evidence (both anecdotal and research based) exists which suggests that such close similarity should be avoided. A well known motivation for ensuring robots avoid becoming too humanlike is to avoid the 'Uncanny Valley' effect(Fig. 2.13). This phenomenon was first described by Mori [109] in the 1970s to serve as a guide to assist designers in building humanoid robots. Mori predicts that when a human observer encounters a robot, their comfort level will depend closely on the human likeness the agent possesses. As the robot agent becomes increasingly human-like, the comfort level (or familiarity) of a human observer grows in proportion. However there reaches a point where the agent becomes too human-like at which its familiarity begins to rapidly decrease. At this point the agent is said to have fallen into the uncanny valley. Only once the agent's likeness becomes indistinguishable from a human will the observer's comfort level rise again. Mori's uncanny valley provides a qualitative upper limit to how human-like humanoid robots should be, both in movement and form. Furthermore it promotes the philosophy of deliberately factoring the aesthetic of the robot into the design process for the purpose of improving human usability.



(a)



(b)

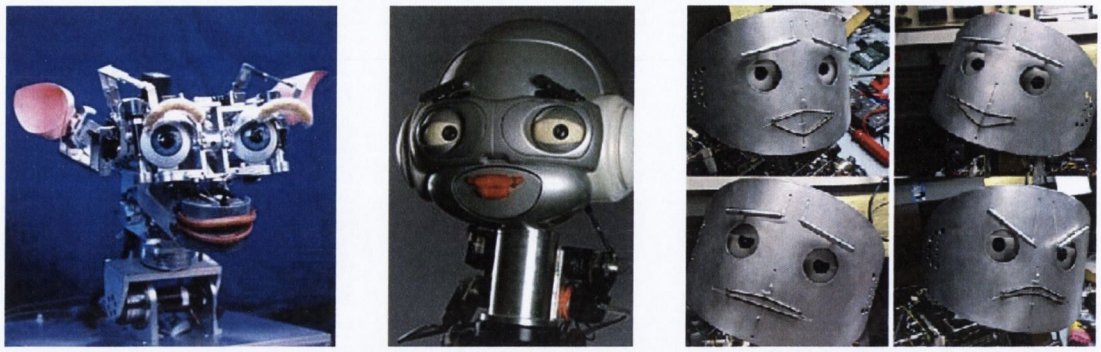


(c)

Figure 2.13: Lifelike robots and the uncanny valley (a) graph describing Mori's uncanny valley (b) Philip K. Dick robot by Hanson robotics (c) Gemenoid F robot by Hiroshi Ishiguro

Other studies which suggest that optimally designed robotic interfaces should possess basic anthropomorphic features/behaviours but retain defined robot features include the nursebot *Pearl* [110] (Fig. 2.14b), *Sparky* [111] (Fig. 2.14c), *Mask-Bot* [112] and *Kismet* [113] (Fig. 2.14a).

An important design principle that arises from research in social robotics is that the complexity of robotic interfaces should loosely map to the overall complexity of the robot's functionality [114]. In other words, since the type of social interface serves as a basis for human users to establish their expectation of the robots intelligence (i.e. what the robot can/can't do), care should be taken to ensure that the expectations formed will align closely with the robot's actual capabilities. Since robots do not currently come close to



(a) (b) (c)

Figure 2.14: Robots retaining basic anthropomorphic social interfaces (a) Kismet (b) Pearl (c) Sparky

matching human levels of intelligence, adherence with such a principle will inherently lead the designer to make a robot that both avoids the uncanny valley and does not intentionally raise user expectation to unreasonably high levels.

2.4.1.2 Review of ISO 13482

As the usage of robots becomes pervasive and as their operation becomes increasingly autonomous, both ethical and safety issues become increasingly relevant. With the service robot industry still in its infancy, few internationally accepted design/usage standards currently exist to guide the design of personal robots. ISO 13482:2014 (Robots and Robotic Devices – Safety Requirements for Personal Care Robots) [115] is the most important document of this type presently available and stipulates that personal service robots manufactured after its publication date must adhere with its design requirements. Unlike ISO 10218:2011 which is targeted at industrial robots, ISO 13482:2014 applies only to personal care service robots. More specifically ISO 13482 is aimed at three categories of service robot (1) mobile servant robot (2) physical assistant robot (3) person carrying robot. In order to achieve ISO certification, developers must show that their robots meet specific standards in mechanical design, control, environmental perception and procedural behaviour as well as adherence with other relevant ISO standards such as ISO 4414 (Pneumatic Fluid Power), ISO 2631 (Mechanical vibration and shock) and ISO 15534 (Ergonomic design for the safety of machinery). Before the ISO standard can be awarded, it stipulates that a detailed risk assessment must be carried out. Furthermore

where potential hazards and hazardous situations are identified, a risk reduction process must be undertaken and improvements which address the issues implemented. Upon completion of the risk reduction process, validation and verification can be made through several methods including visual/acoustic inspection, practical testing, observation during operation and examination of the relevant documents. It is important to observe that owing to the extensive scope of the standard, only robots that are near market ready are likely to develop prototypes/embodiments that adhere fully with the ISO's requirements.

2.4.2 Operating in Human Spaces: The Built Environment

In order to design robots to successfully integrate into civilian life, it is preferable that they can adapt to environments that are optimised for use by human beings. Although human environments are generally flat and reasonably spacious, they also possess architectural barriers that robots must overcome. Traversing stairways, passing between rooms and navigating cluttered environments represent some of the these challenges.

While designing robots capable of exploiting human-centred environments, two factors should be fundamentally considered in the design; ergonomics/human factors and building regulations. In the first instance, the robot should be designed such that it possesses the task space and locomotive ability to do useful tasks in human-centred spaces. Human factors has been the subject of much study in recent decades and many widely accepted conventions now exist to assist architects/builders in designing everyday human environments, both domestic and industrial. However despite the somewhat idealised building guidelines which have emerged from the study of human factors, there is no legal obligation for architects and builders to adhere to these recommendations. It is for these reasons that building regulations, legal documents which set out the design requirements of architectural features, should also guide the design process.

2.4.2.1 Human Factors and Building Regulations

Its important that detailed consideration is given to the relationship between products and the people that use them. Therefore the study of human factors, the scientific discipline concerned with understanding this relationship, plays an increasingly important role in

the present age. As service robots are required to operate in human environments, its important that their designs are influenced by usability and human factors requirements. Through the consideration of human factors in the design of service robots, it should be possible to develop robots that are better capable of overcoming architectural barriers which currently inhibit access to machines and certain demographics of people. Examples of these barriers may include: stairways, doors, floor surfaces, curbs, accessibility of electrical fixtures, control panels and furniture.

Widely recognised as a leading text on the relationship between human anthropometry and the built environment, 'The Measure of Man and Woman: Human Factors in Design' [116] provides an encyclopaedic reference on all of the essential measurements of the human body and its relationship to the human environment. Unless otherwise referenced, all cited ergonomic design recommendations discussed in the proceeding section has been taken from this book.

Official building regulations tend to differ from country to country. Since 2010, countries in the European Union are required to integrate the Eurocodes [117], a set of rules drawn up in an effort to standardise structural design within the EU, with existing building regulations not covered by these rules.

The United Kingdom were the first country in the world to adopt standardised building regulations after the 'Great Fire' of London. The UK Building Regulations contains thirteen sections each pertaining to a particular aspect of architectural design. Each document in the regulations cover both residential and industrial buildings however provisions detail important differences in the architectural/building requirements. In addition to adopting several provisions from the Eurocodes, the Irish Building regulations (falling under the jurisdiction of the Department of the Environment, Community and Local Government) are detailed across ten separate documents, many aspects of which almost directly mirroring corresponding articles in the UK regulations.

Arguably the largest unified effort in standardising building regulations can be observed in the USA. In 1997 the International Code Council (ICC), an organisation combining the efforts of three regional model code groups, began publication of the International Code series (I-Codes). The I-Codes are a complete set of comprehensive, coordinated building

safety and fire prevention codes. The regulations most relevant to the ergonomic design of civilian spaces in this series are the International Building Code (IBC) [118] and International Residential Code 2012 (IRC) [119]. Unlike the UK regulatory documents which address the design of commercial/public and residential buildings in the same document, the ICC separate their respecting requirements into different listings.
Drawing from the UK Building Regulations, the IBC, the IRC and design guidelines set out in [116], the following subsections describe some of the most significant environmental constraints and design challenges that must be overcome in order to develop service robots that can operate robustly within civilian environments.

Doors and Corridors

The dimensions of a door will depend on a number of factors including its function (interior/exterior) and its accessibility requirements. It is recommended that for standard interior doors, they should have have a height of 2030mm and a width of 762-813mm (813mm being the minimum recommended door width for wheelchair access). For exterior doors, a width of 915mm is recommended and a height of 2030mm is suggested. The suggested width for wheelchair access is 915mm [116].
According the IBC, the minimum height of a 'means of egress' doorway is 2032mm and the minimum width is 813mm making it adhere closely with the proposed ergonomic requirements. Additionally thresholds at doorways in dwellings should not exceed 19.1mm above the floor for sliding doors and should not exceed 38.2mm for other doors. When locating doors in series, a space of 1219mm plus the width of the door swinging into the space must be accounted for. Additionally doors located in series should either swing in the same direction or away from the space between the doors. Both the IBC and the IRC further stipulate that landings must be located on both sides of a doorway and that these landings must be at least as wide as the doorway and have a length of at least 914mm for residential buildings and 1118mm for other buildings. The IBC requires that for residential corridors or in buildings where the occupancy is less than fifty, a minimum width of 914.4mm should be observed. For most other buildings with occupancies greater than fifty, a width of 1117mm should be observed. In residential buildings, the IRC states that the minimum height of a 'means of egress ' doorway is 1981mm and the minimum

width is 813mm.

The relevant building regulations in the UK pertaining to doors and corridors is found in 'Document M: Access to and Use of Buildings' [120]. For non-residential buildings, the requirements of the door size depend on (1) whether the building is new or old (2) if the door is internal/external (3) the corridor width and angle of an approach from an access route. For new buildings, doors are required to be wider than for existing buildings; 50mm larger for interior doors and 125mm larger for exterior doors. Doors are also required to be wider if they are located at 90 degrees to an access route. For manual doors fitted with a latch, the door opening mechanism must be operable with one hand using a closed fist (i.e. a door handle). Corridors in non-residential buildings must have an unobstructed width of of at least 1200mm. In corridors where the width is less than 1200mm, they are required to have passing places (at least 1800mm long and 1800mm wide) at reasonable intervals to facilitate the passing of wheelchairs. In the case of residential buildings, exterior doors must have a width of at least 775mm. Additionally the width of internal doors will depend on both the width of the corridor and the angle of approach. Doors located at angles to narrow corridors will require wider frames than those on wider corridors or with head-on access.

Stairways and Landings

Stairways present a significant risk to safety in all buildings. Statistics show that falling represents the most common type of domestic accident (especially high amongst elderly populations) [121] and stairways remain the most common location that falls occur [122]. However despite convincing causal evidence, developing accurate statistical relationships between domestic accidents and their root cause (low lighting, poor ergonomics etc.) is difficult due to the insufficient environmental information typically reported in accident statistics. While for many years, few scientifically rigorous studies had succeeded in finding correlations between stair geometry and the likelihood of accidents [123], several studies have since shown that stair geometry plays a considerable role in the causation of accidents [124] [125] [126]. These studies have strongly suggested that accidents are more common on stairways that have a variability in riser/going lengths and on stairways with

short goings. It is interesting to note that residential environments, where the building regulations are less strict, account for significantly more falls than in utility buildings [127].

It is recommended in a [116] that ergonomically designed stairs should adhere with the guidelines set out in the design guide published by the U.S. Department of Housing and Urban Development, 1972 [128]. In addition to setting upper and lower limits on the riser/going dimensions, the report provides quantitative guidelines for stair variability, places size limits on open risers, stipulates that a landing should be located after eight risers and that 16 risers should not be exceeded in a straight run. Despite considerable potential for slope variability, it also states that an ergonomically designed stairways should possess a rise slope of between 30-35 degrees.

Both the IBC and the IRC provide considerable coverage to stairway requirements. The IRB bans the use of open risers however the IRC makes an allowance for them as long as they don't pose a trap hazard. The IBC stipulates that the maximum rise on a staircase should be 7 inches (177mm) while the minimum going should be 11 inches (279mm) (widely known as the '7-11' standard). This requirement is less stringent in the IRC stipulating that risers should be smaller than 196mm and goings longer than 25.4mm. Both the IBC and IRC require that landings are present before and after a flight of stairs and their length should be at least that of the width of the staircase. Additionally both codes require that a flight of stairs not have a vertical rise larger than 3.65m between floor levels or landings.

The regulations pertaining to stairways in the UK Building Regulations is set out in 'Document K: Protection from Falling, Collision and Impact' [129]. It is observed from this document that stairways in the UK are subject to substantially less strict regulations regarding stair geometry. For general access stairs (i.e. stairs intended for all users of a building on a day-to-day basis), the maximum rise is 170mm and the minimum going is 250mm. For residential buildings, these requirements are relaxed further to a maximum rise of 220mm and a minimum going of 220mm. It is noted however that a provision to this regulation is that for residential buildings the maximum slope/pitch is restricted to 42 degrees. In relation to buildings other than dwellings, Document K prohibits the use of single risers and states that landing should be located after no more than twelve risers.

Additionally Document K states that landings must be located before and after a flight of stairs and that the length of the landing should be at least that of the width of the staircase. Similarly if stairs have more than 36 risers in consecutive flights, at least one change in direction between flights is needed. Like the ICC codes, the UK regulations allows the use of open risers in residences but forbids their use elsewhere.

Fittings, Fixtures and Furniture

Architectural features are not the only aspects of the built environment that present challenges to service robots. As human environments are functional spaces containing furniture and other obstacles that are used by people, it is important that robots are designed such that they too can effectively utilise the space. As men, women and children come in many different shapes and sizes, the variability of furniture and other such items is extremely large. Studies in human factors have led to the standardisation in the size of many commonly encountered household objects. Some important standards include; the standard dining table is 711mm high, kitchen counters are 914mm high and 610mm deep and the highest shelf in a kitchen cabinet should be no higher than 1829mm from the ground. For offices or computer stations, the table height typically ranges from 584-789mm to account for the large variance in body sizes. Additionally bedroom furniture tends to be smaller than 762mm. Human factors also recommends the use of carpets to minimise slippage. Where rugs are used, they should be located on a non-skid material underlay where possible.

In the IBC and IRC relatively little coverage is given to the positioning of fittings and fixtures. However in Document M of the UK Building Code, significant coverage is provided. In non-residential buildings the following regulations are in place:

- wall mounted sockets, telephone points and TV sockets are located between 400mm and 1000mm above the floor (with a preference for the lower end of the range)
- switches for permanently wired applications are located between 400mm and 1200mm above the floor

- all switches/controls that require precise hand movements are located between 750mm and 1200mm above the floor
- simple push button controls that require limited dexterity are not more than 1200mm above the floor
- controls that need close vision are located between 1200mm and 1400mm above the floor so that readings may be taken by a person sitting or standing
- light switches for use by the general public should have large push pads and align horizontally with door handles within the range 900mm to 1100mm above floor level

In residential buildings, the regulations simply state that switches and socket outlets for lighting and other equipment in habitable rooms are located appropriate heights (between 450mm and 1200mm) from the floor level

2.5 Review of Existing Service Robot Technology

It is evident from the literature that the design of several notable robots has been closely influenced by human factors and the requirement for multi-functional use. In this section several such designs and their associated embodiments are discussed.

2.5.1 Honda Asimo

Since the mid-1990s, Honda have been a driving force behind the development of personal assistant service robots. Starting with the *P-Series* and later the *Asimo* robots, Honda have developed a large number of prototype bipedal platforms capable of performing a wide range of tasks in human centred environments. The most recent *Asimo* platform (Fig. 2.15a) has demonstrated the ability to walk on an uneven surface and perform tasks including dynamic stair-climbing, opening/closing a lid on a bottle, serving a table, pouring a drink as well as advanced object recognition and an increased range of autonomous capabilities [130]. Studies of human factors have played a major role in influencing the design of the robot. *Asimo's* height (1200mm for the 2000 version and 1300mm for the

2005/2011/2014 versions) was decided upon as it was considered the minimal height necessary for a humanoid robot to fully exploit human living spaces. *Asimo* was designed such that it utilize on-board power and had a task space that would enable to to operate light switches and door knobs, work at a table and be at eye level when a person who is seated [131]. *Asimo's* size was also influenced by the requirement to climb stairs - specifically stairs with a maximum rise height of 180mm [43]. Additionally *Asimo's* social interface has been refined over successive iterations to simultaneously guide user expectations, avoid the 'Uncanny Valley' and provide continuous feedback to users.

Despite its many successes, *Asimo* possesses several limitations which significantly affects its practical performance. Despite its large configuration space, *Asimo's* range of movement is restricted meaning that it has yet to demonstrate the ability of picking up an object from the ground. As *Asimo* is a legged bipedal robot, it is inherently unstable and requires continuous power to remain upright. This dynamic stability requirement is a major drain on battery and results in a low operational life of approximately one hour [132]. Despite some sophisticated public demonstrations, in recent years Honda has come under criticism for being unable to equip *Asimo* with the levels of behavioural diversity needed to perform in more unstructured environments where increased levels of autonomy are required [133]. *Asimo* has traditionally been actuated using DC servo motors coupled with non-backdrivable harmonic gearboxes. While recent efforts have been made to equip *Asimo* with greater levels of compliance [134], *Asimo* retains a conventional harmonic drive actuation scheme. Despite the fact that *Asimo* can climb stairs, it lacks the ability to sense (and therefore adapt to) unknown stairways with unknown dimensions and depends on preprogrammed knowledge.

2.5.2 Care-O-Bot III

Unlike *Asimo* which was designed using a bottom-up bio-inspired philosophy, the *Care-O-Bot III* (Fig. 2.15b) is a mobile servant robot which was developed using a top-down, functional design approach. The *Care-O-Bot* is a statically stable platform which achieves omni-directional locomotion through the co-ordination of four actively driven, steerable

wheels. This choice of locomotion was chosen to improve the robot's manoeuvrability in cluttered human-centred environments as well as to provide increased usability in human-robot interaction [23]. The robot possesses a lightweight 7 DOF manipulator with an additional 7 DOF gripper that has integrated tactile sensors. The length of this arm was purposefully extended to enable it to pick up objects from the ground as well as reach a typical kitchen shelf [135]. To eliminate the need for the robot to directly engage in object handovers with people, an actively controllable tray was integrated into the robot's morphology. To further improve usability, the robot was designed to possesses two simultaneously active orientations. The front side, known as the 'working side', faces away from the user and is the side where manipulation takes place. The opposing side, known as the 'serving side' is softer appearance and was designed to remove any inhibitions that a human user may have in using a personal service robot. A 50Ahr Li-Ion battery, a full on-board sensor/computer suite and a wide range of advanced software tools and functionalities further increases the robots practical capability. *Care-O-Bot* possesses many impressive built-in features including grasp planning, collision avoidance, 2D-SLAM and object recognition.

Recall from section section 2.4.1.1 that an easily identifiable front facing orientation plays an important role in establishing the user's confidence in using the robot [100]. While the *Care-O-Bot* possesses an easily identifiable front-facing direction (i.e. the 'working side'), the pseudo omni-directional configuration enables it to assume forward motion from any orientation. Therefore it is anticipated that human users may find it somewhat unsettling when the robot with the 'working side' facing forward. With a spatial footprint of 600x600mm and a mass of 180kg, the robot is prohibitively large for practical operation in many (non-wheelchair accessible) human-centred environments. Additionally owing to its morphology and mass, it's not capable of overcoming architectural barriers such a steps/stairways or crevices. The issue of compliance is also not addressed in the robot's design. Despite sophisticated sensing ability, the potential hazard posed by the possible contact from the large reach of a large, non-compliant industrial type arm poses a significant concern. While the robot can provide continuous feedback through a graphical display, the complexity of interaction that is possible is limited when compared with robots that

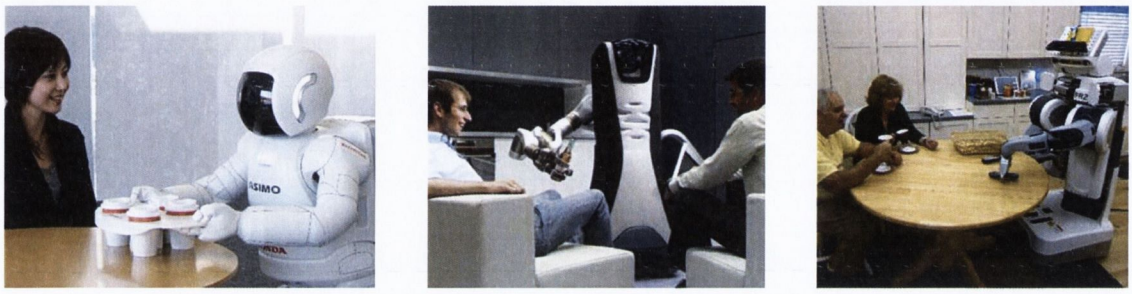
possess more anthropomorphic interfaces.

2.5.3 PR-2

Another project that has successfully succeeded in incorporating human factors into the development of their robot is the *PR-2*(Fig. 2.15c). The *PR-2* (Personal Robot 2) is the second in a series of service robots developed at Willow Garage with the ambition of bridging the gap between the tasks that robots and people can undertake. The *PR-2* was designed such that it could operate in wheelchair accessible spaces and possess the capability of performing a wide range of human tasks including opening doors, serving drinks and performing cleaning tasks [136]. The *PR-2's* design focuses on ensuring a high level of integration between mobility, manipulation and software. It possesses an omni-directional base, two 8 DOF arms and a highly advanced suite of computers and sensors [24]. Most impressively, the *PR-2* was the first robot of such high complexity to receive full ROS (Robot Operating System) support. Through utilisation of the development tools made available through ROS integration [10] (advanced vision libraries, 3D state visualisation (RViz), advanced dynamic simulation (Gazebo), advanced trajectory and grasp planning (MoveIt) to name a few), it is been made possible to achieve impressive performance capabilities in perception, locomotion and manipulation.
Mechanically the *PR-2* is statically stable and carries a 1.3 kWh Li-Ion battery pack giving an operational life of approximately two hours. Its arms have low inertia and are fully back-drivable meaning that it poses a low risk of causing damage in the event of an collision. Despite a price tag of approximately $400k, the *PR-2* remains arguably the most successful development platform of its type and despite its age, it remains one of the most advanced platforms in the field. It is noted that while the *PR-2* does not possess a dedicated social interface to provide continuous feedback, its design remains somewhat anthropomorphic and its head unit serves to provide both a focal point for interaction and a clear indication of the front facing direction of the robot.

Like the *Care-O-Bot*, the spatial footprint of the *PR-2* (668x668mm) makes it impractical for practical operation in buildings that are not wheelchair accessible. Additionally since

it runs on a conventional steered base, it is not capable of traversing over obstacles or climbing stairs and while it has compliant arms. Furthermore while its heavy weight (>100kg) creates a potential usability hazard. The complexity of user interaction that is possible with such a basic interface inherently inhibits communication between the robot and human user. Like the *Care-O-Bot*, the front-facing direction may not always be the direction of forward motion since the steerable base can be adapted to travel in any direction.



(a) (b) (c)

Figure 2.15: Several state-of-the-art personal service robot research platforms (a) Honda Asimo serving coffee (b) Care-O-Bot serving a drink (c) Willow Garage PR-2 attending a table

2.5.4 Other Robots

One of the first examples of successfully applying human factors to the design of service robots was the *Cero* robot project [100]. The platform used for this research was a standard *Nomadic Scout II* wheeled robot customised to also possess a small, interactive anthropomorphic figurine mounted on top (Fig. 2.16a). Through user interviews, task analysis and extensive user testing conducted over long periods of time, researchers identified several interesting psychological requirements of service robots. Insights including the need for providing continuous feedback, the importance of a clearly identifiable front face and the benefit of a pleasing overall aesthetic were all generated by this work.

Another robot developed using a user-centred design approach was the *Movaid* robot [137]. A central tenant of *Movaid's* design is that service robots should be influenced by human social requirements. Reinforcing the lessons learned through the *Cero* project,

the researchers found (through extensive interviews and field testing) that robots should possess a pleasing non-threatening appearance, smooth predictable movement and the user interface should be closely coupled with the end user. A final interesting aspect of this work is that anthropomorphic features were found to not only make the robot morphologically better suited for operation in human-centred spaces but additionally it increased the predictability of the robot's movement making its behaviour more acceptable to human users.

Following from *Movaid*, the *Robutler* robot developed at DLR also initiated some important insights into the design of personal service robots. It was one of the first mobile service robots to incorporate manipulation-driven safety features into the design. This was achieved by adopting a lightweight anthropomorphic arm and gripper. Additionally it succeeded in demonstrating impressive perception and tactile manipulation including the ability to prepare drinks on a table [138].

ARMAR III, developed at the University of Karlsruhe was among the first service robots to integrate a sophisticated anthropomorphic torso and head with a more conventional omni-directional base [139] (Fig. 2.16b). With 43 DOF, *ARMAR III* possessed the potential for high behavioural diversity. Through its use of an artificial tactile sensing skin and integration of force/torque sensors in the wrist, it was among the first service robots to consider the dynamic physical interactions between people and robots. A holonomic, omni-directional base was integrated to improve mobility and to complement a sophisticated bio-inspired control architecture which decomposed into three levels responsible for task planning, synchronization & coordination and task execution respectively.

The *House Exploring Robotic Butler (HERB)* project explored how a distributed system architecture could be leveraged to provide robots with the ability to achieve human-like levels of performance in household manipulation tasks [140] (Fig. 2.16d). Consisting of a *Segway RMP 200* base [12] and a *Barrett* arm, the robot connected wireless to six multi-core computers located throughout the environment. Enabled through almost unlimited computational resources, *HERB* was among the first service-type robots to attempt to

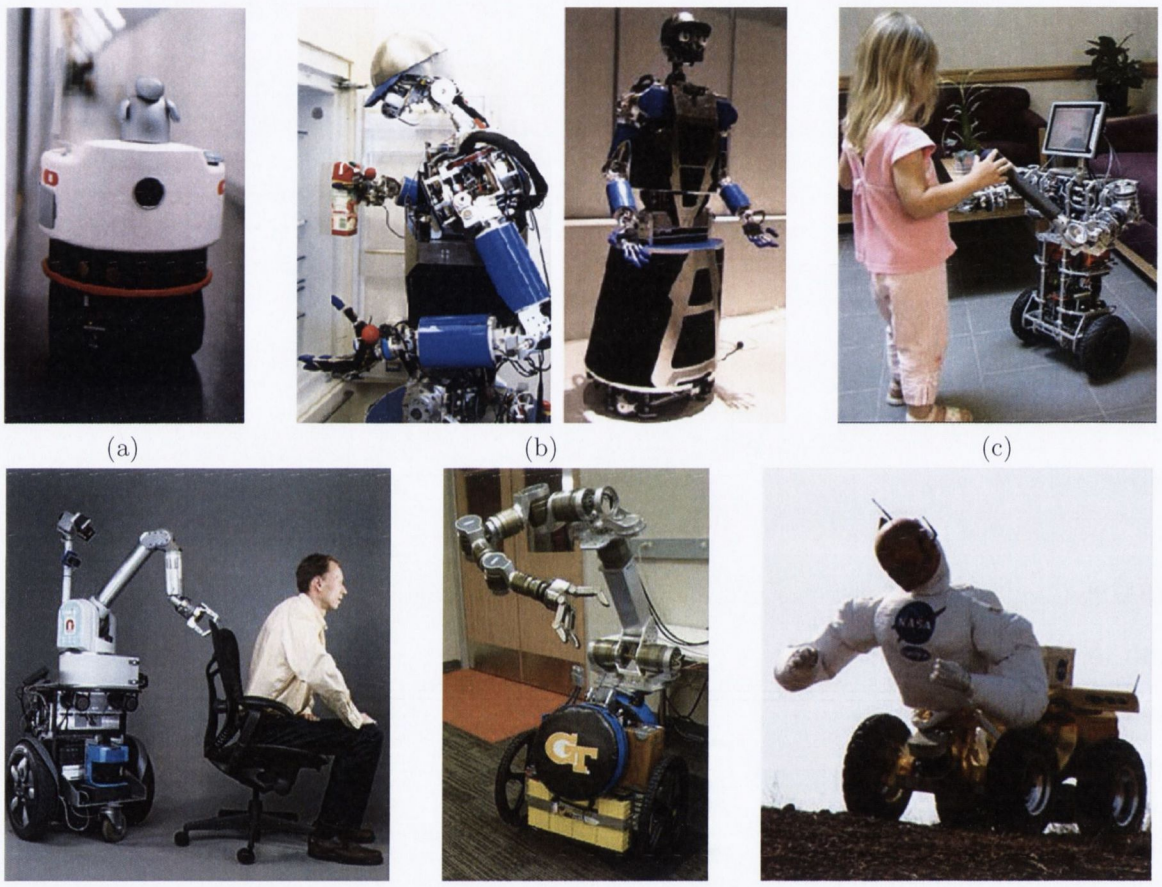
perform tasks in highly cluttered environments. The robot demonstrated the ability to load a dishwasher, manipulate objects, perform handover operations and to locate an object in a room.

Like *Asimo*, both *Golem Krang* [30](Fig. 2.16e) and the *uBot* robot [32] [33] (Fig. 2.16c) are statically unstable robots. While *Asimo* uses legs for locomotion, both *Golem Krang* and *uBot* are self-balancing wheeled platforms. *Golem Krang* consists of a two-wheeled self-balancing base combined with a powerful (non-compliant) robot manipulator. The design of *Golem-Krang* was influenced by ADA design requirements including minimum door and hall widths, minimum floor co-efficients of friction and maximum ramp angles. Unlike most other statically unstable self-balancing platforms, *Golem-Krang* can augment its arm to provide additional balance support thus enabling the robot to exist in a statically stable rest state.

With two anthropomorphic arms, the *uBot* takes a considerably more anthropomorphic form than *Golem Krang*. The *uBot* provides a good example of practical, embodied design as the morphology inherits a 'whole body' approach to both mobility and manipulation [141]. Like *Golem Krang*, it can use its arms to help balance and to exist in low energy states when required. However when more controlled locomotion is required, is capable of adopting a four-wheeled steered configuration where wheels attached to the arms double as steering mechanisms. Additionally another means of locomotion was made possible through adoption of a novel 'knuckle walking gait'.

The final robot of note developed to operate in human centred environments is NASA's *Centaur* [22](Fig. 2.16f). Similar in form to *Workpartner* [142], *Centaur* possesses a humanoid type torso mounted atop a statically stable four-wheeled base. The NASA *Centaur* (so called due to its close similarity with the mythical creature) combines the sophisticated upper body dexterity of the *Robonaut* platform [143] with the ruggedness of an off-road four wheeled base. While this robot does not meet the ergonomic requirements for operation in buildings, it possesses several interesting human-centred features including the manual dexterity to use tools and equipment designed for people, an an-

thropomorphic upper body which is shielded from hazardous contaminants such as dust and water and a highly effective control interface which enables complex actions to be communicated from astronautics located at a distance from the robot.



(a) (b) (c)

(d) (e) (f)

Figure 2.16: Wheeled service robots designed for civilian environments (a) Cero mounted on top of a Nomad Scout (b) ARMAR-III (c) uBot (d) Home Exploring Robotic Butler (HERB) (e) Golem Krang (f) NASA Centaur platform

2.5.5 Robot Stair-Climbing

If service robots are to perform tasks to assist people, it's important that they possess the ability to operate within the same environments as the people they are helping. As stairways are prevalent in virtually all buildings, its important that service robots are capable of ascending and descending them safely when required. This subsection provides some background on robot stair-climbing, and how stair-climbing has been achieved us-

ing various morphological embodiments. While many different morphologies have been developed and adopted to perform this task, the majority remain practically ill-suited for use in indoor civilian environments - either lacking the necessary task space or not possessing the required on-board control/stability/power resources for multi-purpose use. In the preceding sections, unless specifically pointed out, all the research presented (both practical and simulation) has been carried out on stairways typical of public buildings, not residential buildings where the regulations permit significantly more demanding stair geometries.

2.5.5.1 Tracked/Wheeled Solutions

Tracked Systems

Owing to their high mechanical and control simplicity, robots with tracks/crawlers offer the simplest and most reliable means of ascending and descending stairs. As tracked vehicles possess large ground contact areas, they can maintain continuous contact with the stair nosings while retaining static stability.

To increase the environmental adaptability of conventional wheelchairs, several efforts have been made to utilise tracks on manned mobility devices including the *Action Trackchair* [144], *TankChair* [145] (Fig. 2.17a) and *Unimo* wheelchair by Nano-Optics Energy [146](Fig. 2.17b).



(a) (b)

Figure 2.17: Stair-climbing tracked wheelchairs (a) Tankchair mobility platform (b) Unimo wheelchair by Nano Optonics Energy

An excellent overview of the challenges and issues surrounding stair-climbing for tracked vehicles is given by Martins and Newman [147] and Tao et al. [148]. Some important

findings of their research which has since influenced the design of tracked stair-climbing robots include:

- As human tele-operators lack a natural sense of the robot's equilibrium, controlling stair-climbing remotely is an error prone and highly hazardous process, even for trained professionals.
- Maintaining a straight heading direction during stair-climbing is crucial as large steering corrections are very difficult to make on stairs due to the effects of gravity induced drift. This issue was later expanded by Yoneda [149] who observed that the grousers typically provide poor grip at low incidence angles.
- In the absence of specially designed damping mechanisms, stair-climbing can produce large disturbances especially when mounting the landing at the end of the climb.
- The height of the drive axis of the leading track must be greater than that of the stair to be climbed for stair-climbing to be possible.
- Due to the robots high inertia, slip during ascent can be a problem.

While relatively little research has focused on improving how human operators can better improve controllability during stair-climbing, much effort has concentrated on the design of specialised tracked robots with improved stair-climbing abilities. An interesting method of improving the controllability of existing designs involves retrofitting a conventional tracked vehicle with powder filled bags along its tracks. In studies by Yoneda and Hirose [149](Fig. 2.18f), such modifications showed significantly improved handling and reduced vibration during stair-climbing.

Another common way to reduce disturbances and increase adaptability is to add additional articulated tracked arms. Not only does the addition of more arms further improve the robots ability to climb stairs (i.e. enable soft transitions at landings), but its improved reconfigurability enables it to vary its footprint and ground-contact area. These latter traits improve the overall environmental adaptability of the system. This concept has been integrated in the *Urban II* ('Urbie') robot, a joint effort from several research labs [150]

and *PackBot* developed by iRobot [151] (Fig. 2.18a). Further studies which demonstrate the performance improvements that can be attributed to this design are found in [152] [153] [154]. Taking this design concept a step further, both *Silver* [155] (Fig. 2.18b) and *Aladdin* [156](Fig. 2.18d) boast further improved performance levels through utilisation of articulated tracked arms on both extremes of the robot.

Another notable class of tracked designs which show improved performance over conventional tracked mechanisms involve the dynamic reconfiguration of the tracks during operation. The *Linkage Mechanism Actuator (LMA)* robot uses an actuated linage with a tensioner wheel to augment the shape of a track [157] (Fig. 2.18e). This design facilitates a dynamically variable wheelbase that provides the system with levels of terrain adaptability comparable with designs that utilise additional articulated tracked arms.

Some systems have sought to develop hybrid wheel/tracked systems which combine the benefits of wheeled robots (energy efficiency, low vibration/noise etc.) with the benefits of tracked systems (stair-climbing ability, ability to navigate on soft surfaces etc.). The *Andros VI* robot combines a conventional skid-steered wheeled chassis with a tracked mechanism. At a cost of high weight($>$ 150kg), poor energy efficiency and large size, the Andros VI possesses extremely rugged locomotion capabilities and was among the first robots to successfully demonstrate controlled stair-climbing ability [147].

Another wheel-track hybrid which has successfully demonstrated stair-climbing is the *VIPER (Versatile Intelligent Portable Elbit Robot)* system develop by Elbeit systems [158](Fig. 2.18g). This robot utilises the 'Galileo wheel' [159] [160], a clever mechanism which enables a conventional wheel to transform into a tracked mechanism. This feat is achieved through the utilisation of a flexible elastic track belt and a series of actuated pulleys and linkages residing within the wheel's structure.

Yet another effective hybrid wheel-tracked approach involves the installation of active tracked mechanisms in conjunction with a live, independent rotary drive axles. In simpler terms, this design involves using unsymmetrical tracked mechanisms in place of wheels in a conventional multi-wheeled, skid steered vehicle. One such system of note is the *MAC robot (Multi-Active Crawler)* [161](Fig. 2.18c).

A final tracked robot design which has demonstrated stairclimbing involves using an

articulated linkage of small tracked robots [162] [163]. While these robots may possess high levels of modularity and mechanical simplicity in comparison to equivalent designs, their morphology inherently makes them very long which in turn renders them ill suited for indoor, human centred environments.

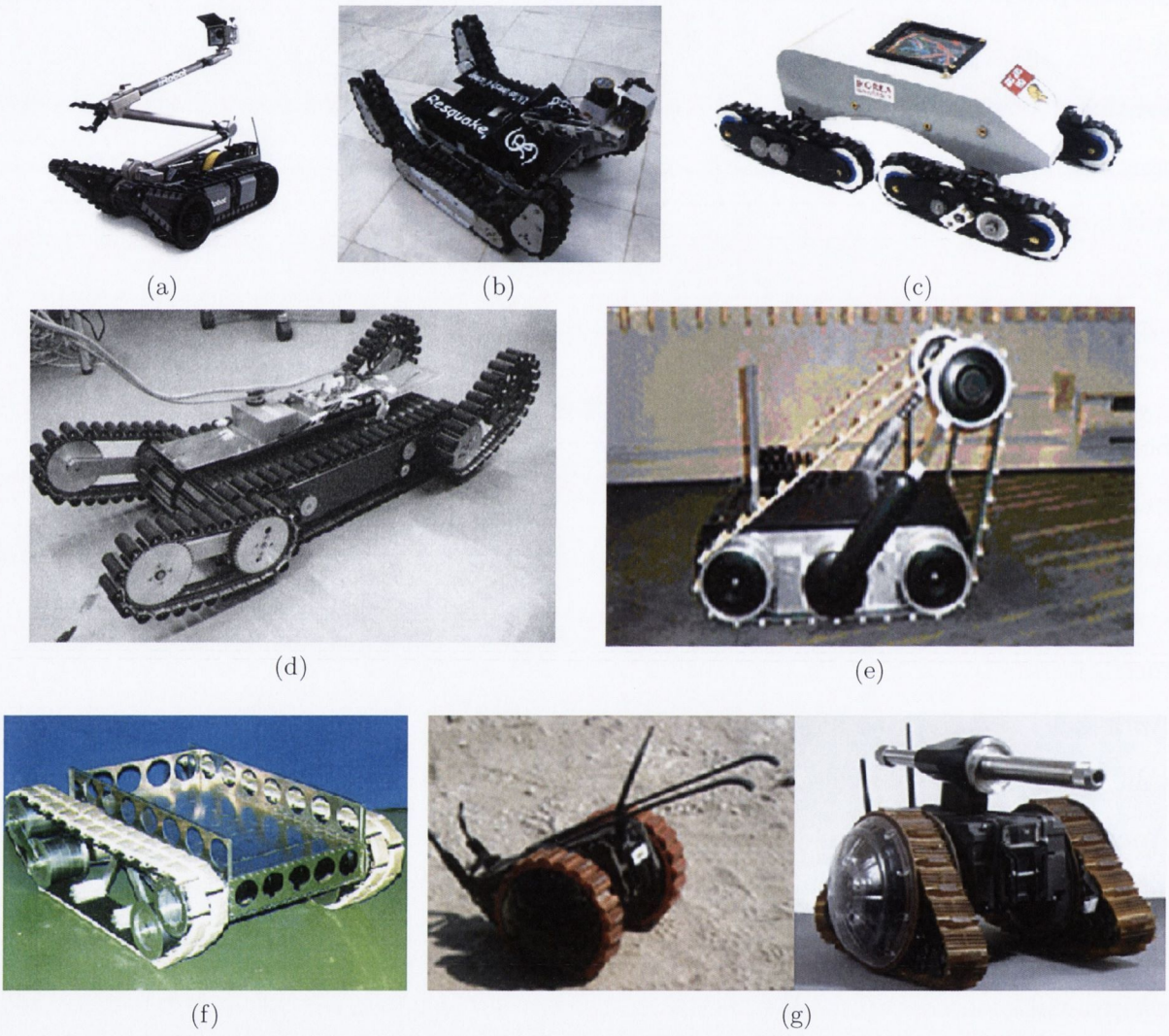


Figure 2.18: Stair-climbing tracked robots (a) PackBot by iRobot (b) double articulated Silver robot (c) MACbot robot (d) Double articulated Aladdin robot (e) LMA robot (f) powder-filled track-belt configuration by Yoneda et al. (g) Reconfigurable VIPeR robot by Elbit systems

Wheeled Systems

Despite their limitations in terrain adaptability, several wheeled morphologies exist which possess the ability to climb stairs. Like tracked vehicles, most wheeled vehicles capable of

such behaviour possess long wheelbases in order to ensure continuous contact with stair nosings.

The *Octal-Wheel* robot is a two-axle wheeled robot. Each axle has four driven wheels - two on either side and each offset symmetrically from the centre of the axle. This morphology enables high levels of environmental adaptability and high traction at the cost of a very long wheelbase, poor manoeuvrability and low energy efficiency [164]. In a design concept similar to that of the *Octal-Wheel*, the *Loper* robot has two axles with three offset wheels on either side of each axle. Arranged symmetrically about the axle in a tripod, this formation provides the robot with high levels of adaptability and traction during locomotion over stairs [165]. An almost identical concept has also been integrated successfully on the stair-climbing mobility device *Wheelchair.q* [166].

The *ROBHA-6W* is a six wheeled vehicle designed to passively adapt to rough terrain. This is achieved through the design of a mechanism which approximates that of a 1 DOF four-bar linkage and which enables the vehicle to passively adapt to uneven ground surfaces [167]. It is through this high level of terrain adaptability that stair-climbing becomes possible although the authors note that the vehicle's stair-climbing performance is correlated with the geometry of the vehicle's design.

Popularised by NASA in its adoption in the *Sojourner* and *Curiosity* rovers (Fig. 2.19a), the 'Rocker-Bogey' mechanism provides a somewhat similar means of achieving stair-climbing. From the findings of a kinematic analysis, Choi et al were able to find the geometric requirements of the linkages needed to successfully climb stairs of a predetermined size [168].

Another six wheeled vehicle capable of stair-climbing is the *HELIOS-V* robot, developed by Shigeo Hirose. Using an articulated mechanism with low pressure pneumatic tires, *HELIOS-V* uses the dynamics of its mass and large wheelbase to climb stairs in a manner comparable with conventional tracked vehicles [169](Fig. 2.20e). While it is capable of climbing stairs, its relatively poor performance in comparison with other systems and its long wheelbase limit its practicality for use in human centric environments. The *Gremlin* robotic system is a distributed set of small wheeled robots that achieves stair-climbing by daisy-chaining themselves together and coordinating a sequence of hoisting actions using

dedicated on-board lifting mechanisms [170].



(a) (b) (c)

Figure 2.19: Wheeled stair-climbing robots (a) NASA Soujourner with rocker-bogey mechanism (b) Helios-V 6-wheeled robot (c) iBot mobility platform

Legged Systems

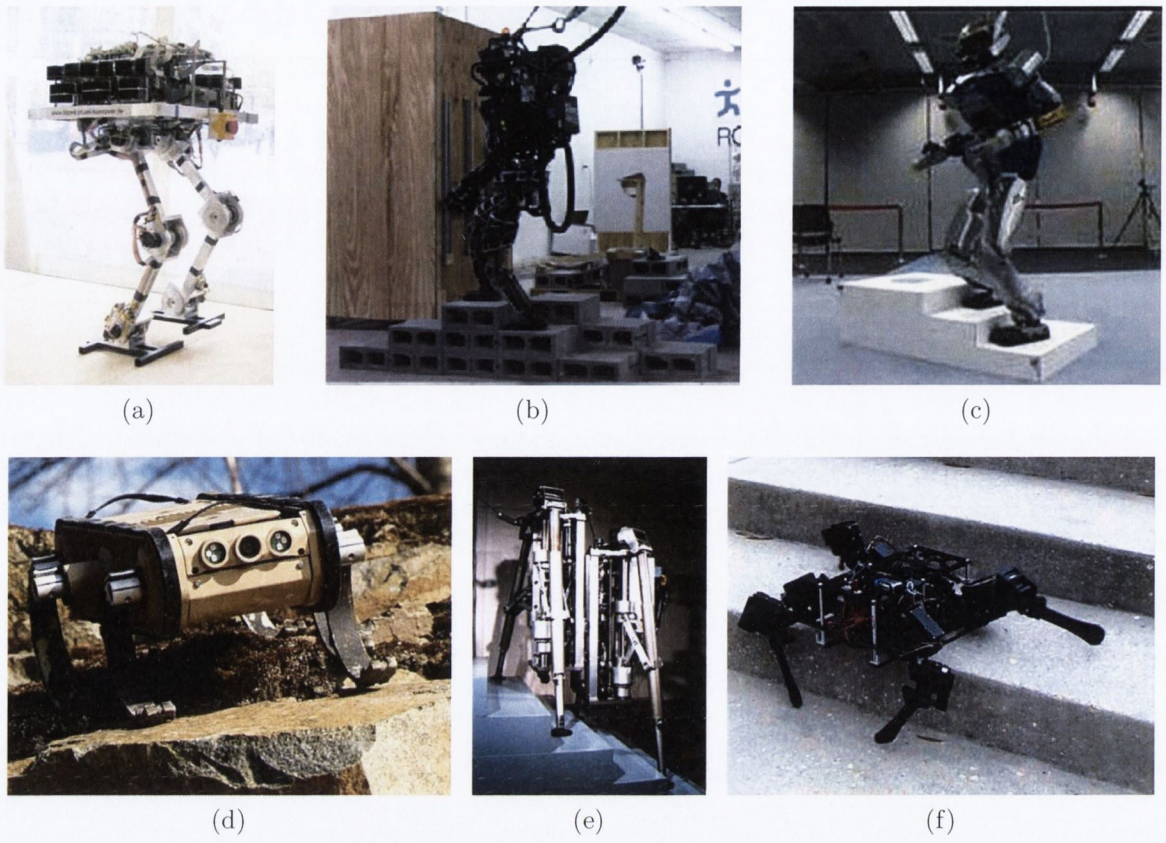
As legged morphologies achieve locomotion through the placement of footholds at discrete points on the ground, they offer a more natural and stable means of overcoming obstacles like stairs. Additionally since they aren't required to span multiple nosings, they can be developed to possess much higher aspect ratios than infinite rotational systems. Despite these potential advantages, stair-climbing remains an inherently demanding process and relatively few legged systems have succeeded in overcoming the inherent difficulties of this process. As legged systems require specific footholds in order to climb stairs effectively, the real-time sensing requirements for stair-climbing is high. Considering that real stairways typically have noticeable deviations in size (major cause of human accidents), even prior knowledge of stair dimensions may not be adequate to ensure safe ascent/descent. The loading of the joints during stair-climbing is also significantly higher than for locomotion on flat terrain. Therefore the power-to-weight requirements for the actuators on stair-climbing robots tend to be higher than for flatland tasks. For quadruped or hexapod type legged robots, the required range of joint rotations for locomotion is increased substantially since the stairs add an offset to relative movement of the upper and lower limbs [171]. Unlike infinite rotational vehicles, the joints in legged robots tend not to be reversible. Therefore simple movements require very complex trajectories when located on a stairway - to the best of the author's knowledge no legged morphology to date has

demonstrated the ability to descend a stairway backwards or to perform a 180 degree turn on a stairway. To date, the vast majority of legged robots require some a-priori knowledge of the shape and/or location of the stairs or alternatively they they tend to carefully execute each stepping-up motion in isolation, choosing not to demonstrate continuous operation [172] [132].

Both statically stable and statically unstable bipedal robots have succeeded in achieving stair-climbing. The *EP-WAR II* is a statically stable robot that used suction cups on its feet which helped it adhere with the ground during stair-climbing [70]. The *BARt-UH* biped robot achieved statically stair-climbing through the utilisation of feet with overlapping geometry [173](Fig. 2.20a). For reasons of environmental adaptability and practical functionality, neither the morphologies of *EP-WAR II* nor *BARt-UH* offer a robust solution. Using a controllable balancing weight to ensure that the robot's centre of gravity remains above its support foot, the *BR-1* robot can maintain static equilibrium while climbing stairs. It is noted that he *BR-1* is not a fully statically stable robot since a dynamic control algorithm is needed during periods of leg movement.

Despite the added complexity, stair-climbing has been more commonly achieved in statically unstable biped robots. Starting with the *P2* and later with the *Asimo* series of robots, Honda have remained at the forefront of humanoid robot stair-climbing research [42] [131]. Other electrically powered humanoid robots which have demonstrated similar stair-climbing ability include *QRIO* [174], *HRP-2* [175](Fig. 2.20c), *Johnnie* [46], *H7* [176] and the robot developed by Li et al [177]. Boston Dynamics and DARPA have also demonstrated impressive stair-climbing ability through the hydraulically powered *Atlas* biped platform [178](Fig. 2.20b). What is particularly impressive about these systems is the dynamic nature of the movement and the natural movement which is emergent from the high levels of joint compliance that the robot possesses.

Other non-biped legged robots which have demonstrated stair-climbing ability include *RHex* [179](Fig. 2.20d), *TITAN VI* [18] and the quadruped robot developed by Brewere et al [180](Fig. 2.20f). While each of these robots possess high stability, their size makes them poorly suited to performing service robot tasks in human centred environments.



(a) (b) (c)

(d) (e) (f)

Figure 2.20: Legged stair-climbing robots (a) BARt-UH robot (b) DARPA Atlas robot climbing steps (c) HRP-2 robot climbing steps (d) Boston Dynamics RHex robot (e) Titan-VI quadruped robot (f) Quadruped stair-climbing robot developed at the Univ. of Maryland

Hybrid Solutions

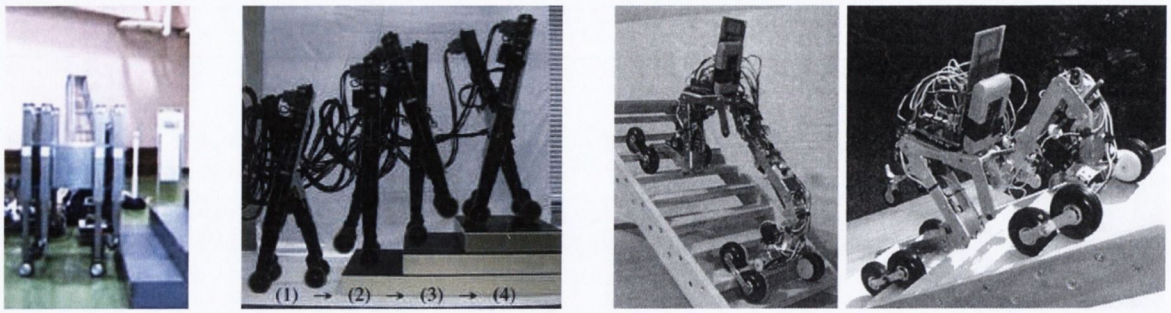
Since wheels and legs possess complementary advantages (wheels tend to be energy efficient, legs are usually environmentally adaptive) and disadvantages (wheels possess poor environmental adaptability, legs have poor energy efficiency), several designers have made efforts to develop optimised morphologies that combine both forms of locomotion in a single mechanism. One of the first robots to do this was *Chariot II*, a robot developed for deployment in forests. *Chariot II* consists of a large drive wheel with four 3 DOF legs, two orientated in front of the robot and two orientated behind the robot. In this system, locomotion is primarily achieved through rotation of the drive wheels however for traversing obstacles (or steps) a walking gait can be adopted. [181].

Matsumoto et al. has developed two interesting hybrid platforms that have each demonstrated stair-climbing ability. In one embodiment, a biped-like legged structure with

wheels on the feet is adopted. As the feet overlap, static equilibrium can be maintained on the stair. Stair-climbing is achieved through the dynamic process of tilting the robot's centre of mass forward such that it is possible to lift and swing the trailing leg up the stairs. This process can be repeated cyclically for each leg. The required shortening of the swing leg is made possible using a linear actuator [182]. The second robot from this group, the *VSTWR (Variable Structure Type Four Wheeled Robot)*, uses a 3D four-bar mechanism with wheels attached at the base of adjacent linkages. Through actuation of the mechanism and development of a self-balancing algorithm which maintains the upright position of one wheeled linkage, its possible to raise the remaining wheeled linkage over a step/obstacle [183](Fig. 2.21b). Since this morphology requires that the tread be larger than the robot's wheelbase, this solution is not well suited for use on conventional stairs or for singular step climbing applications.

The *Zero-Carrier* robot uses eight independently controlled prismatic legs with wheels at their base. The *Zero-Carrier* achieves planar motion through wheeled locomotion and traverses stairs through the coordinated prismatic action of the linear actuators in the legs [184](Fig. 2.21a).

Other hybrid approaches have used articulated mechanisms/linkages to enable the front and rear axles to move relative to each other with increased flexibility. The system developed by Morales et al., uses two actuated four bar linkage mechanisms to connect the wheels at the front/rear with the chassis. A specially designed climbing mechanism which assists the wheels in mounting the stair is also implemented [185]. The solution developed by Lawn and Ishimatsu connects an articulated lifting mechanism with a front and rear driven axle. A pair of independently controlled wheels, symmetrically offset from the drive axis, are located at the extreme of each axle [186] (Fig. 2.21c). With stair-climbing made possible due to the end-over-end action of the wheel mechanisms, the wheelbase is adjusted to suit the stairway through augmentation of the articulated mechanism.



(a) (b) (c)

Figure 2.21: Hybrid stair-climbing robots (a) Zero-carrier robot (b) Matsumoto hybrid wheel-biped robot (c) hybrid stair-climbing wheelchair

2.6 High-level Comparison of Morphologies

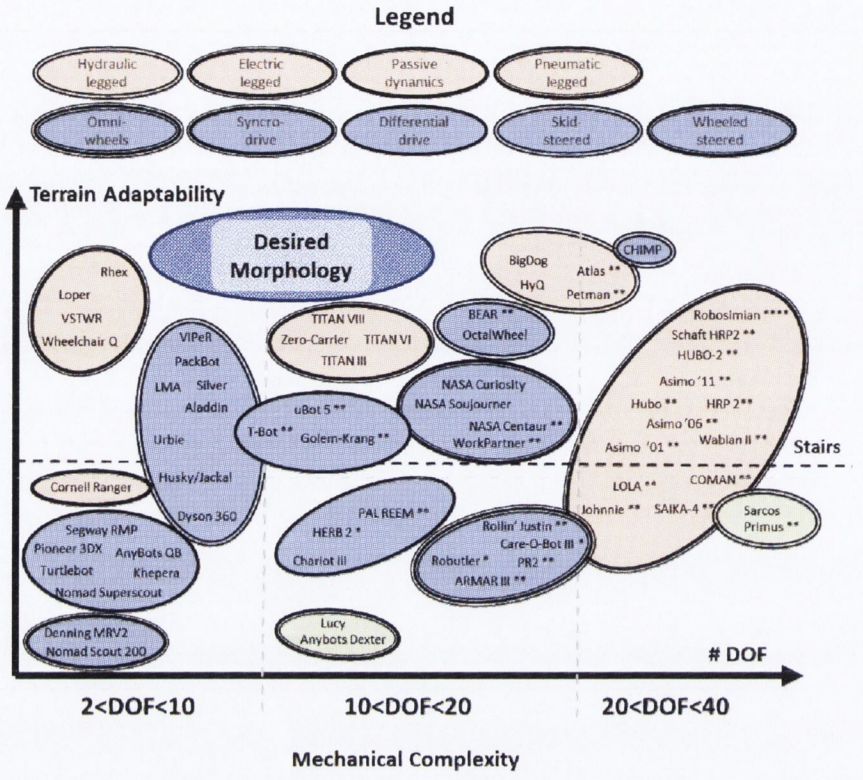
The design of a truly 'general-purpose' robot requires detailed consideration of both kinematic and dynamic factors. In the former instance, high levels of behavioural diversity can only be realised on robots that possess medium-to-high mechanical complexity (i.e. number of DOF), a task space comparable with a person and the capability for advanced terrain adaptability. In the latter case, the robot must be energy efficient and highly stability so that its performance is robust and capable of untethered use for extended time periods. Furthermore to ensure effective communication of its system states (a trait all service robot morphologies should possess), the robot should have an easily identifiable, interactive interface. The complexity of the interface should be in keeping with its degree of behavioural diversity.

From the literature it is observed that a close relationship exists between the terrain adaptability of a robot's morphology, its degree of stability and its overall mechanical complexity (defined in terms of its number of controllable degrees of freedom) (Fig. 2.22). Furthermore in the absence of any widely accepted benchmarks/standards to assess a mobile robot's terrain adaptability, a new metric for assessment is proposed and adopted. Based upon the emergent nature of robotic behaviour, the metric should be performance-based whereby the robot's actual behaviour in the environment is assessed (as opposed to pure simulation etc.). Furthermore as the environment plays an important role in the range of behaviours the robot possesses, it is important that the environment where the robot is tested is similar/relevant to the environments that it was designed to operate

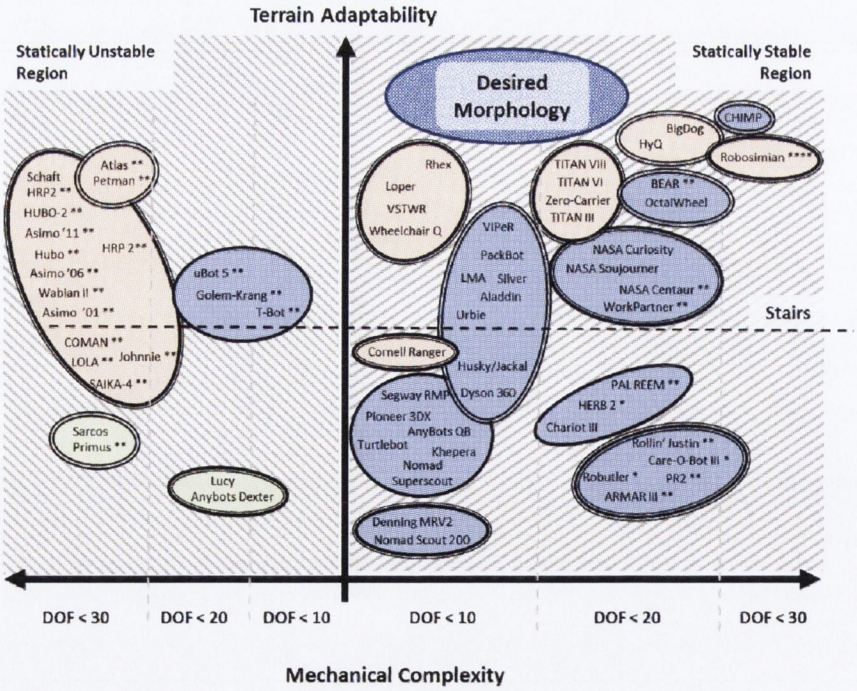
in. With these considerations in mind, it was decided that a suitable metric for determining overall environmental adaptability was to evaluate the system's practical ability to traverse (ascend/descend) stairs. This specific metric was used as stairs pose a major architectural barrier in buildings and systems capable of traversing them must possess advanced kinematic, dynamic and control capabilities.

It is evident from figure 2.22a that low mechanical complexity is often attained through the use of wheeled or tracked morphological configurations. Wheeled configurations (differentially driven, steered, omni-drive etc.) typically suffer poor terrain adaptability as they typically lack the mechanical complexity needed to augment how they move to suit the environment. In order to increase the terrain adaptability of wheeled systems, either very large wheels or additional actuated mechanisms are usually needed. Such design modifications typically have the unwanted consequence of increasing the mechanical complexity and/or decreasing the practical usability of the system (large robots are often not suitable for indoor use etc.). For the same (low) mechanical complexity tracked vehicles possess improved environmental adaptability over equivalent wheeled systems. However stairclimbing is only made possible through utilisation of a large wheelbase. This large wheelbase makes them highly impractical for locomotion in cluttered human-centred environments. Additionally tracked systems require a low centre of mass in order to control pitching and avoid overturning during stairclimbing.

The research indicates that the best attainable terrain adaptability is accomplished using legged systems. This is expected as legged systems are innately adaptable and locomotion is largely independent of the surface properties of the ground. However the cost associated with this performance improvement is that legged systems typically possess increased mechanical complexity. It is noted that the mechanical complexity of legged systems is often proportional to the number of legs the robot possesses. Statically stable four legged systems typically require less than fifteen controllable degrees of freedom (typically three per leg) where as biped robots typically possess more than twenty.



(a) Terrain adaptability Vs. Mechanical Complexity.



(b) Terrain Adaptability Vs. Stability

Figure 2.22: Terrain adaptability of existing morphologies. The number of asterisks indicates the number of manipulators the robot possesses.

This increase in mechanical complexity is due in part to the fact that biped robots are typically statically unstable and therefore require continuous actuation to maintain stability. Also with fewer limbs, greater ranges of joint articulations are needed to enable high agility. Additionally most biped robots possess arms (often with 6 DOF per arm) which require coordination during locomotion but do not necessarily increase the terrain adaptability of the system. On the other hand, the majority of four legged systems are statically stable and locomotion can be achieved using open-loop or less sensitive closed-loop gait pattern generators.

Despite using very similar joint configurations, it is seen that large variances in terrain adaptability exist between legged morphologies. It is noted that iterative refinement of electric actuation schema over decades of legged robotics research has resulted in the state-of-the-art legged robots possessing reasonable levels of efficiency and performance. Newer actuation approaches (i.e. hydraulic and pneumatic) offer improved performance in certain areas (increased compliance, load-carrying etc.) but in most instances they require considerable refinement before they are practical for use on civilian service robots. The terrain adaptability of existing systems is assessed relative to both their mechanical complexity and stability state in figure (2.22b). As well as reducing the computational complexity of the system, the stability of the system plays an important role it's energy consumption. Statically stable systems can conserve power as actuation is only required for deliberative tasks. On the other hand statically unstable robots require continuous actuation for balancing. For statically unstable systems of high mechanical complexity, this results in very high power consumption and generally very low battery life.

Interestingly robots that have high overall terrain adaptability are often practically ill-suited for indoor use in real human-centred environments. This is attributed to the fact that many of these robots adhere poorly with the environmental constraints imposed by building regulations and human factors. The low centre of mass required on conventional tracked vehicles has a practical consequence that tracked systems often have a low vertical height. Considering that human-centred environments are designed for exploitation by agents with taller human-like proportions, there are many common tasks that conventional tracked systems are morphologically poorly suited for (i.e. desktop object recognition/-manipulation, social interaction with people, opening doors). Wheeled robots often need

large wheels and a large wheelbase for static stability and high terrain adaptability. This often renders the robot too large and cumbersome to navigate indoors where the space is tightly confined. Legged systems often require greater levels of perception than are presently feasible for practical usage. Furthermore their power requirements typically limits the robot's battery life to under two hours. Furthermore the use of pump-driven actuation schemas (pneumatic and hydraulic) can be further practically problematic due to the loud noise that the pump makes during the robots operation.

When the complexity of robot interfaces are compared against their respective mechanical complexity (Fig. 2.23), it is apparent that few designers actively incorporate functioning social interfaces into their systems. It is observed that a large number of robot designs possess neither a social interface or a focal point for interaction with people. Furthermore of the robot's that do possess some form of focal point for interaction, typically the capabilities of the interface are very limited (most cases consist of little more than a 2 DOF neck) and little working functionality has been demonstrated. It is interesting to note that the presence of a social interface is correlated with the presence of arms on the robot. The majority of robots possessing social interfaces also possess manipulation capability. There are a few cases where detailed consideration has been given to the realisation of social interfaces on mobile robots. However typically either the complexity of the platform itself has been too low to enable it to perform useful functional tasks (therefore the primary purpose of the robot is to be social) or the interface has been over-designed and consequently fallen into the Uncanny Valley.

As the complexity of the robot's behaviour increases, so too does the user's expectation of the robot. Therefore in the absence of an intuitive interactive interface, the magnitude of the gap between user expectation and actual performance capability is likely to grow in proportion with the behavioural diversity of the robot.

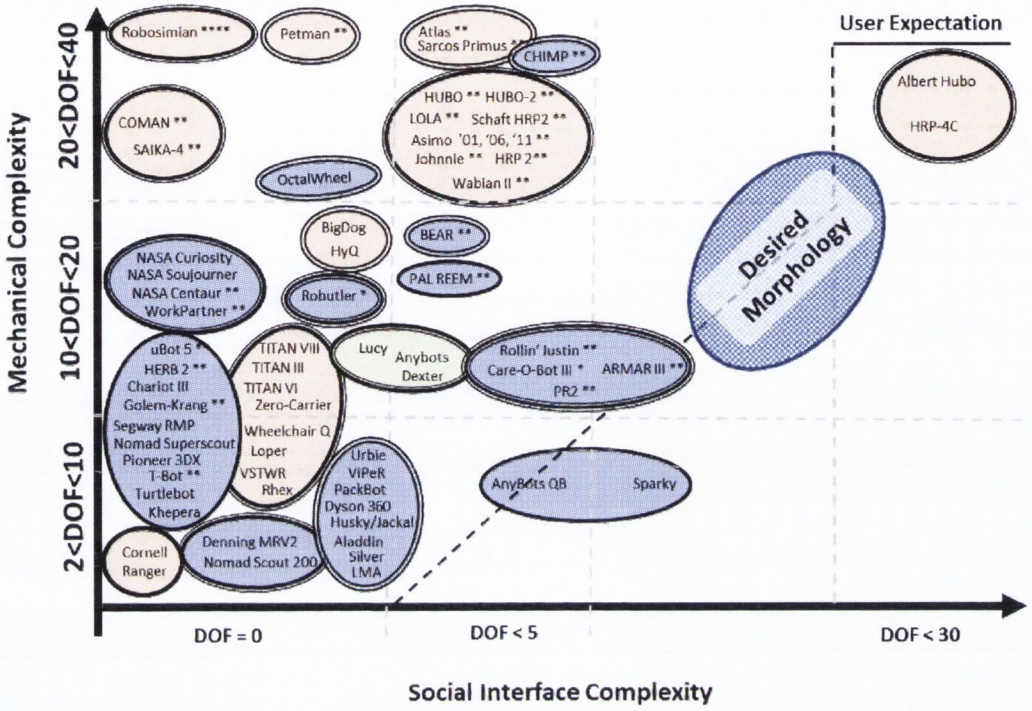


Figure 2.23: Behavioural Diversity Vs. Interface Complexity. The number of asterisks indicates the number of manipulators the robot possesses.

2.7 Summary/Conclusions

For a robot to be capable of performing a range of tasks in human-centred environments, it must possess sophisticated physical, perceptual and cognitive capabilities. The conventional design paradigms which guide the design of these systems were presented with particular focus given to the embodied design approach. This philosophy encourages designers to see intelligence not as a binary, centralised property of an agent or system but as an inherently decentralised property that is manifested as an emergent behaviour that is itself a consequence of the interaction of the system with its own components and with the physical environment around it. Among the many distinctive features of robots designed in accordance with this bottom-up approach include; adherence with the three constituent principle, high system-level redundancy, ecological balance through morphological computation and design iteration/evolution.

According to the three-constituent principle of embodied design, there are three fundamental considerations to be made when designing intelligent systems; the morphology

of the robot, the range of operating environments and the range of desired behaviours. Furthermore this principle states that knowledge of any two considerations provides the foundation for detailed design/engineering of the third. Following this a detailed account of modern robot design (including a detailed review of existing service robots), a discussion of important architectural features in human-centred environments and an account of how stair climbing, a highly challenging behaviour requiring the realisation advanced kinematic/dynamic/control has been realised on mobile robots was presented. In addition to interacting with the surrounding physical environment, service robots must also interact with people. To provide provide appropriate coverage of this area, a comprehensive review of social interaction in robotics was given. This review paid particular attention to the design and control of anthropomorphic social interfaces as well outlining some of the most important design requirements stipulated in ISO 13482, the international standard covering the design of service robots.

The chapter closed with an abstracted comparison of existing robot morphologies. It was shown that wheeled/tracked systems rarely possess the capability for advanced terrain adaptability in human-centred environments. Despite their conventionally desirable levels of static stability and low control complexity, they either lack the required articulations needed for advanced physical tasks such as stair climbing or they are physically unsuited to perform navigation/locomotion in many indoor environments. Furthermore as the aspect ratio of wheeled/tracked vehicles is often low to ensure a low centre of mass, they often do not possess the task space for optimally exploiting human centred environments. Alternatively robots that utilise legs for locomotion possess improved terrain adaptability however this is typically achieved at a cost of increased mechanical complexity. With the required coordination of more controllable degrees of freedom, the control complexity of legged systems rises also. Legged systems can exist in configurations of static instability (2 legs) or static stability (4/6 legs). In the former instance, the robot typically possess the required form and task space to optimally exploit human centred environments. However as the system is statically unstable, they possess very large real-time control, sensing and energy requirements. As statically stable quadruped/hexapod robots do not require continuous actuation and active balance control for stability, they typically possess improved energy efficiency and reduced real-time control/sensing requirements.

Additionally quadruped/hexapod legged robots typically possess large spatial footprints and a non-anthropomorphic task-space making them generally impractical for performing many tasks in indoor human-centred environments.

It was shown that few service robots, in either academia or research, possess the capability for both mobility and advanced social interaction. While several advanced service robots possess a social interface, typically the capability for interaction is extremely low. In the few examples where researchers utilised advanced social interfaces on mobile robots, the interfaces used were too-human in appearance/behaviour and consequently fell into the uncanny valley.

For reasons described in this chapter no robot morphology has yet demonstrated the capability for practical 'general-purpose' use. Such a system would need to possess advanced terrain adaptability, comparable with the best of existing systems, but with reduced overall mechanical and control complexity. While not explicitly needed, it would be advantageous for the proposed system to possess static stability as this would reduce the real-time control, actuation and sensing requirements thus improving energy and computational efficiency. It is desirable that the proposed system would possess a task space that is roughly anthropomorphic in nature such that the robot is morphologically well suited for multi-functional adoption in human-centred environments. The robot's controllable degrees of freedom should be distributed throughout its body thus enabling high reconfigurability/adaptability as well as the capability for redundancy in movement. It is also important that the system possesses a functioning social interface. This interface should be forward-facing and form an obvious focal point for social interaction. Finally the complexity of the interface's appearance and behaviour should be in keeping with overall complexity of the robot (i.e. the complexity of the behavioural diversity that the robot) such that people do not form unrealistic exceptions of the robot.

Chapter 3

Description of Morphology

This chapter introduces the proposed robot morphology. It covers the design approach adopted, the high-level design of the system and the mathematical foundation governing its basic operation. It describes the mechanisms through which considerable behavioural diversity can be realised including how it can pick-up objects navigate stairways, mount obstacles and cross crevices.

3.1 Design Process

A robot morphology fit for practical 'general-purpose' use must possess high levels of terrain adaptability in order to operate between and be used within different civilian environments. In order to obtain high levels of behavioural diversity, the system should possess multiple controllable degrees of freedom. To ensure practical robustness, reduced energy consumption and optimisation of the system's computational resources, it is highly desirable that the system is statically stable or at least is capable of adopting statically stable states. The robot should possess an interface that easily identifies the front facing direction of the robot and provides a focal point for interaction with people and/or other robots. This interface should provide continuous feedback to the user/environment, the level of which should vary depending on the overall behavioural diversity of the robot.
Following the comprehensive review and ensuing discussion of existing systems presented in chapter 2, it emerges that no existing physical system or morphology has met this criteria. Achieving the aspired capabilities is extremely difficult owing to the qualitative nature of the desired design solution, the high overall system complexity and the ad-

vanced system-level integration of the robot's mechanics, electronics and control systems. Rather than approach the problem in a top-down fashion, aspiring to design for a single unified solution that when completed instantly satisfies an explicit quantitative overall design criteria, a bottom-up design approach was favoured. Using a bottom-up approach, the design focus's on developing the robot's fundamental capabilities from the ground up. Through incorporation and exploitation of system redundancy, modularity and reconfigurability, fundamental features of good bottom-up designs, it was expected that a successful robot design would be capable of demonstrating the high levels of adaptability needed for multi-functional operation in unstructured environments. Furthermore owing to the low-level nature of bottom-up designs, the performance of the system typically improves substantially over successive iterations of the design as new improvements build on a firm design foundation.

The embodied design approach, proposed formally by Pfeifer and Bongard [17] provided a series of design principles which both guided and inspired many aspects of the proposed design. These guidelines cover the design and development of intelligent agents over three distinct timespans; the here-and-now, over the lifetime of the agent (ontogenetic) and over successive generations of the agent (phylogenetic). In this work the application of the principles described in the here-and-now perspective helped guide the design of the proposed system such that it possessed the fundamental capabilities and adaptability needed for multi-functional use in human-centered environments. In particular the 'three constituent principle', the guideline/proposition which states that detailed consideration of the range of task behaviours and operating environments should drive the design of the physical embodiment was adopted. Other desirable features covered by the principles mapping the here-and-now timespan include; high system-level redundancy, high sensory-motor coordination, ecological balance through morphological computation and the use of multiple parallel, loosely coupled processes.

The ontogenetic and phylogenetic principles deal with how agents can be designed such that their performance improves over time, firstly over the lifetime of the agent and then over the lifetime of several generations of agents. The principles covering the ontogenetic time frame promote features such as providing the agent with tools for exploration and evaluation as well equipping it with mechanisims that ensure learning can take place

progressively and through social interaction with other agents. With respect to the phylogenetic time scale, principles promoting 'brain-body' co-evolution, elimination of designer bias and the scaling of complexity over successive generations of agent were found relevant in guiding the design of the proposed system. A graphical illustration describing the structure of the bottom-up design process used in this work is presented in figure 3.1.

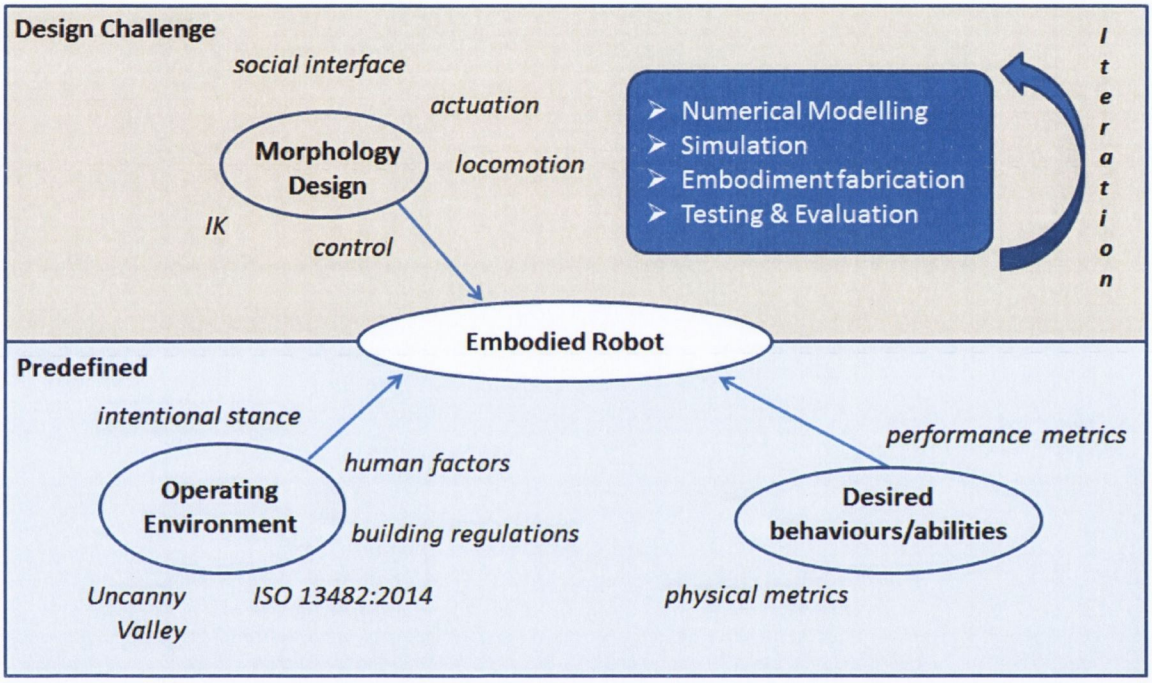


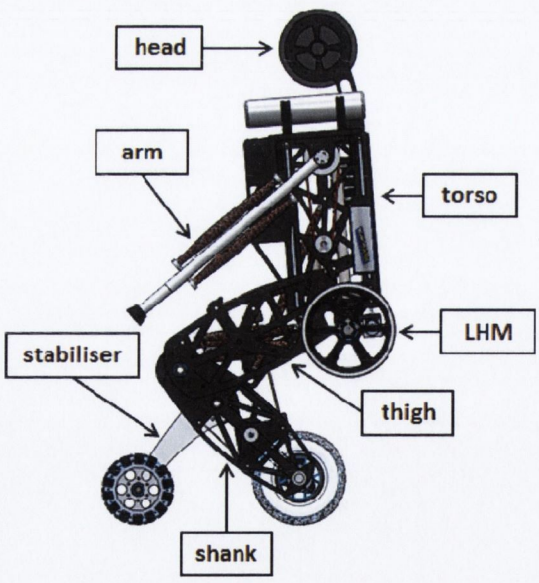
Figure 3.1: Graphical illustration of three-constituent principle as applied to the design of a personal service robot

At the time of writing, two full-scale physical embodiments of the proposed morphology have been design, constructed and subjected to varying degrees of testing. In adherence with the phylogenetic time scale design principles, the second prototype represents a tangible improvement in both performance and functionality. As such its design, development and testing form the basis for the majority of work contained in this thesis. As the assessment of bottom-up robotic design is best achieved through classification of the system's capabilities and adaptabilities, several broadly different performance-based design targets were used. These targets cover the robot's stability, user interface and terrain adaptability.

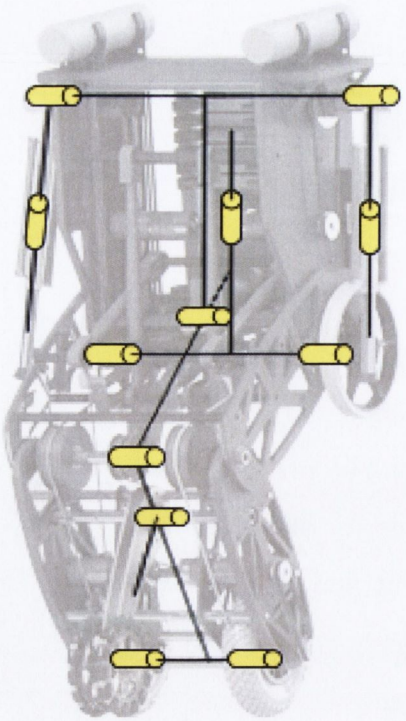
3.2 High Level Description

As domestic and civilian environments are primarily designed to be used by people, robots possessing a human-like form will be morphologically better suited to the environment than robots that do not. Not only are robots of this type likely to offer improved manoeuvring capability but they will also be able to interact with the broader environment in a more diverse and natural way, especially in instances where spatial positioning of limbs is important (engaging in social interaction with a human at eye level, picking up objects from a table etc.).

The proposed robot morphology is broadly anthropomorphic in form. In its most basic configuration the system possesses 12 degrees of freedom (DOF) and is constituted from seven limbs including a shank, stabilising linkage, thigh, torso, head/social interface and two arms (Fig. 3.2).



(a)



(b)

Figure 3.2: Graphical description of the proposed morphology (a) labelled image of primary components (b) visualisation of robot's controllable joints

Driven wheels located at the base of the shank are the primary means for locomotion. An actuated stabilizing link is positioned below the knee in the shank. Actuation of this joint causes a proportional change in the robot's wheelbase. Through coordinated movement of the hip, knee and stabilizer joint, the robot is able to adjust its height and overall centre of mass (COM). An additional feature, hereby referred to as the Lower Hip Mechanism (LHM) is positioned directly beneath the hip. The LHM possesses two actuated wheels and a prismatic actuation mechanism which connects it linearly to the torso.

3.2.1 Locomotion

Residential and other indoor civilian environments typically possess firm, flat floor surfaces which make them well suited to locomotion for wheeled robots. The proposed robot morphology achieves locomotion using a pair of differentially driven wheels located at the base of the shank (at the ankle joint). Differentially driven robots (turning achieved by modifying the speed of one wheel relative to the other) have a greater degree of mobility than steered robots meaning that they can follow more demanding kinematic paths. A passive omnidirectional wheel unit is incorporated at the end of the stabilizer link. Through the actuation of stabiliser linkage, the robot can adjust its height while retaining static stability. Since these wheels have low-lateral resistance, they don't resist turning motion and don't adversely affect the accuracy of the differential drive control system. In this instance, omni-directional wheels [187] were deemed preferable to conventional caster wheels as they possess a larger diameter wheel for the same overall form factor. This increased wheel radius allows the robot to pass over bumps that would be too demanding for equivalent caster systems. For increased levels of traction and stability, a skid-steered configuration can be attained through elongation of the Lower Hip Mechanism (LHM) located at the base of the torso (Fig 3.3).

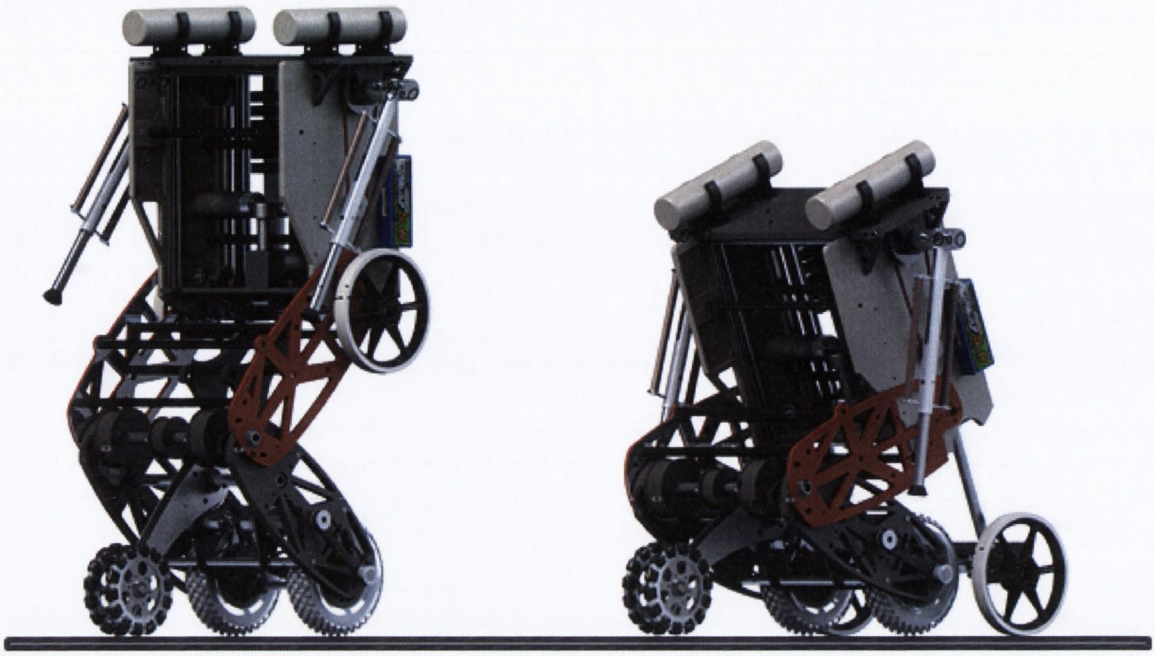


Figure 3.3: Primary modes of locomotion for the proposed morphology (left) the robot in default differential drive mode (right) the robot in high stability 4WD mode

3.2.2 Actuation and Articulation

The robot uses a combination of electrical and pneumatic actuators. For joints requiring fast response times, accurate positioning and low output torques, geared DC motor units are used. Pneumatic air muscles (PAMs) are implemented on joints requiring compliance, large torques, high power-to-weight ratios and/or high levels of customisation.

The arms possess prismatic joints at the elbow. This feature helps enable the robot to pick up objects from the ground (Fig 3.4), to safely navigate stairs and to temporarily increase the size of the its configuration space during manipulation tasks.

In accordance with the findings from the literature, the morphology possesses an easily identifiable 'front-facing' orientation. The front facing direction coincides with the direction of forward motion of the differentially-driven drive wheels. It is observed that owing to the robots' symmetry about the coronal/front plane, much of the robot's morphology can be analysed in two dimensions. This substantially simplifies the inverse kinematics and in turn reduces control complexity.

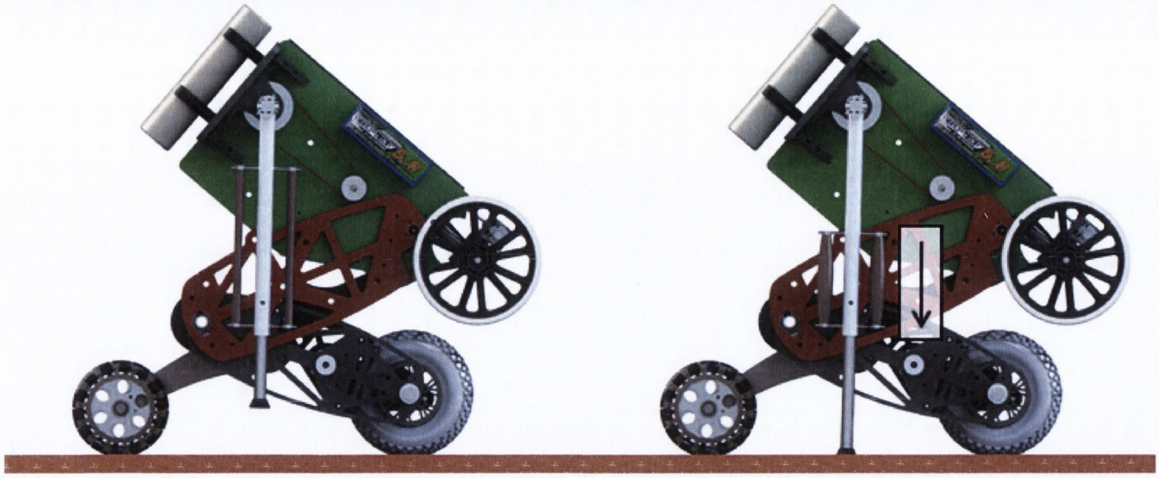


Figure 3.4: Sequence of actions for picking up object from the ground (left) pick-up stance with arm contracted (right) pick-up stance with arm elongated

3.2.3 Embodied Intelligence Philosophy

The embodied design principles described in section 2.1 hypothesise that intelligent agents should evolve and their practical capabilities increase over successive generations of design. While the present embodiment succeeds in providing high levels of practical functionality at a lower cost (mechanical, control, energy etc.) than existing systems, there remains room for substantive improvements to be realised in future iterations of this design. Specifically the robot has been designed to enable future iterations to substantially improve the morphology's manipulation capability. Future generational improvements include incorporating additional flexibility in the shoulder joints, addition of a neck joint and the addition of revolute joints in the arm (i.e. an elbow joint) are anticipated. Since the core functional requirements of the proposed morphology do not relate to manipulation alone and instead require the integration of locomotion, stability and human factors, the incorporation of mechanisms for advanced manipulation tasks remains future work.

3.3 Mathematical Description

To precisely define the proposed morphology, a kinematic description is provided. Firstly the forward kinematics which define the range of postural configurations (configuration space or C-space) that the robot can to have due to its link lengths and joint variables

is given. This is followed by a description of the inverse kinematics algorithm required to ensure safe coordinated adjustment of the body height.

3.3.1 Forward Kinematics

Using the Denavit-Hartenberg (DH) convention [188], the forward kinematics of the robot can be defined. The DH convention provides a systematic mechanism through which homogeneous coordinate transforms can be defined from the specification of just four parameters per link - link length (a_i), link twist (α_i), link offset (d_i), joint angle (θ_i). This expression is given by:

$$T_n^{n-1} = \begin{bmatrix} cos\theta_n & -sin\theta_n cos\alpha_n & sin\theta_n sin\alpha_n & r_n cos\theta_n \\ sin\theta_n & cos\theta_n cos\alpha_n & -cos\theta_n sin\alpha_n & r_n sin\theta_n \\ 0 & sin\alpha_n & cos\alpha_n & d_n \\ 0 & 0 & 0 & 1 \end{bmatrix} \tag{3.1}$$

The DH link segment parameters which describe the 3D projection of the proposed morphology are shown in figure 3.5 and listed in table 3.1. The base reference frame is set at the midpoint of the centreline between the left and right shank drive wheel.

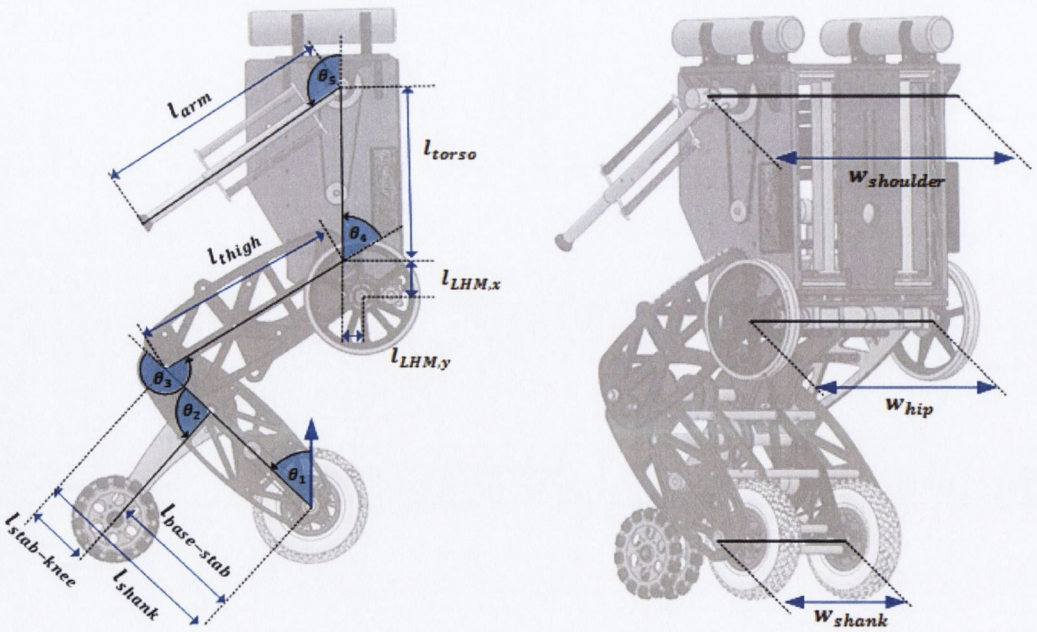


Figure 3.5: Robot Segment Parameters

Description	Ref. Frame	a_i	α_i	d_i	θ_i
Base-Wheel(RHS)	T_0^1	0	0	$\frac{w_{shank}}{2}$	0
Base-Wheel(LHS)	T_0^2	0	0	$-\frac{w_{shank}}{2}$	0
Base-Stab.(Joint)	T_0^3	$l_{base-stab}$	0	0	θ_1
Stab.(Joint)-Stab.(Wheel)	T_3^4	l_{stab}	0	0	θ_2
Stab.(Joint)-Knee(Joint)	T_3^5	$l_{stab-knee}$	0	0	0
Knee(Joint)-Hip(Joint)	T_5^6	l_{thigh}	0	0	θ_3
Hip(Joint)-Shoulder(RHS)	T_6^7	l_{torso}	0	$\frac{w_{shoulder}}{2}$	0
Hip(Joint)-Shoulder(LHS)	T_6^8	l_{torso}	0	$-\frac{w_{shoulder}}{2}$	0
Shoulder(RHS)-End Eff.(RHS)	T_7^9	l_{arm}	$-\alpha_1$	0	θ_4
Shoulder(LHS)-End Eff.(LHS)	T_8^{10}	l_{arm}	$-\alpha_1$	0	$-\theta_4$
Hip(Joint)-LHM(RHS)	T_6^{11}	l_{LHM_x}	$-\alpha_2$	$\frac{w_{hip}}{2}$	$-\theta_5$
	T_{11}^{12}	0	α_2	l_{LHM_y}	θ_5
Hip(Joint)-LHM(LHS)	T_6^{13}	l_{LHM_x}	$-\alpha_2$	$\frac{w_{hip}}{2}$	$-\theta_5$
	T_{13}^{14}	0	α_2	l_{LHM_y}	θ_5

Table 3.1: DH Parameters for robot morphology

Although each base transformation matrix describes the relationship between just two coordinate systems, a larger transformation matrix can be generated by multiplying successive base transformation matrices. For example the transformation matrix which describes the position of the right end-effector relative to the robot's base frame is given by:

$$T_8^0 = T_3^0 \; T_4^3 \; T_5^4 \; T_6^5 \; T_7^6 \; T_8^7 \begin{bmatrix} 0 & 0 & 0 & 1 \end{bmatrix}^T$$

3.3.2 Relating the Shank and Stabiliser Angles

Since the shank angle (θ_1) is coupled with the stabiliser angle (θ_2), the orientation of the shank can be controlled by augmenting the stabiliser mechanism (Fig.3.6). Assuming a flat ground surface, the stabiliser angle is given by:

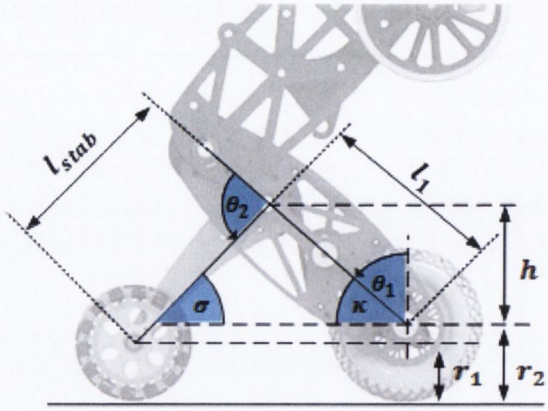


Figure 3.6: Geometrical relationship between shank and stabiliser mechanisims

$$\text{let } \{l_1 = l_{base-stab}\} \text{ and } \{l_2 = l_{stab}\}$$

$$\kappa = (90 - \theta_1)$$

$$h = l_1 sin\alpha = l_2 sin\sigma - (r_2 - r_1)$$

$$\sigma = sin^{-1}\left(\frac{h+(r_2-r_1)}{l_2}\right)$$

$$\theta_2 = 180 - (180 - \sigma - \kappa) = \kappa + \sigma$$

$$\theta_2 = sin^{-1}\left(\frac{h + (r_2 - r_1)}{l_2}\right) + (90 - \theta_1) \tag{3.2}$$

3.3.3 Inverse Kinematics

Inverse kinematics is concerned with determining values for the robot's joint variables in order to achieve a desired end-effector position and orientation. This problem is considerably more difficult than that of forward kinematics as there may exist zero, one or many viable configurations. Additionally the performance of the system will be dependent on the IK algorithm chosen, especially in the vicinity of singularities.

Inverse kinematics algorithms can typically be separated into geometric and Jacobian based methods. In the former class of techniques, trigonometric equations are used to describe the relationship between joint variables and the desired end-effector position. Despite its simplicity, the complexity of the solution scales with the number of joint variables. Also since multiple configurations may exist for a desired orientation, further

heuristic methods are needed to classify and choose between possible configurations. A more efficient (albeit mathematically complicated) class of inverse kinematic methods involve utilisation of the morphology's Jacobian matrix. The Jacobian, a matrix of partial derivatives, defines how the instantaneous position/orientation of the end effector moves relative to the instantaneous orientations of the system's joint variables. This can be approximated to the recorded changes in the robot's joints as shown in eqn. (3.3).

$$J = \frac{\partial e}{\partial \theta} \approx \frac{\Delta e}{\Delta \theta} \tag{3.3}$$

$$\Delta \theta = J^{-1} \Delta e \tag{3.4}$$

While in theory, eqn. (3.4) can be manipulated to solve for the required joint adjustments, this is generally not practical. Finding the inverse Jacobian directly is problematic since it is not guaranteed to be square and is prone to instability caused by singularities brought on by certain joint configurations.

A set of methods exist which do not require the inverse of the Jacobian to be calculated directly. Instead these methods involve formulating an invertible approximation of the Jacobian and then substituting it into the above calculation. Among the most most popular approaches of this type include of the 'pseudo-inverse method' and the 'Jacobian transpose method'The pseudo-inverse method has been adapted in this work owing to its improved accuracy [189]. It is noted that this method is known to possess poor stability in the proximity of singularities. A simple derivation of the pseudo inverse Jacobian is presented below with the final expression given in (3.5).

$$J^T \Delta e = J^T J \Delta \theta$$

$$(J^T J)^{-1} J^T \Delta e = (J^T J)^{-1} (J^T J) \Delta \theta$$

$$J^+ \Delta e = \Delta \theta$$

where

$$J^+ = (J^T J)^{-1} J^T \tag{3.5}$$

So the inverse kinematic problem becomes:

$$\Delta\theta = J^{+}\Delta e \tag{3.6}$$

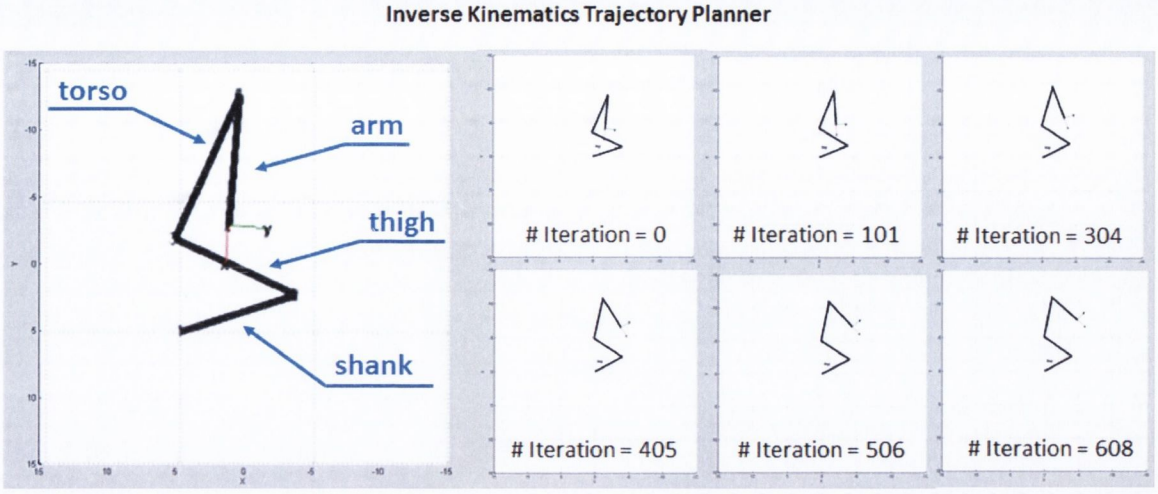
The Jacobian for controlling the position of the left arm end-effector is given in eqn. (3.7). The joint angles and limb lengths used in this analysis are illustrated in figure (3.5). Using this process, it is possible to find suitable joint positions for the range of orientations that the robot possesses.

$$J = \left[\begin{bmatrix} 0 \\ 0 \\ 1 \end{bmatrix} \times \begin{bmatrix} a_1c\theta_1 + a_2c\theta_{12} + a_3c\theta_{123} + a_4c\theta_{1234} \\ a_1s\theta_1 + a_2s\theta_{12} + a_3s\theta_{123} + a_4s\theta_{1234} \\ 0 \end{bmatrix} \begin{bmatrix} 0 \\ 0 \\ 1 \end{bmatrix} \times \begin{bmatrix} a_1c\theta_1 + a_2c\theta_{12} + a_3c\theta_{123} \\ a_1s\theta_1 + a_2s\theta_{12} + a_3s\theta_{123} \\ -d_3 \end{bmatrix} \begin{bmatrix} 0 \\ 0 \\ 1 \end{bmatrix} \times \begin{bmatrix} a_1c\theta_1 + a_2c\theta_{12} \\ a_1s\theta_1 + a_2s\theta_{12} \\ 0 \end{bmatrix} \begin{bmatrix} 0 \\ 0 \\ 1 \end{bmatrix} \times \begin{bmatrix} a_1c\theta_1 \\ a_1s\theta_1 \\ 0 \end{bmatrix} \right]$$

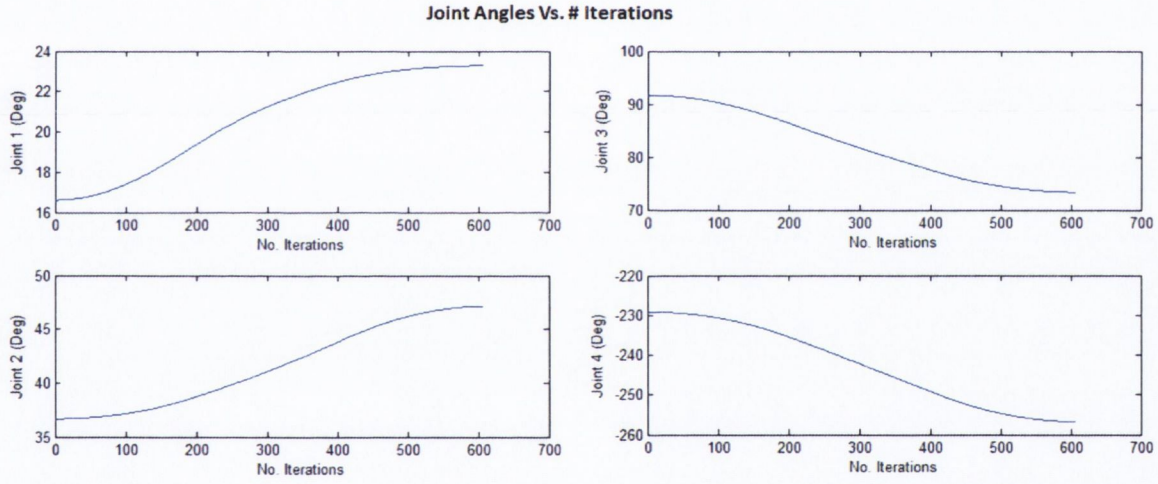
$$J = \begin{bmatrix} -(a_1s\theta_1 + a_2s\theta_{12} + a_3s\theta_{123} + a_4s\theta_{1234}) & -(a_1s\theta_1 + a_2s\theta_{12} + a_3s\theta_{123}) & -(a_1s\theta_1 + a_2s\theta_{12}) & -a_1s\theta_1 \\ a_1c\theta_1 + a_2c\theta_{12} + a_3c\theta_{123} + a_4c\theta_{1234} & a_1c\theta_1 + a_2c\theta_{12} + a_3c\theta_{123} & a_1c\theta_1 + a_2c\theta_{12} & a_1c\theta_1 \\ 0 & 0 & 0 & 0 \end{bmatrix} \tag{3.7}$$

where: $\begin{bmatrix} a_1 = l_{shank} \\ a_2 = l_{thigh} \\ a_3 = l_{torso} \\ a_4 = l_{arm} \end{bmatrix}$

Using Matlab [190] and the Matlab Robotics Toolbox [191], the forward kinematics for the robot were defined. Integrating the FK model with the IK model described in this section, it was possible to demonstrate the ability of the system to perform multi-limb coordinated movement. The output from a simulation demonstrating this capability is given in figure 3.7. For simplicity in the simulation, the stabiliser joint is ignored as the shank and stabiliser are inherently a coupled system.



(a)



(b)

Figure 3.7: Inverse kinematics MATLAB simulation demonstrating the action of placing the end effector on a raised surface (a) wireframe model of the robot's links and joints plotted as a function of the number of solver iterations (b) change in joint angles with respect to the number of solver iterations

3.4 Stability

A novel aspect of this robot's design is that it utilizes a stability mechanism that enables it to perform tasks that were previously reserved for statically unstable robots (i.e. biped legged robots) whilst retaining statically stability. Static stability for the proposed morphology is achieved mathematically if the projection of the robot's centre of mass lies within the support polygon formed by connecting the robot-ground contact points. The margin of static stability is given by the shortest straight line distance from the COM

projection to the nearest edge of the support polygon [40]. Using the 'segmental method', the overall COM of the robot can be computed from the cumulative position and centre of mass of each of the robot's limbs [192]. Thus the expression which defines the overall centre of mass of the robot is given by:

$$(x_{COM}, y_{COM}) = \left(\frac{\sum_{i=0}^{n} m_i x_{COM,i}}{\sum_{i=0}^{n} m_i}, \frac{\sum_{i=0}^{n} m_i y_{COM,i}}{\sum_{i=0}^{n} m_i} \right) \tag{3.8}$$

During periods of rest and when engaged in locomotive tasks on flat ground, the robot operates in its default pose, a configuration of high static stability. However when it's required, the robot can adopt a more upright pose through contraction of the stabiliser and straightening of the knee joint. For the robot described in this work, the SSM is at its maximum when the stabilizer is fully extended and the knees are bent (Fig. 3.8). However when the knees straighten and the stabilizer retracts inwards, the shortening in the robot's wheelbase causes region of stability to shorten which will in turn reduce the SSM and increase the sensitivity of the system to destabilisation.

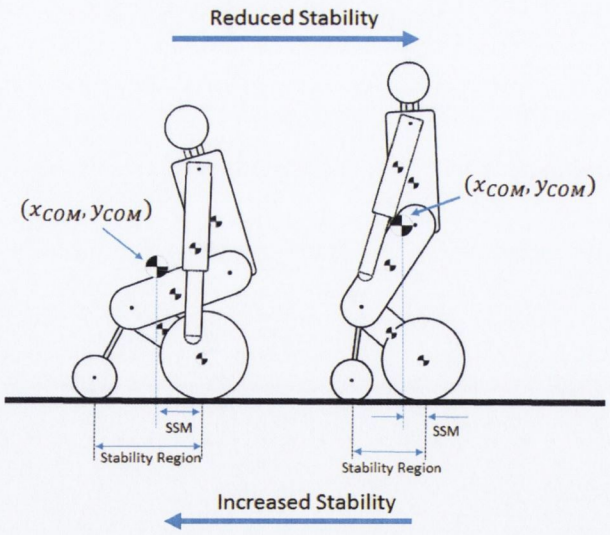


Figure 3.8: Modifying the static stability margin through actuation of the stabiliser linkage

As the joints at the wheel, knee, hip and shoulder are all constrained to rotate in the same plane (saggital plane), the system can be said to possess high lateral stability and the

control problem for stability can be reduced to two dimensions only. This latter property is especially advantageous as it minimises the system's overall control complexity. A high overall degree of lateral stability can also be expected during locomotion as the lateral moment of inertia of the drive wheels is very large and the centre of mass of the morphology can be kept very low. It is noted that should future iterations of the embodied system utilise arms with greater controllable degrees of freedom, the mass of the arms should be minimised such that they don't adversely affect the system's lateral stability.

3.4.1 Control through Self-Balancing

Provided the robot possesses sufficient joint stiffness, situations of instability in the saggital plane (i.e. when the stabiliser wheel has left or is just about to leave the ground) can be modelled as an equivalent 1 DOF wheeled inverted pendulum. It is evident from the equations of motion for an inverted pendulum with a movable base given in figure 3.9 that the angular acceleration of the rotating object is inversely proportional to the distance between the point of rotation and its centre of mass. This means that the higher an object's COM of mass is located, the slower it will rotate about a point at its base.

$$\ddot{\delta} = \frac{\ddot{x}cos\delta + gsin\delta}{l} \tag{3.9}$$

By ensuring the morphology has a high centre of mass (i.e. heavy upper body), a reduced angular acceleration during tipping is ensured. Through integration of a real-time reactive self-balancing controller, deviations in the desired upright set-point can be corrected for through adjustment of the drive wheel velocities. As evident from figures 2.22b and 2.22b, an optimally designed 'general-purpose' robot morphology should possess the minimal number of controllable degrees of freedom needed to achieve high terrain adaptability. By implementing control using a wheeled self-balancing approach, the control problem for the proposed morphology is reduced to one degree of freedom resulting in the real-time control requirements and computational complexity remaining low.

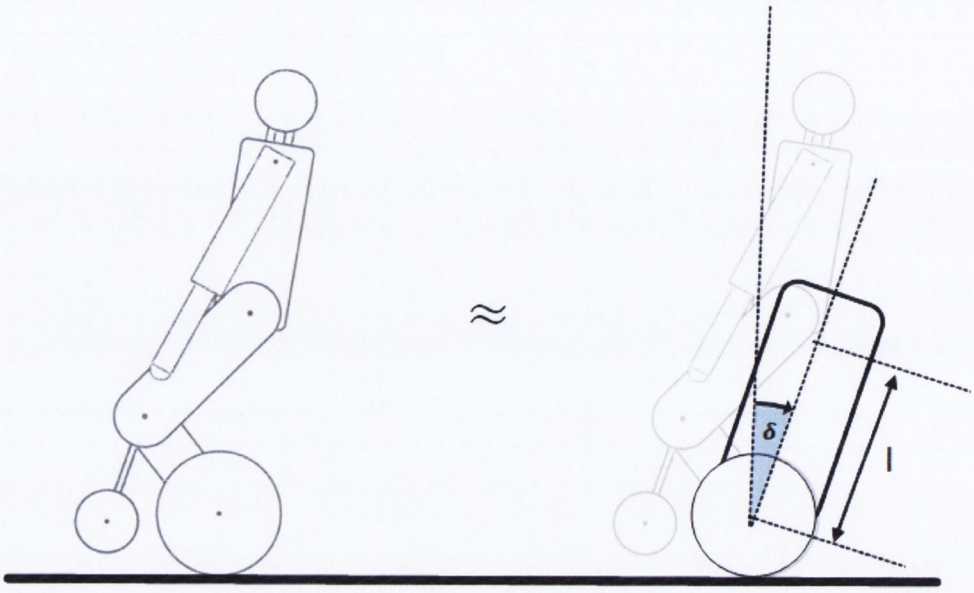


Figure 3.9: Simplifying the stability of the morphology to approximate that of a single degree of freedom wheeled self-balancing platform

3.4.2 Control through Inverse Kinematics

In addition to using the inverted pendulum approach, control through inverse kinematics can also be used to maintain stability. Indeed it is proposed that an optimally designed system would utilise both inverse kinematics and self-balancing to achieve control.

As the robot's SSM is proportional to the relative orientation of the joint angles and the slope of the ground plane, increased stability can be achieved through adjustment of the joints alone. Assuming that the mass of the torso is considerably larger than the mass of the arms, moving the positions of the shoulders, hip and knee to orientations with larger SSMs will have a stabilising effect (Fig. 3.10).

One means to implement this method is through the pseudo-Jacobian method where the Jacobian matrix for the left end-effector is given by eqn. (3.7) and the relationship between the stabiliser angle and the shank angle is given by eqn. (3.2).

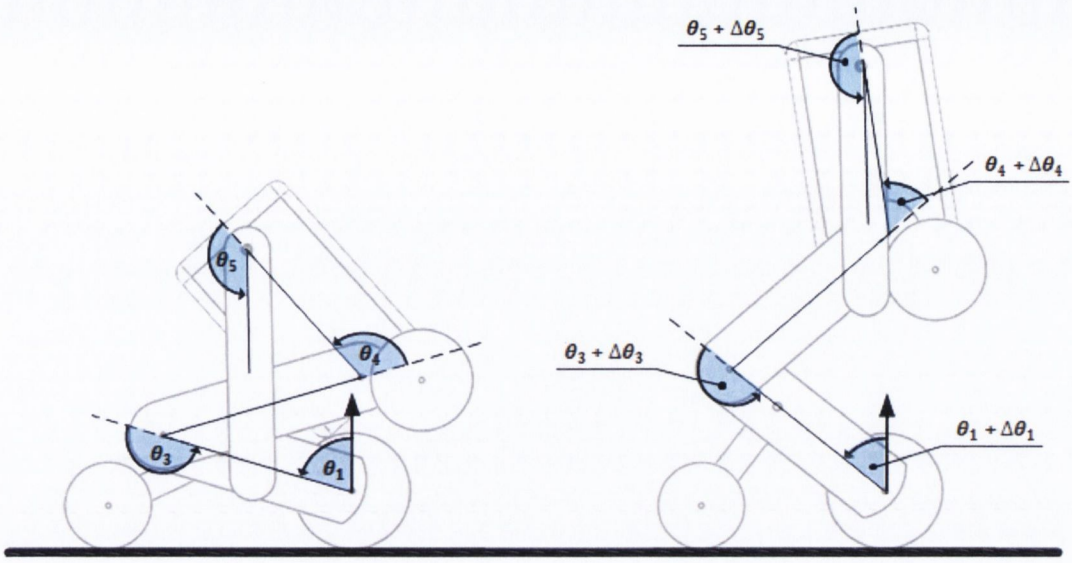


Figure 3.10: The relative joint angles of the robot in positions of varying stability: (left) high stability (right) low stability

3.4.3 Stability on Uneven Surfaces

The stabilising mechanism used on the morphology provides a mechanical support that inhibits forward tipping. As the robot will spend the majority of its operation time travelling in the forward direction, backward instability is not likely. However despite the relatively low-risk, backwards pitching may occur in certain circumstances (traversing uneven terrain, climbing steep slopes). To protect against such occurrence, the torso can be orientated in such a manner that the Lower Hip Mechanism can serve as a reverse stabiliser. This posture is achieved by learning the torso forwards and extending the LHM. When operating in this configuration, changes in the vertical set-point can be augmented not only through wheeled self-balancing and joint angle adjustment but through active control of this mechanism (Fig. 3.11).

3.5 Stair/Obstacle Climbing

To date very few robots, legged or otherwise, have demonstrated the ability to ascend/descend stairs. Fewer still have demonstrated this capability without prior explicit knowledge of the stair geometry. No robots in the literature have succeeded in achieving this

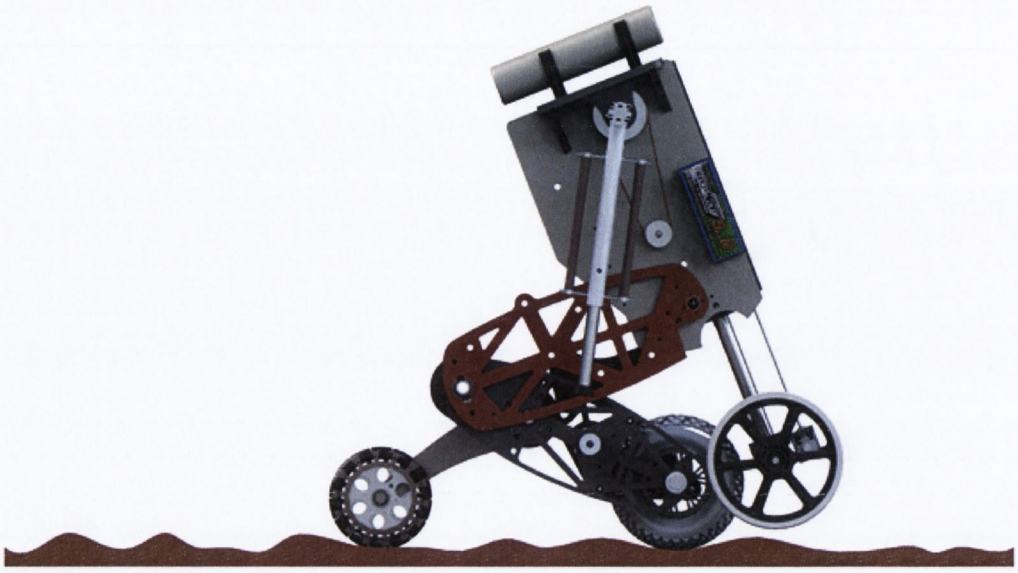


Figure 3.11: The lower hip mechanism providing additional stability during navigation on broken/uneven terrain.

task while retaining a statically stable state without the need to closely control the environment (i.e. ensure that the floor surface will enable suction pads to adhere to it) and/or possessing a high aspect ratio in the saggital plane. Furthermore from the survey of legged robots that possess the ability to climb stairs, none have demonstrated the ability to reverse their direction of motion mid-flight. The primary reason for this limitation can be attributed to the fact that the forward-facing orientation of legged robots with respect to the stairs typically changes depending on whether they are ascending or descending the flight. The complexity of this task is increased further for statically unstable bipedal robots due to demanding real-time control requirements.

The proposed morphology has incorporated an efficient, statically stable and low control cost method of traversing obstacles and climbing stairs (ascent and descent). The orientation of the robot relative to the stairway is the same for both ascent and descent and therefore changing direction mid-flight is a straightforward process. This achievement overcomes a major practical limitation of existing systems. Additionally it is important to observe that the mechanisms used during object and stair climbing are largely decoupled from each other and can operate independently. In this way, pose/gait adjustments

can be made as necessary at both local subsystem and global system level. This feature makes this system fundamentally different from other wheeled morphologies that utilise passively coupled serial linkages such as the 'Rocker-bogey' described in chapter 2.5.5.1.

3.5.1 Traversing an Obstacle

The procedure for traversing an obstacle is illustrated in figure 3.12. The robot approaches the obstacle in reverse and continues backward until the drive wheels contact the surface of the obstacle (Fig. 3.12a). The robot extends the lower hip mechanism until it contacts the ground (Fig. 3.12b). The stabiliser linkage is retracted causing the robot's overall COM to shift backwards (Fig. 3.12c). With the majority of the robot's weight acting over the lower hip mechanism, continued retraction of the stabiliser and rotation of the drive wheels enables the obstacle to be surmounted (Fig. 3.12d). With the obstacle mounted, it is free to resume a standing orientation and proceed with its task (Fig. 3.12e-3.12f).

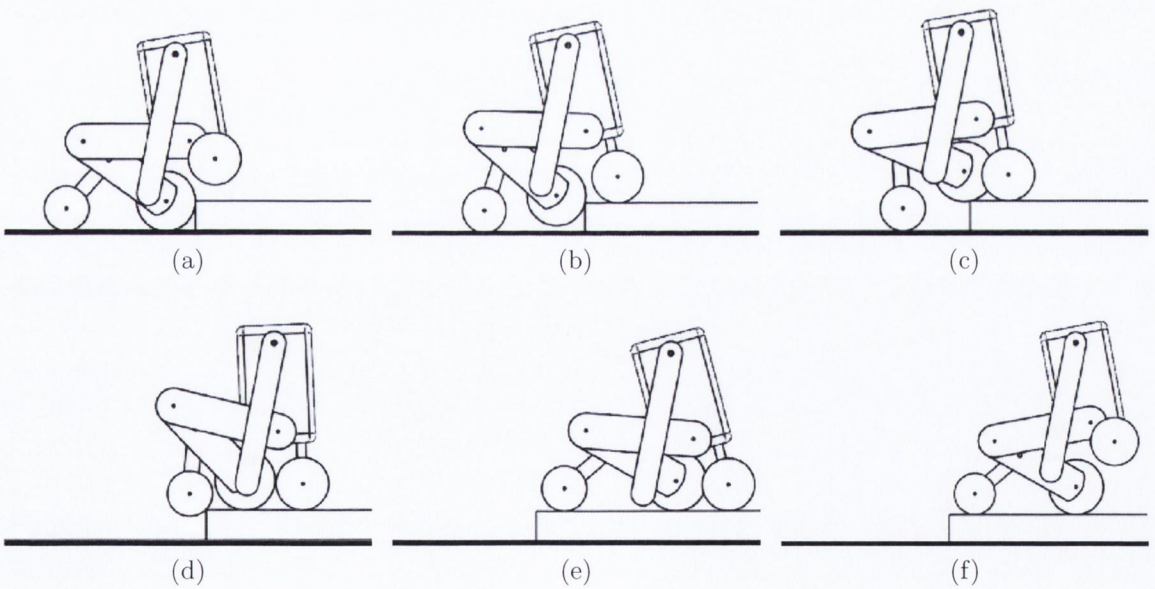


Figure 3.12: Sequence of actions required for traversing an obstacle

3.5.2 Ascending Stairs

The proposed morphology achieves stair-climbing through a repeated sequence of actions. These actions can be broken down into three distinct stages; the approach stage, cyclic stair-climbing stage and the recovery stage. This sequence of actions during the approach stage is illustrated in figure 3.13.

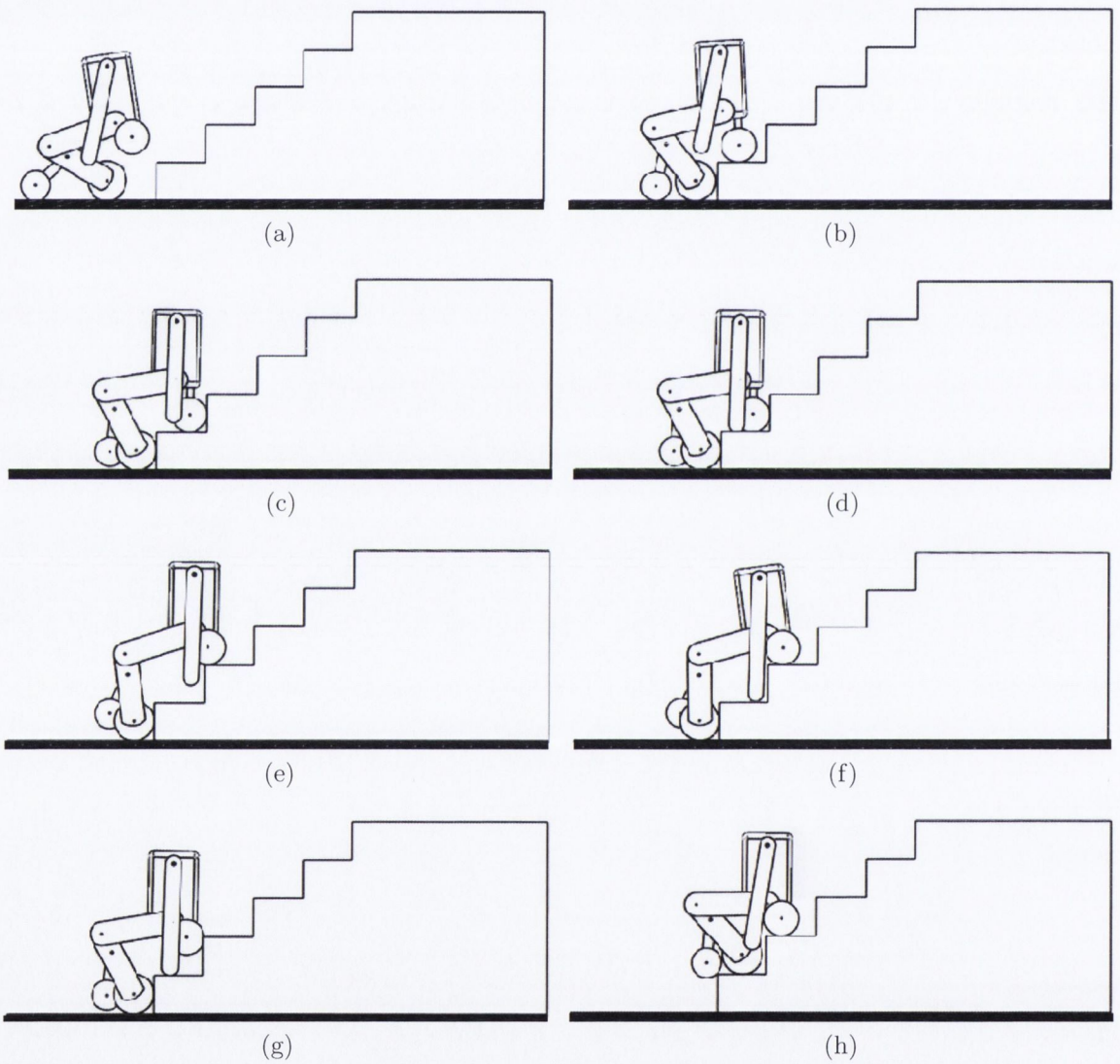


Figure 3.13: Sequence of actions describing the approach stage of stair climbing

The robot approaches the stairs in reverse orientation and upon the drive wheel contacting the first step, the LHM elongates until its wheels contact the stair tread (Fig. 3.13b). At this point the torso is straightened and the arms are positioned parallel to the stair riser. The arms are then elongated to their maximum length (Fig. 3.13d) and the lower torso

mechanism retracted such that the arms carry the load of the body. Once retracted the wheels on the LHM are likely to require a little more lift before they can overcome the stair. To provide this extra leverage, the knee joint is straightened and the LHM wheels are driven forward (Fig. 3.13e).

With two risers separating the LHM from the drive wheels, the next action involves lifting the shank above the stair nosing. This process starts by tilting the torso forward and extending the arms down to the free tread (Fig. 3.13h). This contact forms a tripod support between the body and the arms and provides a firm foundation to resist the overturning moment created when the shank is lifted. At this point the hip muscles are contracted. Any forward pitching is resisted by the arms thus the hip action lifts the thigh upwards. Through the combined action of the hip and arms, the shank rises and mounts the nosing (Fig. 3.14a).

The second stage involves a dual action process that is repeated until the landing is reached. The second stage of stair climbing is depicted in figure 3.14. The first stair climbing action of the cyclic stage commences with the shank wheel and LHM separated by just one riser. Similar to the first part of the approach stage, the robot lowers the LHM while it simultaneously extends the arms beneath it (Fig. 3.14c). Once the arms are fully extended, the LHM is retracted. The stair nosing is crossed through coordinated extension of the knee joint and rotation of the LHM wheels (Fig. 3.13d - 3.13e).

The second stair climbing action is identical to the second action of the approach stage. The torso is tilted forward while the arms are extended and onto the tread below. As the hip muscles contract, the arms resist any overturning/pitching moments ultimately causing the leg to lift (Fig. 3.14f). This action is maintained until the shank clears the nosing. This process is further aided through rotation of the drive wheels. By repeating the first and second actions iteratively, it is possible to ascend flights of any (practical) length. Furthermore since the robot has the ability self adjust (through skid-steering) its orientation/pose, small corrections in heading direction can be made on the fly during the process.

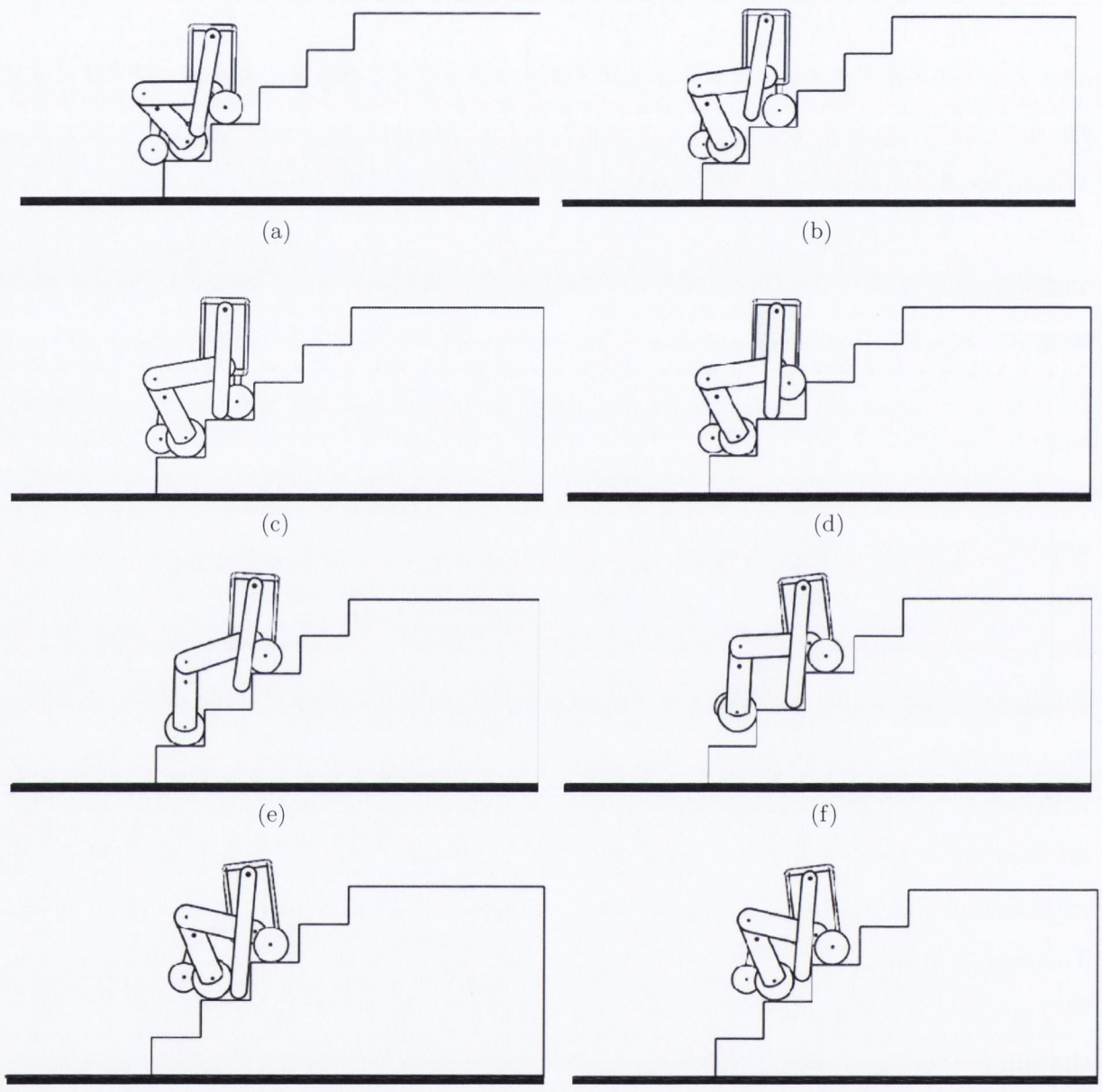


Figure 3.14: The repeated sequence of actions for stair ascent

The final stage in the stair climbing sequence involves mounting the final stair and to return to a standing orientation. This sequence of movements is shown in figure (3.15).

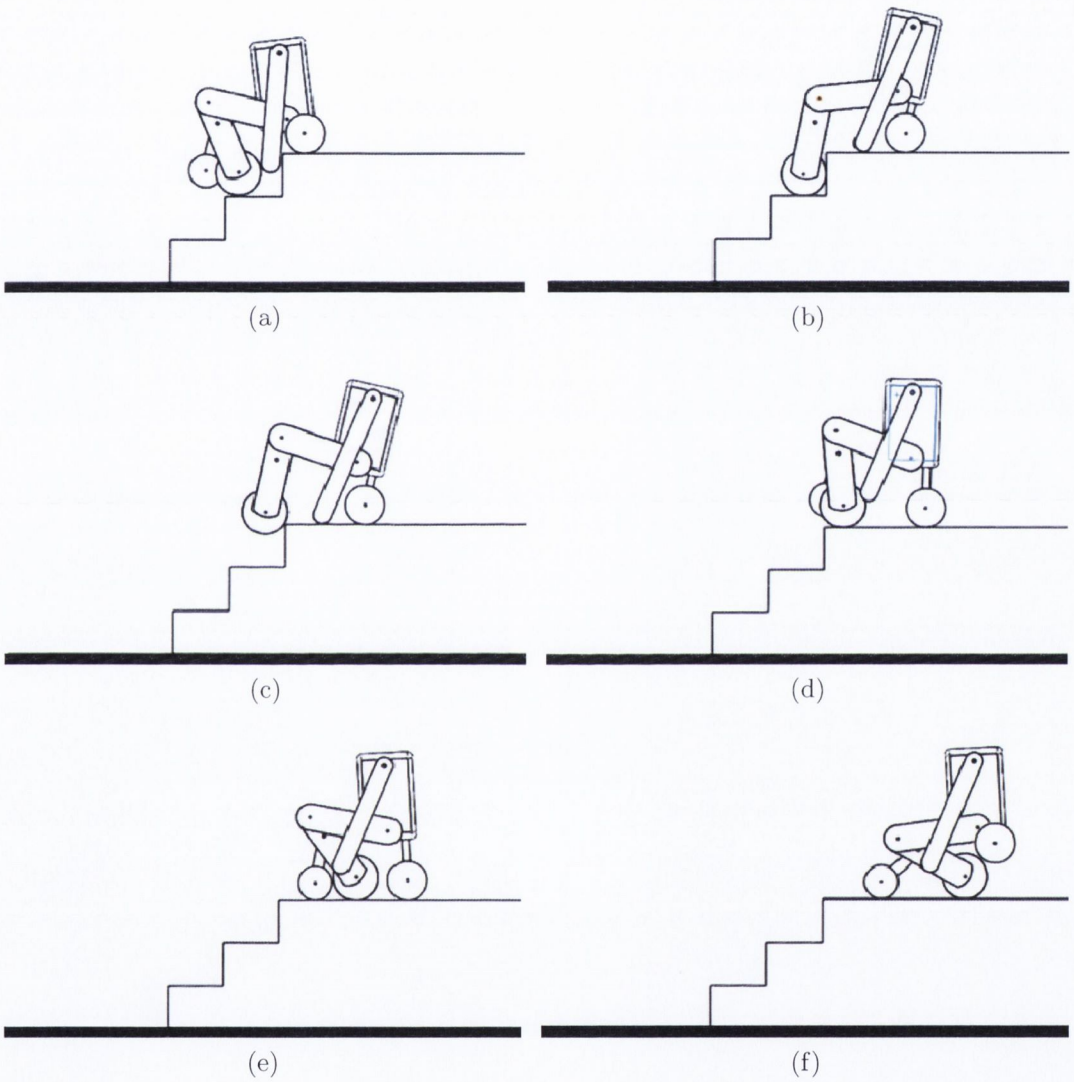


Figure 3.15: Pattern of actions that enable the robot to return to a standing position after climbing the last stair

Upon the torso mounting the last stair, the robot moves backwards and tilts its torso away from the stairway (Fig. 3.15b). The arms are then extended forwards until they contact the ground and form a support tripod with the torso (Fig. 3.15c). In this position, the hip actuators lift the thigh away from the stairs (Fig. 3.15d). This action pulls the shank over the last remaining riser. The shank drive wheels are rotated to provide increased traction during this process. To return to a standing position, an inverse kinematics algorithm

like that described in section 3.4.2 is used (Fig. 3.15e-3.15f).

3.5.3 Descending Stairs

In order to descend the stairs, a similar process to stair ascent (but in reverse) can be adapted. Like stair ascent, the process can be broken into discrete stages; the approach, cyclic stair climbing and landing. The approach is shown in figure 3.16.

The approach stage begins with the robot approaches the stairway in a skid-steered configuration, where the Lower Hip Mechanism (LHM) is extended to the floor (Fig. 3.16b). The arms are then elongated to the floor forming a tripod structural support with the torso (Fig. 3.16c). The shank is moved past the first nosing by driving the drive wheels in the shank and controlled by regulating the rotation of the shank at the knee knee joint (Fig. 3.16c-3.16d).

With a single riser separating the shank and the torso, the LHM is contracted fully and the arms are elongated such that they contact the stair below it, once again forming a support tripod with the torso (Fig. 3.16f). At this point the approach stage is completed.

Like the second stage of stair ascent, the second stage of stair descent involves the use of a cyclical dual action process. The first action of this process commences through by extending of the knee and rotating the the drive wheels forward. This action causes the shank to lower to the next stair (Fig. 3.16g). Once again, any forward pitching moments are resisted by the extended arms.

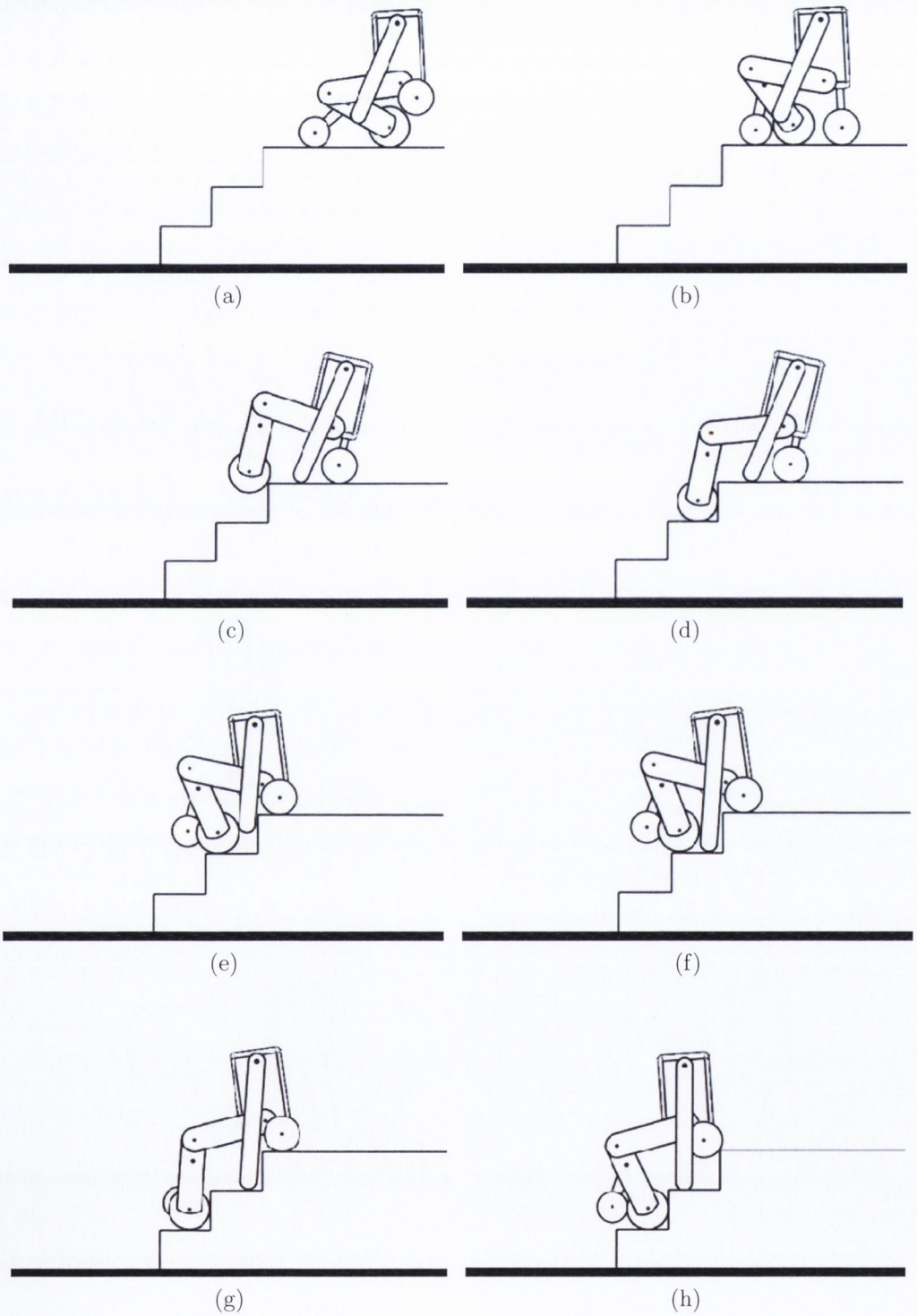


Figure 3.16: The repeated sequence of actions for stair descent

The second action of the cyclic stair descent stage starts with two risers separating the shank drive wheels from the body (Fig. 3.17b). Owing to the close similarity between this action and the landing/recovery stage, they are described together and illustrated in figure 3.17.

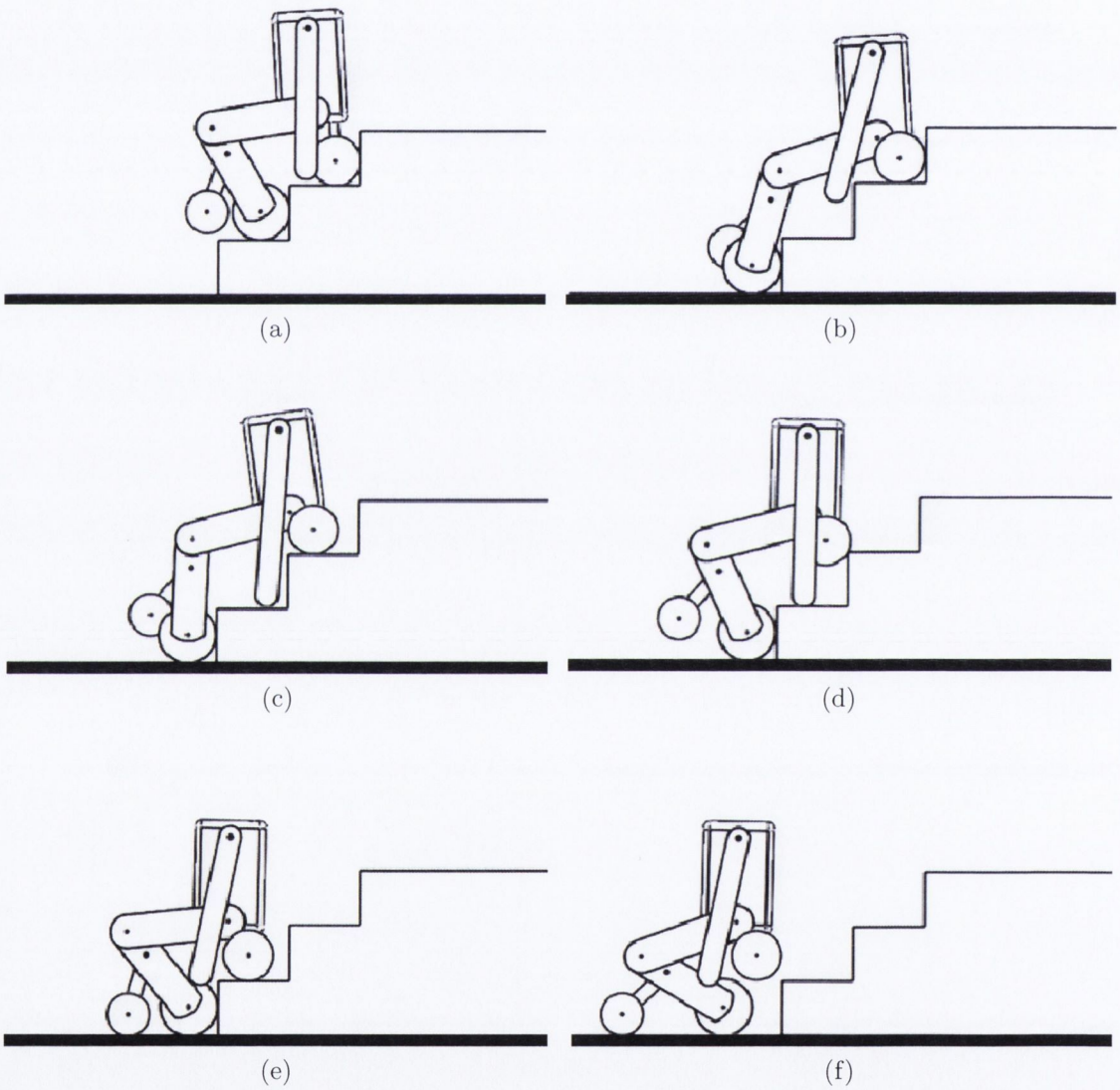


Figure 3.17: Pattern of actions that enable the robot to return to a standing position after climbing the last stair.

Firstly the arms extend and contacting the tread beneath, forming a tripod-like structure (Fig. 3.17c). The LHM wheels are then driven forward causing the torso to pivot about the shoulder. When the the centre-line of the LHM passes the nosing of the stair, a controlled contraction of the arm is commanded and causing gravity to slowly lower the

torso to the tread beneath (Fig. 3.17d).

When the shank wheels have descended the stairway and only one riser separates the shank from the torso, the landing action is performed. This simply involves leaning the torso forward and shifting the weight forward such that the robot's centre of mass moves forward and the stabiliser absorbs some of the robot's load (Fig. 3.17e). At this point, the knee can be straightened and the torso lifted from the stair (Fig. 3.17f). The second action and the descent are described graphically in figure 3.17.

3.5.4 Bridging Crevices

In addition to providing increased levels of stability and stair climbing ability, the lower hip mechanism provides a means of crossing gaps/crevices, a feat that few differentially driven platforms have the ability to accomplish. A graphical description of the process is shown in figure 3.18. Approaching the crevice, the robot elongates the LHM until its wheels contact the ground and a skid-steered form is adopted (Fig. 6.11b). In this configuration, the majority of the robot's mass is distributed between the driven wheels in the shank and LHM resulting in the reaction forces at the stabiliser-ground contact area being small. The stabiliser linkage is raised to ensure clearance while it crosses the gap (Fig. 6.11c). Once the gap is crossed, the stabiliser linkage is contracted until the drive wheels at the shank are lifted into the air (Fig. 6.11d). At this point, the actuated wheels in the lower hip assembly move the robot forward until the shank wheels have bridged the gap. Once this happens, the stability mechanism can be retracted and the robot can assume a standing posture (Fig. 6.11f).

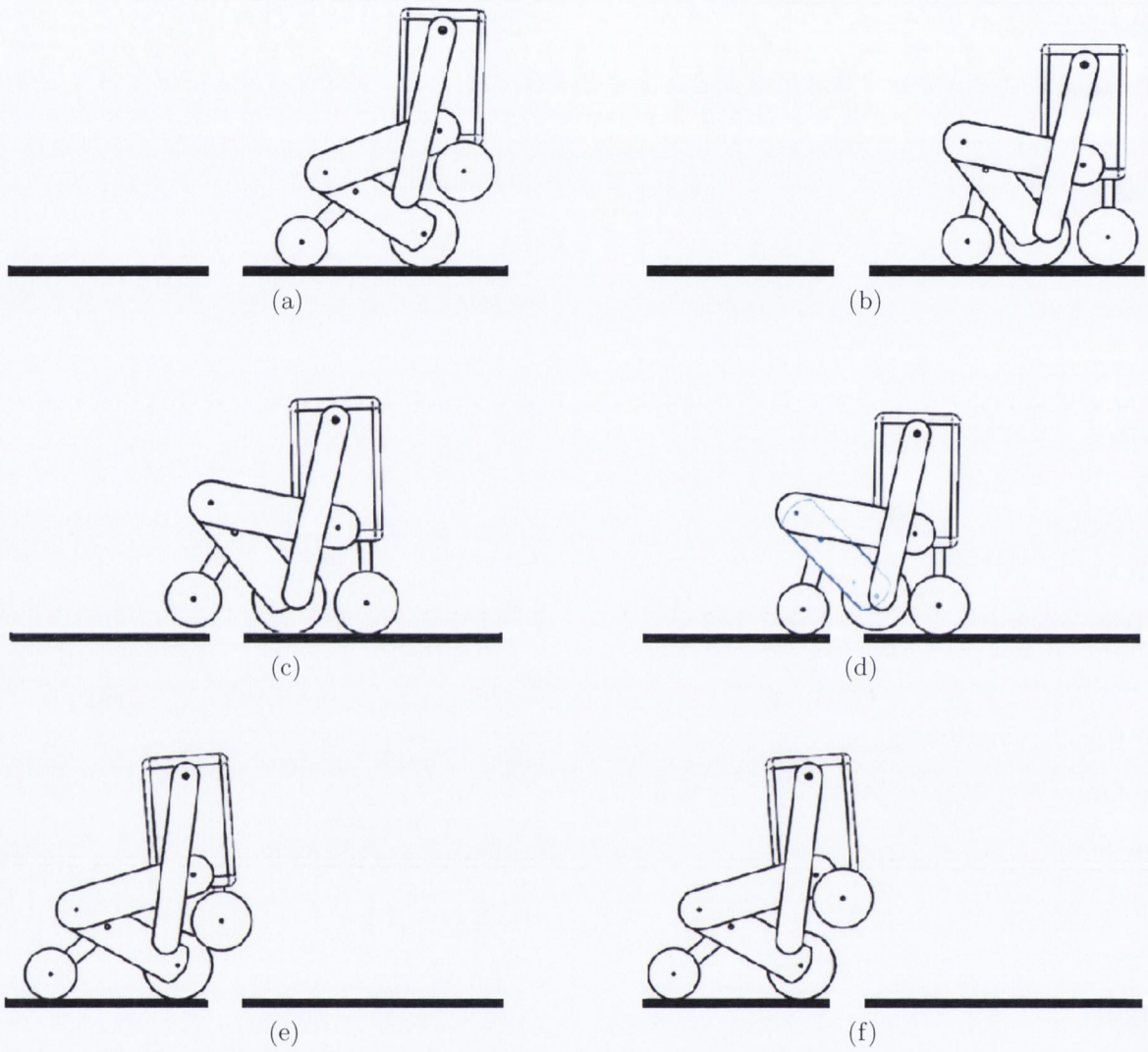


Figure 3.18: Sequence of actions required for crossing a crevice

Chapter 4

Embodiment Design

This chapter introduces the design requirements of the robot. Using data from a dynamic analysis, the mechanical design of the physical embodiment is presented and discussed in detail. A dedicated section is provided on actuation with particular focus on how the PAMs were designed to suit the kinematic and dynamic requirements of the morphology.

4.1 Prior Work

The design of the robot described in this work builds on a first prototype developed in 2013 [193] [194]. This first prototype hereby referred to as *v1.0*, possessed similar (albeit somewhat simpler) kinematics as well as a friendly, intuitively understood social interface. While it maintained morphological similarity to the next generation prototype (*v2.0*), its practical capability was significantly lower. Locomotion was practically limited to flat indoor environments and due to limitations in the electric drive system, it lacked the ability to generate the joint torques needed to achieve standing poses and other more dynamically demanding orientations. Complex manoeuvres such as crevice crossing and stair climbing were not possible and battery life was low due to an inefficient electric drive system. Images of the *v1.0* embodiment can be seen in Appendix B.

4.2 Physical/Performance metrics as Design targets

In order to demonstrate advancement and allow benchmarking of the embodiment against existing systems, a series of physical and performance based metrics were developed.

These targets were created not only to demonstrate the capability for high behavioural diversity but also to show high levels of physical compliance with the task environment. The following physical metrics were defined for the design of the proposed embodiment:

1. Overall mass < 35kg
2. Width < 650mm (for ease of access through doorways)
3. Can possess aspect ratio of at least 2.5 through adjustment of SSM [1]
4. Can possess vertical height of at least 1m
5. Minimum of 12 independently controlled degrees of freedom
6. Arm capable of extending to the ground
7. All limbs must possess high levels of compliance
8. Allow for the modular addition of sensors (hardware and software)
9. Possess adequate on-board power supply for both electronics and actuation systems
10. Have in-built safety features for controlled use during testing
11. Possess the capability for both on-board and off-board high level control
12. Possess a social interface

The following performance metrics were defined for the design of the proposed embodiment:

1. Can perform a zero-point turn
2. Statically stable locomotion in indoor environment
3. Can traverse over door sills and other small obstacles
4. Statically stable locomotion in outdoor environments
5. Can perform pick-and-place tasks between the ground and a raised surface
6. Can lean forward while retaining static stability
7. Can augment vertical height (minimum 2 inches) through modification of the robot's static stability margin
8. Can traverse intermediate sized obstacles (height $\geq$ drive wheel radius)
9. Can cross crevices (gap $\geq \frac{2}{3}$ omni-wheel radius)

[1] With a maximum aspect ratio of at 2.462, the PR-2 robot has the highest aspect ratio for a statically stable robot. Achieving an aspect ratio of 2.5 would mean that the proposed morphology would overtake the PR-2 and become the most slender statically stable mobile robot.

10. Can ascend stairs
11. Can descend stairs

4.3 Dynamic Analysis

Owing to its relatively high kinematic complexity, a dynamic analysis of the proposed robot morphology was was undertaken and has been incorporated into the embodiment presented in this work. Since the dynamic analysis preceded the embodiment design, its purpose was primarily to provide a qualitative description and quantitative estimate of the force/moment distribution throughout the robot's joints and in certain instances to provide an estimate of the force/torques required to achieve actuation.

4.3.1 Inverse Dynamic Analysis

The problem of determining joint forces/moments based on the inertial properties and kinematics of a mechanism is classified as 'inverse dynamics'. Assuming static stability and low limb velocities (negligible inertial effects due to joint accelerations), the joint forces and torques can be solved statically. In the proceeding subsections, the Joint Segment Method (JSM) was used to predict the joint forces and joint torques for various postural configurations and environmental interactions. The JSM is directionally dependent methodology which works through progressive application of the Newton-Euler equations from link to link throughout a kinematic chain [195]. Since the robot's limbs are constrained to move in the sagittal plane, a 2D analysis was performed. The free body diagrams associated with the robot's joint segments is given in figure 4.1.

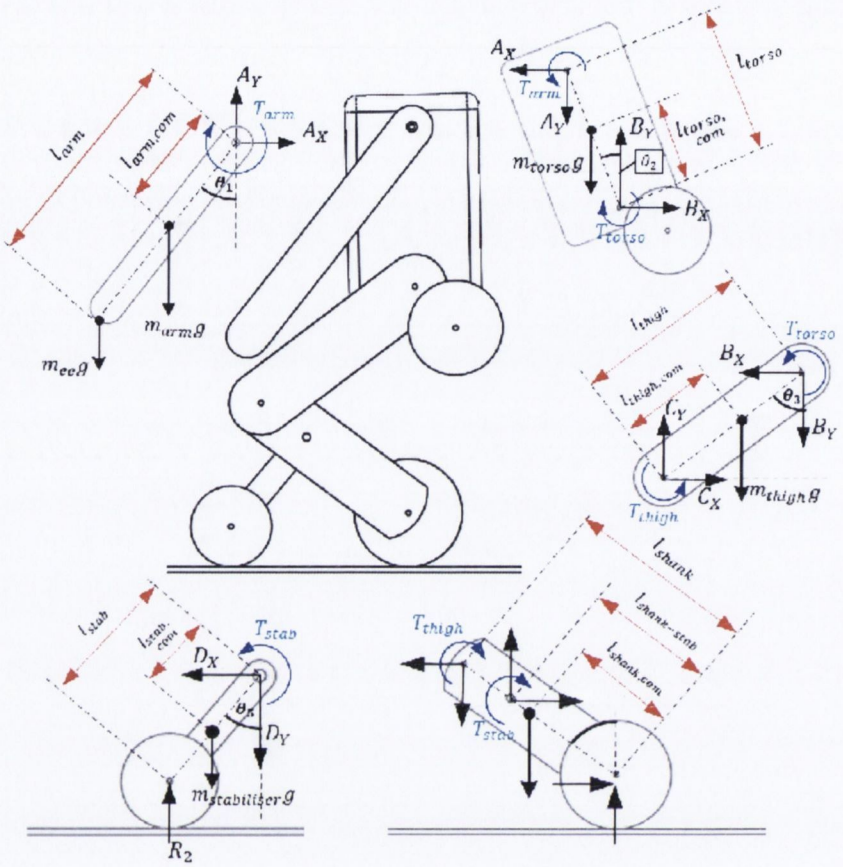


Figure 4.1: Free body diagram of the major limbs for standing poses

For a standing pose, the underlying conditions for joint equilibrium are given by:

$$\begin{bmatrix}
1 & 0 & 0 & 0 & 0 & 0 & 0 & 0 & 0 & 0 & 0 & 0 & 0 & 0 & 0 \\
0 & 1 & 0 & 0 & 0 & 0 & 0 & 0 & 0 & 0 & 0 & 0 & 0 & 0 & 0 \\
0 & 0 & -1 & 0 & 0 & 0 & 0 & 0 & 0 & 0 & 0 & 0 & 0 & 0 & 0 \\
-1 & 0 & 0 & 1 & 0 & 0 & 0 & 0 & 0 & 0 & 0 & 0 & 0 & 0 & 0 \\
0 & -1 & 0 & 0 & 1 & 0 & 0 & 0 & 0 & 0 & 0 & 0 & 0 & 0 & 0 \\
l_{torso}c\theta_2 & l_{torso}s\theta_2 & 1 & 0 & 0 & -1 & 0 & 0 & 0 & 0 & 0 & 0 & 0 & 0 & 0 \\
0 & 0 & 0 & -1 & 0 & 0 & 1 & 0 & 0 & 0 & 0 & 0 & 0 & 0 & 0 \\
0 & 0 & 0 & 0 & -1 & 0 & 0 & 1 & 0 & 0 & 0 & 0 & 0 & 0 & 0 \\
0 & 0 & 0 & l_{thigh}c\theta_3 & -l_{thigh}s\theta_3 & 1 & 0 & 0 & 1 & 0 & 0 & 0 & 0 & 0 & 0 \\
0 & 0 & 0 & 0 & 0 & 0 & -1 & 0 & 0 & 1 & 0 & 1 & 0 & 0 & 0 \\
0 & 0 & 0 & 0 & 0 & 0 & 0 & -1 & 0 & 0 & 1 & 0 & 1 & 0 & 0 \\
0 & 0 & 0 & 0 & 0 & 0 & l_{shank}c\theta_4 & l_{shank}s\theta_4 & -1 & -l'_{shank}c\theta_4 & -l'_{shank}s\theta_4 & 0 & 0 & 0 & -1 \\
0 & 0 & 0 & 0 & 0 & 0 & 0 & 0 & 0 & -1 & 0 & 0 & 0 & 0 & 0 \\
0 & 0 & 0 & 0 & 0 & 0 & 0 & 0 & 0 & 0 & -1 & 0 & 0 & 1 & 0 \\
0 & 0 & 0 & 0 & 0 & 0 & 0 & 0 & 0 & 0 & 0 & 0 & 0 & -l_{stab}s\theta_5 & 1
\end{bmatrix}
\begin{bmatrix}
A_x \\ A_y \\ T_{arm} \\ B_x \\ B_y \\ T_{torso} \\ C_x \\ C_y \\ T_{thigh} \\ D_x \\ D_y \\ R_1H \\ R_1V \\ R_2 \\ T_{stab}
\end{bmatrix}
=
\begin{bmatrix}
0 \\ m_{arm}g \\ -m_{arm}gl_{arm,com}s\theta_1 \\ 0 \\ m_{torso}g \\ -m_{torso}gl_{torso,com}s\theta_2 \\ 0 \\ m_{thigh}g \\ m_{thigh}gl_{thigh,com}s\theta_3 \\ 0 \\ m_{shank}g \\ -m_{shank}gl_{shank,com}s\theta_4 \\ 0 \\ m_{stab}g \\ -m_{stab}gl_{stab,com}s\theta_5
\end{bmatrix} \tag{4.1}$$

where $(l' = l_{shank-stab})$

4.3.2 Dynamic Analysis: Stair Climbing

Recall from section 3.5 that stair climbing (both ascent and descent) requires cyclic application of two distinct sequences of actions. Action #1 of stair climbing requires that the robot is capable of lifting the shank above the nosing located two risers away from the ground contact point of the LHM. To ensure static stability is maintained, the horizontal projection of the robot's COM must remain between the ground contact points of the arms and the LHM respectively (Fig. 4.2).

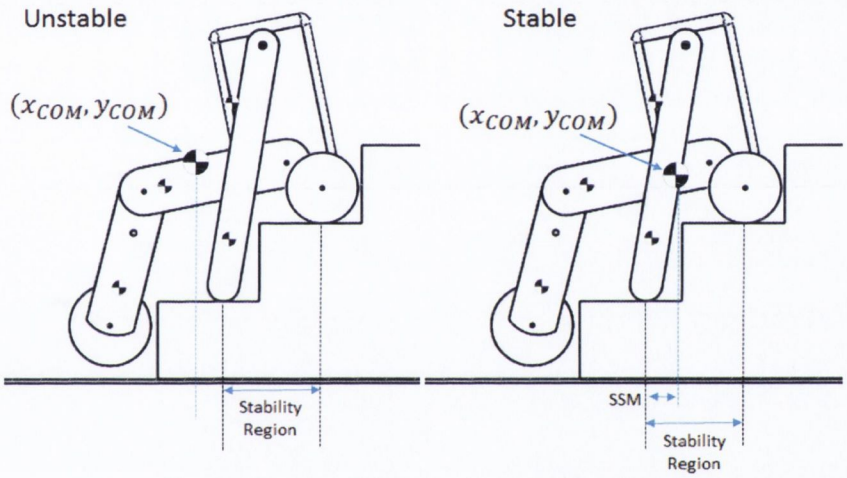


Figure 4.2: Static stability criteria for proposed morphology during stair-climbing

Using the segmental method (Eqn. 3.8), the overall COM of the robot can be computed from the cumulative position and centre of mass of each of the robot's limbs.

There are two distinct poses pertaining to action #2 of stair climbing that warrant further investigation. In the first instance, the LHM is extended and the knee straightened (Fig. 4.3). In this instance, the underlying conditions for joint equilibrium are given by:

$$\begin{bmatrix} 1 & 0 & 0 & 0 & 0 & 0 & 0 & 0 & 0 \\ 0 & 1 & 0 & 0 & 0 & 0 & 0 & 0 & 0 \\ 0 & 0 & -1 & 0 & 0 & 0 & 0 & 0 & 0 \\ -1 & 0 & 0 & 1 & 0 & 0 & 0 & 0 & 0 \\ 0 & -1 & 0 & 0 & 1 & 1 & 0 & 0 & 0 \\ 0 & 0 & 1 & -l_{torso}c\theta 3 & -l_{torso}s(\theta 3) & \sqrt{(w^2+h^2)}s(\theta_3+\beta) & 0 & 0 & -1 \\ 0 & 0 & 0 & -1 & 0 & 0 & 1 & 0 & 0 \\ 0 & 0 & 0 & 0 & -1 & 0 & 0 & 1 & 0 \\ 0 & 0 & 0 & 0 & 0 & 0 & l_{arm}c\theta_4 & -l_{arm}s\theta_4 & 1 \end{bmatrix} \begin{bmatrix} B_x \\ B_y \\ T_{thigh} \\ A_x \\ A_y \\ R_2 \\ R_{1h} \\ R_{1v} \\ T_{arm} \end{bmatrix} = \begin{bmatrix} 0 \\ g(m_{thigh}+m_{shank}+m_{wheels}) \\ -\nabla \\ 0 \\ m_{torso}g \\ -m_{torso}gl_{torso,com}s\theta_3 \\ 0 \\ m_{arm}g \\ -m_{arm}gl_{arm,com}s\theta_4 \end{bmatrix} \tag{4.2}$$

where $\left(\nabla = gm_{thigh}\left(\frac{l_{thigh}}{2}s\theta_1\right) + gm_{shank}\left(l_{thigh}s\theta_1 + \frac{l_{shank}}{2}s\theta_2\right) + gm_{wheel}\left(l_{thigh}s\theta_1 + l_{shank}s\theta_2\right)\right.$

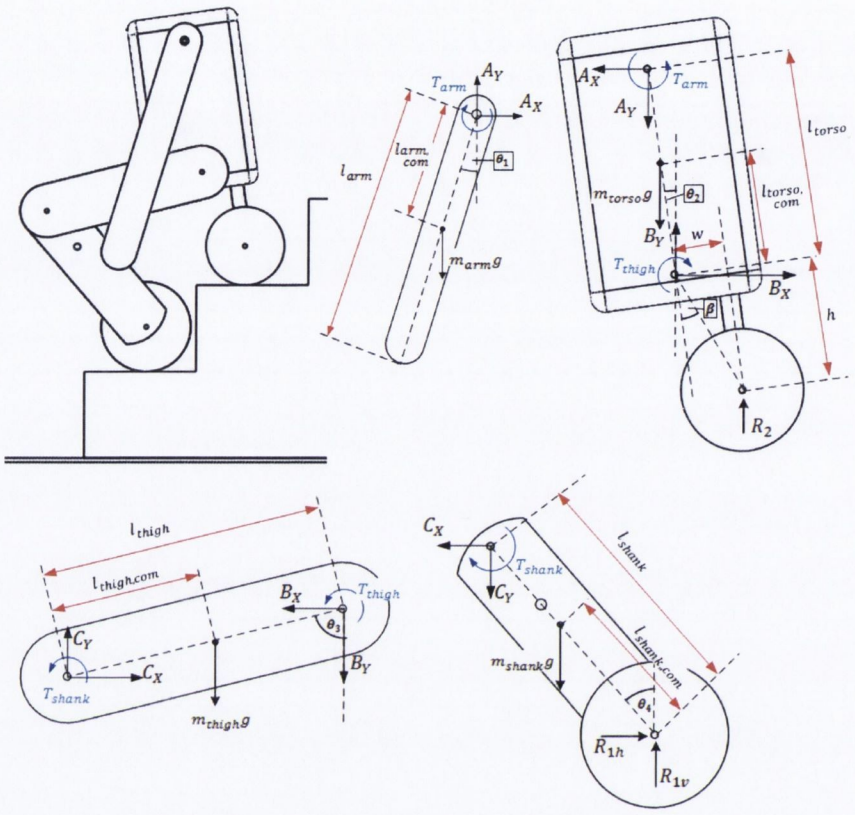


Figure 4.3: Free body diagram of the major limbs during stair climbing (Robot at rest on stair)

In the second pose of interest in action #2, the mass of the torso is transferred from the LHM to the arms which are extended beneath it (Fig. 4.4). In this pose, the underlying conditions for joint equilibrium are given by:

$$\begin{bmatrix} -1 & 0 & 0 & 0 & 0 & 0 & 0 & 0 & 0 & 0 & 0 & 0 \\ 0 & -1 & 1 & 0 & 0 & 0 & 0 & 0 & 0 & 0 & 0 & 0 \\ 0 & 0 & l_{arm}s\theta_1 & -1 & 0 & 0 & 0 & 0 & 0 & 0 & 0 & 0 \\ 1 & 0 & 0 & 0 & 1 & 0 & 0 & 0 & 0 & 0 & 0 & 0 \\ 0 & 1 & 0 & 0 & 0 & 1 & 0 & 0 & 0 & 0 & 0 & 0 \\ -l_{torso}c\theta_2 & l_{torso}s\theta_2 & 0 & 1 & 0 & 0 & -1 & 0 & 0 & 0 & 0 & 0 \\ 0 & 0 & 0 & 0 & -1 & 0 & 0 & 1 & 0 & 0 & 0 & 0 \\ 0 & 0 & 0 & 0 & 0 & -1 & 0 & 0 & 1 & 0 & 0 & 0 \\ 0 & 0 & 0 & 0 & l_{thigh}c\theta_3 & -l_{thigh}s\theta_3 & 1 & 0 & 0 & 1 & 0 & 0 \\ 0 & 0 & 0 & 0 & 0 & 0 & 0 & -1 & 0 & 0 & 1 & 0 \\ 0 & 0 & 0 & 0 & 0 & 0 & 0 & 0 & -1 & 0 & 0 & 1 \\ 0 & 0 & 0 & 0 & 0 & 0 & 0 & l_{shank}c\theta_4 & l_{shank}s\theta_4 & -1 & 0 & 0 \end{bmatrix} \begin{bmatrix} A_x \\ A_y \\ R_2 \\ T_{arm} \\ B_x \\ B_y \\ T_{thigh} \\ C_x \\ C_y \\ T_{shank} \\ R_{1H} \\ R_{1V} \end{bmatrix} = \begin{bmatrix} 0 \\ m_{arm}g \\ m_{arm}gl_{arm,com}s\theta_1 \\ 0 \\ m_{torso}g \\ -m_{torso}gl_{torso,com}s\theta_2 \\ 0 \\ m_{thigh}g \\ m_{thigh}gl_{thigh,com}s\theta_3 \\ 0 \\ m_{shank}g \\ -m_{shank}gl_{shank,com}s\theta_4 \end{bmatrix} \tag{4.3}$$

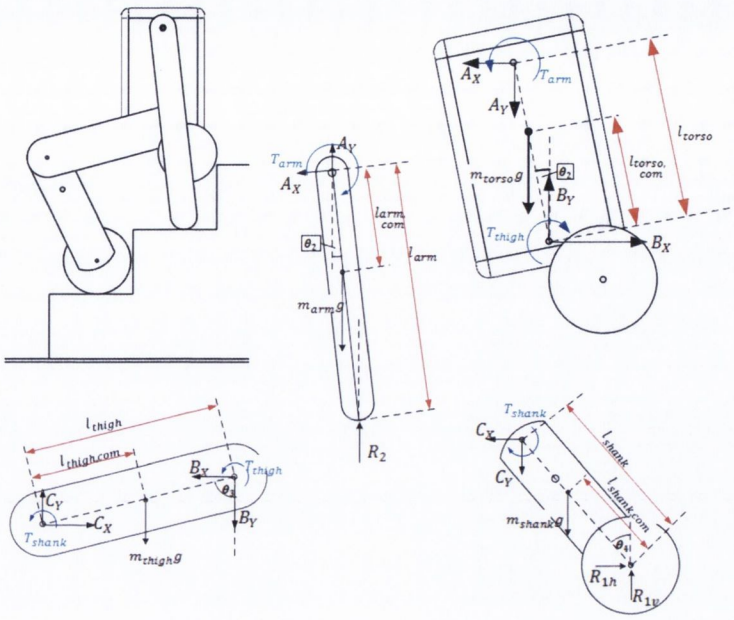


Figure 4.4: Free body diagram of the major limbs during stair climbing (Robot ascending nosing)

4.4 Leg Design

The legs consist of three limbs; the shank, the stabiliser and the thigh (Fig. 4.5). Two differentially driven wheels are attached at the base of the shank and provide the primary ground contact point. A hollow cylindrical rod, called the 'knee joint', is located at the top of the shank. In addition to physically connecting the shank and thigh assemblies, the knee joint adds lateral stability and is used to mount cable driven pulleys used to actuate the knee and stabiliser joints. The stabiliser joint, located near the top of the shank, is is coplanar with and realised using a similar embodiment to the knee joint. Efforts have been made to minimise the mass of the leg in order to reduce the torque requirements of the hip during the leg lift phase (action #2) of the stair climbing gait.



(a) (b) (c)

Figure 4.5: Design of the lower body assemblies (a)shank assembly (b) stabiliser assembly (c) thigh assembly (pneumatic air muscles omitted)

4.4.1 The Shank

Two highly geared DC drive motor units are mounted in the middle of the shank. Actuation of the drive wheels is decoupled from the drive motors through a tensioned timing-belt system. Decoupling the motors from the wheels facilitates gearing, simplifies assembly/disassembly and prevents shocks/vibration being transmitted from the drive wheels to the motor drive shafts. Further damping is achieved through the use of two 8in pneumatic drive wheels. Using these pneumatic wheels reduces vibration and since their tractive properties can be tuned simply by adjusting their internal pressures, they can be tuned in response to the terrain requirements. The walls of the shank are made from 20mm PVC sheet plastic. To reduce mass, cut-outs are introduced in low-stress regions. Not only does this material offer high levels of stiffness and fracture toughness (in comparison with equivalent plastics), but its also highly machinable and its density is approximately half that of aluminium making it a lightweight solution. The use of a lightweight plastic with high thickness was favoured over a stiffer (but heavier) metal with lower thickness for several reasons. Firstly the added thickness dramatically cut down on the number of mechanical fixtures (i.e. nuts, washers) needed to mount the shank components. Secondly a thicker material allowed for electronic pcb boards to be mounted securely and unobstructively within recesses cut in the plastic. Finally the added thickness facilitated wider bearings to be used to support the joints. These wider bearings could only be incorporated on more slender side supports through the integration of additional structural components and thus a more complex overall design. An inertial measurement unit (IMU)

is attached at the top of the shank, in close proximity to knee joint. Wires connecting the shank to the torso are neatly fed through the cylindrical knee joint and along the thigh.

4.4.2 The Stabiliser

The stabiliser mechanism is a pulley-driven linkage which provides the robot with increased stability in the sagittal plane. Two aluminium linkages cut from sheet aluminium are rigidly fixed on either side of a cable driven pulley located in the centre of the stabiliser joint. Rotation of this pulley causes a proportional change in the orientation of the stabiliser linkage. At the opposite end of the linkage, two passive omni-directional wheels are mounted. These wheels generate negligible rolling and lateral resistance due to internal bearings in the hub and small passive rollers located along the perimeter. An inertial measurement unit (IMU) is attached at the top of the stabiliser linkage, in close proximity to its centre of rotation.

4.4.3 The Thigh

The side walls of the thigh are made from of 8mm PVC sheet plastic reinforced with 3mm sheet aluminium. In this embodiment, the thickness of the plastic eliminates the need for bolt fixtures and provides a secure means to friction-fit both the bearings at the knee joint and the carbon fibre tubes that laterally reinforce the assembly. The aluminium composite layer adds increased stiffness to the structure such that weight reducing cut-outs in the plastic can be made without compromising the limbs overall integrity. Custom brackets mounted to the carbon fibre tubes house the PAMs that connect to the knee and stabiliser joints. An inertial measurement unit (IMU) is attached at the base of the thigh, in close proximity to knee joint.

4.4.4 Leg Geometry

The dimensions of the legs are influenced by two important factors. Firstly the legs must be long enough such that the robot possesses the ability to significantly augment its height while remaining statically stable. The second factor to affect the leg geometry is the

ability to climb stairs. Since a longer leg length increases the torque requirement of the hip during the leg lift phase of the stairclimbing gait (action #2), it is desirable to minimise the sum of the shank and thigh lengths. Additionally smaller limb lengths are desirable as they reduce the torque requirements of the knee joint when it's required to support the mass of the upper body during standing modes. Since the range of orientations of the limbs are constrained by their width and the positions relative to the stair geometry, the optimisation is not straightforward.

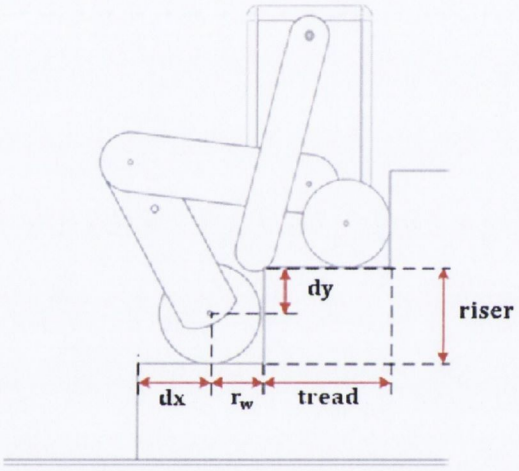


Figure 4.6: Geometry of stairs with respect to the robot during stair climbing

Using the solver add-on in Microsoft Excel, an optimisation study was undertaken which sought to find the smallest suitable limb lengths that would enable the robot to climb stairs. As the optimisation was an inherently non-linear one, the NRG Non-linear method was deemed most suitable. In order to ensure that the robot is capable of climbing stairways in both residential and non-residential buildings, the optimisation process was performed using the most demanding stair geometry in accordance with the IRC regulations (riser height = 196mm, tread length = 254mm). The geometry of the stairs with respect to the robot is illustrated in figure 4.6 while the robot's leg geometry during stair-climbing is presented in figure 4.7. It is noted that since the shank and the thigh have considerable thickness, the range of acceptable joint angles is practically constrained by the stair geometry (Fig. 4.8).

The optimisation problem is stated as:

Objective: Find values of (l_1, l_2) such to minimise $|l_1 + l_2|$

Subject to the following constraints:

1. $l_1 cos\theta_1 + l_2 cos\beta_1 = \sqrt{X_1^2 + Y_1^2}$
2. $l_1 sin\theta_1 = l_2 sin\beta_1$
3. $\pi - \theta_1 - \beta_1 > 0$
4. $\theta_1 >= \theta_{min}$
5. $\beta_1 >= \beta_{min}$
6. $l_2 cos\beta_2 + l_2 cos\theta_2 = \sqrt{X_2^2 + Y_2^2}$
7. $l_1 sin\theta_2 = l_2 sin\beta_2$
8. $l_2 > l_1$
9. $\pi - \theta_2 - \beta_2 > 0$
10. $\theta_2 >= \theta_{min}$
11. $\beta_2 >= \beta_{min}$

where:

$$\theta_{min} = \left[tan^{-1}\left(\frac{dy}{r_w}\right) - \psi\right] + \left[sin^{-1}\left(\frac{t}{\sqrt{dy^2 + r_w^2}}\right)\right]$$

$$\beta_{min} = \left[tan^{-1}\left(\frac{dx}{r_w}\right) - \phi\right] + \left[sin^{-1}\left(\frac{t}{\sqrt{dx^2 + r_w^2}}\right)\right]$$

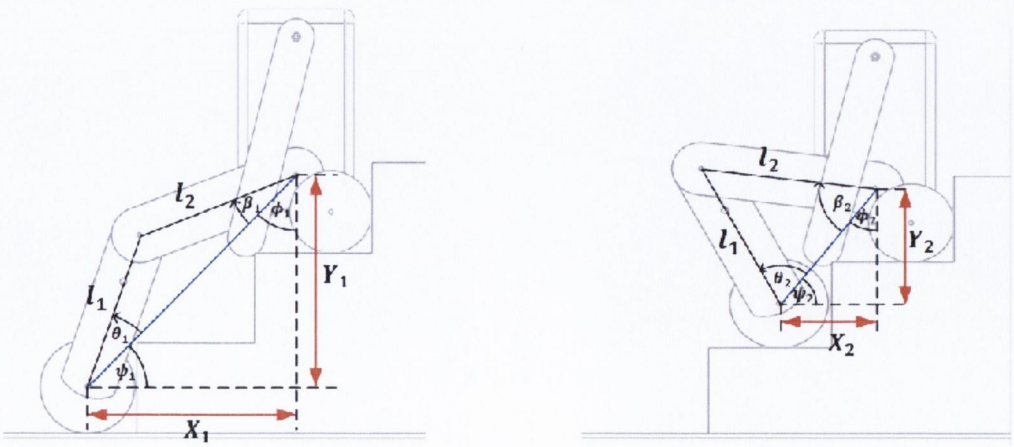
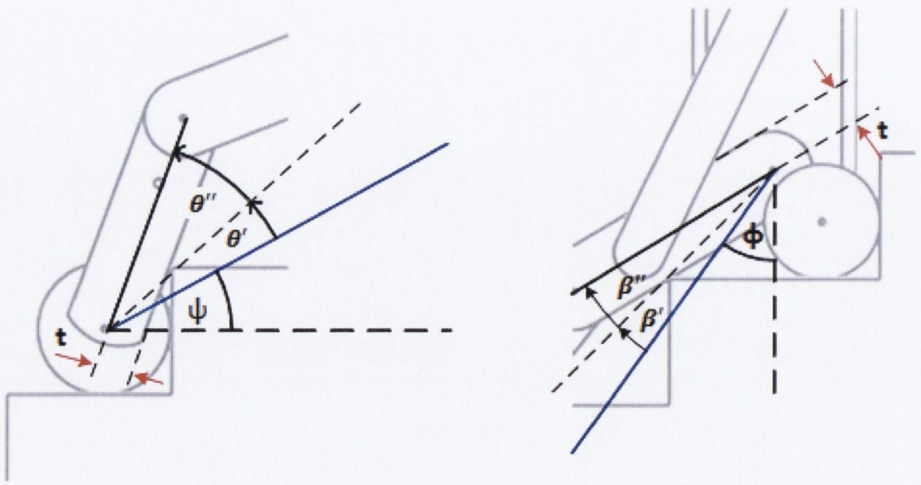


Figure 4.7: Geometry of legs during stair climbing

4.5 Design of Torso and Lower Hip Mechanism

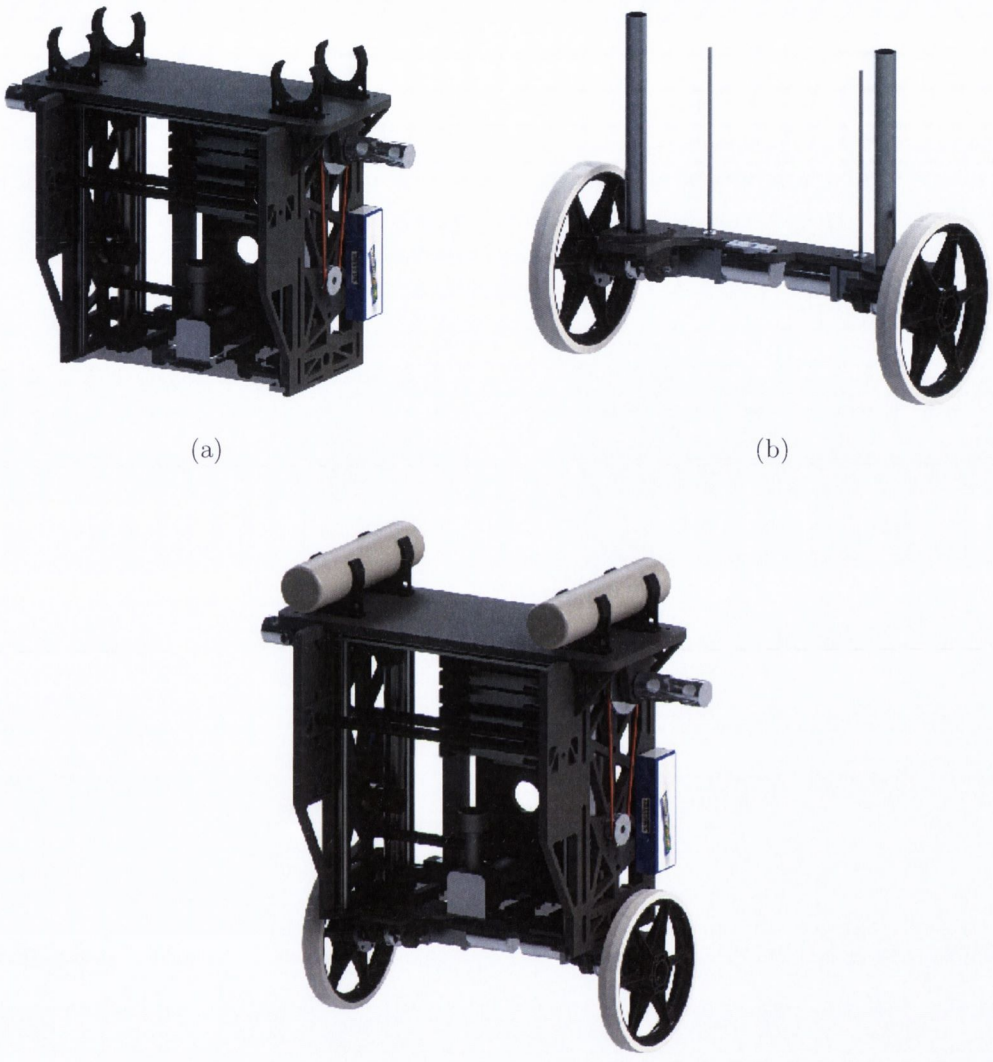
The upper body of the robot contains the four primary components; the torso, the lower hip mechanism (LHM) and two arms (Fig. 4.9). The majority of the robot's mass is located in the upper body and LHM. Although high mass in the torso increases the torque requirements of the knee actuator, it has the benefit of reducing the torque requirements at the hip during stair climbing and dampening the destabilising effect caused by retracting the stabiliser and extending the knee. The torso houses an on-board air compressor, two 14.8V 4000mAhr Lipo batteries, an aluminium pneumatic valve manifold with eight solenoid controlled valves, two DC gearmotors, a pneumatic pressure regulator, a pressure release lever, two plastic air tanks and two pneumatic linear actuators which connect to the LHM. The torso's structure consists of two plastic side panels reinforced by a metallic frame (aluminium strut - 20x20mm section). These plastic supports are made from 12mm PVC sheet plastic and were machined to size using a CNC milling process. A top panel, termed the 'shoulder plate' is meshed with the frame and side panels and is used to mount the electronics. Three hollow carbon fibre tubes are installed to provide increased lateral rigidity and to provide mounting supports for the PAMs that actuate the hip joint.

The shoulders are actuated using a round belt-drive system which connects the DC gearmotors in the torso with an aluminium shoulder joint. A round belt was favoured over



(a) (b)

Figure 4.8: Geometric constraints on leg angles during stair climbing



(a) (b)

(c)

Figure 4.9: Design of the upper body (a) torso (b) lower hip mechanism (LHM) (c) torso with LHM attached (pneumatic air muscles omitted)

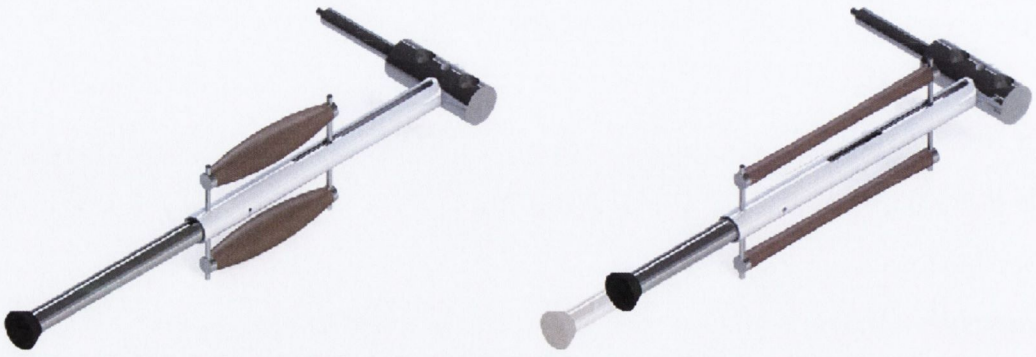
a timing belt since it will slip under a smaller load, a compliant characteristic that is desirable in such a joint.

The lower hip mechanism assembly consists of a metallic plate which houses two drive wheel assemblies. Each assembly contains a DC gearmotor, an eight inch rubber wheel and a timing belt drive mechanism. The belt drive mechanism serves to both protect the motor drive unit from shocks/vibration but also to ensure a more efficient use of space. The lower hip mechanism is linearly connected to the torso at four points; two attached to the pneumatic linear actuators in the torso and other two attached to hollow telescoping

support tubes. Wires connecting the LHM to the torso pass through these tubes, avoiding tangling or other mechanical interference.

4.6 Design of Arms

In its present embodiment, the arms possess only two degrees of freedom; one rotational at the shoulder and one prismatic at the elbow. To facilitate prismatic motion, the arm is comprised of two concentric overlapping tubes, the larger of which is rigidly mounted to the shoulder joint. In this configuration, the smaller of the tubes is constrained to perform linear telescoping motion. Care was taken to reduce the length of the arm in order to reduce the overall torque required at the shoulder. A CAD model of the arm is given in figure 4.10. A length of elastic is stretched from the shoulder joint to the end effector to ensure that the arm is naturally contracted. Two PAMs are mounted on each arm and implemented such that their contraction causes the arm to elongate (Fig. 4.10). In the present configuration, the arms are capable of elongating by approximately 10cm under the action of the PAMs. At the base of the arm is a rubber gripper that was originally designed to provide grip for manual walking aids. An IMU is located in close proximity of the rotational axis of the shoulder joint and calculates the angular orientation of the arm. The pneumatic tubes supplying power to the arms are connected to the valve manifold located in the torso.



(a) (b)

Figure 4.10: Design of the arm (a) arm extended when muscle is contracted (b) arm retracted when muscle is at environmental pressure (note: image not drawn to scale)

4.7 Actuation

As discussed in 2.3.4, pneumatic air muscles (PAMs) provide a simple, low-cost, powerful, easily customisable, compliant actuation solution for use on robots. It was for these reasons that they are used as the actuator of choice for the stabiliser, knee, hip and elbow joints. As the drive wheels (in the shank and LHM) and the joints in the shoulder require more accurate, continuous control and require less torque, electric drives were favoured in these locations. In the present configuration, the shank drive wheels use a 12V 188:1 DC planetary geared motor unit by AndyMark. The motors used to control the shoulders are 12V 270:1 DC planetary gear motor distributed by RobotShop. The wheels in the LHM are driven by a 256:1 planetary geared motor unit by Banebots. A full partlist is given in Appendix C.

Since the McKibben air muscle is relatively easily constructed and its performance has been well studied, it was deemed the most suitable air muscle to use on the robot. After a period of testing combinations of muscle components, the muscle which was ultimately adopted on the robot included flexible silicon tubing (12mm OD, 1mm wall thickness), braided nylon mesh (12mm ID) from TechFlex and custom made aluminium stoppers with 6mm push fit connectors for connection to pneumatic tubing. Steel hose clips were used to bind the mesh and silicon tubing to the stoppers. In the stabiliser, knee and hip joint, an antagonistic configuration was chosen. The antagonistic muscle configuration achieves actuation through the linear contraction of two counteracting muscles (Fig. 2.11).

4.7.1 Characterisation of McKibben Air Muscle

Owing to the high level of actuator customisation required, custom-made actuators were developed in-house rather than acquiring commercially available air muscles that were physically less suited. The first step in determining the number of actuators to use was to characterise the performance of the custom-made muscles. While several studies have attempted to model and characterise the behaviour of McKibben muscles [85], significant deviations (up to 15 percent) [196] have been observed between predictions and real-world data using these models. For this reason a series of experiments were conducted to evaluate the actual performance of the muscles used on the robot. More specifically,

these tests were conducted to investigate how the contraction of the muscle varied with respect to both load and default muscle length. Measured at pressures ranging from 0-100psi (6.9bar), the contraction of muscles of three default lengths (100mm*, 150mm and 200mm*) was measured subject to incremental loading. Each experiment was repeated three times to ensure consistency. The results of these experiments are tabulated in table 4.1 and charted in figure 4.11.

Contraction @ 100psi (relative to length at 0 psi)			
	100mm*	150mm	200mm*
0 N	24.56%	26.00%	22.36%
23.96 N	27.53%	28.33%	29.01%
33.78 N	26.10%	27.33%	29.05%
43.48 N	25.62%	28.05%	28.15%
53.32 N	25.53%	27.44%	27.83%

Contraction @ 80psi (relative to length at 0 psi)			
	100mm*	150mm	200mm*
0 N	23.86%	26.00%	21.51%
23.96 N	26.78%	27.13%	28.17%
33.78 N	25.11%	26.09%	27.85%
43.48 N	24.56%	27.44%	26.80%
53.32 N	24.07%	26.22%	26.71%

Contraction @ 60psi (relative to length at 0 psi)			
	100mm*	150mm	200mm*
0 N	22.98%	24.67%	20.92%
23.96 N	25.64%	25.52%	26.73%
33.78 N	23.16%	25.05%	26.20%
43.48 N	22.59%	25.30%	25.00%
53.32 N	22.28%	23.88%	24.26%

Contraction @ 20psi (relative to length at 0 psi)			
	100mm*	150mm	200mm*
0 N	17.44%	18.22%	15.22%
23.96 N	15.02%	15.31%	16.40%
33.78 N	11.86%	12.84%	14.19%
43.48 N	9.29%	11.48%	11.41%
53.32 N	8.62%	9.55%	9.82%

Table 4.1: Mechanical properties of pneumatic air muscles used on robot

The data indicates that for loads of approximately 50N, the contraction produced at 80psi is approximately equivalent to that produced at 100psi. For this reason the maximum working pressure of the muscles in the system was designed for 80psi. A key observation is that the achieved overall contraction as a percentage of initial length is greater for pre-tensioned than initially relaxed muscles. This characteristic can be attributed to stretching effect caused by the load which effectively lengthens the muscle but is later recovered during contraction. To emulate this effect on the muscles used on the robot, they were manually pre-tensioned until they stretched to approximately 5% of their total length. The tests confirmed that the pressure needed to achieve muscle contraction is proportional to the load acting on the muscle. Thus as the load increases, the pressure required to achieve contraction increases. It was found experimentally that for the designed muscles, the operating pressure should be kept below 90psi as higher pressures tended to accelerate the rate of muscle wear and increase the probability of leakages occurring.

* Using the in-house fabrication process, it was not possible to reliably manufacture muscle actuators to 1mm accuracy. The 100mm and 200mm muscles referenced in these experiments actually measured 95mm and 195mm respectively.

To ensure safe working pressures for actuation, several PAMs were installed in parallel allowing the total actuation force to distribute across the muscles.

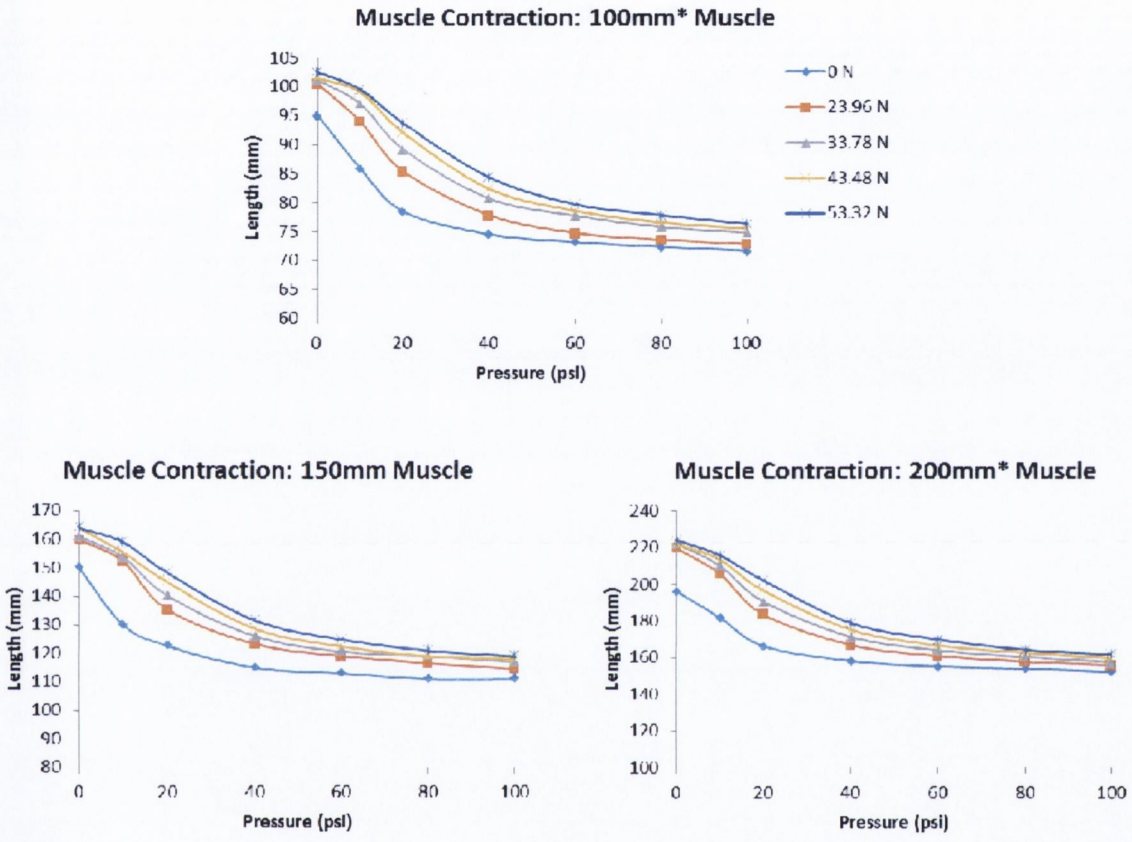
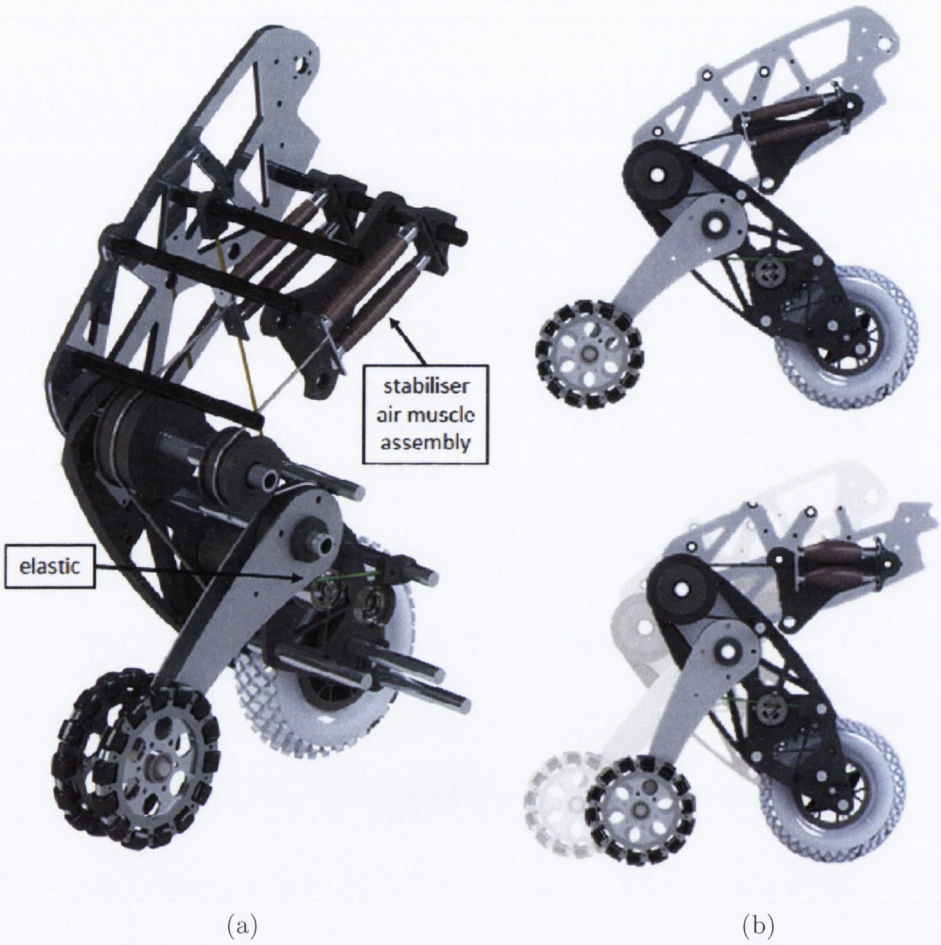


Figure 4.11: Muscle Contraction data for various muscle lengths

4.7.2 Actuation of Stabiliser Joint

The PAM which actuates the stabiliser joint is connected to a mounting bracket in the thigh and to a steel cable which runs from the PAM to a cable tensioner in the stabiliser assembly (Fig. 4.12). A pulley is used at the stabiliser joint to maximise the torque transmitted at the joint. With prior knowledge of the PAM contraction rates, the desired range of joint rotation and the maximum permissible length of the PAM, it is possible to design for the pulley of largest radius using eqn. 4.4. It was determined from a geometric analysis that the required stabiliser angle rotation ($\Delta\theta_{stab}$) was 90°.

$$\Delta l_{muscle} = r\Delta\theta_{muscle} r = \frac{\Delta l_{muscle}}{\Delta\theta_{muscle}} \tag{4.4}$$



(a) (b)

Figure 4.12: Design of the stabiliser actuation system (a) labelled cross section of assembly (b) action of stabiliser muscle assembly (note: image not drawn to scale)

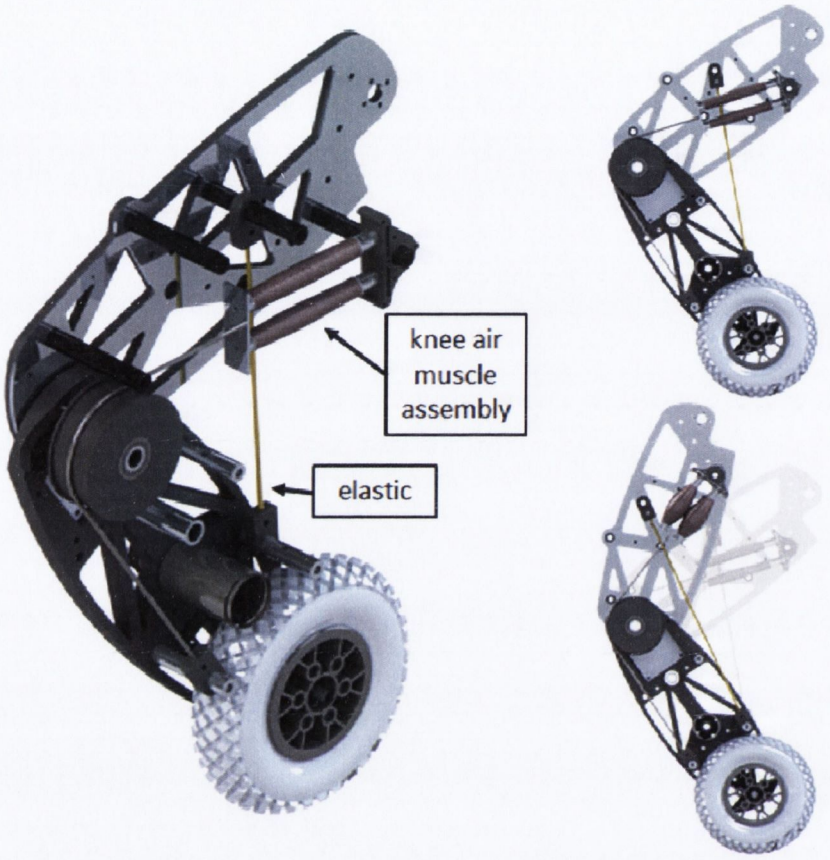
The stabiliser angle is physically constrained to remain within its operating range by the aluminium knee joint and a similar sized aluminium bar that laterally spans the shank. The reaction force at the ground contact point of the stabiliser (i.e. at the omni-wheel) generates a large clockwise torque about the stabiliser joint axis. For this reason just one PAM assembly (acting in the counter-clockwise direction) is used to actuate the joint. This design eliminates the need for an additional muscle and the more complex antagonistic configuration that would otherwise be required to ensure reliable joint control. Using the predicted torques in the joints from the dynamic analysis as a guide, four PAMs were installed to control the stabiliser joint. To retain antagonistic properties without additional control complexity, a linear spring is fitted in the place of the omitted PAM such that antagonistic behaviour can be realised in postural configurations where the

stabiliser linkage is not in contact with the ground. To limit the forces in the stabiliser muscles during periods of rest/high stability (i.e. periods when the stabiliser angle is at a maximum), the stabiliser muscle cable is tensioned such that when the stabiliser linkage is in contact with the aluminium knee bar, the cable is in low tension and the resisting moment is primarily provided by the mechanically rigid knee joint.

4.7.3 Actuation of Knee

The PAM which actuates the knee joint is connected to a mounting bracket in the thigh and to a steel cable which runs from the PAM to a cable tensioner in the shank assembly (Fig. 4.13). A pulley is used at the knee joint to maximise the torque transmitted at the joint. With prior knowledge of the PAM contraction rates, the desired range of rotation of the joint and the maximum permissible length of the PAM, it is possible to design for the pulley of largest radius using eqn. 4.4. It was determined from a geometric analysis that the required angle rotation ($\Delta\theta_{knee}$) was 130°.

Since controllability in both directions is required and as gravity may not be able to provide the actuation force necessary in all cases, an antagonistic configuration is implemented. Using the predicted torques in the joints from the dynamic analysis as a guide, eight PAMs (four located either side of the stabiliser) were installed to enable the straightening of the knee joint. As the required restoring forces are low due the robot's mass and the effects of gravity, a passive elasticated cable was implemented. Using this passive means of actuation further reduces the complexity (mechanical and control) of the system, cuts down on the number of valves needed for actuation and helps conserve compressed air stored in the on-board tanks.



(a) (b)

Figure 4.13: Design of the knee actuation system (a) labelled cross section of assembly (b) action of knee muscle assembly (note: image not drawn to scale)

4.7.4 Actuation of the Hip Joint

The PAMs which actuate the hip joint are mounted to brackets in the thigh and connected to similar brackets within the torso assembly. Since controllability is required in both directions, an antagonistic configuration was designed and implemented. To ensure a large torque was transmitted at the joint by the muscles, the point of action of the PAM was offset from the joint axis. This distance is practicality limited by the volume occupied by the robot. To ensure a torque arm large enough to lift the legs during step/stair climbing, an additional muscle was installed higher up in the torso which is capable of delivering more torque. The positioning of these muscles is shown graphically in figure 4.14.

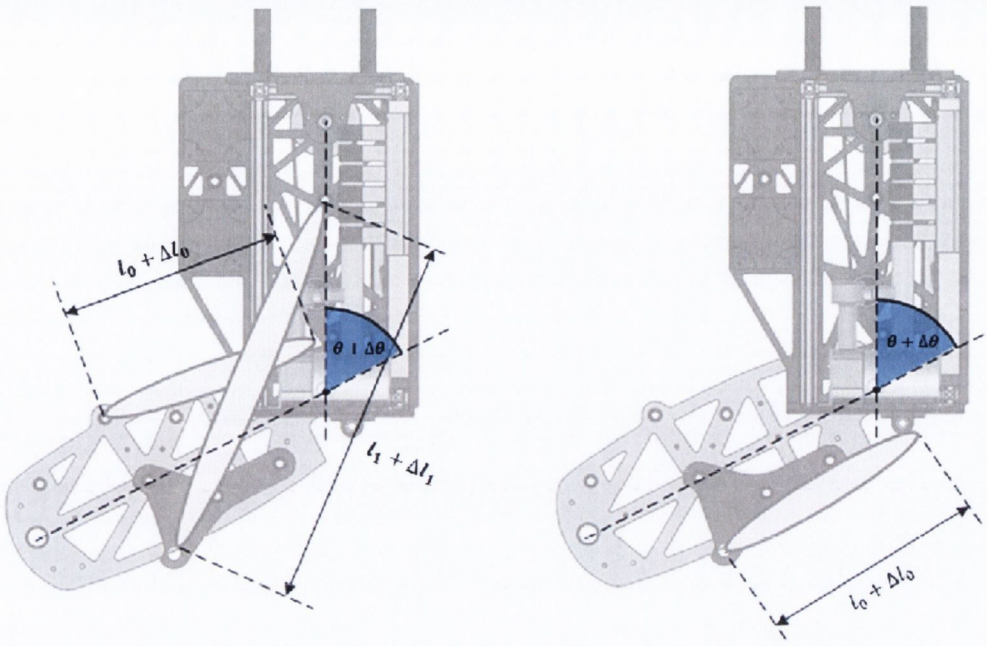


Figure 4.14: Antagonistic muscle configuration in the Hip

Antagonistic Muscles in the Hip

When designing the antagonistic muscle configuration in the hip, care was taken to ensure that contraction of one antagonistic muscle did not cause overextension of the opposing muscle. This was achieved through the design of a system which ensured that both muscles were of equal default length and configured symmetrically about the axis bisecting the thigh when the thigh is centred within its range of rotation. Due to the mechanical complexity of the embodiment's design, suitable mounting locations in both the torso and thigh are severely limited. To reduce the required actuation force, it is desirable to mount the PAMs at a fixed distance from the hip joint such that a large torque is developed upon contraction of the muscle. It is observed that the size of the available torque arm is restricted primary by the limited space beneath the hip joint where it is possible to mount a PAM. A final observation is that the torque applied at the joint due to PAM contraction is not constant across the full range of joint rotations. It is observed that the torque will vary with the thigh-torso angle.

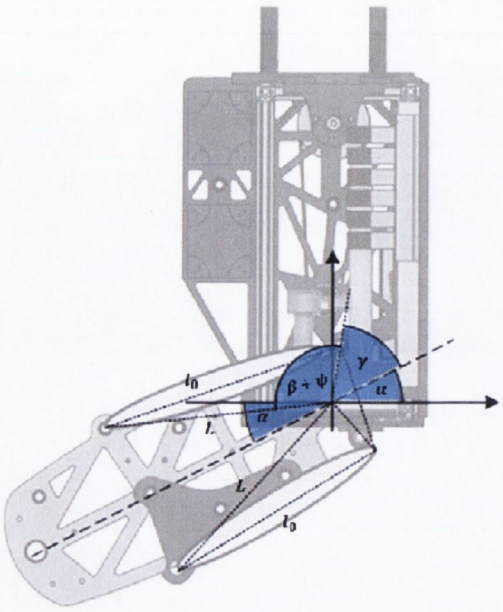


Figure 4.15: Design variables for antagonistic hip muscle configuration

The locations of the muscle mounting points in the torso were determined by finding the furthest location beneath the hip joint that it was practical to mount a muscle. The corresponding muscle mounting point was determined by mirroring this point about the axis bisecting the thigh when the thigh-torso angle was mid-range. An optimisation study was conducted to determine the most suitable locations to mount the muscles in the thigh and to determine the corresponding muscle lengths required to achieve a rotation of 75°(determined from a geometric analysis). This optimisation was conducted using the 'GRG non-linear' solver add-on in Microsoft Excel.

The optimisation problem is stated as:

Objective: Find values of (β, L) such that $\left(\frac{l_1}{l_2}\right) = \left(\frac{0.875l_0}{1.125l_0}\right) = 0.78$

Subject to the following constraints:

1. $l_1 <= l_2$
2. $Lsin\zeta < \frac{w_{thigh}}{2}$

where the following relationships hold:

1. $\delta = \gamma + \alpha$
2. $\zeta = 2\pi - \alpha - (\beta + \psi) - \gamma$
3. $l_1^2 = z^2 + L^2 - 2zLcos\beta$
4. $l_2^2 = z^2 + L^2 - 2zL\left[cos\beta cos(2\psi) - sin\beta sin(2\psi)\right]$
5. $\frac{l_1}{l_2} = \left(\frac{\sqrt{z^2+L^2-2zLcos\beta}}{\sqrt{z^2+L^2-2zL[cos\beta cos(2\psi)-sin\beta sin(2\psi)]}}\right)$

As the torque required to rotate the torso about the legs is relatively low, a passive elasticated cable was installed on the embodiment as the preferred means of connecting the underside of the thigh to the torso. Using this passive means of actuation further reduces the complexity (mechanical and control) of the system, cuts down on the number of valves needed for actuation and helps conserve compressed air stored in the on-board tanks.

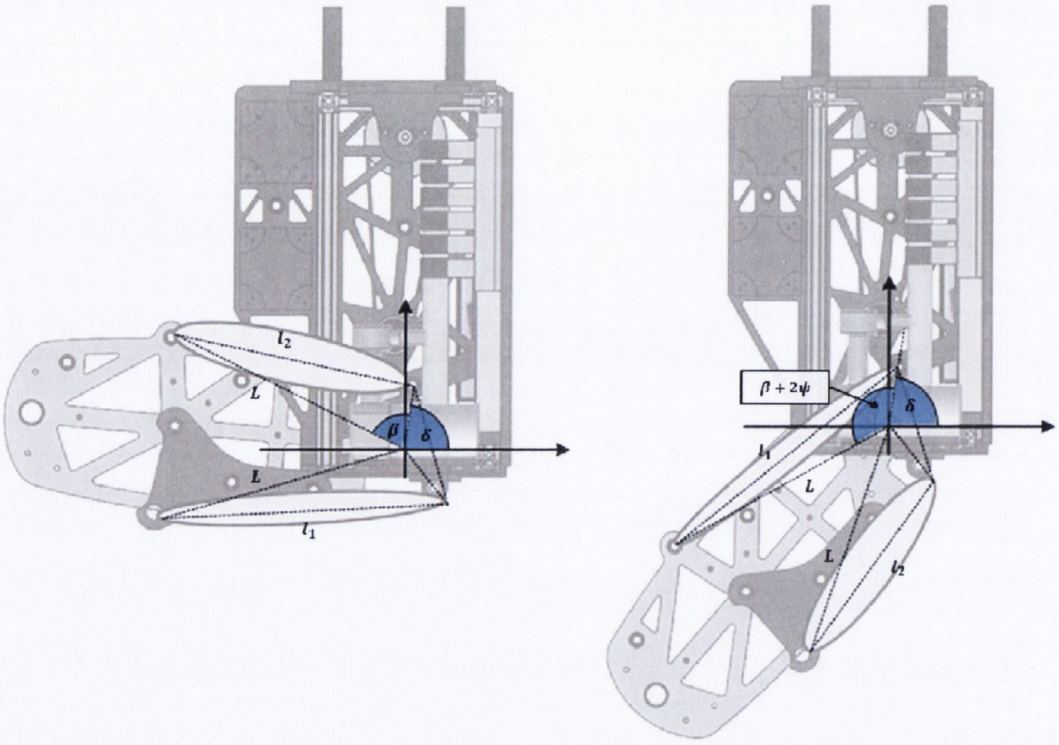


Figure 4.16: Variability of pneumatic muscle length over the range of hip rotation for hip muscles

Additional Hip Muscle

The primary role of the additional hip muscle is to provide the extra torque required to lift the shank and stabiliser above the stair riser during stair climbing. Therefore it is designed to possess a large torque arm and to be located in a position that ensured it will deliver a large torque regardless of the thigh-torso angle. The location of the muscle mounting point in the thigh was chosen to coincide with an existing muscle mount which already possessed a large offset from the hip joint and with an unobstructed path to the torso. Once again an optimisation study was undertaken in Microsoft Excel using the 'GRG non-linear' solving function to determine the location in the torso to mount the muscle and the required muscle length such that it could operate across the range of joint rotations. The primary constraints for this solver related to the relatively small volume of space that was available inside the torso to mount the muscle.

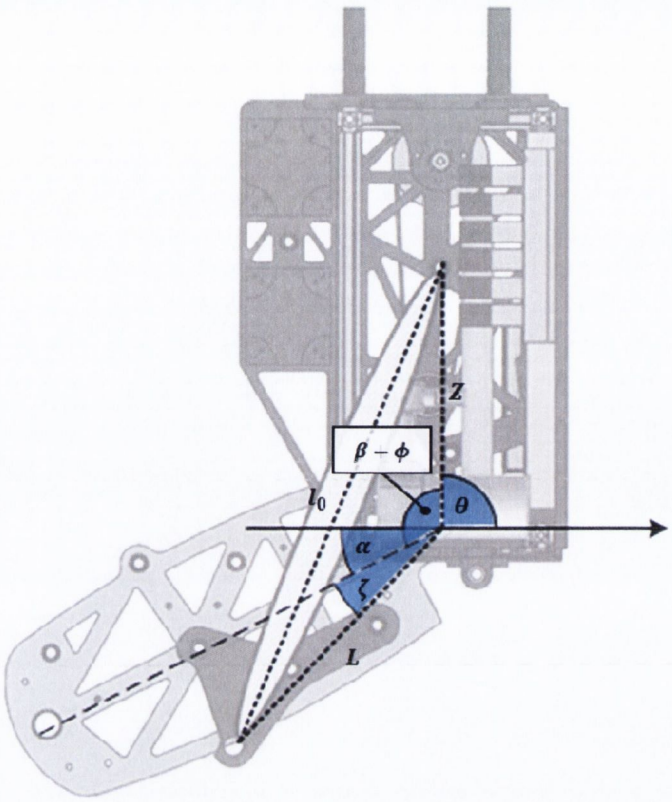


Figure 4.17: Design variables for additional hip muscle configuration

The optimisation problem is stated as:

Objective: Find values of (β, L) such that $\left(\frac{l_1}{l_2}\right) = \left(\frac{0.875l_0}{1.125l_0}\right) = 0.78$

Subject to the following constraints:

1. $l_1 \leq l_2$
2. $\beta \geq 0.3$
3. $0 \leq zcos\theta <= 70$
4. $zsin\theta \geq 200$

where the following relationships hold:

1. $\theta = \pi - \beta - (\phi - \alpha)$
2. $l_1^2 = L^2 + z^2 - 2Lzcos(\beta + \zeta)$
3. $l_2^2 = L^2 + z^2 - 2Lzcos(\beta + \zeta + 2\psi)$

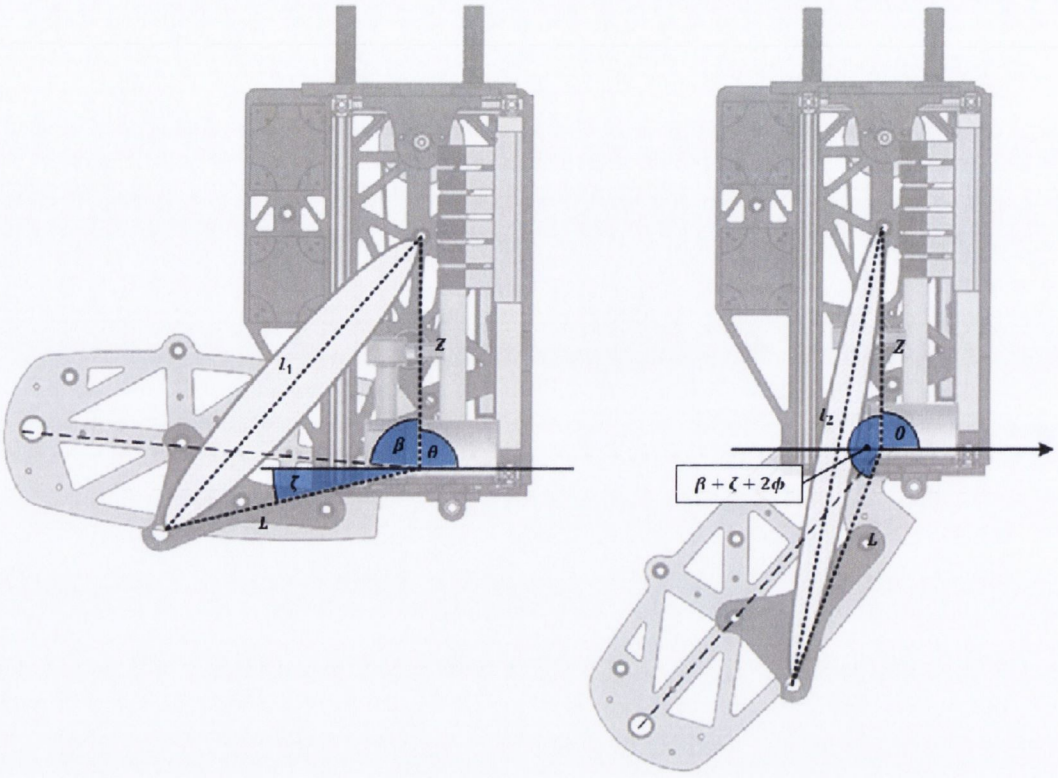


Figure 4.18: Variability of pneumatic muscle length over the range of hip rotation for additional hip muscle

Chapter 5

Sensing and Control

This chapter describes the development of the control architecture deployed on the robot. Particular attention is given to how low-level control is attained. The robot's sensing capability is described with special focus given to proprioception, the process of ascertaining the values of its internal states. The means through which the robot can interact with people is discussed with particular focus given to the design and implementation of a novel semi-autonomous controller.

5.1 Robot Control Architecture

High behavioural diversity is an emergent property which arises from complex interaction between a system and its operating environment. While the robot's morphology plays a critical role in the realisation of complex behaviour, so too does the robot's control schema. For robots to autonomously perform tasks, they require the ability to perceive and extract information from the environment after which they must perform actions. As discussed in section 2.1, these actions are typically either reflex-based or deliberative. In the former instance, control is inherently reactive and arises in direct response to a stimulus (i.e. modifying the wheel velocities of a self-balancing robot in response to its angular displacement from the vertical). In the latter case, control is higher level process where the performance of the controller is measured over longer periods of time and requires increased levels of planning and environmental perception (i.e. navigation between rooms in a house, picking up an object from the ground etc.).

Recall from the three-constituent principle outlined in section 3.1 that the desired be-

haviour, the task environment(s) and the embodied morphology form the three fundamental considerations in the design of an 'intelligent' agent. In an abstract sense the control architecture can be described as the physical embodiment of the coupling between the morphology and realisation of desired behaviours. In practical terms, it represents the manner through which the system's control systems operate and the configuration through which the system's sensors, electronics, computers and actuators are connected.

Robots built using conventional top-down approaches have the advantage that the exact sensing, control and actuation requirements can be accurately predicted explicitly at the beginning of the design process. As robots developed using a bottom-up approach must be capable of high adaptability and are often subjected large degrees of design iteration, it is often not possible to accurately anticipate the exact performance requirements in advance. In such instances, system traits such as modularity, reconfigurability, redundancy and expandability are especially desirable. In order to integrate these traits into a system architecture, it is proposed that a holistic system-level design approach is needed whereby the design of the architecture is tightly coupled with both the mechanical design of the physical embodiment and the range of its desired behaviours. In other words, the physical design of a given morphological embodiment (joint/link positions, sensing/actuation requirements, suitable mounting locations, mass distribution etc.) as well as the type of tasks that the robot should perform should all factor into the design and configuration of the architecture.

It is observed from the literature that the majority of state-of-the-art mobile robot platforms achieve high-level modularity through utilisation of dedicated middlewares such as ROS [10], YARP [11], OROCOS etc. Typically implemented on conventional linux-based PC computers, dedicated robotic middlewares enable software modularity as they facilitate a wide range of generic software libraries (OpenCV, PCL, ODE etc.)and specific program functions to be easily downloaded and configured to control a robot. Furthermore these middlewares can operate across a distributed network of computers thus allowing for reconfigurability and expandability. Despite these advantages, these middlewares are (typically) not built for real-time performance, have bad inter operating system compat-

ibility and possess poor integrated hardware support. This bad hardware support makes connecting the robot's high level controllers (typically in form of PCs) to its low-level controllers (typically in the from of microcontrollers/SBCs), especially when the low-level system is responsible for performing perception and meeting real-time control requirements.

The novelty of the proposed architecture lies mostly in its distributed form and the system-wide modularity it possesses. The architecture is innately distributed as it uses a distributed network of computers (controlling both low and high level functionality) which can be located both on and off-board the robot. The architecture is divided into two tiered structures; one tier containing computational modules dedicated to tasks pertaining to low-level control and the second containing modules dedicated to high-level control. Within both tiers, each computational module is configured in a 'loosely coupled' fashion, responsible in isolation for it's own specific function(s) but also capable interacting with other modules in the tier to perform tasks etc. Modules can be connected directly to sensors/actuators and adding them within each tier can be done in an almost ad-hoc manner. Computation modules are connected in parallel within in each tier and communicate with each other across a common bus using a generic tier-specific API. A second, different API is responsible for maintaining communication between tiers. A dedicated computer module located in the low-level control tier is responsible for controlling the bidirectional flow of information between tiers. As the inter-tier data communication API is implemented in a generic way independent of any specific software, high levels of hardware/software reconfigurability can be achieved without any discernible loss in the architecture's generality. Additionally as this API is innately lightweight, it can be modified/added to in accordance with the functional requirements of the system.

5.1.1 Overview of Architecture

The proposed architecture can be described as a two-tiered system separated into low and high-level partitions. A simplified graphical representation of the architecture is

presented in figure 5.1. The architecture developed in this work proposes that tasks requiring reflex-based, real-time control (balancing, stabilisation during stair climbing etc.) are most appropriately accomplished on dedicated hardware capable of implementing reliable feedback control with minimal human intervention. The lower tier, or Low Level System (LLS), contains the on-board hardware required for performing all low-level data acquisition and control tasks. Low bandwidth data acquisition (encoder readings, IMU values etc.) is accomplished through the use of multiple interconnected general-purpose input/output (GPIO) modules distributed throughout the robot. These GPIO modules can be designed to possess a range of form factors and capabilities such that they can be embedded appropriately throughout the system. A dedicated computer, hereby referred to as the Specialist Computation module (SCM), is used to process data from high bandwidth sensors (cameras, laser scanners etc.). Once processed, all sensory information from the GPIO modules and SCM is then passed to the 'master' module where it is both used to maintain reactive low-level control loops and also transmitted as an encoded data stream via the switch to the upper tier of the architecture.

Higher level deliberative tasks which are not subjected to the same robustness and real-time requirements as those in the lower tier are more appropriately undertaken using more standardised hardware platforms such as PCs and single-board computers (SBCs). The upper partition, or the High Level System (HLS), contains the computational hardware necessary for the system to perform computationally expensive high-level control algorithms. On-board computers are tethered to the switch whereas off-board computers access the switch via a wireless link. Encoded actuator command values are sent from the computers in the HLS to the MM via the switch. At the MM, the actuation instructions are processed within a scheduler function and the resultant commands are executed by the systems actuators.

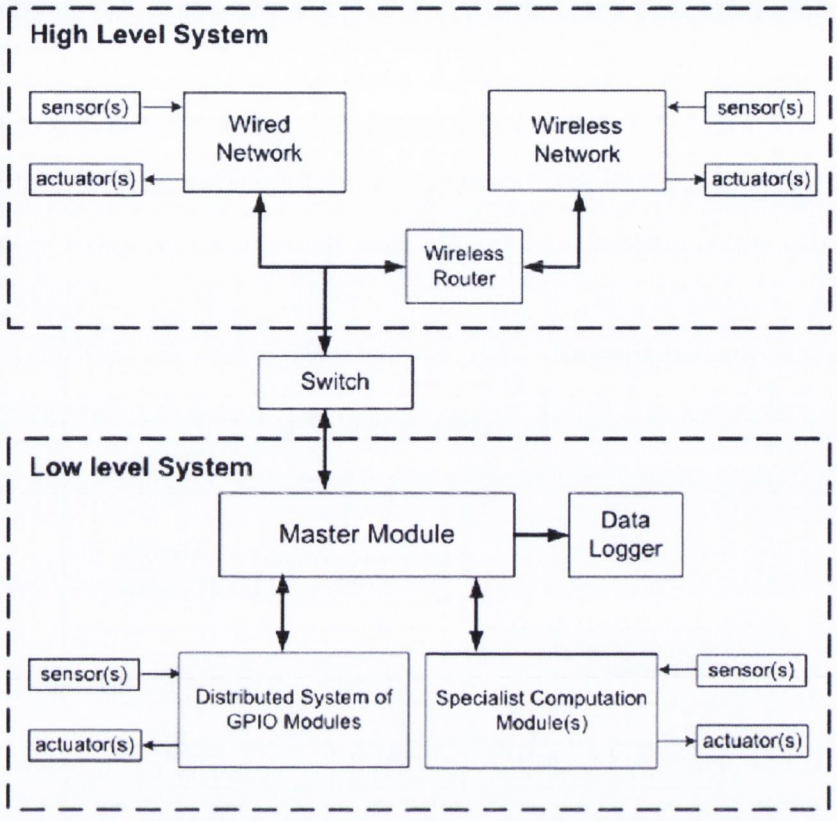


Figure 5.1: High-level description of the two-tiered architecture. Direction of arrows indicate the direction of information/data exchange. The thickness of arrows indicates the relative data bandwidth of the communication channel.

5.1.2 Low Level System Design

The three core components within the low-level system (LLS) are the distributed system of GPIO modules, the 'master' module and the Specialist Computation Module (SCM). A graphical representation of the LLS topology is given in figure 5.2. The GPIO modules are distributed throughout the robot's structure and serve several core functions (1) process (low bandwidth) sensor values and/or generate low-level actuator control signals (2) filter and perform error-checking on sensor data (3) publish filtered sensor data to a high-speed data bus or trigger an error if data is corrupted (4) enable the distribution of control hardware to reduce the electro-mechanical complexity (5) provide a simple and modular means to (re)configure the robot (6) ensure redundancy in the instance that a GPIO module might fail. As the GPIO modules are simply required to read/transmit data from a high speed bus, they can be engineered to be added and configured ad-hoc and with

little practical difficulty.

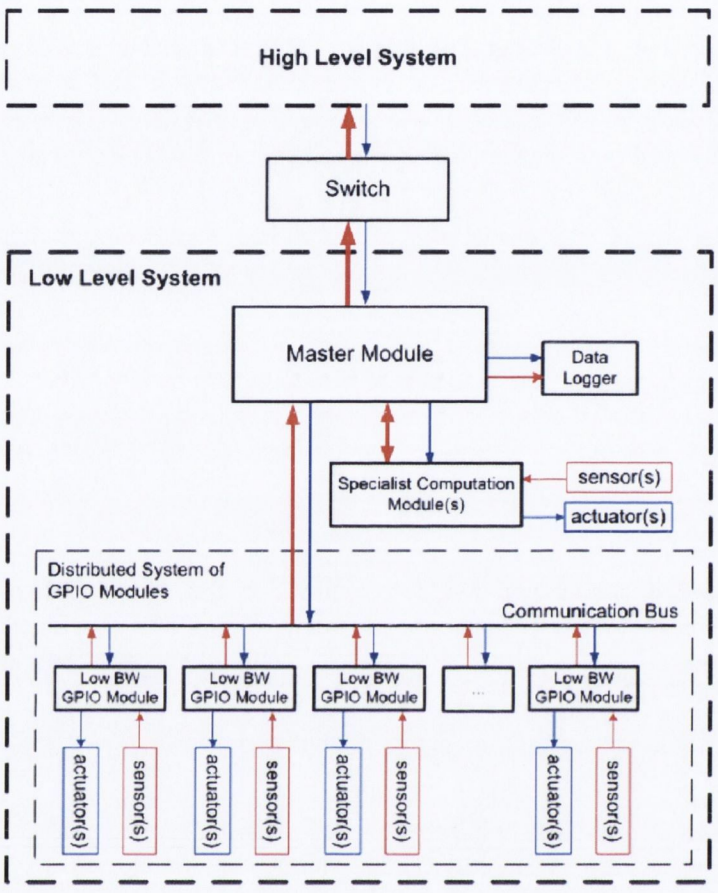


Figure 5.2: Graphical description the of architecture focusing on the low-level tier. Blue lines indicate actuator control commands. Red lines indicate sensor information. The directions of the arrows indicate the direction of information/data exchange. The thickness of the arrows indicates the relative bandwidth of the communication channel.

The MM is the primary processing center within the LLS. Connected to the GPIO modules, the SCM and the network of computers in the HLS, it serves the following key functions (1) read/process filtered sensor data from GPIO bus (2) calculate the proprioceptive state of the robot (static stability margin, forward kinematics, battery levels etc.) (3) perform inverse kinematics (IK) and generate associated actuator commands (4) maintain closed-loop feedback control on joints (5) publish actuator commands on GPIO communication bus (6) process abstract actuator commands from HLS via sequencer function (7) transmit sensor stream (consisting of data from GPIO modules and SCM) to the HLS. As the MM is responsible for maintaining proprioception, performing IK and generating actuator commands, it is possible for the robot to maintain stability using the LHS

alone. Therefore in the event of failure of the switch connecting the LLS and HLS, the robot can remain stable while a warning is raised. The Specialist Computation Module (SCM) can be interpreted as an extension of the MM. It can be adopted to serve several purposes including (1) high bandwidth sensor processing (camera stream, laser scans etc.) (2) computational overflow resource for MM (3) local perception (object detection, tracking etc.). To justify its presence as a separate unit in the architecture and not merely an extension of the MM, the SCM uses dedicated hardware that is optimized for parallel processing applications. A data-logging module can be connected directly to the MM or alternatively at the hardware switch. Its primary function is to record sensor/actuator control data.

5.1.3 High Level System Design

The high-level system (HLS) consists of several interconnected computational modules. Sensory data from LLS is streamed to each module via the switch. Computational modules can attach to the switch through either a wired (in the case of on-board modules) or wireless (for remote modules) connection. This configuration is shown in figure 5.3. The proposed system is designed to support a distributed array of computing platforms. Since the architecture is designed to promote generic, multifunctional applications, it is intended that each module should perform differing functionalities. Any sensors/actuators that are needed but are not already connected to the LLS can be connected directly within the HLS to the local computer(s) that requires them. By so doing this minimizes the code modifications engineers need to make when adding additional hardware. Additionally the sensor readings can then be processed locally without affecting the performance of other modules on the system. While the specific function of individual computation modules is likely to vary from robot to robot and from application to application, it is proposed that for civilian applications a dedicated on-board module should be devoted to human-robot interaction (HRI). This module should possess specific actuators which are capable of providing continuous feedback to human users and have the prerequisite sensors and cognitive structure needed for social interaction. In most instances the output from the computation modules takes the form of abstracted actuator commands. These commands

are sent from the computation modules in the LHS to the hardware switch where they are then routed to the MM in the LLS. Since these desired actuation commands will likely be in conflict at times, a sequencer function in the MM is required. In times of conflict, the role of this sequencer is to determine which of the high-level actuation commands should be executed. As the sequencer function which interprets the series of actuator commands from computation modules in the HLS does not possess an accurate model of the system to guide its decision making, it may perform poorly at times. However when applied effectively, approaches including machine learning , fuzzy logic, generic algorithms and/or neural networks offer a promising means of ensuring reliable and satisfactory system behaviour.

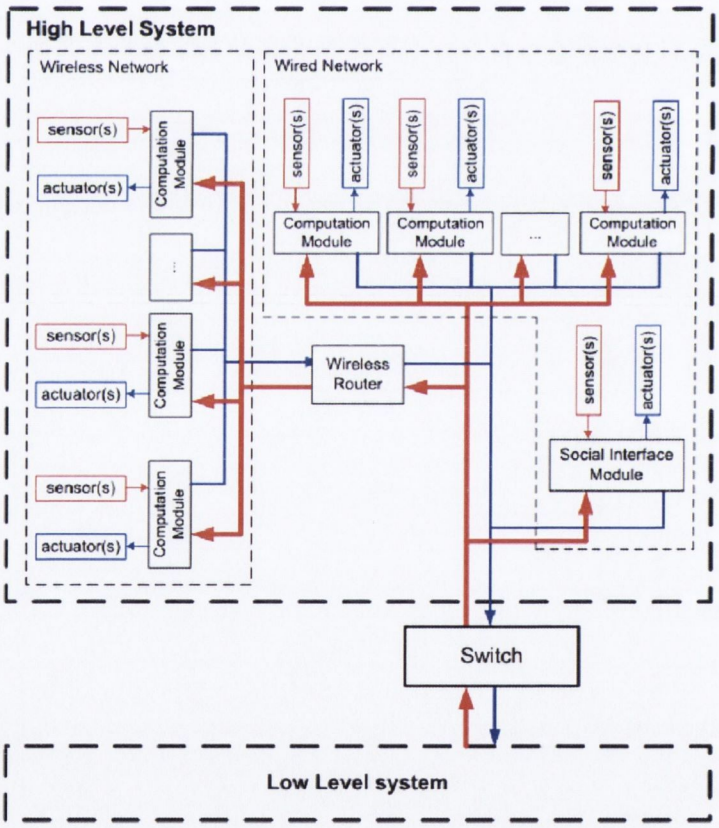


Figure 5.3: Graphical description the of architecture focusing on the higher-level tier. Blue lines indicate actuator control commands. Red lines indicate sensor information. The directions of the arrows indicate the direction of information/data exchange. The thickness of the arrows indicates the relative bandwidth of the communication channel.

5.1.4 Embodiment Design

A small-scale physical embodiment of the proposed system architecture has been designed and integrated with the physical embodiment of the proposed robot morphology. A fully labelled graphical description of the implemented architecture is given in 5.4.

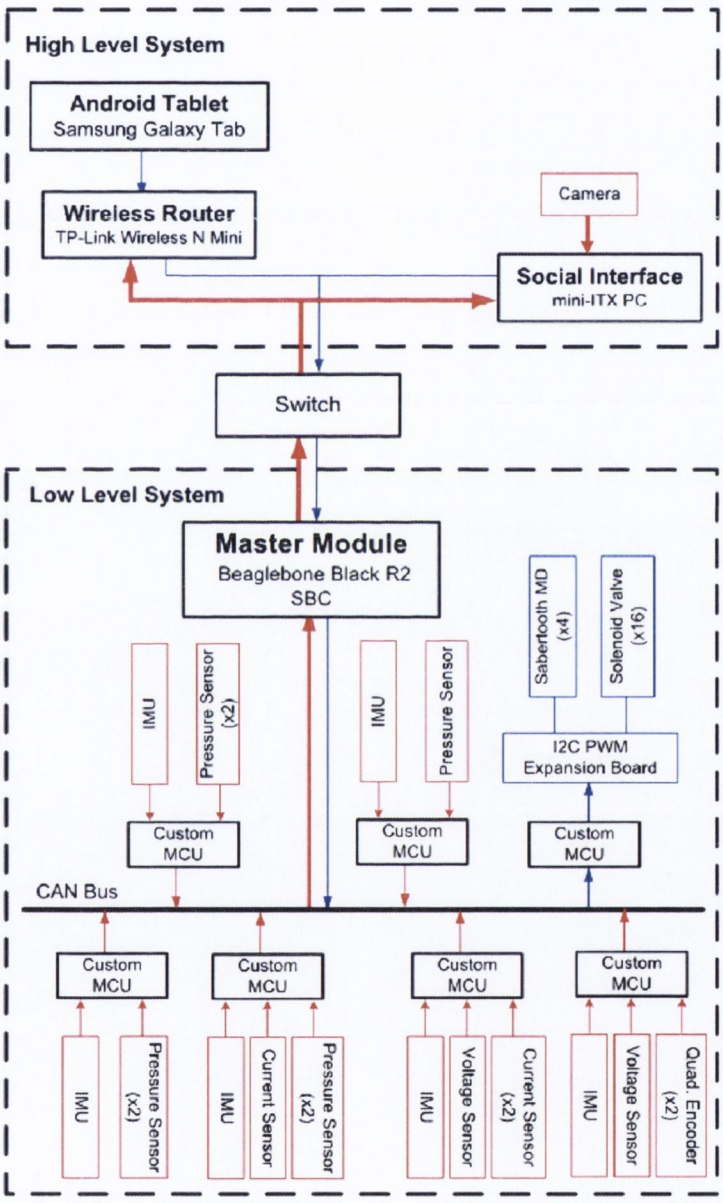


Figure 5.4: Graphical description of prototype architecture. Blue lines indicate actuator control commands. Red lines indicate sensor information. The direction of the arrows indicates the direction of information/data exchange. The thickness of arrows indicates the relative bandwidth of the communication channel.

The robot presented in this work makes use of seven GPIO modules in its low-level system

architecture (six for sensing, one for actuation). Each GPIO module uses identical hardware, a custom made printed circuit board (PCB) designed using Eagle from CADSoft [197] and manufactured professionally by Seed Studios (Fig. 5.5). Each board contains an 8-bit programmable microprocessor, hardware for CAN communication, several GPIOs and an amplifier circuit which can read two differential pressure sensors for the PAMs. A voltage regulator is used to reduce the 11.1V supply battery voltage to a 5V circuit voltage. The board has a spatial footprint of 100x100mm and contains connectors for I2C, RS-232, CAN communication.

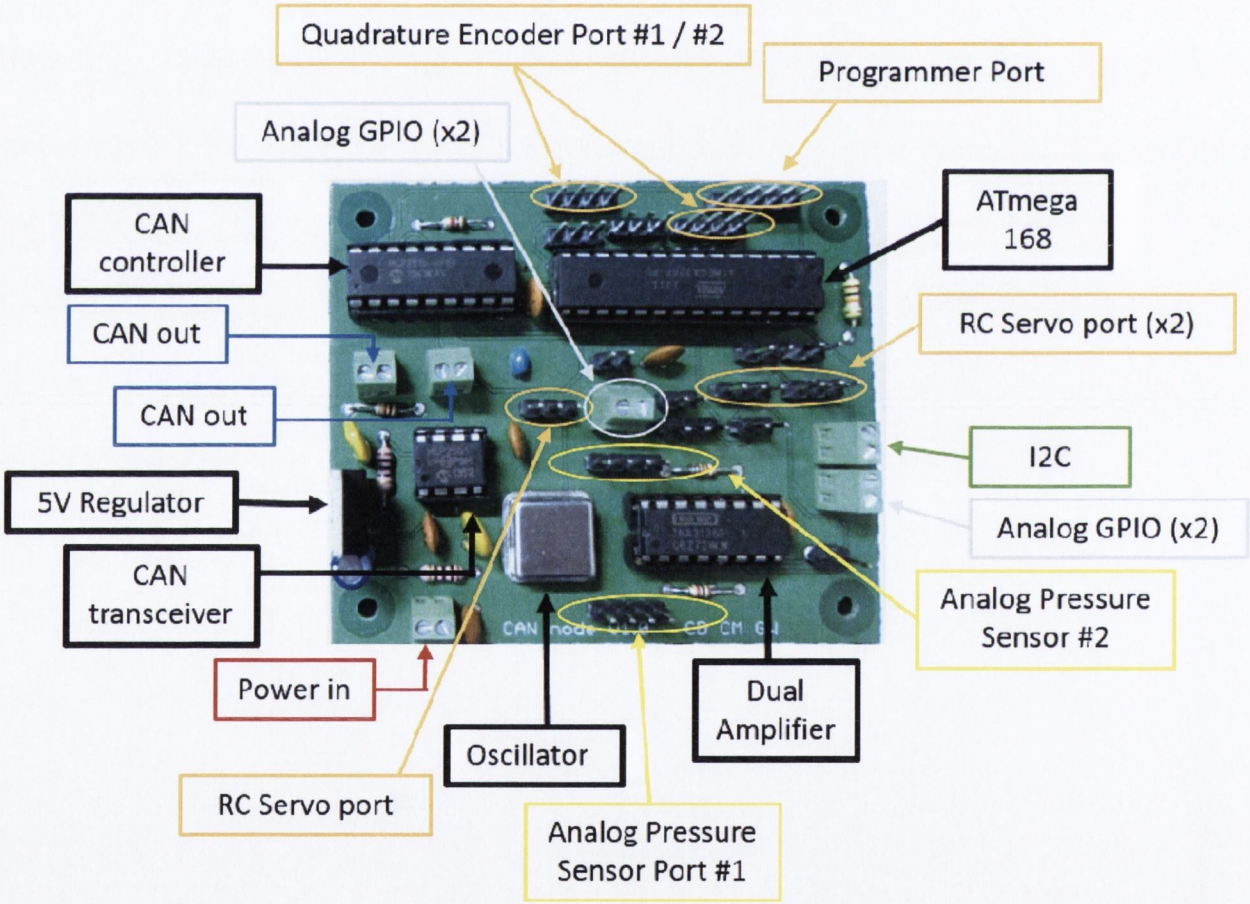


Figure 5.5: The design of the GPIO module v1.0 printed circuit board

The board utilises the popular 8-bit Atmega328 microprocessor. The Arduino bootloader is installed such that the board can be programmed using the conventional Arduino IDE [198]. Not only does this provide a simpler means of programming using the Processing language [199] but it permits the use of the vast collection of libraries that have been

developed for the Arduino platform. Using an off-the-shelf Arduino Uno as a programmer, code can easily be uploaded to each GPIO module using a custom made programmer cable which connects to a specially designed connection port on the module. The method used is similar to that recommended on the Arduino website [200]. The full specifications of the GPIO module boards are listed in table 5.1.

Feature	Specification
Size	100x100mm
Microcontroller	ATmega328 (with Arduino Bootloader)
Communications	CAN, RS-232, I2C
Supply Voltage	7-24V
GPIO	11 (7 digital, 4 analog)
Specialist Ports	Analog Pressure Sensor (x2)
	Quadrature Encoder (x2)
	RC Servo (x3)

Table 5.1: Hardware specifications of the GPIO module v1.0

The 'master' module takes the form of a SBC that serves as an interface between the robot's actuators, the computers performing high-level control tasks and the robot's low-level sensory system. In the current embodiment, the MM is implemented using a BeagleBone Black R3, a SBC developed by the Beagleboard.org Foundation (Fig.5.6).

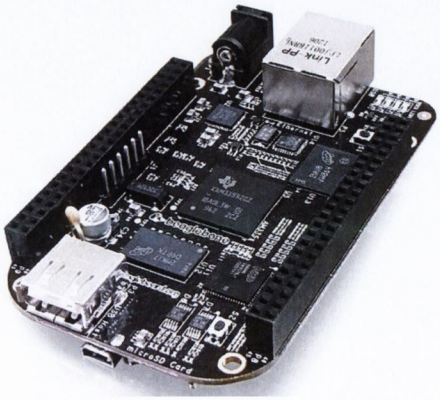


Figure 5.6: The BeagleBone Black SBC used as the 'master' module on the v2.0 demonstrator embodiment

This board possesses a 1GHz Arm Cortex A8 processor, 512MB DDR3 RAM, 4GB eMMC flash memory and a 3D graphics accelerator. In its current configuration, the system runs a lightweight Debian operating system. The control program is written entirely in C++ and threading is accomplished through use of the Boost C++ libraries [201].

When installed on the robot, the MM is programmed remotely through the use of a SSH server which gains accesses to the board (at TCP port 22) through the on-board wireless switch. While the Beaglebone possesses an internal CAN controller, it was necessary to configure a simple external circuit containing a CAN transceiver and logic level converter before it was possible for the BeagleBone to gain access to the CAN bus. An external voltage regulator is used to convert the 11.1V battery supply voltage to the stable 5V needed to power the system. All of the control code used on this board is hosted at a github repository and is freely available to download [202]. An image of the robot showing the location of the GPIO and 'master' module is given in figure 5.7.

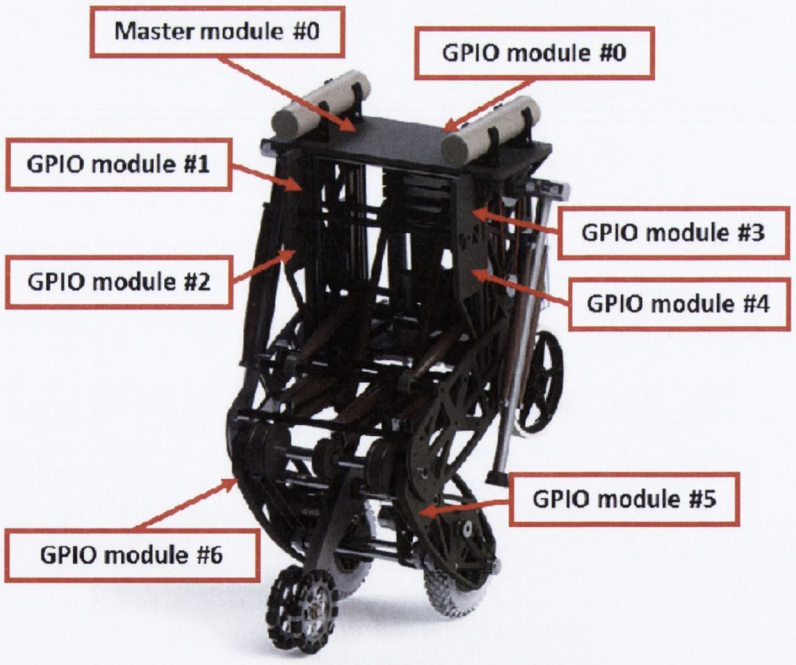


Figure 5.7: The distribution of the GPIO modules and 'master' module throughout the robot

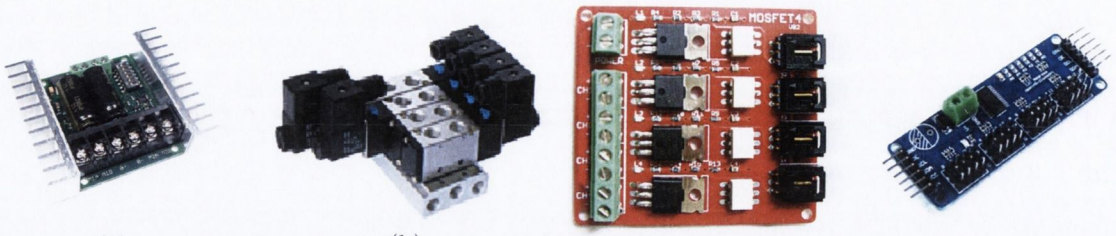
5.1.5 Actuation Control

The robot is actuated using both conventional DC gearmotors and pneumatic air muscles (PAMs). In both instances the control commands are computed in the 'master' module and immediately sent to the GPIO module responsible for actuator control. It is the job of the action module to then relay these control commands to the dedicated hardware responsible for supplying electricity/air to the actuators.

In the case of the DC gearmotors, actuation requires the use of motor driver pcb boards which use a low current PWM signal voltage to modulate the supply voltage across the terminals of the motors. The *v2.0* embodiment uses four Sabertooth 2x25 motor drivers each connected to the regulated on-board 12V supply rail (Fig. 5.14a). In total, there are the eight on-board motors to be controlled (shank drive wheels (x2), LHM drive wheels(x2), shoulder joint(x2), air compressor (large), air compressor (small)). Each motor driver can control two motors per board, support currents up to 25Amps per channel and possesses a switching frequency of 32kHz.

Fast switching solenoid operated valves are used to control the air flow to the PAMs. Since these mechanisms open and close mechanically, substantially lower switching speeds are attainable in comparison with MOSFETS or other equivalent solid state switching mechanisms. The valves used on the robot are normally closed (NC) 5/2 3-position valves manufactured by Stcvalves and are assembled in a six-way manifold (Fig. 5.14b). Each valve has two solenoids which connect the PAM to the high pressure supply line and the ambient environment respectively. As the default state of the valves is 'normally closed', if neither solenoid is turned on, the PAM becomes an isolated system and retains its pressure. An additional one way solenoid control valve is connected between the compressed air tank and the on-board pressure regulator. This is used to prevent leakage when the pressure in the supply tank rises above that set for the regulator. As powering the solenoid valves requires more current than is safe to supply from a microprocessor alone, dedicated solid state MOSFET driver boards are implemented. These boards are physically located between the solenoid and the actuator GPIO module and are used to the regulate the supply of voltage from the 12V supply rail based on the on associated

control signal (Fig. 5.14c).



(a) (b) (c) (d)

Figure 5.8: Hardware for controlling actuators: (a) Sabertooth 2x25 motor driver (b) Stc 5/2 valves with manifold (c) MOSFET board to control solenoids (d) Adafruit PWM Breakout board

As the number of control variables that require a PWM control signal significantly exceeds the available PWM pins on the actuator GPIO Module, additional hardware was attained to provide the necessary expansion. Through integration of two, 16-channel Adafruit PWM Driver breakout boards (Fig. 5.8d), it was possible to provide 12-bit resolution PWM signals for both the motor and PAM control signals. These boards are connected to the actuator GPIO Module across an I2C connection. In addition to providing the ability to expand the number of available PWM lines, the board offers the ability to vary the default frequency of the control signal. This features facilitates tuning of the solenoid switching frequency to its maximum achievable value (found to be at approximately 40Hz for the valves used). A schematic which conveys the overall actuator setup is shown in figure 5.9.

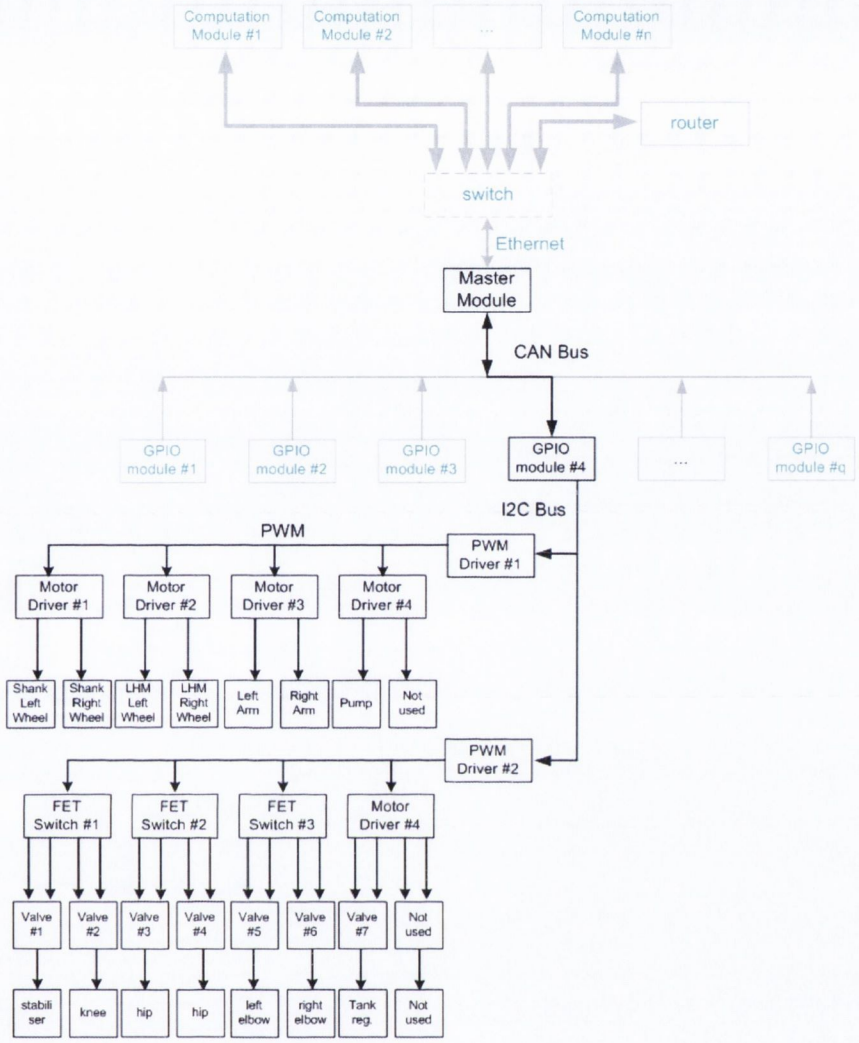


Figure 5.9: Low-level actuator control topology

The 'shoulder plate', the flat plate mounted on top of the torso, was designed to house the system's electronics and pneumatics control hardware. Among the components mounted on the shoulder plate include; the social interface mounting brackets, the maser module, the actuator GPIO module, a wireless router, five MOSFET boards (for activating the solenoid valves), two plastic pneumatic air tanks, a manual pressure release lever, two electric kill switches, two PWM breakout boards for actuator signal processing, a pressure relief valve and an on-board pressure regulator (Fig. 5.10).

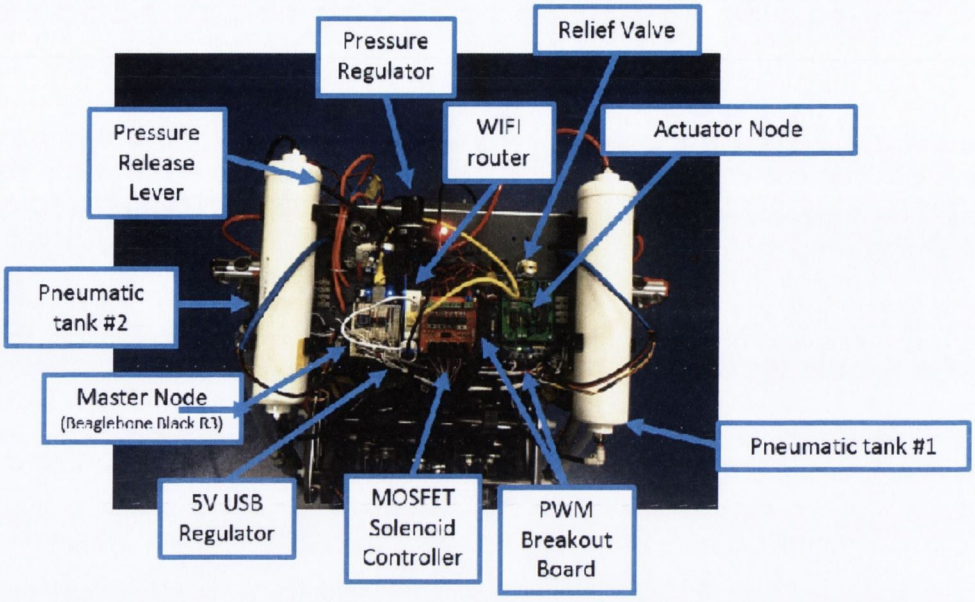


Figure 5.10: Physical layout of the electronics and pneumatics control hardware in the *v2.0* demonstrator embodiment

5.2 Sensing

5.2.1 Sensor Overview

Robot sensing can be broadly classified into proprioceptive and exteroceptive sensing. Sensors in the former category are responsible for sensing the internal state of the robot (joint angles, battery voltage etc.) while sensors in the latter category are responsible for external sensory perception (vision, sonar, tactile sensors etc.). In the robot architecture developed in this work, proprioceptive sensing takes place at the low-level GPIO modules while the networked computers are responsible for performing the (typically higher bandwidth) exteroceptive sensing tasks. It is noted that since the scope of the thesis does not cover the high-level control of the robot system, further discussion of the exteroceptive sensing system beyond this section is omitted. The *v2.0* embodiment possesses a diverse range of sensors including IMUs, rotary encoders, linear encoders, voltage sensors, pressure sensors and current sensors. The physical distribution of the sensors is shown in figure 5.11.

In section 5.1, the details of how proprioceptive sensing is integrated within the control architecture is given. Using a two-tiered architecture, low-level proprioceptive sensing/-control is achieved with the help of an integrated system of GPIO modules while higher

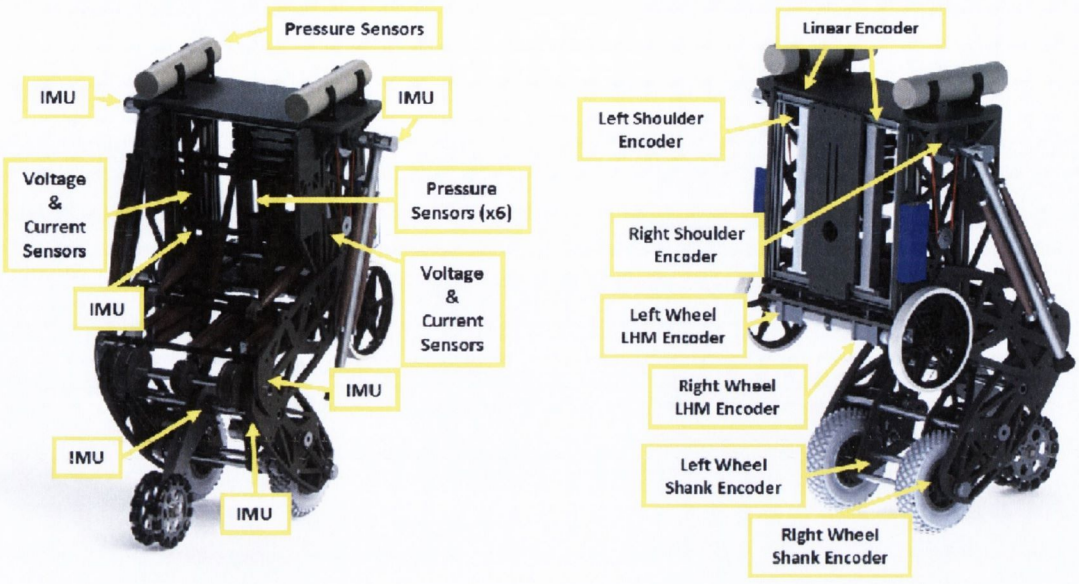


Figure 5.11: Distribution of low-level sensors throughout the demonstrator embodiment

level control/perception is carried out by dedicated computer systems. This configuration provides high-levels of practical reliability, modularity and computational efficiency since computers performing computationally demanding tasks are not constrained by the latency issues of processing/filtering low-level sensor values or meeting exact real-time control requirements.

It is observed that the low-level proprioceptive sensing system (using distributed array of custom designed GPIO modules connected across a CAN bus) possesses increased levels of system integration when compared with the higher level exteroceptive sensing system (consisting of networked computers connected at the hardware switch). There were several reasons behind this design.

Firstly, since the required level of proprioceptive sensing is likely to remain constant for a given robot morphology, detailed consideration can be given to the sensing requirements of the robot in the design stage. This is not necessarily the case with exteroceptive sensing which is often highly task specific.

Secondly since the sensors commonly used for proprioceptive sensing (rotary encoders, IMUs, voltage sensors etc.) use stable and mature technology, the requirement for hardware retrofitting is minimised thus facilitating closer morphological coupling. Conversely

the degree of exteroceptive sensing needed is constantly subject to change depending on the required tasks, the required autonomy and the availability of new/improved sensor technologies. In order to facilitate hardware retrofitting of this type, a more adaptive design was required for the higher level system.

Thirdly since the morphology has reactive, real-time control requirements which depend on proprioceptive sensor values, the proprioceptive system requires intricate coupling with the actuation system. High-level tasks undertaken on the networked PCs typically do not have the same real-time requirements and therefore can connect to the low-level actuation system using a standardised API.

5.2.2 Proprioception

Using a combination of pressure sensors, voltage sensors, current sensors, rotary encoders, linear encoders, and inertial measurement units, the robot's internal states are measured. Two voltage sensors are used to measure the voltage of the batteries supplying the actuators and electronics respectively. These sensors are particularly important since the high density Lithium Polymer batteries that the robot uses cannot fall below a threshold voltage (3 Volts per cell). Two current sensors are used to measure the current drawn by both the electronics system and actuator system respectively. By measuring the rate at which power is being used, it is possible to estimate the remaining operating time.

The rotation of the drive wheels in the shank and the drive wheels in the LHM is measured using 360 count quadrature encoders from US Digital. Using encoders on the shank drive wheels, odometry by dead-reckoning is performed to track the robot's orientation and position. Furthermore these sensors are used to detect unintended rotation of the wheels should the robot be subjected to a disturbance or should the wheels slip. As the LHM drive wheels are used to assist the torso in mounting/dismounting stair nosings, encoder feedback from the encoder is used to regulate traction between the stair and the wheel.

Rotary encoders connected to the left and right shoulder joints are used to infer the relative position of the arms with respect to the torso. It is noted that these encoders are connected to the shoulder joint (as opposed to the joint supplying the actuation) as the pulley belt is designed to slip under load/contact. The position of the lower arms

and the LHM relative to the upper arms and the torso respectively is detected using a linear encoder. This encoder takes the form of a string potentiometer, a multi-turn rotary potentiometer connected to a retractable string mechanism. With the potentiometer located on one side of the joint and the string attached to the other, the value of any subsequent elongation/contraction can be mapped to the change in resistance across the potentiometer.

The relative positions of the stabiliser, shank, thigh and torso are computed in real-time using data from IMUs located close to the joints (Fig. 5.12). Since the IMU provides

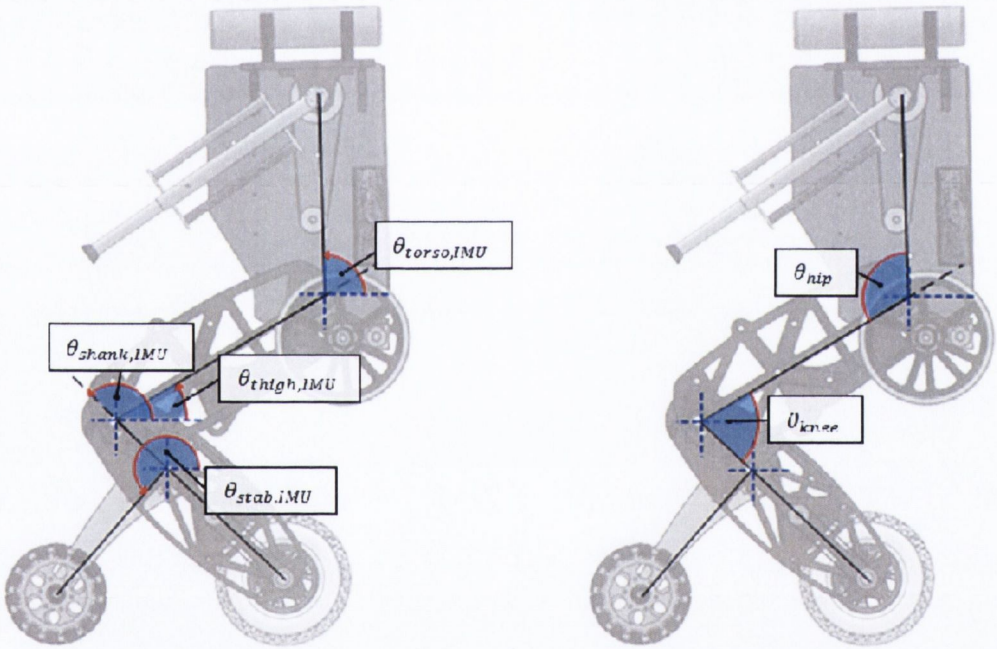


Figure 5.12: Determining joint angles from IMU readings

rotations relative to a global reference frame, the relative position of the limbs must be inferred from combining this data with the robot's kinematics. The following relations are used to determine the joint orientations:

$$\theta_{stab} = (\theta_{shank,IMU} + \pi) - \theta_{stab,IMU} \tag{5.1}$$

$$\theta_{knee} = (2\pi - \theta_{shank,IMU}) + \theta_{thigh,IMU} \tag{5.2}$$

$$\theta_{hip} = (\pi + \theta_{thigh,IMU}) - \theta_{torso,IMU} \tag{5.3}$$

A pressure sensor is connected to each PAM grouping and is used to monitor for air leaks

and provide a control input for joint position control. The pressure sensors currently used on the robot are temperature compensated gauge pressure transducers manufactured by Honeywell. Additionally as the required actuation pressure increases with load, these sensor values can be used to infer the instantaneous loading on the joints.

5.2.3 Safety

As the demonstrator robotic platform presented in this work is not being immediately developed for commercialisation, it has not been designed to adhere fully with the ISO standard for personal robots described in section 2.4.1.2. However as it is anticipated that future versions of the robot will require adherence with this standard, efforts have been made to ensure that the robot morphology possesses features that are considered safe in accordance with this standard. While a full safety and risk analysis of the present embodiment is outside the scope of this work, mention should be given to several important safety issues and the design steps that have been taken to minimise their occurrence.

Arguably the most significant safety risk posed by full-scale commercial personal service robots involve the uncontrolled movement of the robot due to a software glitch or hardware failure. To ensure that the robot can be shut down instantly, three hardware based kill-switches are implemented. Two switches take the form of toggle switches which isolate the batteries from the actuator control boards and electronics respectively. The third kill-switch takes the form of an easy-break connector in the battery supply cable. This connector is located in an easily accessible harness located on top of the robot and when tugged, it creates a break in the power line thus preventing the flow of electricity through the circuit. A mechanical release lever is connected to the compressed air tanks and is used to regulate the escape of compressed air when appropriate.

An important requirement of the ISO 13482:2014 standard (part 5.13) is that wheeled robots should not have exposed rotating drive wheels. In the majority of wheeled service robot embodiments, this leads to designers adopting shell-like fairings which shield the wheels from the surrounding environment. Using these structures has the practical effect of compromising the robot's ground clearance and therefore adversely affecting its terrain adaptability. By locating the drive wheels inside the shank, they become shielded from the

outside environment thus eliminating the need for a design feature which will compromise the robot's performance capability. As the stabiliser wheel is passive, its exposure poses a far less significant threat. Similarly since the wheels in the LHM are used only occasionally, rotate relatively slowly and are only used under certain conditions, the potential risk they pose is also very small.

Since the robot's joints use pneumatic actuation, they are innately compliant and offer little impedance on contact. In instances where electric motor driven belt drives are used (i.e. the shoulder muscles), a round belt is used and tensioned such that belt slippage occurs upon contact thus making the joints easily back-drivable.

As the electronics/computers/sensors draw a constant current (approx. 0.8 Amps), battery life prediction can be done with high accuracy and reliability (assuming the availability of voltage sensing). In the present configuration, the system will stop operating as soon as the voltage in either the actuator or electronics supplies falls below a predetermined threshold value (typically below 3.1V per cell). Two separate power supplies are used to supply the system's computers/electronics and actuators. This was done in an attempt to ensure that the on-board computers/electronics do not lose power before the actuators and to protect sensitive electronic components against the threat of power surges and back-emfs generated by the electric motors.

5.3 Human-Robot Interaction and Control

5.3.1 Design of Social Interface

Human-robot interaction plays a central role in the design of user-centred service robots. Robots of this type require some form of social interface, a focal point for interaction that provides some form of continuous feedback to the human user and to the surroundings during operation. According to the Life-like Agents Hypothesis discussed in section 2.4.1.1, it was suggested that robots possessing face-like interfaces will perform better than those that do not owing to the innate ability of humans to read human emotions and expressions. Since the practical requirements of the facial features will vary from person-to-person and from task-to-task, it is desirable that a face possesses many degrees of freedom and that the expressions can be easily customised.

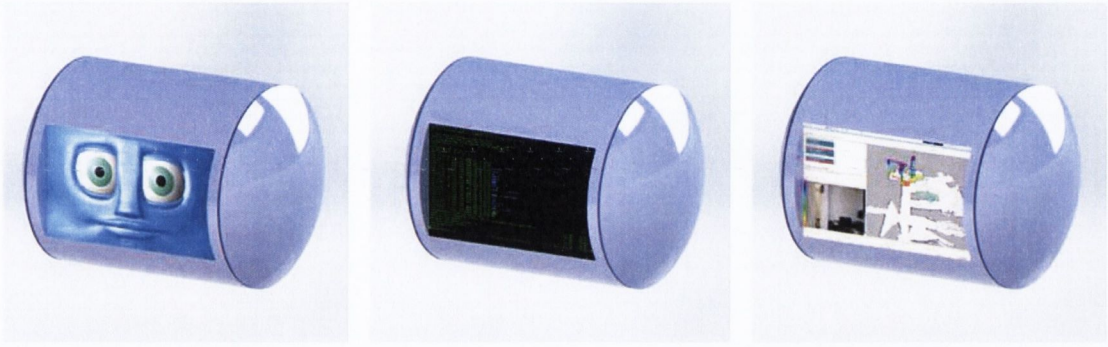
For these reasons, a social interface has been included among the primary features of the robot morphology developed in this work. An image of the social interface utilised on the v2.0 demonstrator platform is shown in figure 5.13. This interface is made up of a physical head constructed from model foam, two plastic mounting brackets and an 7in LCD monitor. The LCD is driven by a Cubieboard V2 single board computer and is responsible for rendering an interactive virtual face. The social interface is integrated as a high-level computer within the robot's control architecture (described in section 5.1). Both the LCD screen and SBC is powered from the on-board electronics supply rail.



Figure 5.13: Embodiment of the social interface on *v2.0* demonstrator

The social interface is designed to be highly customisable; both the head itself and the face animation are easily modified to suit the requirements of the user. In the present embodiment, the animation was developed using the Blender Game Engine, developed by the Blender Foundation [203]. Face movement can either be generated locally (by control code running on the SBC) or through the transmission of an API-based control command

to one of the SBC's TCP ports. A particularly attractive feature of this interface design is that since the interface is connected directly to the computer controlling the robot, it can serve secondary functions as both a programming interface and a medium to directly communicate the robot's internal states (joint orientations, sensor visualisation, belief states and joint trajectory plans) (Fig. 5.14).



(a) (b) (c)

Figure 5.14: Core functionalities of social interface (a) interactive customisable face (b) programming interface (c) sensor visualisation

5.3.2 Human-in-the-Loop Control

Since service robots are required to operate under the instruction of human operators, the means through which they receive instruction and communicate with people forms an important design consideration. As few general-purpose robotic systems have come close to demonstrating full autonomous capability, it is observed that at present semi-autonomous control offers the most practical, effective and efficient means of controlling robots of this type. Robots operating under semi-autonomous control possess a certain level of autonomous functionality but can also be controlled directly by a human operator. The research conducted in this work set out to demonstrate two important hypothesises concerning the effective control of service robots. The first one postulates that in human-centred environments, manual control by a human user cannot consistently meet the performance levels (number of collisions, navigation time etc.) delivered by an equivalent autonomous controller for high-level navigation-based tasks. Secondly the research set out to show that the overall performance of a semi-autonomous controller improves with

increased levels human interaction. In other words, the more the human is 'in-the-loop', the better the robot's overall performance.

Hypothesis #1

The first hypothesis states that manual control of a mobile service robot by a human user cannot consistently meet the performance (number of collisions, navigation time etc.) delivered by an equivalent autonomous controller for navigation-based high-level tasks. There are several reasons for this assertion:

1. The performance of the robot under manual control is dependent on the operator's field of view. When parts of the robot are occluded or the robot is out of the operator's field of vision, collisions become significantly harder to avoid. Even with a real-time video feed from an-board camera, practical factors including image latency, the small field of view and the first person viewpoint further increase the risk of an accident.

2. In certain instances when reactive real-time control is needed, manual human control is often not suitable. In these cases human operators simply do not possess the ability to process and react to the system's proprioceptive sensors in the required fashion. For example it was observed by Martens and Newman that since a robot operator lacks the ability to sense the robot's equilibrium point, tasks such as stair-climbing are extremely hazardous for manual human control, even for highly experienced robot operators [147].

3. Manually controlled robots typically process control commands given relative to their own local coordinate systems (i.e. a 'go-forward' command is almost always with respect to the robot's local coordinates). As the robot moves, the orientation of the its local coordinates will vary with respect to the local coordinates of the human operator (global coordinates). Therefore control instructions given with respect to where the operator is standing may result in the robot performing an undesired action.

4. The tuning of a controller and its physical embodiment will have a direct effect on

the robot's performance. Therefore manual performance levels cannot be guaranteed from the control schema alone but require consideration of the physical controller device.

Hypothesis #2

The second hypothesis proposes that the overall performance of a semi-autonomous robot increases in proportion with the degree of human interaction in the control loop. To rationalise this proposition consider first that communication between robots and people is both an implicit and explicit process. While the explicit aspect of the communication is clear (human gives explicit command, robot performs explicit action etc.), the implicit aspect is more subtle. When people observe a robot in action they will naturally form beliefs and opinions based on their observations of the robot's behaviour. They might be able to (without prior knowledge) ascertain the task the robot is carrying out, its relative ease/difficulty in performing the task and perhaps even anticipate any mistakes that robot is likely to make. As human observers possess the ability to provide such a powerful means of instantaneous feedback during a robot's operation, it is proposed that a control schema which provides human users with the ability to augment the robot's behaviour implicitly (in real-time while the robot engages in the task) as well as explicitly will offer improved performance over conventional manual and semi-autonomous controllers that operate in a more binary fashion.

Furthermore it is proposed that since the physical form of a controller directly affects the performance of the robot it controls, any effort to increase the degree of human interaction in a semi-autonomous control system warrants the detailed design and system integration of a specialised controller embodiment.

5.3.3 Semi-Autonomous Control Schema and Embodiment Design

An integral feature of the proposed robot morphology is the integration of a cooperative control schema that necessitates continuous human feedback throughout the robot's operation, regardless of whether the robot is acting under manual or autonomous instruction.

In other words, the proposed control schema requires the operator to provide continuous input to the control system, regardless of whether the robot is under direct or automatic control.

The controller embodiment consists primarily of two elements, a tactile touch-pad and a joystick. The controller can be implemented using a dedicated hardware embodiment or using a custom application developed on a smartphone/tablet (Fig. 5.15).



(a) (b)

Figure 5.15: The two controller embodiments designed for use in the proposed control schema (a) Hardware embodiment (b) Android application installed on tablet computer

When the user operates the joystick, the robot automatically enters 'manual mode' and the robot moves in accordance with the joystick commands. However when the user places their fingers on the touchpad, the robot switches to 'autonomous mode' and executes the command action generated by the robot's on-board computers. The touchpad is designed such that it can detect the number of fingers that are touching it. The robot interprets the number of fingers touching the touch-pad as a discrete confidence rating, an implicit measure of how well the robot is performing at that time (four fingers equating to high confidence, one finger to low confidence). Using this form of feedback, the robot can adjust its behaviour in real-time to incorporate the feedback of the person controlling it. When the user neither touches the touchpad nor the joystick, the robot will remain at rest. If the user happens to simultaneously activate the touchpad and the joystick, then

the manual joystick commands are executed.

Several features of this controller make it novel. Firstly, unlike conventional semi-autonomous controllers, the switching mechanism between autonomous and manual modes is not a binary process. Instead it requires continuous feedback to be provided by the operator (joystick control during manual mode, communication of user confidence during autonomous mode). In this way, the operator maintains varying levels of control throughout the operation of the robot.

Secondly the robot switches between autonomous and manual control in a manner opposite to interrupt-driven systems. Unlike interrupt-driven systems that await a discrete command before switching control modes, the proposed system is driven by a continuous, sustained command signal. This schema provides an inherent safety feature as, should the controller be dropped, the signal will break and the robot will halt.

Finally as the control of the robot is closely coupled with human feedback, it provides a natural means of integrating machine learning methods (supervised learning in particular) in order to improve the robot's ability to autonomously perform tasks over time. Incorporation of machine learning algorithms in this manner is currently an area of future research.

Owing to the mechanical simplicity of the controller and the broad range of semi-autonomous systems that may benefit from its use, the precise physical embodiment of the controller may vary across morphologies. To date, two physical embodiments have been developed, the first a purpose built controller and the second a application for an Android-based smartphone/tablet.

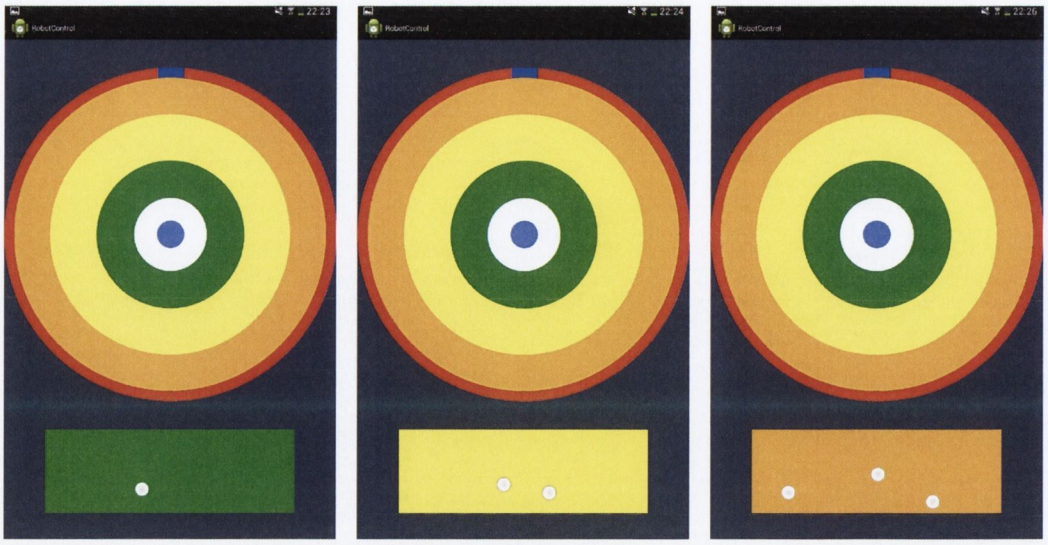
5.3.3.1 Hardware Controller Implementation

The hardware implementation of the proposed controller embodiment consisted primarily of an arcade joystick (8-bit resolution), Arduino microcontroller [198] and capacitive tactile sensors made up from thin copper strips (Fig. 5.15a). The joystick, tactile sensors and an 'on/off' button were connected to the microcontroller which was programmed to relay the control command to a the host computer across a RS-232 connection. A simple networking program running on the host relayed the commands wirelessly to the robot. When the joystick is depressed, micro-switches are triggered and the direction is ascer-

tained. The conductive copper strips are connected (at separate locations) to a digital output pin and an analog input pin on a microcontroller. A medium to high value resistor (100 kilohm - 50 megohm) is connected in series between the output pin and the copper strip. As copper is conductive, its voltage will increase in proportion with the voltage at the output pin. The time it takes for the voltage of the copper to rise will depend on the conductance of the material and its volume. Therefore when a person touches the strip, the time it takes for the voltage to rise will increase. By implementing a timer that counts how long it takes for the voltage to rise at the input pin, it is possible to determine if and to what degree a person is touching the strip. This sensing capability was integrated using the CapSense library [204].

5.3.3.2 Software App Control Implementation

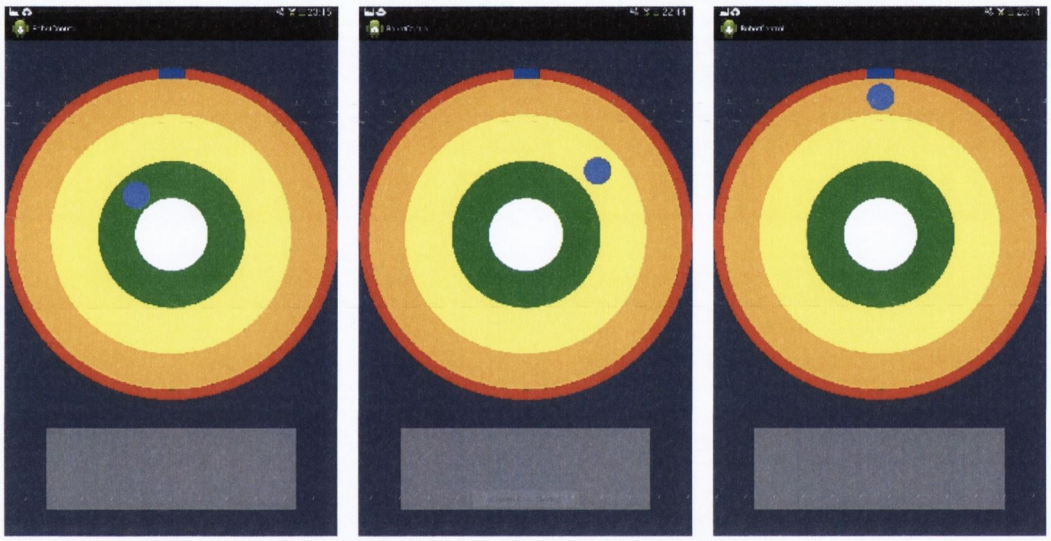
An Android application was developed to evaluate the proposed controller design (Fig. 5.15b). The application was developed and tested on a Android tablet computer. Autonomous mode is engaged when the operator places their fingers on the touchpad located at the base of the controller. The multi-touch feature enabled multiple contact points to be selected at once. The colour of the touchpad was programmed to change with the confidence rating (number of fingers contact points) (Fig. 5.16).



(a) 1 finger touch (b) 2 finger touch (c) 3 finger touch

Figure 5.16: Semi-autonomous control mode using the touchpad (a) low confidence (b) medium confidence (c) high confidence

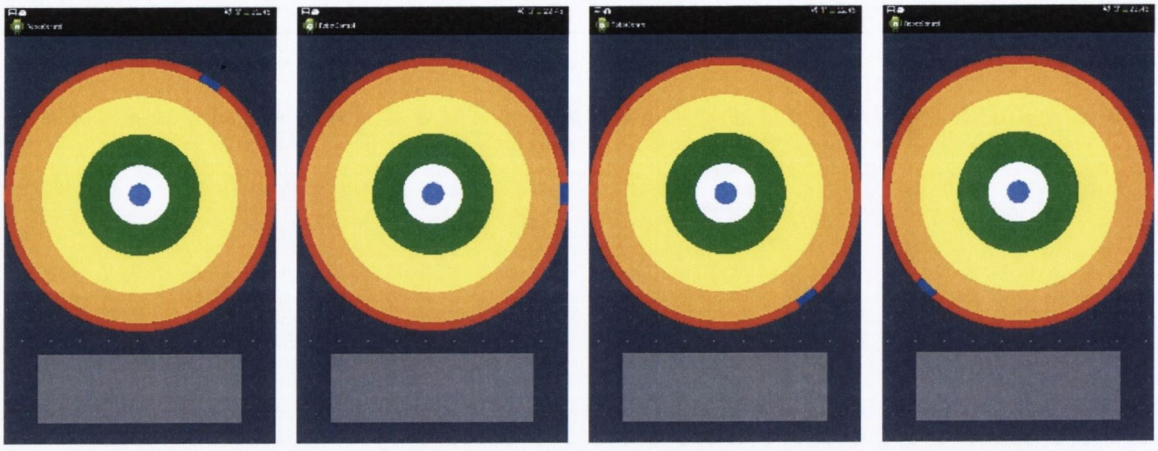
A novel joystick design which incorporates variable speed control was developed. The joystick is operated by dragging the purple control point (located in the centre of the joystick by default) towards the desired heading direction. The control point is programmed to snap to one of three concentric rings. The speed of the robot can be modified by changing the ring at which the control point lies (speed increases with circle diameter). Manual control in this fashion is depicted in figure 5.17.



(a) (b) (c)

Figure 5.17: Manual control using the control app (a) low speed in the forward-left direction (b) medium speed in the forward-right direction (c) fast speed in the forward direction

It was found that neither the physical joystick nor the application joystick possessed the ability to easily perform zero-point turns. To address this issue, an additional control point was added to the control application. This control point (located at the top of the joystick by default) is responsible for controlling the pose/orientation of the robot. The zero-point turn control point is constrained to rotate along an outer ring and is controlled simply by tracing a circle inside the joystick with a finger (Fig (5.18)).



(a) (b) (c) (d)

Figure 5.18: Performing a zero-point turn. Actions (a)-(d) finger dragged clockwise within the joystick area

Chapter 6

Results

The ability of a robot to perform tasks is dependent on the practical capability of the robot's morphology, its adaptability to the task environment and how it's controlled. It is reasonable that a platform's suitability should therefore be assessed based on the integrated combination of its physical characteristics, practical capabilities and control architecture.

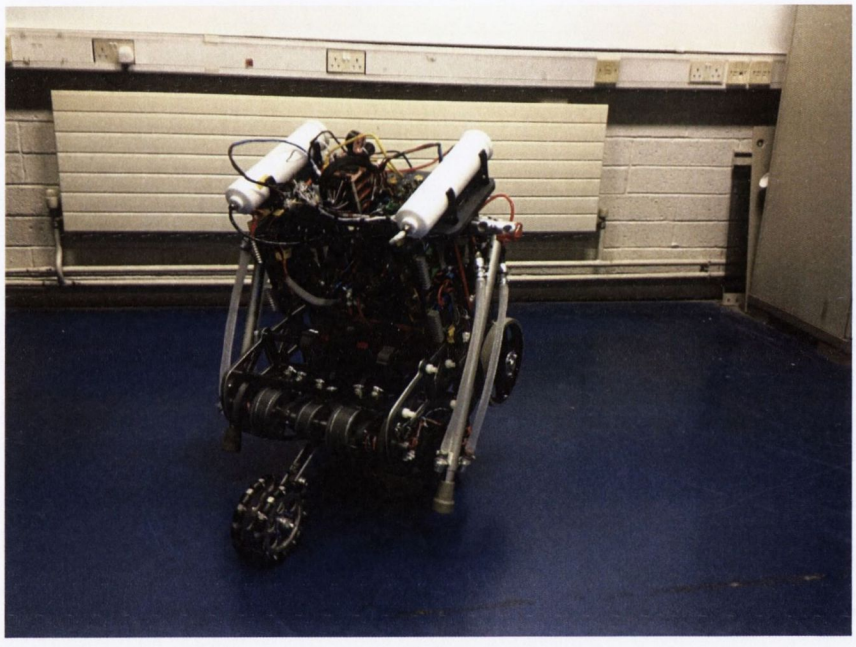
Since the requirements of the robot's physical characteristics and practical capabilities can be easily defined, quantitative design metrics were created to facilitate the assessment, benchmarking and validation of the proposed morphological embodiment. The creation of these metrics (defined and discussed in section 4.2) was guided by the findings of the literature review detailed in section 2.7. Achieving these targets would suggest that the proposed morphology possesses a unique combination of high terrain adaptability, high stability, low system complexity and user-interface complexity.

While most aspects of the design can be validated through the practical accomplishment of pre-defined targets, certain qualitative elements pertaining to robot controllability require separate consideration. Specifically this research set out to define the architectural barriers that affect manual control of service robots, investigate whether semi-autonomous control offers an inherent advantage over manual control in navigation-based tasks and to establish whether the performance of systems using semi-autonomous control schema improves with increasing levels of human-robot interaction.

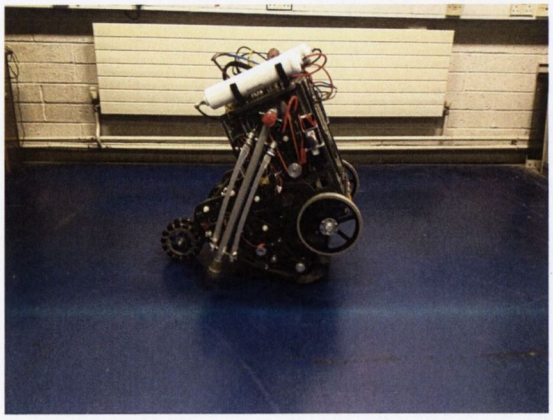
6.1 Physical Metrics

6.1.1 Robot dimensions and inertial properties

To date, two demonstrator embodiments of the proposed morphology have been designed, built and subjected to varying degrees of testing. The most recent demonstrator (*v2.0*) offers the highest level of performance and forms the central basis of this work. Several images of the *v2.0* embodiment are shown in figure 6.1. A table describing the robot's physical parameters is given in table 6.1.



(a)



(b)



(c)

Figure 6.1: Several views of the demonstrator embodiment

The overall mass of the demonstrator robot is approximately 28kg. As per design requirements, the majority the mass (16kg) is located in the upper body with the remainder distributed between the shank (8.1kg), thigh (2.8kg) and arm (0.5kg per arm) sub-assemblies. The mass of the arms was minimised to ensure that arm movement alone wouldn't destabilise the robot in states of low static stability.

Property	Value
Height	920mm (default), 1100mm (max)
Width	600mm
Depth	600mm (default), 440mm (min)
Aspect Ratio	1.33 (default), 2.5 (maximum)
Mass	28kg (approx)
# DOF	12 (8 compliant)
Power	8000mAhr LiPo (Actuator), 3000mAhr LiPo (Electronics)
Computing	Master Node: BeagleBone Black R3 (x1) Slave Nodes: Custom Board with Atmega 168 (x8) Android Device (control) CubieBoard R2 (social interface)
Connectivity	TP-Link TL-WR702N nano wireless router

Table 6.1: Physical parameters of the demonstrator

The *v2.0* demonstrator was designed to possess the shortest limbs required for successful operation in civilian environments. As the torque acting at the joints increases with limb length, shortening the limbs served to significantly reduce the system's actuation requirements. The length of the shank and thigh was determined through an optimisation process described in section 4.4. This study found that a knee-to-hip length of 363mm and a wheel-to-knee shank length of 348mm [1] were the minimum proportions required to permit stair climbing (using the proposed gait) on the most geometrically severe stairways allowed by the IRC standards.

The vertical length of the torso (356mm) was chosen such that the demonstrator could achieve the required aspect ratio of 2.5 stipulated in the physical design requirements. Again this height was minimised for this embodiment to reduce actuation requirements

[1] the analysis assumed a shank drive wheel of 100mm (approx 4 inches) radius. Therefore in practise the ground-to-knee length will be approximately 448mm

at the hip. The arms of the robot were designed to be capable of extending to the ground from both the default orientation of high static stability and from an elevated height during stair climbing. In total the arm was designed to be capable of extending by 100mm, approximately 18% of its total default length.

6.1.2 System modularity

The demonstrator achieves computational modularity through the integration of the system architecture described in section 5.1. Low-level modularity is achieved through implementation of a distributed network of seven custom-made micro-controller GPIO modules. Each module possesses an identical form factor and was designed to be easily reprogrammable and highly customisable. Six of these modules are dedicated to low-level sensing while the seventh is responsible for interfacing with the demonstrator's actuators (both pneumatic and electric). Each module is capable of interacting with a wide range of devices and since the Arduino IDE is used to program the robot, a wide range of software libraries can be used. The modules are interconnected via a CAN bus and adding more GPIO modules to the system only requires little more than the addition of a few lines of code within the 'master' module's control program. A more complete description of these modules is given in section 5.1.

High level modularity is achieved through the formation of a distributed network of computers which connect to each other (and the 'master') module at a wireless ethernet switch/router. Since these computers communicate using a standardised API, the addition of high-level computers using different computer architectures is possible. In the *v2.0* demonstrator embodiment, three high-level computers have been integrated in this fashion; an off-board android tablet running a control application, an off-board laptop computer running a control program and a SBC computer responsible for animating the social interface (Fig. 6.2).

6.1.3 Actuation and Safety

In total the demonstrator possesses 12 degrees of freedom as described in section 3.2. All of the demonstrator's major joints possess high levels of compliance. Pneumatic



(a) (b)

Figure 6.2: Implementation of interactive social interface on *v2.0* demonstrator

Air Muscles (PAMs) are used for actuation of the knee, stabiliser, hip and elbow joints. The Lower Hip Mechanism (LHM) is actuated using two telescoping pneumatic linear actuators. The shoulder joint is actuated using a round pulley belt that is designed to slip under load. The robot's wheels (at the base of the shank and in the LHM) are the only non-compliant joints on the robot. In an effort to isolate the motors from ground vibrations and to facilitate hardware modularity, the motors are physically decoupled from the wheels through a geared timing belt pulley system.

Electrical power is supplied to the demonstrator through two separate sources. Two 4000mAhr 14.8V Lithium Polymer batteries provide power to the system's actuators while one 3000mAhr Lithium Polymer battery powers the on-board computers, sensors and electronics. Not only does this configuration isolate the power going to the control electronics but it possesses the practical benefits of facilitating on-the-fly changes of actuator batteries. Additionally since the current consumption of the electronics/computer system is constant (approx. 0.8Amps), the battery voltage decreases linearly allowing accurate battery life predictions to be made. These predictions allow for the development of a robust and reliable shut-down procedure that prevents the system operating under low battery capacity. On the *v2.0* embodiment, voltage/current monitoring is processed locally by a GPIO module and their values subsequently passed to the 'master' module for further dissemination.

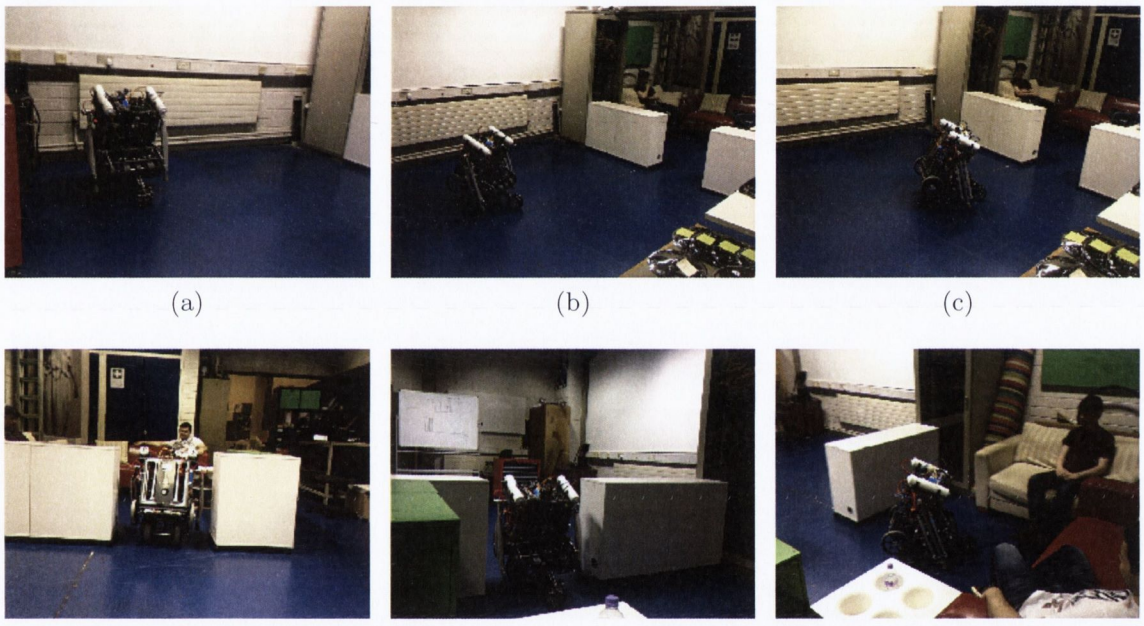
To facilitate safe usage, several hardware switches are installed to connect/disconnect

the batteries from the actuators/electronics. A toggle switch with an LED indicator is used to connect/disconnect the power electronics. A (key-access) turn switch is used to engage/disengage the computational electronics. In the event that the robot malfunctions and it is not possible to reach either power switches, s software kill switch is implemented and can be triggered through either a control application running on a smart device or a test program running on a connected PC. If all else fails, an easily accessible break-cable is installed which ensures the physical disconnection of the actuator power cable.

6.2 Performance Metrics

6.2.1 Locomotion

Testing has shown that the demonstrator is capable of smooth, stable and reliable locomotion across a range of indoor and outdoor human-centred environments. A time lapse of the robot moving within the lab is shown in figure 6.3.

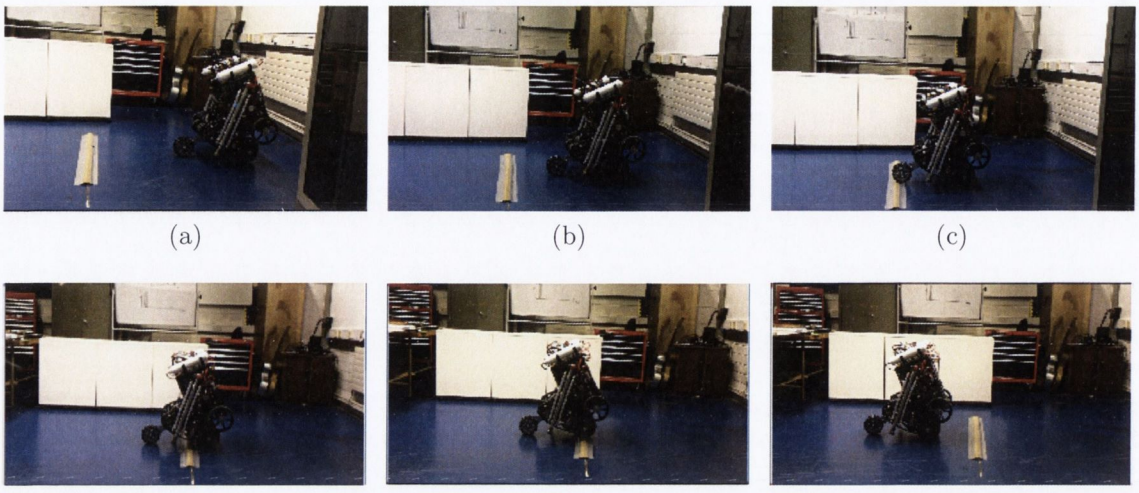


(a) (b) (c)

(d) (e) (f)

Figure 6.3: The demonstrator embodiment demonstrating indoor locomotion capability and the physical ability to comfortably pass through a gap equivalent to a typical residential doorway.

In addition to demonstrating the ability to operate effectively across a range of floor surfaces (hardwood, carpet, ceramic etc.), the demonstrator has also shown the ability to traverse over small architectural features (door sills, draught guards etc.). A time lapse of the robot traversing a door sill (12mm high, 80mm long) is shown in figure 6.4.



(a) (b) (c)

(d) (e) (f)

Figure 6.4: Indoor locomotion and traversal over a large door sill

The *v2.0* demonstrator embodiment has also demonstrated impressive outdoor locomotion capability. The pneumatic tires and compliant joints provide high levels of damping and since the robot has relatively high ground clearance, small obstacles provide little impediment to motion. Additionally since the majority of the robot's mass lies over its rear driven wheels, the stabiliser linkage remains relatively unconstrained during locomotion. This state enables the platform to traverse uneven terrain without components jamming or becoming stuck and ensures that small disturbances do not adversely affecting overall system stability. Images of the robot moving on a grassy plane and across cobblestone are given in figure 6.5 and figure 6.6 respectively. Although it is safer to maintain a large SSM during outdoor locomotion, it is possible to achieve a 2 inch increase in vertical height through coordinated extension of the LHM alone.



(a) (b) (c)

Figure 6.5: Outdoor locomotion on grass

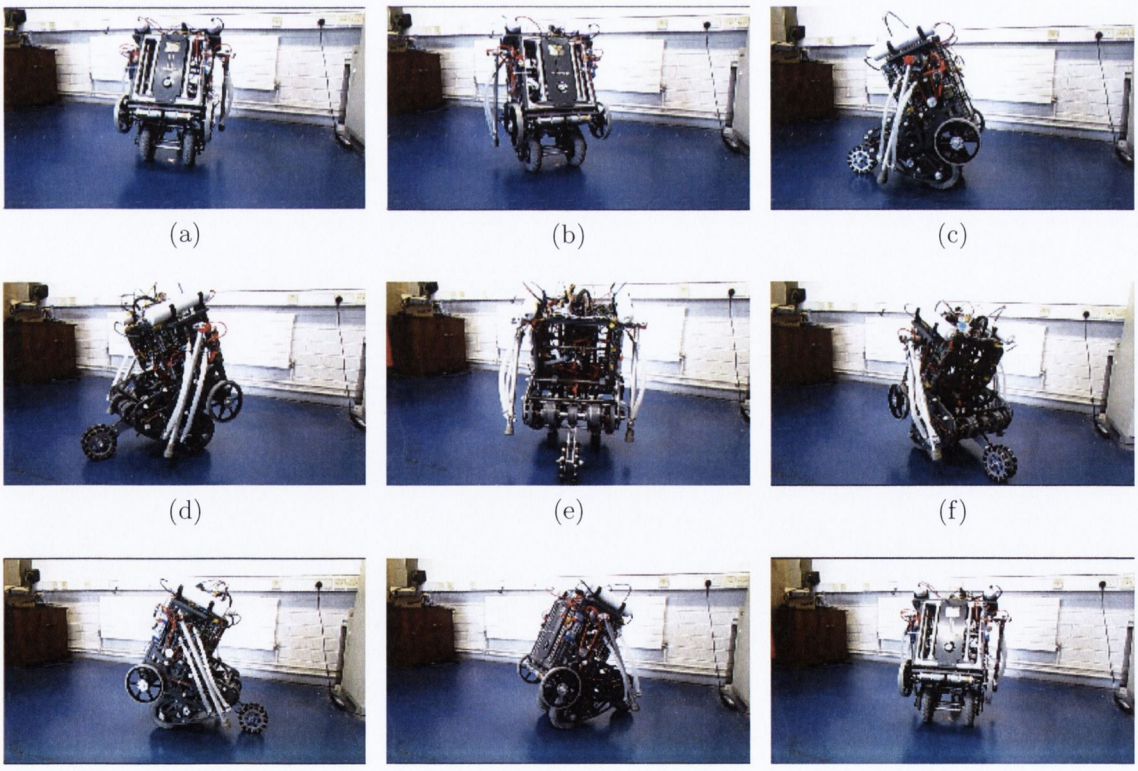


(a) (b) (c)

Figure 6.6: Outdoor locomotion on cobblestone

6.2.1.1 Zero-point turn

The ability of the *v2.0* demonstrator to perform a zero-point turn was evaluated and is depicted in figure 6.7. It was found that under normal indoor conditions (i.e. on flat, hard surfaces) the robot was capable of undertaking this task with ease while retaining high levels of static stability.



(a) (b) (c)

(d) (e) (f)

(g) (h) (i)

Figure 6.7: Demonstrator embodiment performing a zero point turn

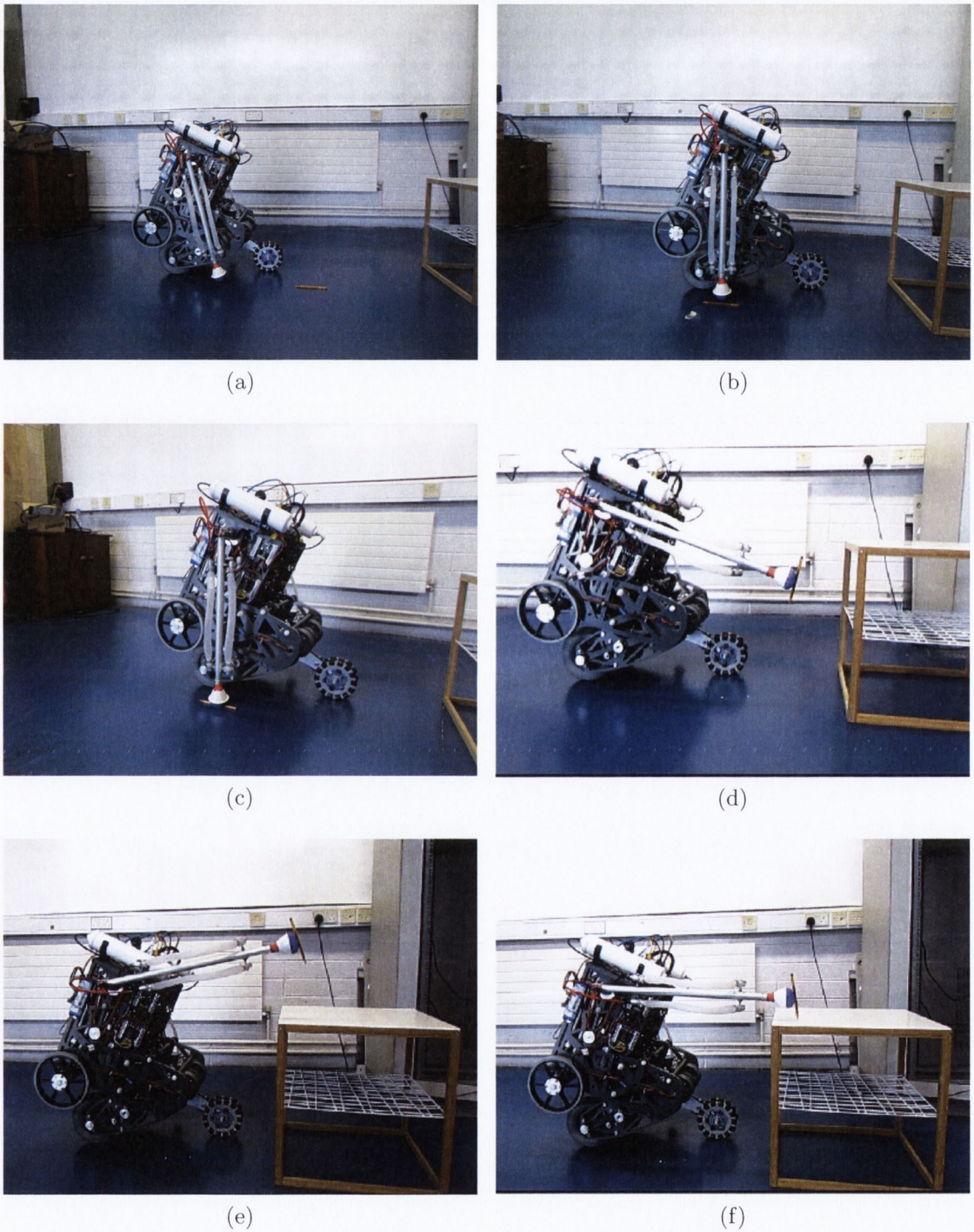
In grassy conditions, effective zero-point turns were also demonstrated however it is worth noting that the decrease in adhesion between the wheels and the ground surface meant

that the actuators needed more current and slip was observed at lower turning speeds.

6.2.2 Pick-and-Place

Many of the most desired applications of personal service robots requires the robot to pick-up items and pass them to human users [205] [206][207]. The *v2.0* demonstrator has demonstrated several impressive functionalities in this respect. Firstly it has demonstrated the ability to pick-up small objects from the ground using a simple particle-jamming end-effector (Fig. 6.8). This end-effector consists of a plastic housing containing a rubber balloon filled with ground coffee beans. An air-hose connects the volume inside the balloon to a two-way vacuum pump. Activation of the pump in 'negative-pressure' mode creates a vacuum that in turn causes the granules to bind together. This binding process causes the granules to apply a gripping force around any objects that it had previously formed/moulded around. Reversal of the pressure (i.e. application of 'positive-pressure' to the balloon) removes the the vacuum and allows the granules to loosen thus releasing any gripped objects. A more complete description and performance characterisation of this type of end-effector is given in [208].

For the proposed morphology, the procedure of picking an object from the floor is initiated by firstly positioning the arm directly above the object (preferably at 90 degrees to the ground plane). The arm is then elongated until the particle-jamming end-effector moulds around the object to be grasped. Since the elbow joint is inherently compliant, this process does not require great positional sensitivity - reaction forces induced by excess arm extension get mostly absorbed in the PAM rather than inducing roll about the robot base (as would happen using a conventionally stiff actuator). With the end-effector in place, the vacuum pump is engaged causing the granules in the gripper to tighten, forming a grip around the object. Once all the air is removed from the balloon and the object is clasped by the gripper, the pump is turned off and the robot is free to move to wherever it needs to deposit the object. The object is released through application of positive pressure at the pump. This sequence of actions being undertaken by the *v2.0* demonstrator is given in figure 6.8.



(a) (b)

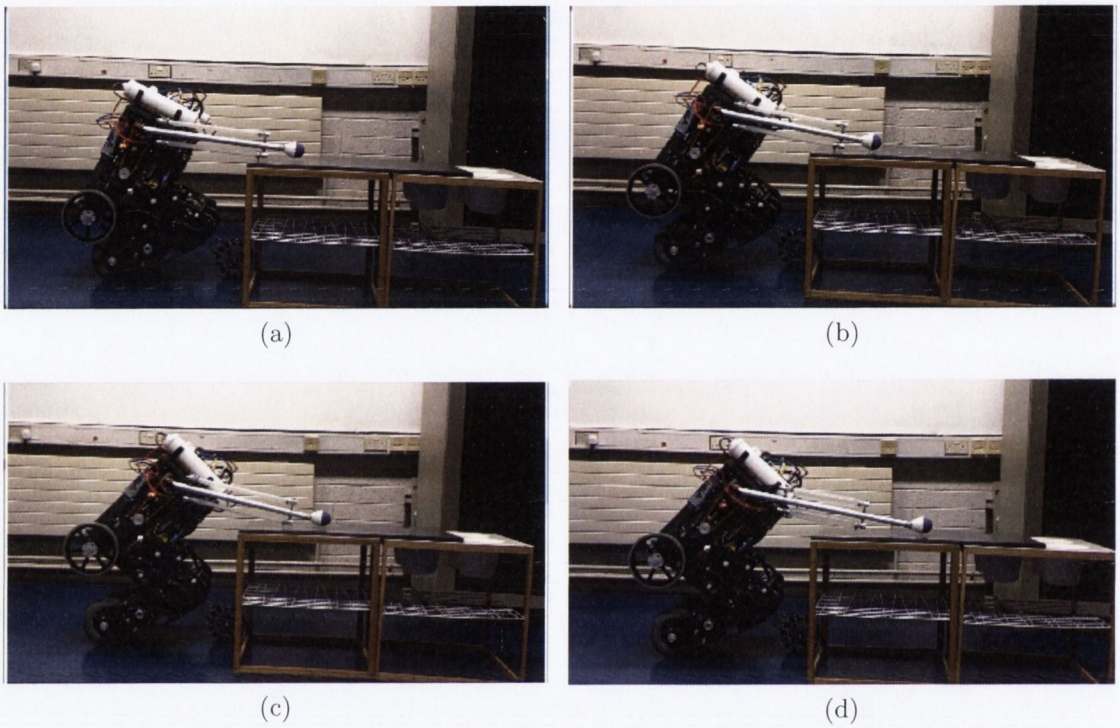
(c) (d)

(e) (f)

Figure 6.8: Demonstrator embodiment picking up a small object from the floor

Since the arm is capable of linear extension, it is possible for the robot to position the object at a radius of between 556-566mm from its shoulder joint. Additionally since rotation at the knee (in the default orientation) actually serves to increase the demonstrator's overall SSM, it is possible for the robot to lean forward during object hand-overs (Fig

6.9). This action not only increases the demonstrator's task space but it can be used to provide an important behavioural 'object handover' cue to human users with whom the demonstrator is interacting.

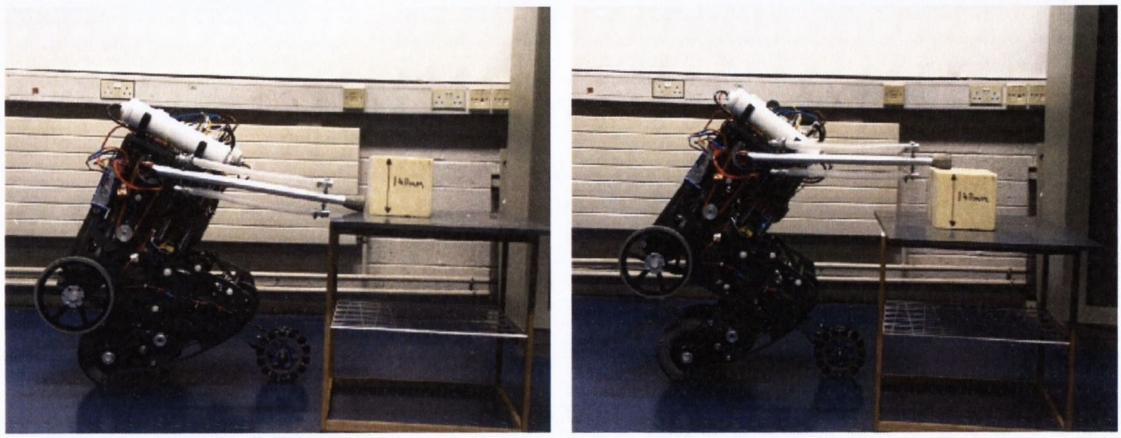


(a) (b)

(c) (d)

Figure 6.9: Demonstrator embodiment leaning forward to increase task space or to engage in a hand-over

Through the coupled actuation of the stabiliser and knee linkage, it is possible to increase the aspect ratio of the demonstrator. While actuation of the hip will further increase the robot's aspect ratio, so doing noticeably decreases the robot's static stability margin. Changing the aspect ratio is useful when the robot needs to navigate constrained spaces or if the robot needs to increase its vertical height. In its present embodiment, the robot can increase its vertical height by over three inches while retaining comfortable levels of static stability. Beyond an increase in height of four inches, active control of the static stability margin is required. A depiction of the robot augmenting its height by approximately three inches through adjustment of its SSM is shown in figure 6.10.



(a) Sitting orientation (b) Rising/Standing orientation

Figure 6.10: Demonstrator embodiment performing vertical height adjustment through modification of static stability margin

6.2.3 Crevice Crossing

Through utilisation of the LHM, it has been demonstrated that the demonstrator possesses the ability to cross crevices and small gaps, a task traditionally reserved exclusively for legged robots (Fig. 6.11). Upon detecting the crevice, the robot deploys the LHM causing its centre of mass to fall between the pneumatic drive wheels and the LHM wheels. With no load acting on the stabiliser linkage and with its associated PAM relaxed, it is lifted off the ground under the action of its elastic antagonistic support. With the robot in a position of high static stability, it drives forward until the stabiliser clears the crevice. At this point the robot's centre of mass is shifted forward and the stabiliser linkage once again supports the platform. The LHM is extended further. This action causes the knee's to straighten until their mechanical limits are reached. Further elongation of the LHM causes the pneumatic tires to lift from the ground. At this point the LHM wheels are driven forward until the shank has fully cleared the gap. Once the stabiliser and shank has crossed safely, the LHM is retracted and the pneumatic wheels return to the ground. With the LHM retracted the robot has fully traversed the gap and can continue forward.

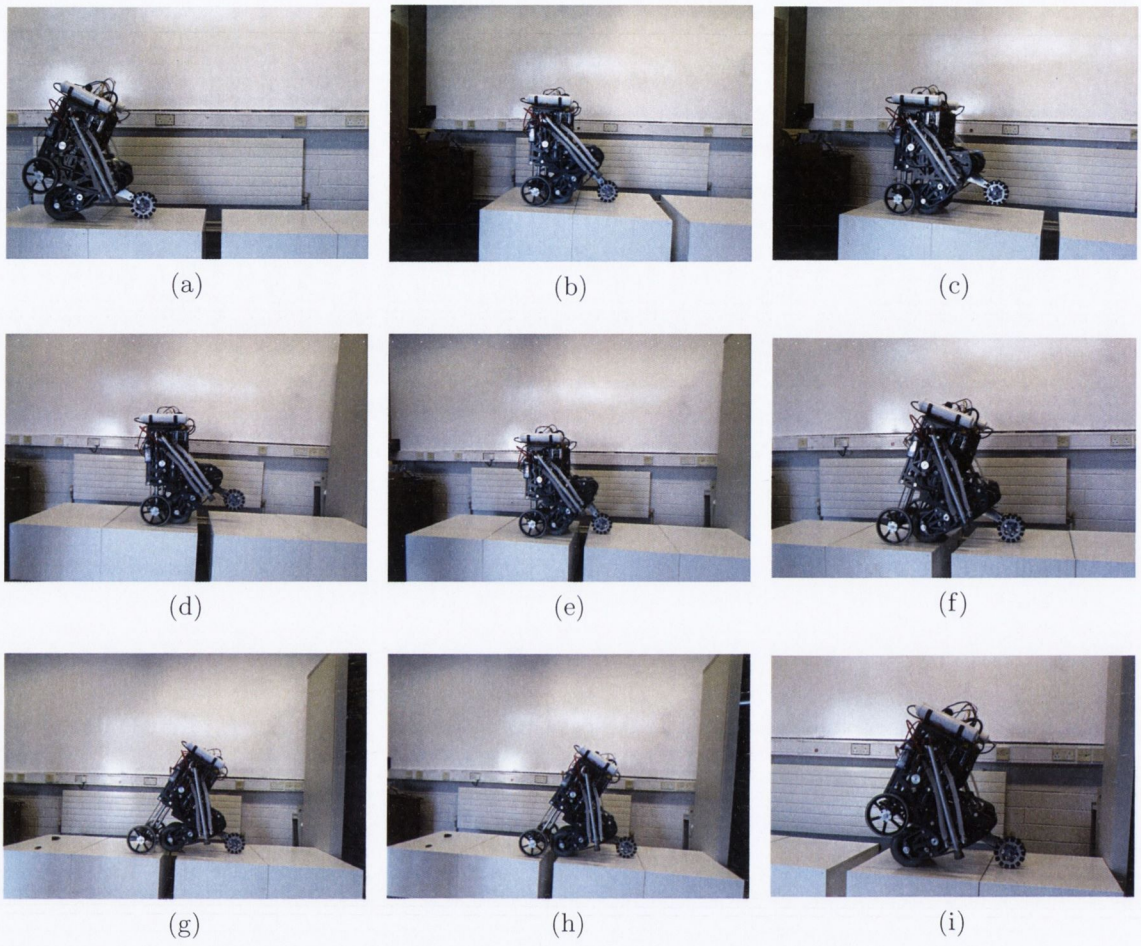
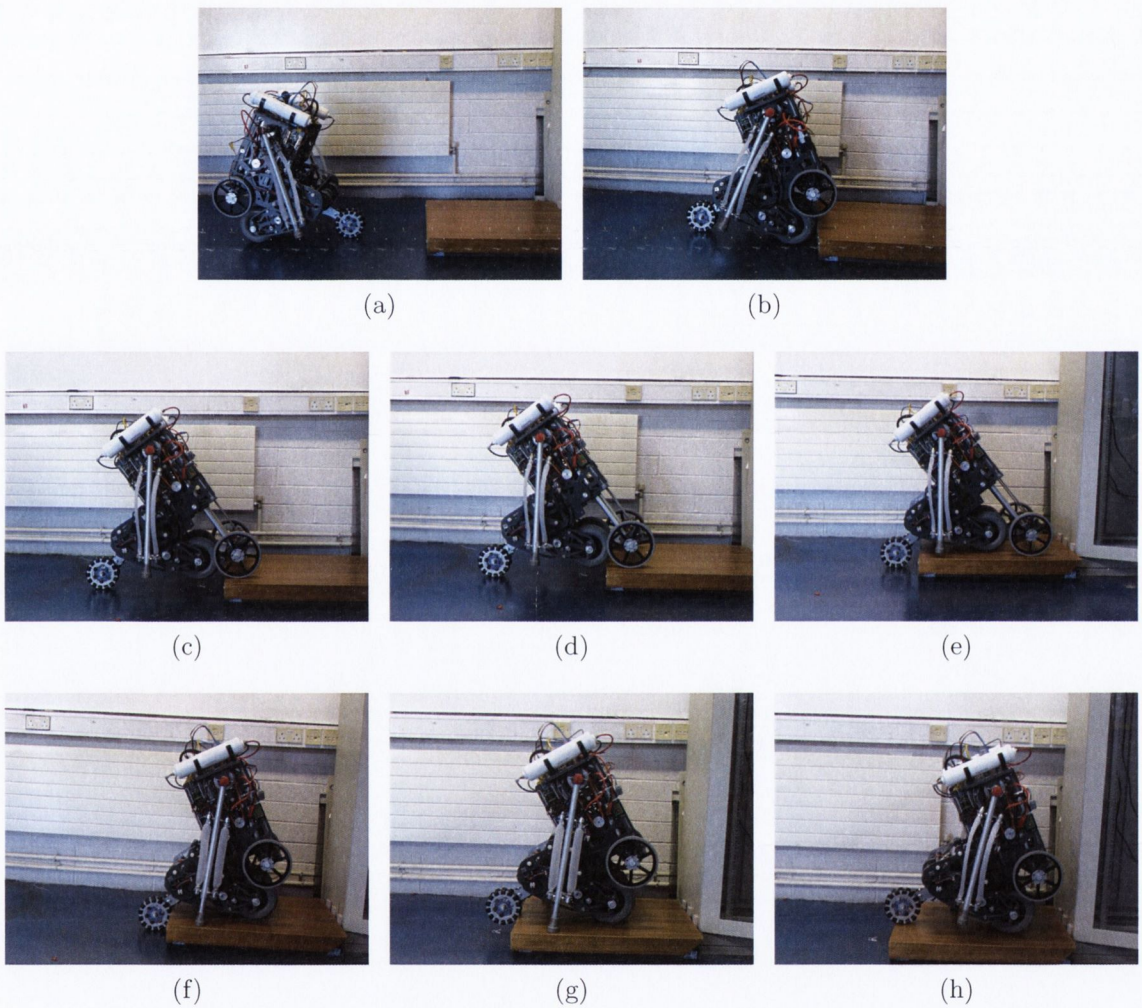


Figure 6.11: Demonstrator embodiment crossing a 100mm crevice

6.2.4 Traversing Obstacles

The *v2.0* embodiment has demonstrated the capability of traversing obstacles taller than the radius of both the stabiliser and shank drive wheels (Fig. 6.12). To traverse a large obstacle, the robot must approach it from its reverse orientation. When the pneumatic wheels contact the obstacle, the LHM is elongated while the knee and hip joints are secured in place. With further extension of the LHM, the pneumatic wheels lift above the ground and a bridge forms between the stabiliser and the LHM wheels. The LHM wheels are then driven forward until the pneumatic wheels next contact the edge of the obstacle. If the axis of rotation of the wheel is above the nosing, the wheels can be driven forward and the robot will mount the obstacle. If further height is needed, it can be provided through contraction of the stabiliser linkage. With only the stabiliser remaining on the floor beneath the obstacle, the robot pitches about the drive wheels extending the

arm down to the floor while simultaneously locking the knee and hip joints in position. This action causes the stabiliser to raise from the floor. Then by driving forward while continuing to extend the arms, the stabiliser mounts the obstacle thus completing the action.



(a) (b) (c) (d) (e) (f) (g) (h)

Figure 6.12: Demonstrator embodiment traversing a 110mm obstacle

6.2.5 Stairclimbing - Ascent

In addition to the static analysis conducted in section 4.3.1, a dynamic analysis was undertaken to investigate the practicality of stair-climbing using the proposed gait pattern. This study was undertaken using MSC Adams, a dynamic simulation software package commonly used for analysis of this type. These simulations were developed to both guide the development of the stair-climbing gait and also to help predict the joint reaction forces as well as the necessary joint rotations and joint torques. It is noted that for reasons of computational efficiency, the robot was modelled using simple primitives rather than the complex geometry realised in the embodiment. Screen-grabs capturing some of these simulations are given in figure 6.13.

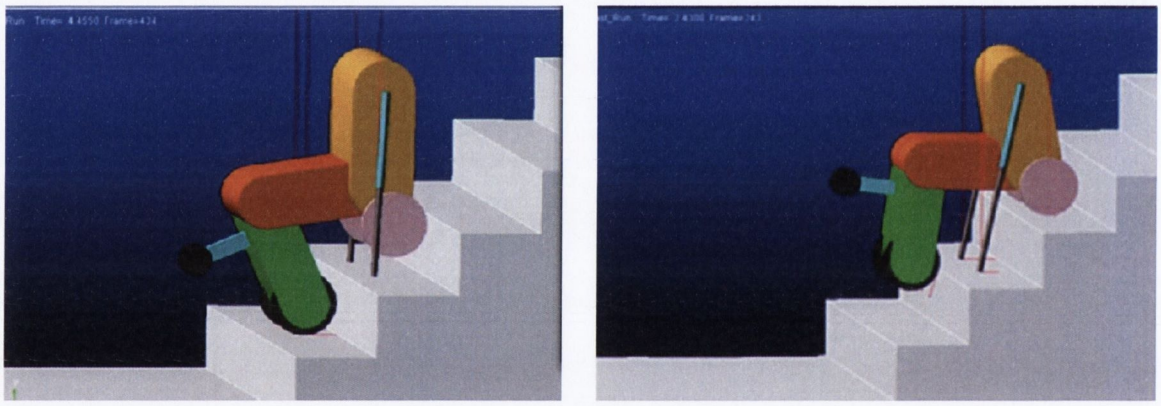


Figure 6.13: Simulations using MSC Adams

The practical capability of the robot to ascend/descend stairs was investigated using a custom-made flight of stairs. The flight consisted of three risers and two treads. The tread depth was 254mm which is the smallest permissible length according to both the UK and ICC building codes across both residential and utility buildings. The riser height was 120mm making an overall slope of 25.3°.

For stair ascent, the robot approaches the flight in backwards orientation. The robot reverses on approach and when the pneumatic wheels make contact with the stair, the LHM is extended while the stabiliser is contracted. This movement causes the robot to sit backwards onto the stair. Action #1 of stair ascent begins with the controlled elongation of the LHM in combination with the straightening of the knee. This action maintains the vertical orientation of the torso and provides the clearance necessary to position the end-

effector in parallel with the adjacent riser. The arm is then elongated until it contacts the ground and supports the weight of the torso and LHM. With the shoulder joint fixed in place, the system is statically stable and the LHM is retracted until the axis of rotation of its wheels is located above the stair nosing. At this point, the LHM wheels are activated and the knee straightens further. These actions causes the robot's torso to mount the stair. The second action of stair ascent commences by minimising the thigh-torso angle through contraction of the hip muscle. With the robot's arms angled forward the elbow is elongated until the end-effector contacts the unoccupied tread. As the arm continues to elongate, the magnitude of the reaction force at the end-effector increases. With the thigh-torso angle and torso-arm angle fixed in place, the reaction force at the end-effector provides a pitching moment about the ground contact point at the base of the LHM. This action causes the robot undergo a rigid body rotation about this ground contact point cumulating in the pneumatic wheels leaving the ground. When the axis of rotation of the pneumatic wheels exceeds the stair nosing, the wheels are rotated forward propelling the shank onto the tread. Through iterative repetition of action #1 and action #2 movement sequences, the robot can ascend the stairs in a statically stable, cyclic fashion. It was found that mounting the final stair in the fashion described in section 3.5 was not practically feasible on the *v2.0* embodiment without further increasing the elongation capability of the arms. However a modified (somewhat less elegant) gait proved effective in accomplishing this task. In this new gait, the robot minimises the thigh-torso angle and simply drives the LHM wheels forwards. Increased grip and traction can be attained by angling the arm towards the stairs and extending it such that the lateral component of the ground reaction force pushes the robot in the opposite direction. Once again, the pneumatic wheels are driven forward once their axis of rotation exceeds the stair nosing causing the shank to mount the stair. It is noted that mechanical stoppers impede the rotation of the knee such that it remains slightly bent. The robot returns to a standing position through the coupled extension of the LHM and rotation of the pneumatic drive wheels while the thigh-torso angle remains locked.

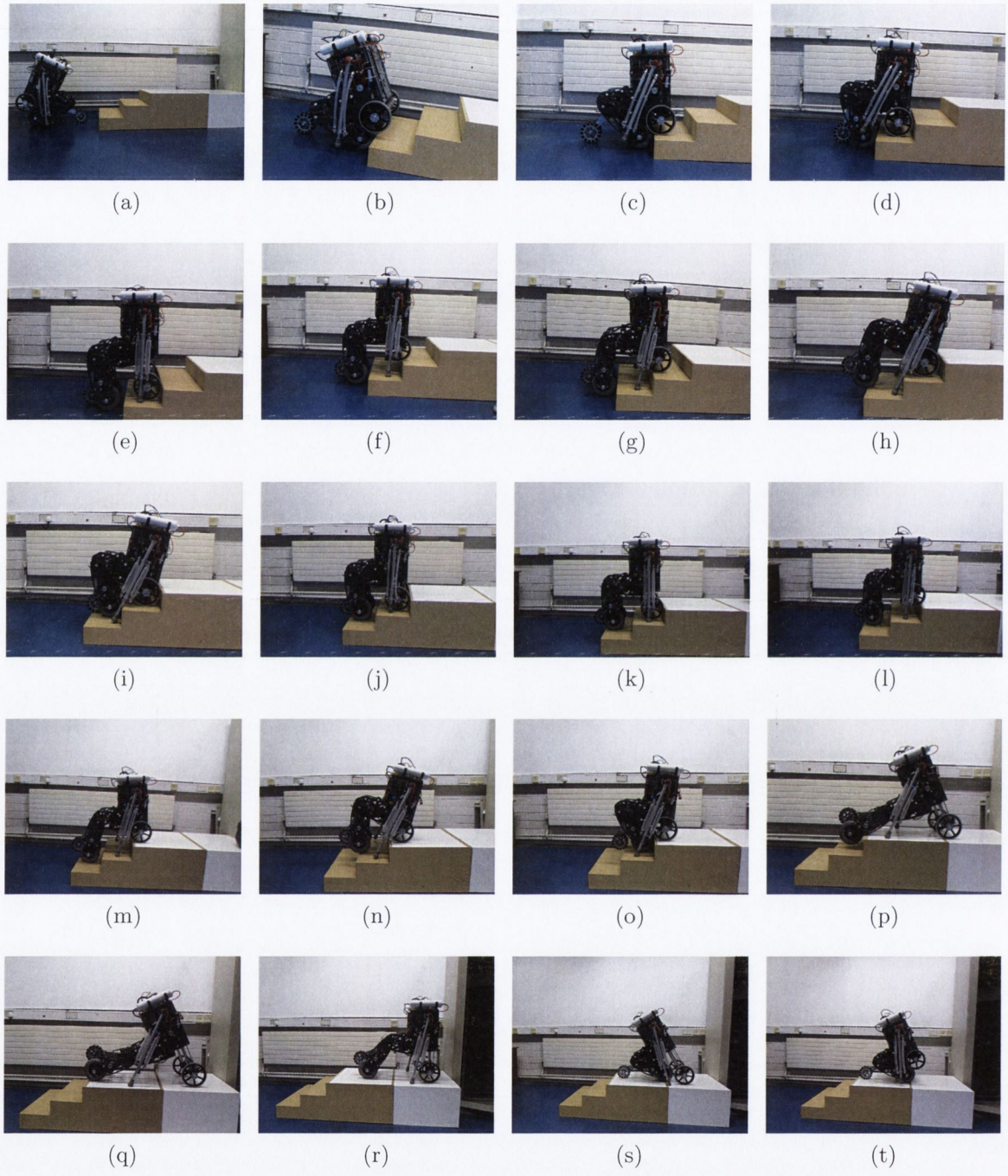


Figure 6.14: The process of stair ascent on the *v2.0* demonstrator (a)-(c) stair approach (d)-(f),(j-l) action #1 (g)-(i),(m)-(o) action #2 (p)-(t) stair recovery

6.2.6 Stairclimbing - Descent

To commence stair descent, the robot approaches the stairs in the forward orientation. Recall that a novel aspect of this morphology is that the orientation of the robot (with respect to the stairs) is the same for both stair ascent and descent. The LHM is extended and the stabiliser is contracted. This action causes the robot's centre of mass to shift backwards transferring the majority of the robot's weight to the LHM wheels. The shank drive wheels are driven forward and the knee extended until the shank drive wheels reach the stair nosing. The robot is driven forwards (using both the shank drive wheels and the LHM wheels) until the shank has crossed the nosing and stabilised on the tread below. The torso is then lowered through contraction of the LHM.

The first action of stair descent commences with the robot being driven forward until the shank once more passes the stair nosing and settles on the tread below. At this point, one tread separates the torso from the shank.

The second action begins by first contracting the hip muscle, minimising the thigh-torso angle. The arm is angled toward the empty riser and extended until it makes contact with the ground surface. The LHM wheels are then driven forward until the wheels cross the stair nosing and the majority of the torso's weight is transferred to the arms. At this point PAMs in the arms are slowly deflated and the action of gravity guides the torso to the tread below. Through iteration between action #1 and action #2, the robot can descend an arbitrary number of stairs in a statically stable manner. Once the robot reaches the final stair, it contracts the stabiliser inwards. It then simultaneously contracts the hip muscle and elongates the LHM causing the robot to lean forward. The PAM controlling the stabiliser is released slowly, ensuring that the robot does not fall forwards. Once this process is complete, the robot is free of the stair and can retract the LHM.

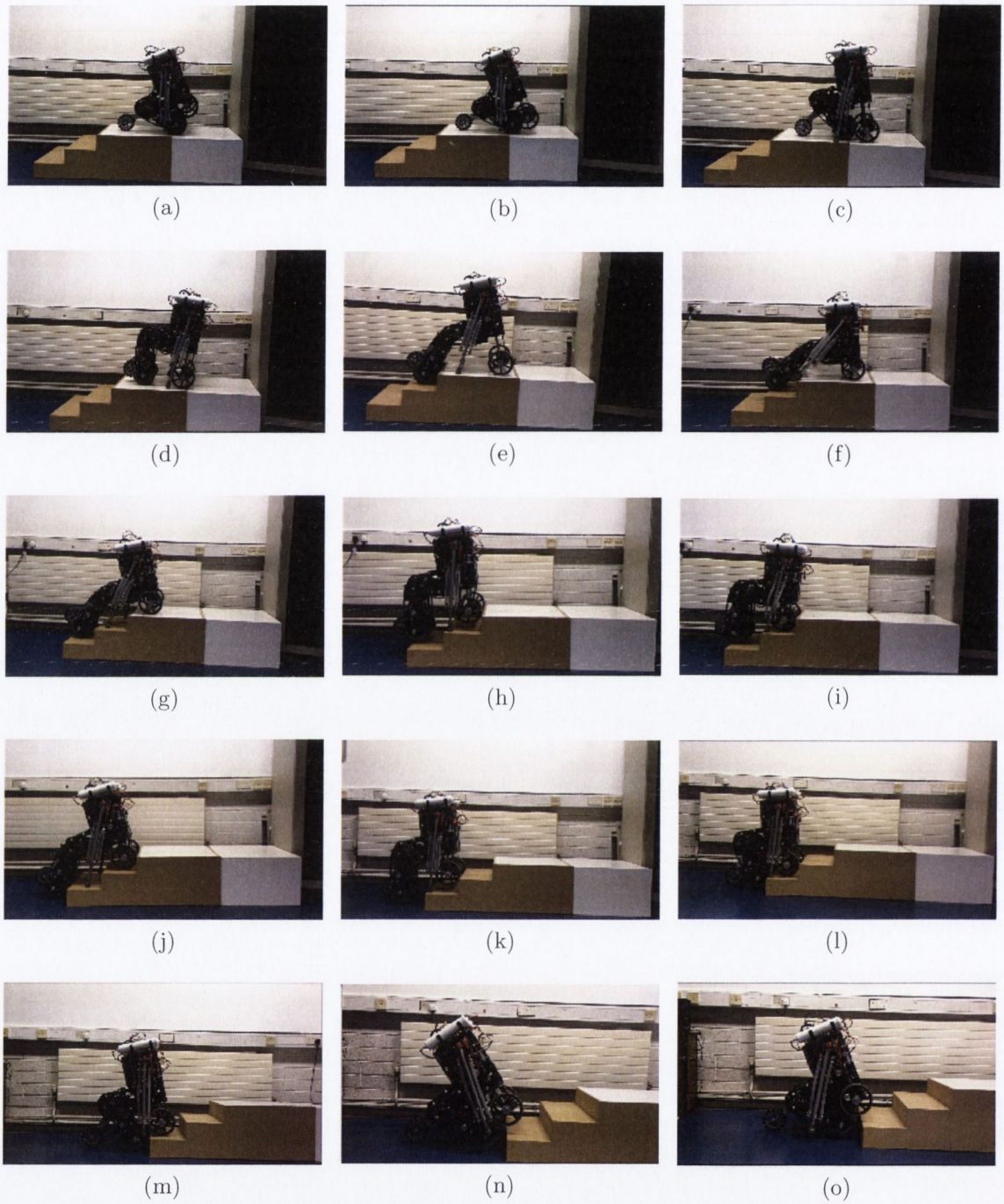


Figure 6.15: The process of stair descent on the *v2.0* demonstrator (a)-(g) stair approach (h-i) action #1 (j) action #2 (k-o) stair recovery

6.3 Human control of service robots

A robot's actions and behaviour are dependent on the means through which it's controlled. This is especially true for semi-autonomous robots where autonomous capability and manual control are closely coupled. Therefore the implementation of a suitable controller (both the physical embodiment and its integration within the overall control schema and system architecture) represents a very important aspect of the robot's overall design. In this work, an integrated semi-autonomous control schema is proposed and implemented on the *v2.0* embodiment. The system was designed in accordance with two hypothesises pertaining to the human control of robots.

1. In human-centred environments, manual control by a human user cannot consistently meet the performance delivered by an equivalent autonomous controller for navigation-based high-level tasks

2. The overall performance of a semi-autonomous robot increases in proportion with the degree of human interaction in the control loop.

6.3.1 Experimental Procedure

An interactive simulation was developed where a human participant controlled the movement and actions of a robot in a 3D virtual environment modelled closely on a large modern one-bedroom apartment. The environment contained four rooms (kitchen, bedroom, bathroom, sitting room with hall) and was populated with furniture and other common fixtures. Dynamically moving objects including a dog and a robotic vacuum cleaner were implemented also. The objective of the simulation was to instruct a personal assistant service robot (modelled closely on the proposed embodiment) to perform a series of tasks between different rooms in the house. The performance of human volunteers completing these designated tasks was measured and analysed. By comparing the participant's performance across the same tasks using several different controllers, it was possible to find correlations between the effectiveness of the controller embodiment and the underlying control schema. The simulation involved the operator performing the following tasks:

1. Moving the robot from the sitting room into the kitchen where it locates and collects a purple drinks can.
2. Delivering the drinks can to a person located in the bedroom.
3. Returning to a charge station in the hallway

In this case, a virtual simulation was favoured over conventional live testing for several key reasons:

1. **Architectural hazards**

   As the study sought to investigate the relationship between human tele-operated control and the specific properties of the task environment, particular attention was given to the design of the apartment and its contents. It would not have been feasible to construct an equivalent scale model of the space to the same degree as allowed by simulation.

2. **Quantification and data collection**

   The simulation is programmed to accurately and automatically capture behaviour and performance-based information throughout the completion of tasks. The quality and degree of data generation would not have been possible using a real-life setup.

3. **Environmental consistency**

   For comparison purposes, its important that each test is conducted under identical environmental conditions (lighting, clutter etc.). Through simulation, it was possible to ensure each participant partook in the exact same experiment under the same operating conditions.

4. **Human behaviour test**

   While the simulator uses the state-of-the-art Bullet physics engine, it provides a relatively poor technical model for the realisation of real-world robot dynamics. However as the purpose of the simulation is to investigate human behaviour, a non-realistic yet believable robot model is appropriate.

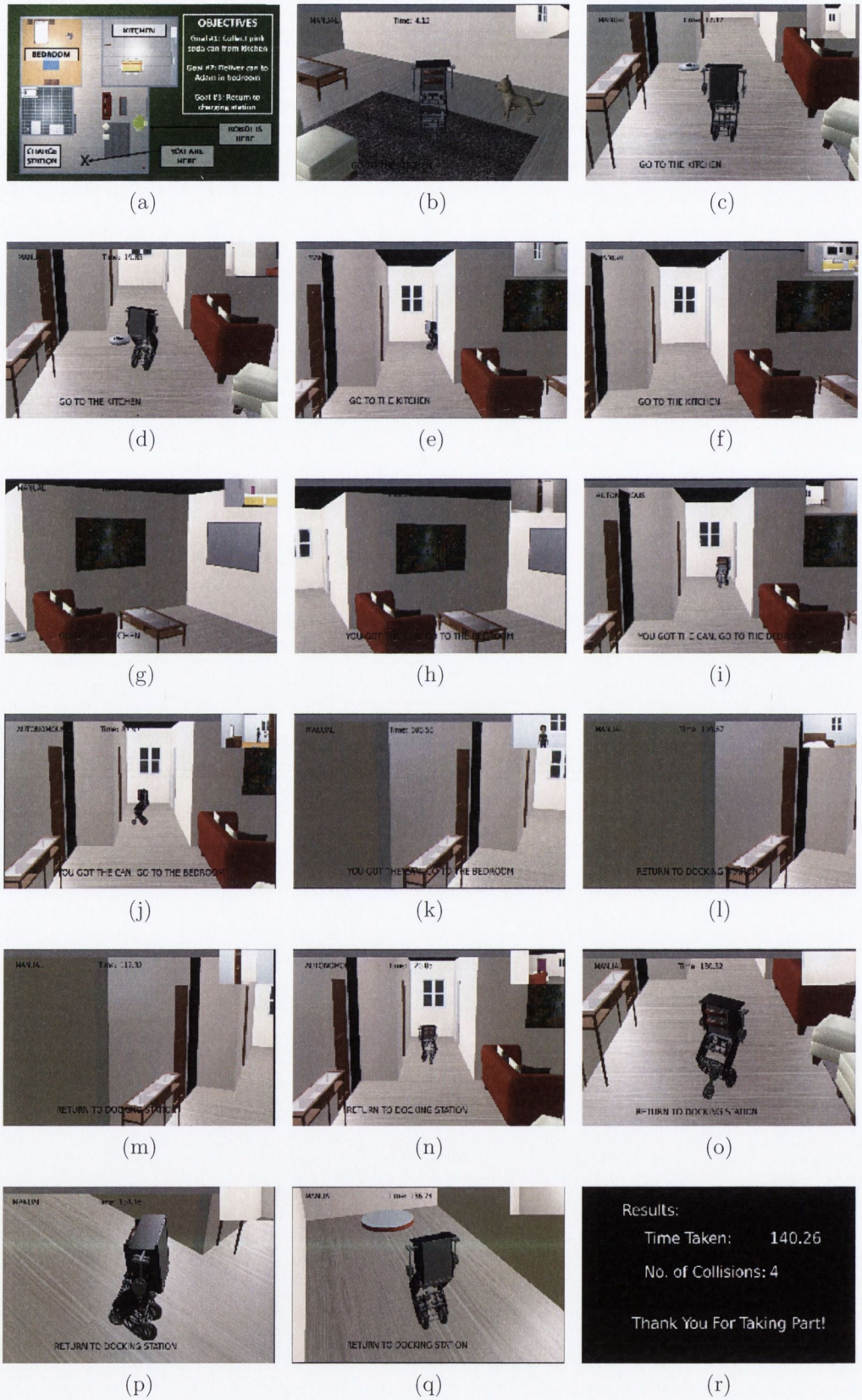
5. **Practical efficiency**

   Medium to large scale testing of robots causes several practical issues. Firstly complex robots can be unreliable and unsuitable for the kind of sustained use that such

tests require. Mobile robots typically require on-board power supplies that deplete over time. Not only does a diminishing power supply often effect system-level performance (reduce top-speed etc.) but it may also directly affect the period that the robot can operate for. As the setup requirements for real-world testing are typically high, the time required, cost and resources needed to perform real-world experiments is significant. Using simulation, these issues are largely averted.

The simulation was developed using the Blender Game Engine developed by the Blender foundation [203]. A typical sequence of completing each of the tasks is shown in fig 6.16. The camera is positioned in a fixed, first person viewpoint and implemented at eye-level to emulate the field-of-view (FOV) of a human operator standing in the room. While the position of the camera is fixed in space, it automatically tracks the robot as it moves throughout the house.

A second view emulating that of a camera positioned on the robot itself is visible in the top right hand-corner of the simulation window. Its field-of-view is restricted to approximate that of a 1080x720 pixel camera.



(a) (b) (c)

(d) (e) (f)

(g) (h) (i)

(j) (k) (l)

(m) (n) (o)

(p) (q) (r)

Figure 6.16: A walk-through of the 3D simulation where the user is challenged to guide a personal service robot as it performs some useful tasks

The simulation was designed so that achieving each goal required overcoming at least one architectural barrier or control challenge. Where possible, these impediments were unique to the specific goal that the participant was attempting.

When trying to reach the first goal (collecting the can in the kitchen) the robot must avoid two moving objects (a dog and a vacuum cleaner), one static object (sofa) and navigate through a door where the robot's local coordinate system was aligned with that of the human operator (Fig. 6.16b-6.16i).

To reach the second goal (deliver the can to the person), the robot must execute a zero-point turn, exit the door it previously came through and enter another door where this time the robot's local coordinate system is flipped 180° relative to the human operator (Fig. 6.16j-6.16l).

To reach the third goal (return to charging station), the robot must once again perform a zero-point turn, exit back through the door it came through (low visible contrast between the open doorway and the wall in the hallway) and to travel a curved trajectory to the charge station (Fig. 6.16m-6.16q). It is noted that both zero-point turn manoeuvres and two of the doorway traversals are accomplished outside the FOV of the human operator and with only the view from the robot's on-board camera to serve as a guide.

The participant is required to instruct the robot using varying levels of manual and semi-autonomous control implemented across two separate physical embodiments, a conventional Microsoft Xbox game controller and a purpose-built control application running on an Android tablet (Fig. 6.17). The simulation permits the robot to have a limited range of autonomous functionality. When in 'semi-autonomous' mode, the robot is capable of autonomously navigating between rooms, a capability that has been subject to a lot of study and is presently implemented on many service robots. Tasks requiring the robot to complete more specific, cognitively demanding instructions that requires specialist knowledge (i.e. 'find the can', 'deliver the can to a person') are only possible (for the purposes of the simulation) using manual human control.



(a) (b)

Figure 6.17: The control embodiments used during the simulation testing (a) Xbox game controller (b) custom built tablet control application

The status of the controller ('manual' or 'autonomous') is printed in the top left corner of the simulation window. Additionally a running timer is located in the top-centre of the screen. At the end of the simulation, once the user has successfully delivered the robot to the charging station, a score screen appears reporting the time taken (including penalties) and the number of collisions encountered.

The test required the user to complete the simulation five times, each time varying either the control schema (manual/semi-autonomous) and/or the physical embodiment (Xbox controller/app). Two different physical embodiments were evaluated for two distinct reasons.

Firstly since a significant proportion of those involved with the study were competent computer game users, it was predicted that they would possess an inherent advantage over participants that were unfamiliar and untrained with using conventional computer game controllers. Ensuring that at least one controller was unfamiliar to all participants provides a means of desensitising against such an issue.

Secondly since the study sought to investigate how the robot's performance changes with increased levels of human interaction, it was felt that a purpose built controller would better facilitate higher levels of interaction than purely retrofitting a generic game controller built for multi-functional use. A full description of the design and operating principles of the control application used in this experiment is given in section 5.3.

The five simulations were carried out in the following order:

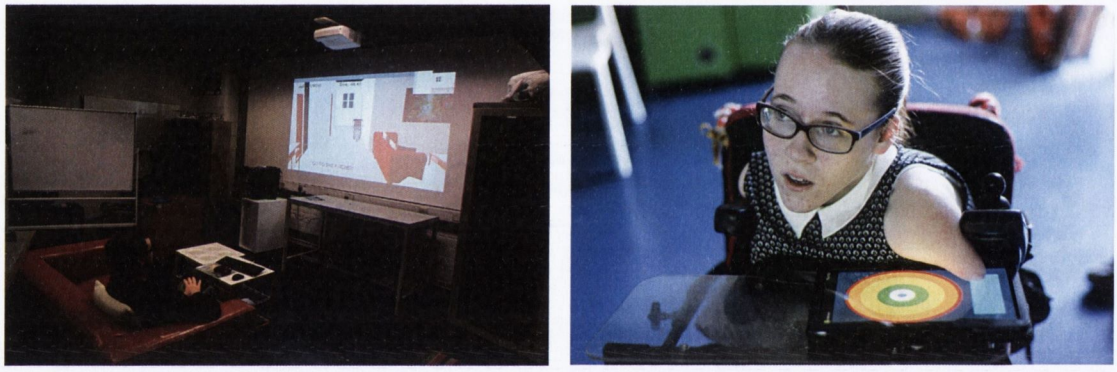
1. Xbox controller, full manual control
2. Xbox controller, semi-autonomous control (discrete switching)
3. Xbox controller, semi-autonomous control (continuous switching)
4. Application, full manual
5. Application, semi-autonomous (continuous switching, manual speed variance, autonomous confidence)

In manual mode, the user was responsible for assuming full control of the robot's movement and actions. When using the Xbox controller, the robot could be controlled at a constant speed using the device's 'left thumbstick'. When the app was used, manual mode required the user to control the robot using the novel joystick interface described in section 5.3. Since speed control is integrated into the application's manual joystick, increased levels of interaction is possible using the manual controller.

When semi-autonomous control with discrete switching is enabled, the robot switches between autonomous mode and manual mode using a discrete button press on the Xbox controller. When the 'right trigger' button was pressed, the robot entered autonomous mode and stayed in this mode until the 'left trigger' was pressed when it would return back to manual mode.
In semi-autonomous mode with continuous switching, operating in autonomous mode required continuous input to be provided by the user, regardless of whether the system was being manually or automatically controlled. When using the Xbox controller, autonomous mode was engaged when the user pressed and held the 'left trigger'. Once released, the robot automatically reverted to manual mode and was then only responsive to commands from the 'left thumbstick'. When using the control app, autonomous mode was activated when the user touched the dedicated touchpad located below the manual joystick. With multi-touch enabled, the number of discrete points of contact detected in this region determined the confidence level which in turn adjusted the autonomous speed of the robot. If the operator removed their fingers from the touchpad, the controller reverted to manual mode. A full description of this controller and the psychology behind its design is given

in section 5.3.

Each user was given the opportunity to familiarise themselves with the floor plan of the house (shown in figure 6.16a). This was done firstly through visually displaying the floor plan on the loading screen at the start of each simulation. An additional hard-copy of the floor plan was also located on the table in front of each participant. To familiarise themselves with using the physical controllers and performing the control tasks, each user was given one unrecorded test run using both the Xbox controller and the tablet device running the control application.



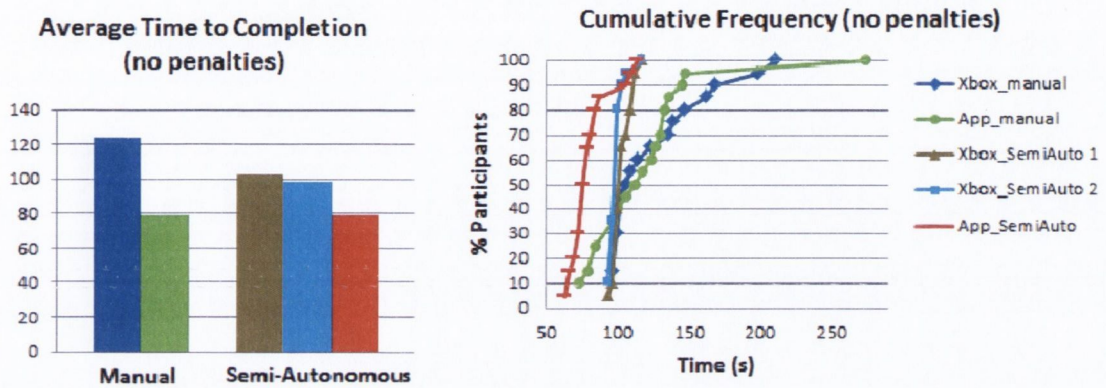
(a) (b)

Figure 6.18: Practical testing of the control schema and custom control embodiment (a) user testing in lab in Trinity (b) field testing with personal service robot user

6.3.2 Results from Simulation study

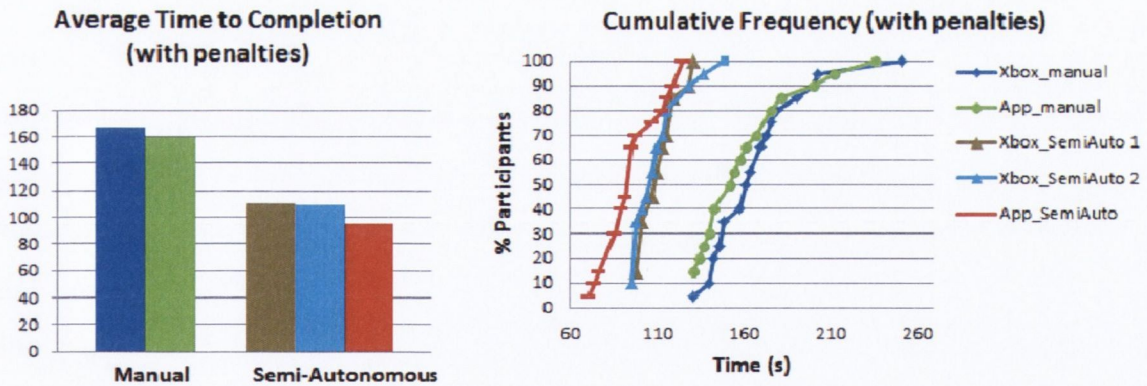
A study was undertaken whereby twenty volunteers partook in the experiment outlined in section 6.3.1. Of the sample set, 80% were students under the age of 25 and 90% of them were male. The overall performance of the users was assessed based on two metrics; firstly their ability to complete the level in the fastest time and secondly their ability to avoid collisions in the process. It was found during preliminary testing that in an effort to record the fastest time, users often placed little priority on avoiding collisions. To remedy this, a ten second penalty was added for every collision that the user incurred during the simulation.

A cumulative frequency distribution and bar chart conveying the overall time taken (with and without time penalties) for each controller across the sample set is given in figure 6.19 and figure 6.20.



(a) (b)

Figure 6.19: Overall performance of each controller (time penalties not included) (a) bar chart (b) cumulative frequency plot



(a) (b)

Figure 6.20: Overall performance of each controller (time penalties included) (a) bar chart (b) cumulative frequency plot

A bar chart contrasting the performance of each control method with respect to the number of collisions is shown in figure 6.21.

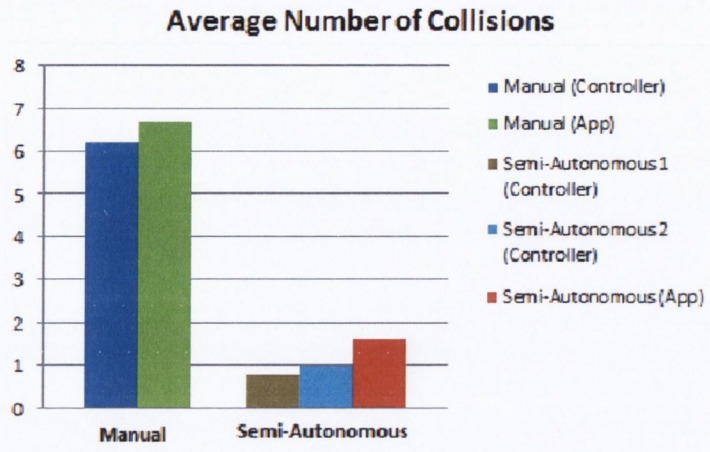


Figure 6.21: Number of collisions recorded for each controller

A breakdown of the time taken to progress through the level is shown in figure 6.22. The time on this graph is representative of the actual time taken plus collision penalties.

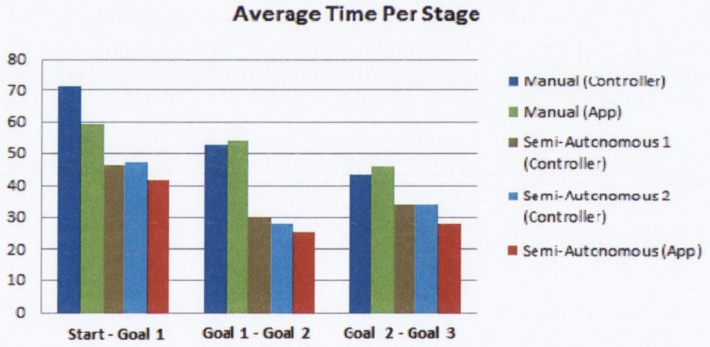


Figure 6.22: Average time recorded per stage

6.3.3 Findings from Simulation study

It is clear from both figure 6.19 and figure 6.20 that the semi-autonomous controllers consistently outperformed the manual controllers, independent of any specific embodiment. It is evident from figure 6.19 that when the robot is manually controlled, significantly faster completion times were achieved using the control app than with the Xbox controller. This improvement is attributed to the increased level of human interaction facilitated by the app controller. However the improvement was less apparent when time penalties were considered (Fig. 6.20, Fig. 6.21) as users tended to have more accidents when using the

app. The increased number of collisions from the control app is primarily attributed to (1) many of the participants in the study had prior experience of using a Xbox controller and were unfamiliar with the control app control interface (2) several users complained that the control app was too responsive and required further tuning (3) the control app did not provide tactile feedback and users often had to take their eyes off the simulation to look at the controller.

It is also observed from these figures that the semi-autonomous control mode is better realised through a process of continuous switching than the less involved discrete-switching approach when implemented using the Xbox control embodiment. Once more this indicates that increased levels of operator interaction improve the performance of semi-autonomous controllers.

From figures 6.19 and 6.20, it is apparent that the semi-autonomous control schema implemented on the control app offers the best overall performance. This is largely due to the fact that the user has the ability to vary the speed of the robot (in both manual and autonomous modes) with virtually no additional control effort. It was observed that arising from the ease of interaction permitted by the custom-designed controller, users tended to control the robot with increased efficiency. For example in scenarios where the robot required straight-line movement to be carried out within the operator's FOV, high-speed manual control was efficiently performed. However for tasks performed outside the operator's FOV, manoeuvres that required fine control and for navigation when the robot's local co-ordinates were misaligned with that of the operator, users naturally delegated control to the autonomous controller. Based on these results, it is reasonable to deduce that increased performance and controllability is emergent from controllers that facilitate higher levels of machine-user interaction.

Another objective the study was to investigate and identify the environmental barriers and control hazards that may affect the performance of a service robot in a civilian environment. From figure 6.21, it is clear that collisions were commonly incurred throughout the level and were particularly common during manual operation. As the incidence of col-

lisions does not change significantly between controller embodiments, this suggests that collisions can be attributed predominantly to human-error.

From the study it was observed that the action which caused the most number of collisions involved passing through doorways where fine control was required and the spatial awareness of the operator with respect to the robot and the doorway is low. The operator's ability to manually traverse through doorways was generally improved when exiting rooms as the path to the doorway was usually straighter than when first entering the door from the hallway corridor.

The second most significant navigation issue was steering mistakes caused when the operator was tasked with driving the robot towards the operator. Users often tended to steer the robot in the wrong direction since the robot's local co-ordinate system is misaligned with that of the operator. Since the vacuum cleaner is only visible when it was in front of the robot or in the FOV of the operator, dynamically moving objects also negatively affectively affected the reliability of the system under manual control.

6.4 Summary

Despite being only the second physical embodiment of the proposed morphology, the *v2.0* embodiment has demonstrated a wide range of impressive performance capabilities while simultaneously maintaining the physical practicality required for operation in both indoor and outdoor civilian environments. As the embodiment has succeeded in meeting each of the proposed design targets, it is evident that the proposed morphology is practically realisable. Furthermore it is reasonable to expect that future embodiments of the will possesses the potential to realise levels of behavioural diversity required for robust general-purpose operation in civilian environments.

When the mechanical complexity of the proposed morphology is compared against equivalent systems or alternative morphologies, it is observed that very high levels of terrain adaptability are possible using relatively few controllable degrees of freedom. Recall that an additional reduction in system complexity is possible under certain ideal conditions described in section 3.4.1, thus further enhancing the desirability of the system. Comparing the demonstrable terrain adaptability of the system with its overall mechanical

complexity, the proposed morphology in the desired region of the graph shown in figure 2.22a. Additionally since the system is statically stable, it also exists within the desired region of figure 2.22b.

As the v2.0 system possesses an interactive social interface, it is one of the few practical mobile service robots with the capability of engaging in meaningful social interaction with people. With over five degrees of freedom, the social interface is too positioned within the desirable region of the graph in figure 2.23.

A more thorough comparison of the *v2.0* robot prototype against equivalent morphological embodiments is given in table 6.2. It is clear from this comparison that in addition to possessing a unique combination of practical traits (static stability, terrain adaptability, low mechanical complexity etc.), the morphology is also possesses a unique set of practical performance when compared against equivalent, state of the art robot platforms

	Static stability	Indoor locomotion	Zero-point turn	Soft terrain locomotion	Crevice crossing	Obstacle climbing	Stair climbing	Interactive social interface	Compliant joints	Modular software	Modular hardware	Dual arms	On-board power	On-board high-level controller	Ground pick-up
HERB 2.0	✓	✓	✓	✗	✗	✗	✗	✗	✓	?	✓	✓	✓	✓	✓
HUBO-2	✗	✓	✓	✓	✓	✓	✓	✗	✗	✓	✗	✓	✓	✗	✓
Asimo '11	✗	✓	✓	✗	✓	✓	✓	✓	✗	✗	✗	✓	✓	✗	✗
Care-O-Bot	✓	✓	✓	✗	✗	✗	✗	✓	✗	✓	✗	✗	✓	✓	✓
PR-2	✓	✓	✓	✗	✗	✗	✗	✗	✓	✓	✓	✓	✓	✓	✓
Atlas	✗	✓	✓	✓	✓	✓	✓	✗	✗	✓	✗	✓	✓	✗	✗
BEAR	✓	✓	✓	✓	✓	✓	✓	✗	✗	?	✗	✓	✓	✗	✓
uBot v5	✗	✓	✓	✗	✗	✗	✗	✗	✗	?	✗	✓	✓	✗	✓
COMAN	✗	✓	✗	✓	✓	✓		✗	✓	✓	✗	✓	✓	✗	✗
V2.0	✓	✓	✓	✓	✓	✓	✓	✓	✓	✓	✓	✓	✓	✓	✓

Table 6.2: Comparison of existing platforms

In addition to validating the practical capability of the robot, a novel method of semi-autonomous control has been developed and subjected to a practical evaluation. Using a

purpose-built virtual simulator, the proposed control schema (and controller embodiment) was evaluated against conventional systems. It was found that semi-autonomous control schema perform consistently better than equivalent manual systems for navigation-based control tasks. Furthermore it was shown that through utilisation of control schema that necessitate increased levels of operator interaction, increased performance levels can be realised.

Chapter 7

Conclusions

Existing robot morphologies have typically failed to demonstrate the full range of terrain adaptability, physical practicality and behavioural diversity needed for general-purpose use, as the most suitable morphologies for certain tasks are highly unsuitable for others. This work set out to develop a robot morphology that is capable not only of passing a range of assessment metrics that demonstrate proficiency in each of these areas but also to demonstrate that the overall system design possesses unique capabilities that make it additionally advantageous over equivalent systems as a general-purpose morphology. In light of this, this work contributes primarily towards the morphological design of service robots. The core hypothesis that underlies this study is that the successful design of a complex, multi-functional system capable of general-purpose use can be made possible through the adoption of an embodied design approach and through detailed integration of the mechanical design (kinematics, dynamics, actuation etc.), the design of robotic system architecture (low/high level sensing and control) and design of the human-robot interface as well as through detailed consideration of the range of task environments. Two full-scale embodiments of the proposed morphology were designed and built. To validate the hypothesis, the second of these prototypes was subjected to a range of performance tests and physical assessments. In so doing, several significant contributions are made including:

1. The design, analysis and practical embodiment of a novel robot morphology capable of high behavioural diversity including the ability to pick-up objects from the ground, traverse a wide range of civilian environments and overcome several significant architectural barriers including small vertical obstacles, crevices and stairways.

2. A robot morphology capable of pose adjustment through active control of its static stability margin.
3. A novel electro-pneumatic actuation schema that utilises electric motors for accurate wheeled locomotion and pneumatics for actions requiring high compliance and the generation of large forces.
4. A robust, modular and distributed robot control architecture capable of integrating low-level proprioceptive sensing and reactive actuation with high-level perception and control. In addition to providing autonomous capability, this control architecture facilitates integration with a range of manual and semi-autonomous control schemes.
5. A novel embodiment of a semi-autonomous controller which when integrated with the proposed control architecture, offers increased levels of performance over conventional manual or semi-autonomous control mechanisms.

Firstly a literature review was undertaken to ascertain the state-of-the-art in robot design philosophy, morphology design and robotic actuation. It was evident from this review that no practical service robot morphology currently facilitates the possession of both low system complexity and high terrain adaptability (see Fig. 2.22a). With safety and energy efficiency being important properties of all service robots, it was further observed that no statically stable robot morphology has the capability for both high terrain adaptability and high task-based behavioural diversity (see Fig. 2.22b). Few state-of-the-art mobile robot systems possess an interface that provides continuous visual feedback and fewer still possess interactive social interfaces. Of the robots that do possess interactive social interfaces, they are typically implemented on systems of low behavioural diversity or the interfaces themselves fall into the 'uncanny valley' (see Fig. 2.23).

Following the literature review, a high-level description of the proposed robot morphology was given. This was then followed by a mathematical description of the system's basic kinematics. Using the DH-convention, the set of homogeneous equations needed to describe the location and orientation of the robot's joints relative to a global reference frame, was presented. The inverse kinematics were explored by deriving the Jacobian matrix of

one of the system's end effectors. Using the pseudo inverse of the Jacobian, a description was given of how the system's inverse kinematics can be performed effectively. Using the Robotics toolbox for Matlab[191], a 3D computer model of the system's forward kinematics was created. Using this model, the effectiveness of the inverse kinematics algorithm was assessed and validated. Using the Static Stability Margin as a metric to quantify a robot's static stability, the stability of the proposed morphology was assessed. Since the robot is capable of dynamically adjusting its static stability margin, the system was said to be quasi-statically stable. The final section in the chapter provided a high-level description of how various gaits/action sequences can be used to perform demanding tasks (i.e. crevice crossing. stair-climbing). It was observed that the proposed robot morphology is unique in its capability to ascend/descend stairways facing the same direction. This trait is highly advantageous as it eliminates the need for zero-point turns to be carried out under especially demanding environmental conditions.

The mechanical design of the embodiment is presented in the fourth chapter. A dynamic analysis was undertaken to predict the reaction forces in the joints and the torques required to achieve desirable postural configurations. Since the robot is statically stable and joint accelerations are typically low, the analysis was conducted using the joint segment method. This allowed for the creation of a parametric model which was then used to predict the actuation requirements of the robot over a range of postural configurations. A description is given of the unique electro-pneumatic system of actuation used by the robot with special attention paid to the custom design, in-house fabrication and integrated morphological optimisation of the network of pneumatic air muscles used. The remainder of the chapter covers the detailed mechanical design of the legs, torso, lower hip mechanism and arms of the *v2.0* embodiment.

A highly reconfigurable, modular robot system architecture was developed and integrated into the robot morphology. The high-level design of a novel distributed system architecture is discussed in chapter five. Through the use of discrete, distributed computing hardware and modular software development, the architecture succeeds in integrating three layers of control - low-level reactive control, high-level deliberative control and direct

tele-operated control. The custom hardware design of the architecture's GPIO modules (generic low-level microprocessor based pcb boards for interfacing with sensors and actuators) is presented. A description of the *v2.0* prototype's low-level proprioceptive system is outlined. Following this, the design of the social interface, the integration of the social interface with the system architecture and the design of a novel semi-autonomous control schema which promotes increased levels of human interaction is presented and discussed.

Based on the limitations of existing morphologies, a practical list of design targets that aseesess the capabilities of the *v2.0* demonstrator was presented. These targets were drawn up to provide a basis to facilitate benchmarking against existing embodiments and to assess the morphology's potential for general-purpose use. The *v2.0* demonstrator embodiment was subjected to a range of tests to evaluate the degree to which it meets the proposed targets. Amongst the capabilities that the robot successfully demonstrated include height adjustment through augmentation of the static stability margin, the ability to cross crevices, obstacle traversal and stair climbing (both ascent and descent). Based the demonstrators ability to achieve the proposed metrics, it is evident that the robot possesses a combination of physical traits and performance capabilities (pertaining to terrain adaptability, behavioural diversity, human-robot interaction and stability) unmatched by any other morphology developed to date. It is observed that while the development of the embodiment presented in this work remains somewhat immature in comparison with the majority of the platforms that it has been compared against, it can be expected that many further improvements and upgrades will be possible with increased financial investment, further design iteration and from the anticipated findings of future academic study.
Through user-testing on a custom-made virtual simulator, it was found that semi-autonomous control offers inherent performance improvements over manual control in human-centred environments. It was evident that during instances where perception is limited and/or in the presence of architectural barriers, manual control becomes a highly error prone process. Additionally the efficiency of the manual controller will depend heavily on the physical embodiment of the controller and the degree to which it is tuned. This latter consideration is especially significant considering the high practical desirability of using smartphones, tablets and other non-optimised controller embodiments for service robot

applications. Furthermore it was shown that the best overall task performance was consistently achieved using the integrated semi-autonomous control schema described in chapter five. This improvement in performance over conventional semi-autonomous controllers is primarily attributed to the increase in the degree of human interaction made possible through integration with the proposed system architecture and through the custom design of a complimentary hardware embodiment. With this controller, improved levels of performance were realised when the user delegated control to the robot in instances when manual control is impractical (robot out of operator's field of view, robot moving through doorway etc.) and later resumes manual control when safe and appropriate to do so (when robot is in their field of view, when robot is operating in uncluttered environment etc.). It was found that by facilitating increased interaction through enabling the user to vary the speed of the robot (both in manual and autonomous mode), further improvements in task performance were made possible.

7.1 Future Work

Despite demonstrating several impressive performance capabilities, considerable work remains before the robot is fully capable of demonstrating truly robust, general-purpose performance levels. The three areas of future work most important to the realisation of this potential include include embodiment design, social interface integration and increased autonomous functionality.

In order that an embodiment of the proposed morphology can meet the safety standards required for use by civilians, its design must adhere fully with the ISO 13482. To address this requirement, future work will require a detailed risk analysis to be conducted and the required improvements incorporated through a top-down design approach. Some examples of required design modifications include covering any exposed belts, protecting the electronics from dust/water, improving battery accessibility and integrating safe and reliable start-up, shutdown and emergency control procedures.
Based on practical evaluation of the present prototype, several other design modifications are recommended.

1. **Incorporate cable tensioner on PAMs**

   It was found that slack often developed when the PAMs were at normal pressure and the limbs positioned in certain configurations. This problem was most notable when attempting stair-climbing when the knee was allowed to extend towards the limit of its mechanical capability. This slack often caused the cable to misalign from the connecting pulley thus requiring manual realignment. To remedy this problem, an additional spring loaded tensioning pulley should be integrated to maintain a minimum tension in the cable and to ensure accurate pulley alignment.

2. **Increased on-board computation**

   In its current embodiment the height of the torso was minimised to reduce the torque requirements of the hip. Future iterations should possess a larger torso which would enable more computer hardware to be mounted within the robot.

3. **Faster valve response times**

   It was found that despite being possible to vary the flowrate through the valves, the valves presently installed on the robot are poorly suited to accurate control applications. It is recommended that valves with substantially lower response times (¡5ms) be used for all other embodiments. It is noted that although manual throttling valves proved extremely effective on the *v2.0* prototype however their poor reconfigurability makes them a unsuitable long term solution.

While the framework required to support the social interface has been developed and implemented within the robot's architecture, work remains on developing behaviours and features required to enable fluid natural interaction to take place between the robot and humans in its vicinity. The following are representative of some of the key capabilities that remain to be incorporated:

1. **Attention and Emotion Modelling**

   At a given instant, the attention of the robot should be concentrated to the region within its local environment that it is most concerned with. Attention modelling should be realised primarily through control of the eyes and head (when additional degrees of freedom are incorporated). The system should possess the ability to track faces, local movements and objects with high saliency (certain colours, shapes

etc.). The robot should possess an emotional model that can be updated and will (over time) provide meaningful feedback to human users. The sophistication of the emotional model (both in appearance and behaviour) should be in line with the overall complexity of the robot platform to ensure the alignment with the user's perceived expectation of the robot.

2. **Turn-taking behaviour**

   The social interface should provide a focal point for turn-taking behaviour to take place. Turn-taking behaviour is an example of a complex capability that requires the interaction and co-operation of many of the robot's sensors, actuators and computers.

3. **Voice/Gesture Control**

   Communication between people is a highly layered process that is accomplished using many overlapping actions (speech, body language, gestures etc.). Equipping the robot with the ability to verbally and physically understand human behaviour would help provide the basis for increased levels of interaction. Additionally gesture recognition through the use of point cloud data is currently an area of much academic interest and one that promises impressive capabilities in the near/intermediate future.

The third significant area of future work relates to the integration of autonomous capability on the robot embodiment. In its present embodiment, most of the performance achieved to date has been done using open loop control. This has been made possible owing to the robot's high static stability and the mechanical limits of its joints. To ensure that the capabilities of the robot can be realised in a self-regulated system, a range of feedback controllers are required.

Furthermore, to fully realise the morphology's practical utility, higher level autonomous control should be incorporated. This will require the addition and integration of at least one dedicated computer running the Robot Operating System (ROS) environment. Through utilisation of ROS, it will be possible to use a wide range of state-of-the-art software libraries, simulation tools and monitoring capabilities. It is noted that ROS integration will require the further development of an architecture specific communication

protocol and/or additional software drivers that facilitate the transmission of information between the 'master' module and the ROS-based high-level computers. To provide the environmental perception necessary for high-level autonomous functionality, exteroceptive sensors including IR depth sensors, vision systems and LIDAR need to be implemented. With the system possessing high sensing ability and increased computational resources available, the robot will be ready for the programming and implementation of advanced autonomous capability. Autonomous functionalities presently of great interest include:

1. Advanced locomotion including (autonomous stair climbing, crevice crossing etc.)
2. Simultaneous Localisation and Mapping (SLAM)
3. Autonomous pick-and-place
4. Performance of specific tasks relevant to assistant living applications (cleaning, carrying objects, providing interface for communication etc.)

Bibliography

[1] Aristotle, "Politics," in *Book 1*, Batoche Books, 350BC. [Online]. Available: http://classics.mit.edu/Aristotle/politics.html.

[2] International Federation of Robotics (IFR). (2014). Service robots, Definition of service robots, [Online]. Available: http://www.ifr.org/service-robots/ (visited on 2014).

[3] "Robots and robotic devices - vocabulary," International Organization for Standardization, ISO 8373:2012, 2012.

[4] B. Gates, "A robot in every home.," *Scientific American*, vol. 296, no. 1, pp. 58–65, Jan. 2007, ISSN: 0036-8733. [Online]. Available: http://www.ncbi.nlm.nih.gov/pubmed/17186834.

[5] K Henriksen, J. Battles, and M. Keyes, "Home health care patients and safety hazards in the home: Preliminary findings," *Advances in Patient Safety: New Directions and Alternative Approaches*, vol. 1, pp. 1–16, 2008. [Online]. Available: http://www.ncbi.nlm.nih.gov/books/NBK43619/.

[6] L. H. Chen, M. Warner, L. Fingerhut, and D. Makuc, "Injury episodes and circumstances: national health interview survey, 1997-2007.," *Vital and health statistics. Series 10, Data from the National Health Survey*, no. 241, pp. 1–55, 2009, ISSN: 0083-1972. [Online]. Available: http://www.ncbi.nlm.nih.gov/pubmed/20187342.

[7] *Global report on falls prevention in older age*, World Health Organisation, 2008, ISBN: 9789241563536.

[8] P. L. Jackson and H. Cohen, "An in-depth investigation of 40 stairway accidents and the stair safety literature," *Journal of Safety Research*, vol. 26, no. 3, pp. 151–159, 1995, ISSN: 00224375. DOI: 10.1016/0022-4375(95)00014-H. [Online]. Available: http://linkinghub.elsevier.com/retrieve/pii/002243759500014H.

[9] J. Sheldon, "On the natural history of falls in old age," *British Medical Journal*, 1960. [Online]. Available: http://www.ncbi.nlm.nih.gov/pmc/articles/PMC2098310/.

[10] M. Quigley, K. Conley, B. Gerkey, J. Faust, T. B. Foote, J. Leibs, R. Wheeler, and A. Y. Ng, "Ros: An open-source robot operating system," in *ICRA Workshop on Open Source Software*, 2009.

[11] G. Metta, P. Fitzpatrick, and L. Natale, "Yarp: Yet another robot platform," *International Journal on Advanced Robotics Systems*, vol. 3, no. 1, pp. 43–48, 2006.

[12] H. Nguyen, J. Morrell, K. Mullens, A Burmeister, S. Miles, N. Farrington, K. Thomas, and D. Gagee, "Segway robotic mobility platform," *SPIE Mobile Robots XVII*, 2004.

[13] E Guizzo, "Rescue-robot show-down," *IEEE Spectrum*, pp. 52–55, 2014. [Online]. Available: `http://ieeexplore.ieee.org/xpls/abs\_all.jsp?arnumber=6701433`.

[14] R. Murphy, "Introduction to ai robotics," in. The MIT Press, 2000, ISBN: 0-262-13383-0.

[15] R Brooks, "Intelligence without representation," *Artificial Intelligence*, vol. 47, pp. 139–159, 1991.

[16] R. A. Brooks, "Intelligence without reason," in *Proceedings of the 12th International Joint Conf. on Artificial Intelligence - Volume 1*, ser. IJCAI'91, Sydney, New South Wales, Australia: Morgan Kaufmann Publishers Inc., 1991, pp. 569–595, ISBN: 1-55860-160-0. [Online]. Available: `http://dl.acm.org/citation.cfm?id=1631171.1631258`.

[17] J. Bongard and R. Pfeifer, *How the Body Shapes the Way We Think: A New Version of Intelligence*. The MIT Press, 2006, ISBN: 9780262162395.

[18] S. Hirose, "Three Basic Types of Locomotion in Mobile Robots, journaltitle = Robots in Unstructured Environments: Fifth Intl. Conf. on Advanced Robotics, '91 ICAR," vol. 1, 1991.

[19] R. Siegwart and I. Nourbakhsh, "," in *Introduction to Autonomous Mobile Robots*. The MIT Press, 2004, ch. 2, p. 30, ISBN: 0-262-19502-X.

[20] J. Wong and W. Huang, ""'wheels vs. tracks" a fundamental evaluation from the traction perspective," *Journal of Terramechanics*, vol. 43, pp. 27–43, 1 2006.

[21] L. Laursen, "Google is building its own self-driving car prototypes," *IEEE Spectrum*, 2014. [Online]. Available: `http://spectrum.ieee.org/cars-that-think/transportation/self-driving/google-is-building-selfdriving-car-prototypes`.

[22] J. Mehling, P. Strawser, L. Bridgwater, W. Verdeyen, and R. Rovekamp, "Centaur: Nasa's mobile humanoid designed for field work," in *Robotics and Automation, 2007 IEEE International Conference on*, 2007, pp. 2928–2933. DOI: `10.1109/ROBOT.2007.363916`.

[23] C. Connette, C. Parlitz, B. Graf, M. Hagele, and A. Verl, "The mobility concept of care-o-bot 3," *39th International Symposium on Robotics (ISR)*, pp. 737–758, 2008.

[24] J. Bohren, R. Rusu, E. Jones, E. Marder-Eppstein, C. Pantofaru, M. Wise, L. Mosenlechner, W. Meeussen, and S. Holzer, "Towards autonomous robotic butlers: Lessons learned with the pr2," in *IEEE International Conference on Robotics and Automation (ICRA)*, 2011, pp. 5568–5575. DOI: `10.1109/ICRA.2011.5980058`.

[25] A. Chopra, M. Obsniuk, and M. Jenkin, "The nomad 200 and the nomad superscout: Reverse engineered and resurrected," *The 3rd Canadian Conf. on Computer and Robot Vision*, 2006.

[26] V. Tucakov, M. Sahota, D. Murray, A. Mackworth, J. Little, S. Kingdon, C. Jennings, and R. Barman, "Spinoza: A stereoscopic visually guided mobile robot," *Proc. of the Thirtieth Hawaii International Conf. on System Sciences*, 1997.

[27] B. Gerkey and K. Conley, "Ros topics: Robot developer kits," *IEEE Robotics and Automation Magazine*, p. 16, 2011. [Online]. Available: `http://ieeexplore.ieee.org/stamp/stamp.jsp?tp=&arnumber=6016608`.

[28] L. Wang, K. Tan, and V. Prahlad, "Developing khepera robot applications in a webots environment," *Proc. of 2000 International Symposium on Micromechatronics and Human Science*, pp. 71–76, 2000.

[29] S. Zaman, W. Slany, and G. Steinbauer, "Ros-based mapping, localization and autonomous navigation using a pioneer 3-dx robot and their relevant issues," *2011 Saudi International Electronics, Communications and Photonics Conference (SIECPC)*, pp. 1–5, 2011.

[30] M. Stilman, J. Olson, and W. Gloss, "Golem krang: Dynamically stable humanoid robot for mobile manipulation," *IEEE International Conf. on Robotics and Automation (ICRA)*, 2010.

[31] V. Ragusila, S. Emami, J. Rebula, and T. Hutcheson. (2010). Tbot: The self-balancing transformer robot, [Online]. Available: `http://www.shervinemami.info/tbot.html`.

[32] S. Kuindersma, E. Hannigan, D. Ruiken, and R. Grupen, "Dexterous mobility with the ubot-5 mobile manipulator," in *Proc. of the 14th International Conference on Advanced Robotics (ICAR)*, 2009, pp. 1–7.

[33] D. Ruiken, M. Lanighan, and R. Grupen, "Postural modes and control for dexterous mobile manipulation: the umass ubot concept," in *Proc. of the 13th IEEE-RAS International Conference on Humanoid Robots*, 2013).

[34] E. Guizzo, "Anybots qb telepresence robot lets you be at the office ... without being there," *IEEE Spectrum*, 2010. [Online]. Available: `spectrum.ieee.org/automaton/robotics/industrial-robots/051810-anybots-qb-new-telepresence-robot`.

[35] D. Theobald, "Mobile extraction-assist robot," pat. US7719222 B2, 2010. [Online]. Available: `http://www.google.com/patents/US7719222`.

[36] J. Falconer, "Cmu's chimp humanoid robot moves like a tank," *IEEE Spectrum*, 2013. [Online]. Available: `http://spectrum.ieee.org/automaton/robotics/humanoids/cmu-chimp-humanoid-robot-moves-like-a-tank`.

[37] L. Caracciolo, A. De Luca, and S. Iannitti, "Trajectory tracking control of a four-wheel differentially driven mobile robot," *IEEE International Conf. on Robotics and Automation*, vol. 4, pp. 2632–2638, 1999.

[38] B. M. Yamauchi, "Packbot: A versatile platform for military robotics," in *Unmanned Ground Vehicle Technology VI*, G. R. Gerhart, C. M. Shoemaker, and D. W. Gage, Eds., ser. Society of Photo-Optical Instrumentation Engineers (SPIE) Conference Series, vol. 5422, Sep. 2004, pp. 228–237. DOI: `10.1117/12.538328`.

[39] P. Hebert, M. Bajracharya, J. Ma, N. Hudson, A. Aydemir, J. Reid, C. Bergh, J. Borders, M. Frost, M. Hagman, J. Leichty, P. Backes, and B. Kennedy, "Mobile manipulation and mobility as manipulation - design and algorithms of robosimian," *Journal of Field Robotics*, October 2013 (submitted)),

[40] E. G. Armada, J. Estremera, and P. G. d. Santos, "A classification of stability margins for walking robots," 2002),

[41] V. Miomir, S. Dragoljub, and E. Yury, *Dynamics and Robust Control of Robot-environment Interaction*. River Edge, NJ, USA: World Scientific Publishing Co., Inc., 2008, ISBN: 9789812834751, 9812834753.

[42] K. Hirai, M. Hirose, Y. Haikawa, and T. Takenaka, "The development of honda humanoid robot," *1998 IEEE International Conference on Robotics and Automation*, vol. 2, 2007.

[43] M. Hirose and T. Takenaka, "Development of humanoid robot asimo," *Proc. of IEEE/RSJ Int. Conference on Intelligent Robots and Systems*, 2001.

[44] K. Nishiwaki, T. Sugihara, S. Kagami, F. Kanehiro, M. Inaba, and H. Inoue, "Design and development of research platform for perception-action integration in humanoid robot: H6," *Proc. of 2000 IEEE/RSJ International Conference in Intelligent Robots and Systems (IROS 2000)*, vol. 3, 2000.

[45] K. Nishiwaki, J. Kuffner, S. Kagami, M. Inaba, and H. Inoue, "The experimental humanoid robot h7: A research platform for autonomous behaviour," *Philosophical Transactions of the Royal Society A: Mathematical, Physical and Engineering Sciences*, vol. 365, 1850 2007.

[46] S. Lohmeier, K. Loffler, M. Gienger, H. Ulbrich, and F. Pfeiffer, "Computer system and control of biped johnnie," *Proc. of IEEE International Conference on Robotics and Automation (ICRA'04)*, vol. 4, 2004.

[47] Y. Ogura, H. Aikawa, K. Shimomura, A. Morishima, H. ok Lim, and A. Takanishi, "Development of a new humanoid robot wabian-2," *Proc. of 2006 IEEE International Conf. on Robotics and Automation, (ICRA)*, 2006.

[48] K. Kaneko, F. Kanehiro, S. Kajita, H. Hirukawa, T. Kawasaki, M. Hirata, K. Akachi, and T. Isozumi, "Humanoid robot hrp-2," in *Proc. of IEEE International Conference on Robotics and Automation, (ICRA '04)*, vol. 2, 2004, pp. 1083–1090. DOI: 10.1109/ROBOT.2004.1307969.

[49] G. Nelson, A. Saunders, N. Neville, B. Swilling, J. Bondaryk, D. Billings, C. Lee, R. Playter, and M. Raibert, "Petman: A humanoid robot for testing chemical protective clothing," *Journal of the Robotics Society of Japan*, vol. 30, 4 2012.

[50] T. McGeer, "Passive dynamic walking," *The International Journal of Robotics Research*, 1990), volume = 9, issue = 2, pages = 62-82,

[51] P. A. Bhounsule, J. Cortell, A. Grewal, B. Hendriksen, J. G. D. Karssen, C. Paul, and A. Ruina, "Coupled and decoupled actuation of robotic mechanisms," *International Journal of Robotics Research*, vol. 33, 7 2014.

[52] S. Hirose and K. Arikawa, "Coupled and decoupled actuation of robotic mechanisms," in *Proc. of IEEE International Conf. on Robotics and Automation, (ICRA'00)*, vol. 1, 2000, pp. 33–39. DOI: 10.1109/ROBOT.2000.844036.

[53] S. Hirose and K. Kato, "Study on quadruped walking robot in tokyo institute of technology-past, present and future," in *Proc. of IEEE International Conference on Robotics and Automation (ICRA '00)*, vol. 1, 2000, pp. 414–419. DOI: 10.1109/ROBOT.2000.844091.

[54] A. Nagakubo and S. Hirose, "Walking and running of the quadruped wall-climbing robot," in *Proc. of IEEE International Conference on Robotics and Automation (ICRA '94)*, vol. 2, 1994, pp. 1005–1012. DOI: 10.1109/ROBOT.1994.351225.

[55] S. Hirose and K. Arikawa, "Coupled and decoupled actuation of robotic mechanisms," in *Proc. of IEEE International Conference on Robotics and Automation (ICRA '00)*, vol. 1, 2000, pp. 33–39. DOI: 10.1109/ROBOT.2000.844036.

[56] S. Shirata, A. Konno, and M. Uchiyama, "Design and development of a light-weight biped humanoid robot saika-4)," *Proc. of 2004 IEEE/RSJ International Conf. on Intelligent Robots and Systems (IROS 2004)*, vol. 1, 2004.

[57] I.-W. Park, J.-Y. Kim, J. Lee, and J.-H. Oh, "Mechanical design of humanoid robot platform khr-3 (kaist humanoid robot 3: Hubo)," in *5th IEEE-RAS International Conf. on Humanoid Robots*, 2005, pp. 321–326. DOI: 10.1109/ICHR.2005.1573587.

[58] A. Parmiggiani, M. Maggiali, L. Natale, F. Nori, A. Schmitz, N. Tsagarakis, J. S. Victor, F. Becchi, G. Sandini, and G. Metta., "The design of the icub humanoid robot," *International journal of humanoid robotics*, vol. 9, 4 2012.

[59] K. Kaneko, K. Harada, F. Kanehiro, G. Miyamori, and K. Akachi, in *IEEE/RSJ International Conf. on Intelligent Robots and Systems (IROS 2008.*

[60] M. Laffranchi, N. Tsagarakis, F. Cannella, and D. Caldwell, "Antagonistic and series elastic actuators: A comparative analysis on the energy consumption," in *IEEE/RSJ International Conference on Intelligent Robots and Systems (IROS '09)*, 2009, pp. 5678–5684. DOI: 10.1109/IROS.2009.5354349.

[61] G. Pratt and M. Williamson, "Series elastic actuators," *Proceedings 1995 IEEE/RSJ International Conference on Intelligent Robots and Systems. Human Robot Interaction and Cooperative Robots*, vol. 1, 1995), pages = 399-406,

[62] A. R. McNeill, *Elastic mechanisms in animal movement.* Cambridge University Press, 1988.

[63] D. Hobbelen, T. de Boer, and M. Wisse, "System overview of bipedal robots flame and tulip: Tailor-made for limit cycle walking," in *IEEE/RSJ International Conference on Intelligent Robots and Systems (IROS '08)*, 2008. DOI: 10.1109/IROS.2008.4650728.

[64] R. Pfeifer, H. G. Marques, and F. Iida, "Soft robotics: The next generation of intelligent machines," in *Proc. of the 23rd International Joint Conf. on Artificial Intelligence*, ser. IJCAI '13, Beijing, China: AAAI Press, 2013, pp. 5–11, ISBN: 978-1-57735-633-2. [Online]. Available: http://dl.acm.org/citation.cfm?id=2540128.2540131.

[65] H. Dallali, M. Mosadeghzad, G. Medrano-Cerda, V.-G. Loc, N. Tsagarakis, D. Caldwell, and M. Gesino, "Designing a high performance humanoid robot based on dynamic simulation," 2013. DOI: 10.1109/EMS.2013.61.

[66] M. Raibert, K. Blankespoor, G. Nelson, and R. Playter, "Bigdog, the rough-terrain quaduped robot," *Proc. of the 17th IFAC World Congress*, vol. 17, 1 2008.

[67] B. Stephens and C. Atkeson, "Push recovery by stepping for humanoid robots with force controlled joints," in *10th IEEE-RAS International Conf. on Humanoid Robots (Humanoids)*, 2010, pp. 52–59. DOI: 10.1109/ICHR.2010.5686288.

[68] C. Semini, N. G. Tsagarakis, B. Vanderborght, Y. Yang, and D. G. Caldwell, "Hyq-hydraulically actuated quadruped robot: hopping leg prototype," *Proceedings of the Institution of Mechanical Engineers, Part I: Journal of Systems and Control Engineering*, Sept. 2011), pages = 831-849,

[69] G. Figliolini and M. Ceccarelli, "Walking programming for an electropneumatic biped robot," *Mechatronics*, 1999), pages = 941–963, issue = 8, volume = 9, issn = 0957-4158, doi = http://dx.doi.org/10.1016/S0957-4158(99)00040-9, url = http://www.sciencedirect.com/science/article/pii/S0957415899000409,

[70] G. Figliolini and M. Ceccarelli, "Climbing stairs with ep-war2 biped robot," in *Proceedings of the IEEE Conference of Robotics and Automation (ICRA '01)*, vol. 4, 2001, pp. 4116–4121. DOI: 10.1109/ROBOT.2001.933261.

[71] G. Figliolini and M. Ceccarelli, "Descending stairs with ep-war3 biped robot," *Proceedings of IEEE/ASME International Conference on Advanced Intelligent Mechatronics, AIM 2003*, 2003), pages = 747-752, volume = 2,

[72] G. Spampinato and G. Muscato, "Diees biped robot : a bio-inspired pneumatic platform for human locomotion analysis and stiffness control," *6th IEEE-RAS International Conference on Humanoid Robots*, 2006), pages = 478 - 483,

[73] T. Minato, Y. Yoshikawa, T. Noda, S. Ikemoto, H. Ishiguro, and M. Asada, "Cb2: a child robot with biomimetic body for cognitive developmental robotics," in *7th IEEE-RAS International Conference on Humanoid Robots*, 2007, pp. 557–562. DOI: 10.1109/ICHR.2007.4813926.

[74] M. Lacagninaa, G. Muscatob, and S. Rosario, "Kinematics, dynamics and control of a hybrid robot wheeleg," *Robotics and Autonomous Systems*, vol. 45, pp. 161–180, 2003, ISSN: 0921-8890. DOI: http://dx.doi.org/10.1016/j.robot.2003.09.006.

[75] K. K. Tan and A. S. Putra, "Servo hydraulic and pneumatic drive," in *Drives and Control for Industrial Automation*. Springer, 2011, ch. 2, pp. 9–44, ISBN: 978-1848824249. [Online]. Available: http://www.springer.com/engineering/robotics/book/978-1-84882-424-9.

[76] R. Gaylord, "Fluid activated motor system and stroking device," pat. US2844126, 1958. [Online]. Available: http://www.google.com/patents/US2844126.

[77] F. Daerden and D. Lefeber, "Pneumatic artificial muscles: Actuators for robotics and automation," *European journal of Mechanical and Environmental Engineering*, vol. 47, pp. 10–21, 2000.

[78] W. Gurstelle, "Joseph mckibben and the air muscle," *Makezine*, [Online]. Available: http://makezine.com/projects/make-40/joseph-mckibben-and-the-air-muscle/.

[79] D. Caldwell, G. Medrano-Cerda, and C. Bowler, "Investigation of bipedal robot locomotion using pneumatic muscle actuators," in *Proc. of the 1997 IEEE International Conf. on Robotics and Automation*, vol. 1, 1997, pp. 799–804. DOI: 10.1109/ROBOT.1997.620132.

[80] M. More and O. Liska, "Comparison of different methods for pneumatic artificial muscle control," in *2013 IEEE 11th International Symposium on Applied Machine Intelligence and Informatics (SAMI)*, 2013, pp. 117–120. DOI: 10.1109/SAMI.2013.6480957.

[81] Bridgestone Corporation, "Pneumatic actuator for manipulator," pat. US4615260 A, 1986. [Online]. Available: https://www.google.com/patents/US4615260.

[82] M. Ozkan, K. Inoue, K. Negishi, and T. Yamanaka, "Defining a neural network controller structure for a rubbertuator robot," *Neural Networks*, vol. 13, no. 4-5, pp. 533–544, 2000, ISSN: 0893-6080. DOI: 10.1016/S0893-6080(00)00020-4. [Online]. Available: http://dx.doi.org/10.1016/S0893-6080(00)00020-4.

[83] The Shadow Robot Company Limited, "Robotic muscular-skeletal jointed structures," pat. US20120017718 A1, 2012. [Online]. Available: http://www.google.com/patents/US20120017718.

[84] I. Boblan and A. Schulz, "A humanoid muscle robot torso with biologically inspired construction," *41st International Symposium on and 2010 6th German Conference on Robotics (ROBOTIK)*, pp. 1–6, 2010.

[85] C.-P. Chou and B. Hannaford, "Measurement and modeling of mckibben pneumatic artificial muscles," *IEEE TRANSACTIONS ON ROBOTICS AND AUTOMATION*, 1996), pages = 90-102, volume = 10, issue = 1,

[86] G. Klute, J. Czerniecki, and B. Hannaford, "Mckibben artificial muscles: Pneumatic actuators with biomechanical intelligence," in *Advanced Intelligent Mechatronics, 1999. Proceedings. 1999 IEEE/ASME International Conference on*, 1999, pp. 221–226. DOI: 10.1109/AIM.1999.803170.

[87] D. Caldwell, G. Medrano-Cerda, and M. Goodwin, "Control of pneumatic muscle actuators," *IEEE Control Systems Magazine*, vol. 15, no. 1, pp. 40–48, 1995, ISSN: 1066-033X. DOI: 10.1109/37.341863.

[88] T. Hesselroth, K. Sarkar, P. van der Smagt, and K. Schulten, "Neural network control of a pneumatic robot arm," *IEEE Transactions on Systems, Man and Cybernetics*, vol. 24, no. 1, pp. 28–38, 1994, ISSN: 0018-9472. DOI: 10.1109/21.259683.

[89] FESTO, *Fluidic muscle dmsp/mas*, 2008. [Online]. Available: http://www.festo.com/rep/en_corp/assets/pdf/info_501_en.pdf.

[90] B. Vanderborght, B. Verrelst, R. Van Ham, J. Naudet, J. Vermeulen, D. Lefeber, and F. Daerden, "Lucy, a bipedal walking robot with pneumatic artificial muscles," *IEEE Conf. on Mechatronics and Robotics*, 2004.

[91] B Vanderborght, "Dynamic stabilisation of the biped lucy powered by actuators with controllable stiffness," PhD, Vrije Universiteit Brussel, 2007.

[92] Editors. (2011). Interview w/ trevor blackwell from anybots, Pilot Presence, [Online]. Available: http://www.pilotpresence.com/2011/02/interview-w-trevor-blackwell-from-anybots/.

[93] E.P.W., "Rubber muscles take robotics one step further," *Rubber Developments*, 1984), pages = 117-119, volume = 37, issue = 4,

[94] R. Walker. (2013). The shadow biped, The Shadow Robotics Company, [Online]. Available: http://www.shadow.org.uk/projects/biped.shtml.

[95] S. R. Company, *Shadow dexterous hand technical specification, Shadow dexterous hand e1 series*, 2013. [Online]. Available: http://www.shadowrobot.com/wp-content/uploads/shadow_dexterous_hand_technical_specification_E1_20130101.pdf.

[96] D. Buckley. (2005). Shadow robotic-leg, The Shadow Robotics Company, [Online]. Available: http://foundation-robotics.com/FR/ShadowLeg/ShadowLeg.html.

[97] R. Colbrunn, G. Nelson, and R. Quinn, "Design and control of a robotic leg with braided pneumatic actuators," in *Intelligent Robots and Systems, 2001. Proceedings. 2001 IEEE/RSJ International Conference on*, vol. 2, 2001, pp. 992–998. DOI: 10.1109/IROS.2001.976298.

[98] "Ergonomics of human-system interaction – part 210: Human-centred design for interactive systems," International Organization for Standardization, ISO 9241-210:2010, 2010.

[99] J. Schulte, C. Rosenberg, and S. Thrun, "Spontaneous, short-term interaction with mobile robots," in *Proc. of 9th IEEE International Workshop on Robot and Human Interactive Communication (RO-MAN)*, vol. 1, 1999, pp. 658–663. DOI: 10.1109/ROBOT.1999.770050. [Online]. Available: http://ieeexplore.ieee.org/lpdocs/epic03/wrapper.htm?arnumber=770050http://ieeexplore.ieee.org/xpls/abs_all.jsp?arnumber=770050.

[100] A. Green, H. Huttenrauch, M. Norman, L. Oestreicher, and K. Severinson Eklundh, "User centered design for intelligent service robots," in *Robot and Human Interactive Communication, 2000. RO-MAN 2000. Proceedings. 9th IEEE International Workshop on*, 2000, pp. 161–166. DOI: 10.1109/ROMAN.2000.892488.

[101] S. Kiesler and J. Goetz, "Mental models of robotic assistants," in *Proc. of Conf. on Human Factors in Computing Systems*, ser. CHI EA '02, Minneapolis, Minnesota, USA: ACM, 2002, pp. 576–577, ISBN: 1-58113-454-1. DOI: 10.1145/506443.506491. [Online]. Available: http://doi.acm.org/10.1145/506443.506491.

[102] E. Ackerman, "Dyson's robot vacuum has 360-degree camera, tank treads, cyclone suction," *IEEE Spectrum*, 2014. [Online]. Available: http://spectrum.ieee.org/automaton/robotics/home-robots/dyson-the-360-eye-robot-vacuum.

[103] J. Aron, "How innovative is apple's new voice assistant, siri?" *New Scientist*, vol. 212, p. 24, 2836 2011. [Online]. Available: http://www.sciencedirect.com/science/article/pii/S026240791162647X.

[104] D. Dennett, *The Intentional Stance*. 1989, ISBN: 978-0262540537. [Online]. Available: http://static.freelibr.org/fiction/Daniel%20C%20Dennett%20-%20The%20Intentional%20Stance%20(pdf).pdf.

[105] F. Thomas and O. Johnston, *The Illusion of Life: Disney Animation*. 1995, ISBN: 978-0786860708.

[106] K. Dautenhahn, "Socially intelligent agents and the primate social brain-towards a science of social minds," *Proc. of AAAI Fall Symposium Socially Intelligent Agents–The Human in the Loop*, 35–51, 2000. [Online]. Available: http://www.aaai.org/Papers/Symposia/Fall/2000/FS-00-04/FS00-04-008.pdf.

[107] E. Guizzo, "David hanson's incredible robot heads," *IEEE Spectrum*, 2011. [Online]. Available: http://spectrum.ieee.org/automaton/robotics/humanoids/david-hanson-robot-heads.

[108] E. Guizzo, "Robots for real: the amazing androids of hiroshi ishiguro," *IEEE Spectrum*, 2009. [Online]. Available: http://spectrum.ieee.org/podcast/robotics/artificial-intelligence/the-amazing-androids-of-hiroshi-ishiguro.

[109] M. Mori, "The uncanny valley," *Energy*, vol. 7, no. 4, pp. 33–35, 1970. [Online]. Available: http://www.androidscience.com/theuncannyvalley/proceedings2005/uncannyvalley.html.

[110] C. F. DiSalvo, F. Gemperle, J. Forlizzi, and S. Kiesler, "All robots are not created equal: The design and perception of humanoid robot heads," in *Proc. of the 4th conference on Designing interactive systems: Processes, practices, methods, and techniques*, ser. DIS '02, London, England: ACM, 2002, pp. 321–326, ISBN: 1-58113-515-7. DOI: 10.1145/778712.778756. [Online]. Available: http://doi.acm.org/10.1145/778712.778756.

[111] M. Scheeff, J. Pinto, K. Rahardja, and S. Snibbe, "Experiences with sparky, a social robot," *Socially Intelligent Agents: Multiagent Systems, Artificial Societies, and Simulated Organizations*, vol. 3, pp. 173–180, 2002. [Online]. Available: http://www.springerlink.com/index/H8K18422181606P8.pdf.

[112] T. Kuratate, Y. Matsusaka, B. Pierce, and G. Cheng, ""'mask-boti: A life-size robot head using talking head animation for human-robot communication," in *11th IEEE-RAS International Conference on Humanoid Robots (Humanoids)*, 2011, pp. 99–104. DOI: 10.1109/Humanoids.2011.6100842.

[113] C. Breazeal, "Toward sociable robots," *Robotics and Autonomous Systems*, vol. 42, no. 34, pp. 167–175, 2003, ISSN: 09218890. DOI: http://dx.doi.org/10.1016/S0921-8890(02)00373-1. [Online]. Available: http://www.sciencedirect.com/science/article/pii/S0921889002003731.

[114] T. Fong, I. Nourbakhsh, and K. Dautenhahn, "A survey of socially interactive robots," *Robotics and Autonomous Systems*, vol. 42, no. 34, pp. 143–166, 2003.

[115] "Robots and robotic devices – safety requirements for personal care robots," International Organization for Standardization, ISO 13482:2014, 2014.

[116] A. R. Tilley and H. D. Associates, *The Measure of Man and Woman: Human Factors in Design*. Wiley, 2001, ISBN: 978-0471099550.

[117] (2014). The en eurocodes, [Online]. Available: http://eurocodes.jrc.ec.europa.eu/.

[118] International Code Council (ICC), *International building code (ibc)*, 2012. [Online]. Available: http://publicecodes.cyberregs.com/icod/ibc/2012/index.htm.

[119] ——, *International residential code for one- and two-family dwellings (irc)*, 2012. [Online]. Available: http://publicecodes.cyberregs.com/icod/irc/2012/index.htm.

[120] The Building Regulations, *Park m: Access to and use of buildings*, 2010. [Online]. Available: http://www.planningportal.gov.uk/uploads/br/BR_PDF_ADM_2004.pdf.

[121] L. Currie, "Chapter 10: fall and injury prevention," in *Patient Safety and Quality: An Evidence-Based Handbook for Nurses*. 2008. [Online]. Available: http://www.ncbi.nlm.nih.gov/books/NBK2653/.

[122] H. H. Cohen and J. R. Abele, "Chapter 10: fall injury information," in *Slips, Trips, Missteps, and Their Consequences*. 2008, p. 112. [Online]. Available: http://www.ncbi.nlm.nih.gov/books/NBK2653/.

[123] "Stair safety - a review of the literature and data converning stair geometry and other characteristics," NAHB Research Center, Prepared for U.S. Department of Housing and Urban Development, 1992. [Online]. Available: http://www.toolbase.org/PDF/CaseStudies/stair_safety.pdf.

[124] M. S. Roys, "Serious stair injuries can be prevented by improved stair design," *Applied Ergonomics*, vol. 32, pp. 135–139, 2 2001.

[125] M. S. Roys and M. Wright, "Accidents on english dwelling stairs are directly related to going size," *Proc. of the International Conf. on Contemporary Ergonomics (CE2008)*, vol. 32, 632–637, 2 2008.

[126] D. A. Johnson and J. Pauls, "Systemic stair step geometry defects, increased injuries, and public health plus regulatory responses," *Proc. of the International Conf. on Contemporary Ergonomics and Human Factors*, 453461, 2010.

[127] P. L. Jackson and H. Cohen, "An in-depth investigation of 40 stairway accidents and the stair safety literature," *Journal of Safety Research*, vol. 26, 151159, 3 1995.

[128] B. E. Co, *A Design Guide for Home Safety*. U.S. Department of Housing and Urban Development, 1972. [Online]. Available: http://books.google.ie/books?id=zofRnQEACAAJ.

[129] The Building Regulations, *Park k: Protection from falling, collision and impact*, 2010. [Online]. Available: http://www.planningportal.gov.uk/uploads/br/BR_PDF_AD_K_2013.pdf.

[130] Honda. (2014). Asimo specifications, [Online]. Available: `http://asimo.honda.com/asimo-specs/`.

[131] *Asimo: The honda humanoid robot*, Honda Motor Co. Ltd., Public Relations Division, 2007.

[132] *Asimo: Frequently asked questions*, Honda Motor Co. Ltd., Public Relations Division. [Online]. Available: `https://asimo.honda.com/downloads/pdf/asimo-technical-faq.pdf`.

[133] J. Falconer, "Honda developing disaster response robot based on asimo," *IEEE Spectrum*, 2013. [Online]. Available: `http://spectrum.ieee.org/automaton/robotics/humanoids/honda-new-disaster-humanoid-robot`.

[134] T. Yoshikawa and O. Khatib, "Compliant humanoid robot control by the torque transformer," in *IEEE/RSJ International Conference on Intelligent Robots and Systems (IROS '09)*, 2009, pp. 3011–3018. DOI: 10.1109/IROS.2009.5353907.

[135] U. Reiser, C. Connette, J. Fischer, J. Kubacki, A. Bubeck, F. Weisshardt, T. Jacobs, C. Parlitz, M. Hagele, and A. Verl, "Care-o-bot 3 - creating a product vision for service robot applications by integrating design and technology," in *IEEE/RSJ International Conference on Intelligent Robots and Systems (IROS '09)*, 2009, pp. 1992–1998. DOI: 10.1109/IROS.2009.5354526.

[136] K. Wyrobek, E. Berger, H. Van der Loos, and J. Salisbury, "Towards a personal robotics development platform: Rationale and design of an intrinsically safe personal robot," in *IEEE International Conf. on Robotics and Automation (ICRA '08)*, 2008, pp. 2165–2170. DOI: 10.1109/ROBOT.2008.4543527.

[137] P. Dario, E. Guglielmelli, C. Laschi, S. Superiore, and S. Anna, "Humanoids and personal robots : design and experiments," *Journal of Robotic Systems*, vol. 18, pp. 673–690, 12 2001.

[138] U. Hillenbrand, B. Brunner, C. Borst, and G. Hirzinger, "The robutler: A vision-controlled hand-arm system for manipulating bottles and glasses," *35th International Symposium on Robotics (ISR)*, 2004.

[139] T. Asfour, K. Regenstein, P. Azad, J. Schroder, A. Bierbaum, N. Vahrenkamp, and R. Dillmann, "Armar-iii: An integrated humanoid platform for sensory-motor control," in *6th IEEE-RAS International Conference on Humanoid Robots*, 2006, pp. 169–175. DOI: 10.1109/ICHR.2006.321380.

[140] S. Srinivasa, D. Ferguson, C. Helfrich, D. Berenson, A. Collet, R. Diankov, G. Gallagher, G. Hollinger, J. Kuffner, and M. Weghe, "Herb: A home exploring robotic butler," *Autonomous Robots*, vol. 28, no. 1, pp. 5–20, 2010, ISSN: 0929-5593. DOI: 10.1007/s10514-009-9160-9. [Online]. Available: `http://dx.doi.org/10.1007/s10514-009-9160-9`.

[141] S. Kuindersma, E. Hannigan, D. Ruiken, and R. Grupen, "Dexterous mobility with the ubot-5 mobile manipulator," in *Advanced Robotics, 2009. ICAR 2009. International Conference on*, 2009, pp. 1–7.

[142] A. Halme, I. Leppnen, and S. Salmi, "Development of workpartner-robotdesign of actuating and motion control system," *2nd International Conference on Climbing and Walking Robots*, 657–666, 1999.

[143] M. Diftler and R. Ambrose, "Robonaut: a robotic astronaut assistant," in *Proc. of the 6th International Symposium on Artificial Intelligence and Robotics & Automation in Space: i-SAIRAS 2001*, 2001.

[144] T. R. Swenson, "Multi-terrain motorized wheelchair apparatus," pat. US8789628 B2, 2009. [Online]. Available: `http://www.google.com/patents/US8789628`.

[145] TC Tankchair. (2013). The original tank chair, [Online]. Available: `http://www.tankchair.com/tankchair/`.

[146] Nano Optics. (2014). Unimo wheelchair, [Online]. Available: `http://www.nano-opt.jp/`.

[147] J. Martens and W. Newman, "Stabilization of a mobile robot climbing stairs," in *Proc. of IEEE International Conf. on Robotics and Automation*, vol. 3, 1994, pp. 2501–2507. DOI: `10.1109/ROBOT.1994.351135`.

[148] W. Tao, Y. Ou, and H. Feng, "Research on dynamics and stability in the stairs-climbing of a tracked mobile robot," *International Journal of Advanced Robot Systems*, vol. 9, 657–666, 146 2012. DOI: `10.5772/52850`.

[149] K. Yoneda, Y. Ota, and S. Hirose, "High-grip stair climber with powder-filled belts," *The International Journal of Robotics Research*, vol. 28, no. 1, pp. 81–89, 2009, ISSN: 0278-3649. DOI: `10.1177/0278364908098091`. [Online]. Available: `http://ijr.sagepub.com/cgi/doi/10.1177/0278364908098091`.

[150] Y. Xiong and L. Matthies, "Vision-guided autonomous stair climbing," in *Proc. of IEEE International Conference on Robotics and Automation (ICRA '00)*, vol. 2, 2000, pp. 1842–1847. DOI: `10.1109/ROBOT.2000.844863`.

[151] A. Mourikis, N. Trawny, S. Roumeliotis, D. Helmick, and L. Matthies, "Autonomous stair climbing for tracked vehicles," *The International Journal of Robotics Research*, vol. 26, no. 7, pp. 737–758, 2007, ISSN: 0278-3649. DOI: `10.1177/0278364907080423` [Online]. Available: `http://ijr.sagepub.com/cgi/doi/10.1177/0278364907080423`.

[152] D. Helmick, S. Roumeliotis, M. McHenry, and L. Matthies, "Multi-sensor, high speed autonomous stair climbing," in *IEEE/RSJ International Conference on Intelligent Robots and Systems*, vol. 1, 2002, pp. 733–742. DOI: `10.1109/IRDS.2002.1041478`. [Online]. Available: `http://ieeexplore.ieee.org/lpdocs/epic03/wrapper.htm?arnumber=1041478`.

[153] S. Steplight and G. Egnal, "A mode-based sensor fusion approach to robotic stair-climbing," *Proceedings of the 2000 IEEE/RSJ International Conference on Intelligent Robots and Systems*, pp. 1113–1118, 2000. [Online]. Available: `http://ieeexplore.ieee.org/xpls/abs\_all.jsp?arnumber=893168`.

[154] Q. Zhang, S. Ge, and P. Y. Tao, "Autonomous stair climbing for mobile tracked robot," in *IEEE International Symposium on Safety, Security, and Rescue Robotics*, 2011, pp. 92–98. DOI: `10.1109/SSRR.2011.6106757`. [Online]. Available: `http://ieeexplore.ieee.org/lpdocs/epic03/wrapper.htm?arnumber=6106757`.

[155] E. Mihankhah, a. Kalantari, E. Aboosaeedan, H. Taghirad, S. Ali, and a. Moosavian, "Autonomous staircase detection and stair climbing for a tracked mobile robot using fuzzy controller," *2008 IEEE International Conference on Robotics and Biomimetics*, pp. 1980–1985, Feb. 2009. DOI: 10.1109/ROBIO.2009.4913304.

[156] K. Ohno, S. Morimura, S. Tadokoro, E. Koyanagi, and T. Yoshida, "Semi-autonomous control of 6-dof crawler robot having flippers for getting over unknown-steps," in *Proc. of the 2007 IEEE/RSJ International Conf. on Intelligent Robots and Systems (IROS '07)*, 2007, pp. 2559–2560. DOI: 10.1109/IROS.2007.4399428.

[157] P. Ben-Tzvi, S. Ito, and A. Goldenberg, "Autonomous stair climbing with reconfigurable tracked mobile robot," in *International Workshop on Robotic and Sensors Environments (ROSE 2007)*, 2007, pp. 1–6. DOI: 10.1109/ROSE.2007.4373976.

[158] E. McCarthy, "Israeli military robot is built to kill (mini-uzi included)," *Popular Mechanics*, 2007. [Online]. Available: http://www.popularmechanics.com/technology/military/robots/4216523.

[159] A. Novoplanski, "Tire for surface vehicle," pat. US20140158268 A1, 2014. [Online]. Available: https://www.google.com/patents/US20140158268.

[160] ——, "Deformable wheel assembly," pat. US20130033099 A1, 2013. [Online]. Available: https://www.google.com/patents/US20130033099.

[161] Q.-H. Vu, B.-S. Kim, and J.-B. Song, "Autonomous stair climbing algorithm for a small four-tracked robot," in *International Conference on Control, Automation and Systems (ICCAS '08)*, 2008, pp. 2356–2360. DOI: 10.1109/ICCAS.2008.4694199.

[162] J. Liu, Y. Wang, S. Ma, and B. Li, "Analysis of stairs-climbing ability for a tracked reconfigurable modular robot," in *IEEE International Workshop on Safety, Security and Rescue Robotics*, 2005, pp. 36–41. DOI: 10.1109/SSRR.2005.1501238.

[163] J. Borenstein, G. Granosik, and M. Hansen, "The omnitread serpentine robot design and field performance," in *Proc. of the SPIE Defense and Security Conference, Unmanned Ground Vehicle Technology VII*, 2005.

[164] Y. Takita, N. Shimoi, and H. Date, "Development of a wheeled mobile robot "octal wheel" realized climbing up and down stairs," in *Proc. of IEEE/RSJ International Conf. on Intelligent Robots and Systems (IROS 2004)*, vol. 3, 2004, pp. 2440–2445. DOI: 10.1109/IROS.2004.1389774.

[165] S. Herbert, A. Drenner, and N. Papanikolopoulos, "Loper: A quadruped-hybrid stair climbing robot," in *Robotics and Automation, 2008. ICRA 2008. IEEE International Conference on*, 2008, pp. 799–804. DOI: 10.1109/ROBOT.2008.4543303. [Online]. Available: http://ieeexplore.ieee.org/xpls/abs_all.jsp?arnumber=4543303.

[166] G. Quaglia, W. Franco, and R. Oderio, "Wheelchair.q, a motorized wheelchair with stair climbing ability," *Mechanism and Machine Theory*, vol. 46, no. 11, pp. 1601–1609, Nov. 2011, ISSN: 0094114X. DOI: 10.1016/j.mechmachtheory.2011.07.005. [Online]. Available: http://www.sciencedirect.com/science/article/pii/S0094114X1100139X.

[167] C.-K. Woo, H. Choi, S. Yoon, S. Kim, and Y. Kwak, "Optimal design of a new wheeled mobile robot based on a kinetic analysis of the stair climbing states," English, *Journal of Intelligent and Robotic Systems*, vol. 49, no. 4, pp. 325–354, 2007, ISSN: 0921-0296. DOI: 10.1007/s10846-007-9139-8. [Online]. Available: http://dx.doi.org/10.1007/s10846-007-9139-8.

[168] D. Choi, J. Oh, and J. Kim, "Analysis method of climbing stairs with the rocker-bogie mechanism," English, *Journal of Mechanical Science and Technology*, vol. 27, no. 9, pp. 2783–2788, 2013, ISSN: 1738-494X. DOI: 10.1007/s12206-013-0725-3. [Online]. Available: http://dx.doi.org/10.1007/s12206-013-0725-3.

[169] Y. Uchida, K. Furuichi, and S. Hirose, "Fundamental performance of a 6 wheeled off-road vehicle ldquo;helios-v rdquo;" in *Proc. of IEEE International Conference on Robotics and Automation*, vol. 3, 1999, pp. 2336–2341. DOI: 10.1109/ROBOT.1999.770454.

[170] J. Gaston, K. Raahemifar, and P. Hiscocks, "A cooperative network of reconfigurable stair-climbing robots," in *Proc. of IEEE International Symposium on Circuits and Systems (ISCAS '06)*, 2006, pp. 2553–2556. DOI: 10.1109/ISCAS.2006.1693144.

[171] S. Hirose, K. Yoneda, K. Arai, and T. Ibe, "Design of prismatic quadruped walking vehicle titan vi," in *Fifth International Conference on Advanced Robotics ('91 ICAR)*, 1991, pp. 723–728. DOI: 10.1109/ICAR.1991.240685.

[172] P. Michel, "Integrating perception and planning for humanoid autonomy," PhD thesis, Robotics Institute, Carnegie Mellon University, Pittsburgh, PA, 2008.

[173] A. Albert, M. Suppa, and W. Gerth, "Detection of stair dimensions for the path planning of a bipedal robot," in *Advanced Intelligent Mechatronics, 2001. Proceedings. 2001 IEEE/ASME International Conference on*, vol. 2, 2001, pp. 1291–1296. DOI: 10.1109/AIM.2001.936909.

[174] J.-S. Gutmann, M. Fukuchi, and M. Fujita, "Stair climbing for humanoid robots using stereo vision," in *Proc. of IEEE/RSJ International Conference on Intelligent Robots and Systems (IROS 2004)*, vol. 2, 2004, pp. 1407–1413. DOI: 10.1109/IROS.2004.1389593.

[175] J. Chestnutt, S. Kagami, K. Nishiwaki, J. Kuffner, and T. Kanade, "Gpu-accelerated real-time 3d tracking for humanoid locomotion," in *Proc. of the IEEE/RSJ International Conf. on Intelligent Robots and Systems*, 2007.

[176] K. Nishiwaki, S. Kagami, Y. Kuniyoshi, M. Inaba, and H. Inoue, "Toe joints that enhance bipedal and fullbody motion of humanoid robots," in *Proc. of IEEE International Conference on Robotics and Automation (ICRA '02)*, vol. 3, 2002, pp. 3105–3110. DOI: 10.1109/ROBOT.2002.1013704.

[177] T. Li, Y.-T. Su, C.-H. Kuo, C.-Y. Chen, C.-L. Hsu, and M.-F. Lu, "Stair-climbing control of humanoid robot using force and accelerometer sensors," in *SICE Annual Conference 2007*, 2007, pp. 2115–2120. DOI: 10.1109/SICE.2007.4421336.

[178] DARPA Defense Advanced Research Projects Agency. (). Darpa robot masters stairs, [Online]. Available: https://www.youtube.com/watch?v=aqCmX5dMYHg.

[179] E. Moore, D. Campbell, F. Grimminger, and M. Buehler, "Reliable stair climbing in the simple hexapod 'rhex'," in *Proceedings 2002 IEEE International Conference on Robotics and Automation*, vol. 3, 2002, pp. 2222–2227. DOI: 10.1109/ROBOT.2002.1013562.

[180] T. Brewer, K. Kaipa, and S. K. Gupta, "A quadruped robot with on-boarding sensing and parameterized gait for stair climbing," in *15th International Conf. on Climbing and Walking Robots (CLAWAR)*, 2012.

[181] N. Eiji and N. Sei, "Leg-wheel robot: A futuristic mobile platform for forestry industry," in *Proceedings of IEEE/Tsukuba International Workshop on Advanced Robotics*, 1993, pp. 109–112. DOI: 10.1109/ICAR.1993.337208.

[182] O. Matsumoto, S. Kajita, M. Saigo, and K. Tani, "Dynamic trajectory control of passing over stairs by a biped type leg-wheeled robot with nominal reference of static gait," in *Proc. of IEEE/RSJ International Conference on Intelligent Robots and Systems*, vol. 1, 1998, pp. 406–412. DOI: 10.1109/IROS.1998.724653.

[183] O. Matsumoto, S. Kajita, K. Tani, and M. Oooto, "A four-wheeled robot to pass over steps by changing running control modes," in *Proc. of IEEE International Conference on Robotics and Autornation*, vol. 2, 1995, 1700–1706 vol.2. DOI: 10.1109/ROBOT.1995.525518. [Online]. Available: http://ieeexplore.ieee.org/xpls/abs_all.jsp?arnumber=525518.

[184] J. Yuan and S. Hirose, "Actualization of safe and stable stair climbing and three-dimensional locomotion for wheelchair," in *IEEE/RSJ International Conf. on Intelligent Robots and Systems (IROS 2005)*, 2005, pp. 1538–1543. DOI: 10.1109/IROS.2005.1545335.

[185] R. Morales, V. Feliu, A. Gonzlez, and P. Pintado, "Kinematic model of a new staircase climbing wheelchair and its experimental validation," *The International Journal of Robotics Research*, vol. 25, pp. 825–841, 9 2006, ISSN: 0921-0296. DOI: 10.1177/0278364906069149.

[186] M. Lawn and T. Ishimatsu, "Modeling of a stair-climbing wheelchair mechanism with high single-step capability," *Neural Systems and Rehabilitation Engineering, IEEE Transactions on*, vol. 11, no. 3, pp. 323–332, 2003, ISSN: 1534-4320. DOI: 10.1109/TNSRE.2003.816875.

[187] R. Rojas. (2006). A short history of omnidirectional wheels, [Online]. Available: http://robocup.mi.fu-berlin.de/buch/shortomni.pdf.

[188] M. W. Spong, S. Hutchinson, and M Vidyasagar, *Robot modeling and control*. John Wiley & Sons, 2006, ISBN: 978-0471649908.

[189] S. R. Buss. (2009). Introduction to inverse kinematics with jacobian transpose, pseudoinverse and damped least squares methods, [Online]. Available: http://www.math.ucsd.edu/~sbuss/ResearchWeb/ikmethods/iksurvey.pdf.

[190] MATLAB, *Version 7.10.0 (R2010a)*. Natick, Massachusetts: The MathWorks Inc., 2010.

[191] P. I. Corke, *Robotics, Vision & Control: Fundamental Algorithms in Matlab*. Springer, 2011, ISBN: 978-3-642-20143-1.

[192] I. W. Griffiths, "Chapter 4: equilibrium," in *Principles of Biomechanics & Motion Analysis*. Lippincott Williams & Wilkins, 2006, pp. 94–100.

[193] C. McGinn, K. Kelly, and D. Holland, "Towards the design of a new humanoid robot for domestic applications," in *IEEE International Conf. on Technologies for Practical Robot Applications (TePRA)*, 2014.

[194] C. McGinn and K. Kelly, "A practical humanoid robot morphology for operation in civilian environments," *Trinity Journal of Postgraduate Research*, vol. 13, 2014.

[195] S. N. Whittlesey and D. G. Robertson, "Chapter 5: two-dimensional inverse dynamics," in *Research Methods in Biomechanics*, 2nd ed. 2001, pp. 1591–1593.

[196] E. Roche. (2014). Pneumatic artificial muscles, [Online]. Available: `http://softroboticscom/book/pneumatic-artificial-muscles` (visited on 2014).

[197] CadSoft. (2014). Cadsoft eagle pcb design software, [Online]. Available: `http://www.cadsoftusa.com/eagle-pcb-design-software/?language=en`.

[198] *Arduino*, 2014. [Online]. Available: `http://www.arduino.cc/`.

[199] *Processing*, 2014. [Online]. Available: `https://www.processing.org/`.

[200] Arduino. (2014). Using an arduino as an avr isp (in-system programmer), [Online]. Available: `http://arduino.cc/en/Tutorial/ArduinoISP`.

[201] Boost. (2014). Boost c++ libraries, [Online]. Available: `http://www.boost.org/`.

[202] C. McGinn, *Robbie_v2.0*, `https://github.com/Lane252/Robbie_v2.0`, 20014.

[203] *Blender foundation*. [Online]. Available: `http://www.blender.org/` (visited on 2014).

[204] P. Badger. (2014). Capacitive sensing library, [Online]. Available: `http://playground.arduino.cc/Main/CapacitiveSensor?from=Main.CapSense`.

[205] L. Oestreicher and K. Eklundh, "User expectations on human-robot co-operation," in *15th IEEE International Symposium on Robot and Human Interactive Communication (ROMAN '06)*, 2006, pp. 91–96. DOI: `10.1109/ROMAN.2006.314400`.

[206] M. L. Walters, K. Dautenhahn, S. N. Woods, and K. L. Koay, "Robotic etiquette: Results from user studies involving a fetch and carry task," in *Proceedings of the ACM/IEEE International Conference on Human-robot Interaction*, ser. HRI '07, Arlington, Virginia, USA: ACM, 2007, pp. 317–324, ISBN: 978-1-59593-617-2. DOI: `10.1145/1228716.1228759`. [Online]. Available: `http://doi.acm.org/10.1145/1228716.1228759`.

[207] H. R. Lee, J. Sung, S. Sabanovic, and J. Han, "Cultural design of domestic robots: A study of user expectations in korea and the united states," in *RO-MAN, 2012 IEEE*, 2012, pp. 803–808. DOI: `10.1109/ROMAN.2012.6343850`.

[208] J. Amend, E. Brown, N. Rodenberg, H. Jaeger, and H. Lipson, "A positive pressure universal gripper based on the jamming of granular material," *IEEE Transactions on Robotics*, vol. 28, no. 2, pp. 341–350, 2012, ISSN: 1552-3098. DOI: `10.1109/TRO.2011.2171093`.

Appendix A

V1.0 Robot

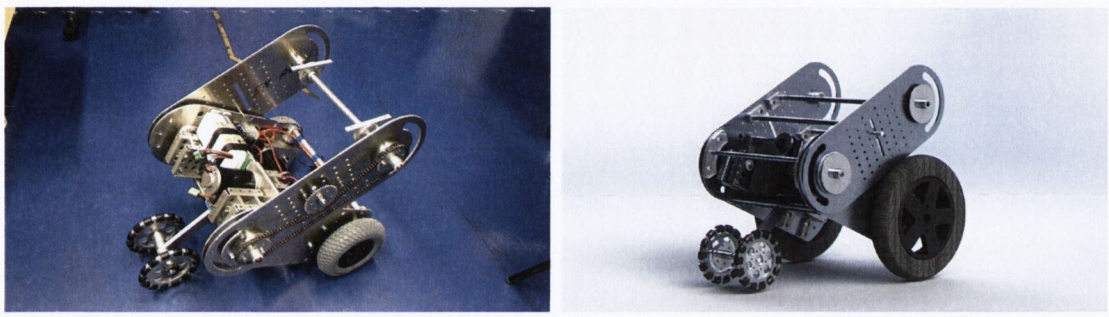


Figure A.1: Leg assembly on the v1.0 robot

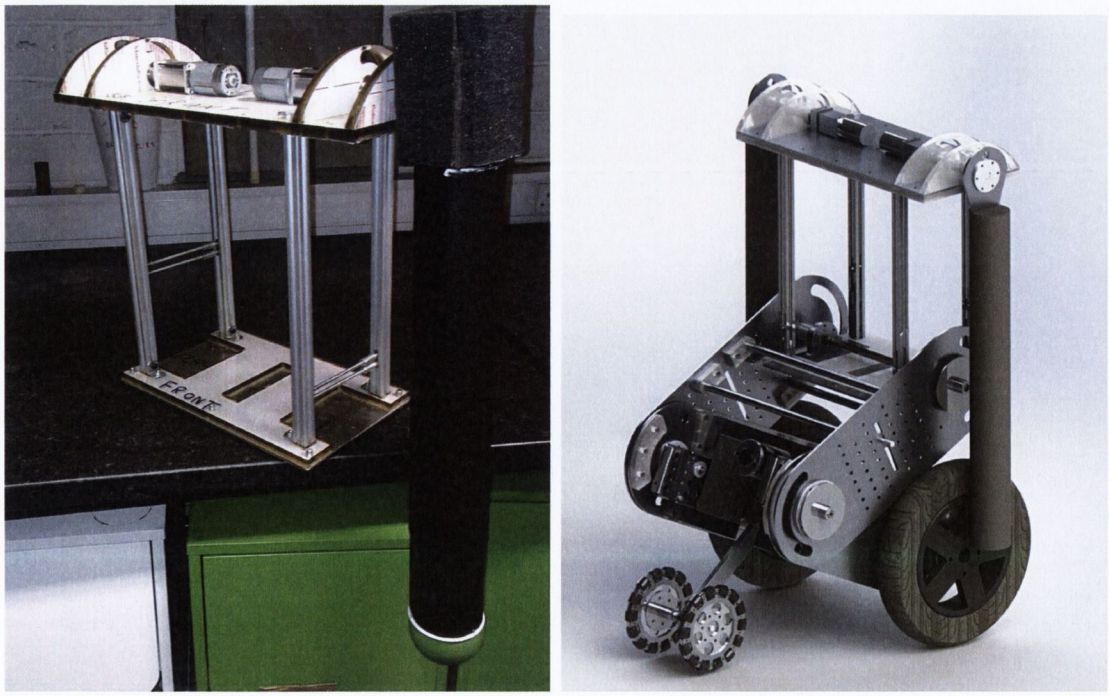


Figure A.2: The upper body structure (left) v1.0 protype upper body in the lab (b) CAD model showing upper body structure integrated with leg assembly



Figure A.3: v1.0 robot moving around the lab



Figure A.4: v1.0 robot interacting with a wheelchair user



Figure A.5: v1.0 robot (left) the v1.0 social interface (right) the engineering team behind the design/construction of the v1.0 robot

Appendix B

V2.0 Robot

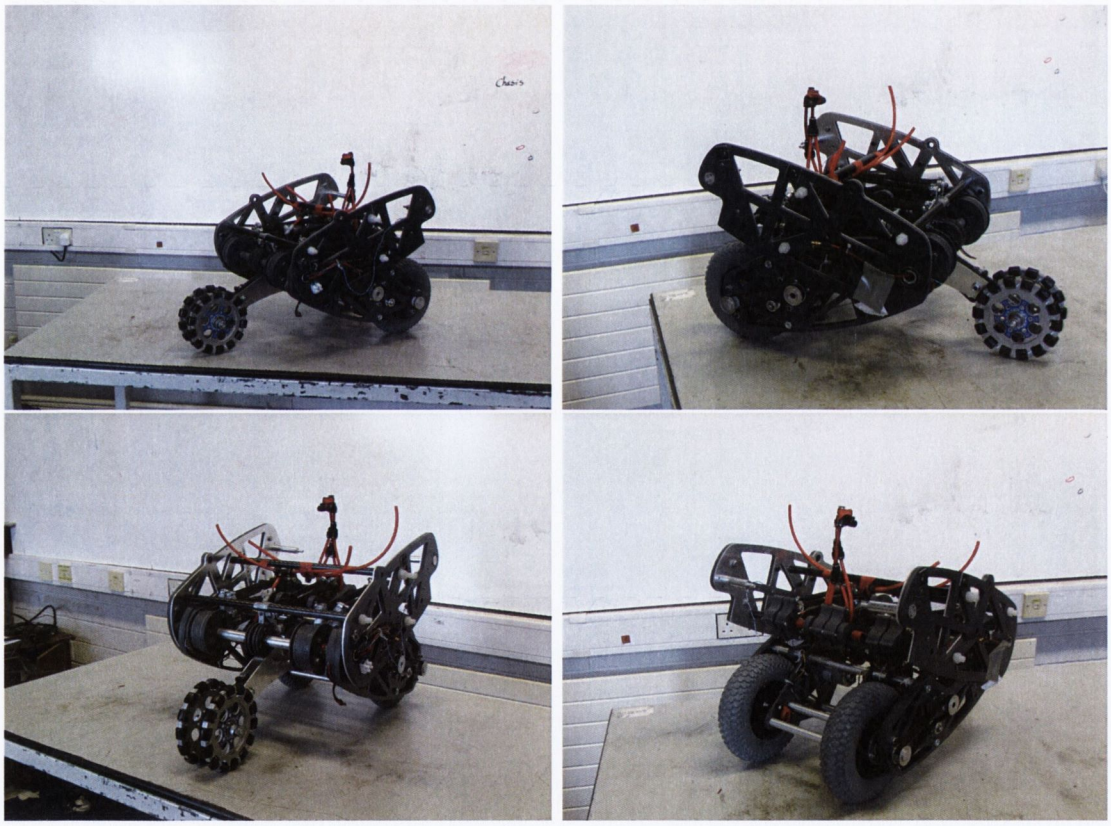


Figure B.1: Leg assembly on the v2.0 robot



Figure B.2: Range of motion of the v2.0 leg assembly

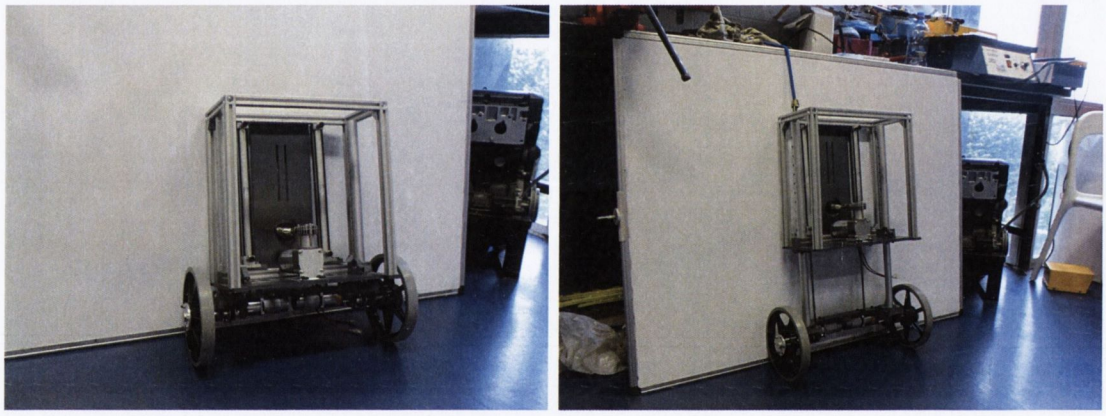


Figure B.3: Action of the lower hip mechanism (LHM)

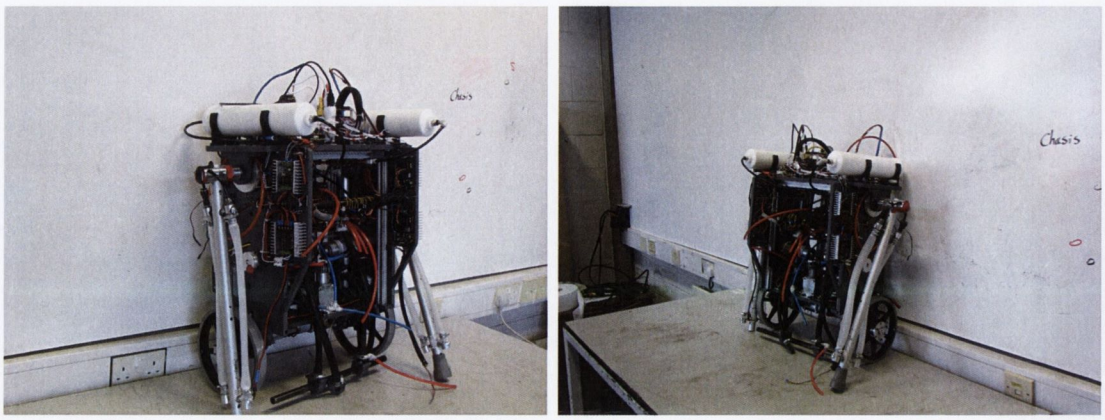


Figure B.4: Assembly of the torso, lower hip mechanism (LHM) and arm structures on the v2.0 embodiment

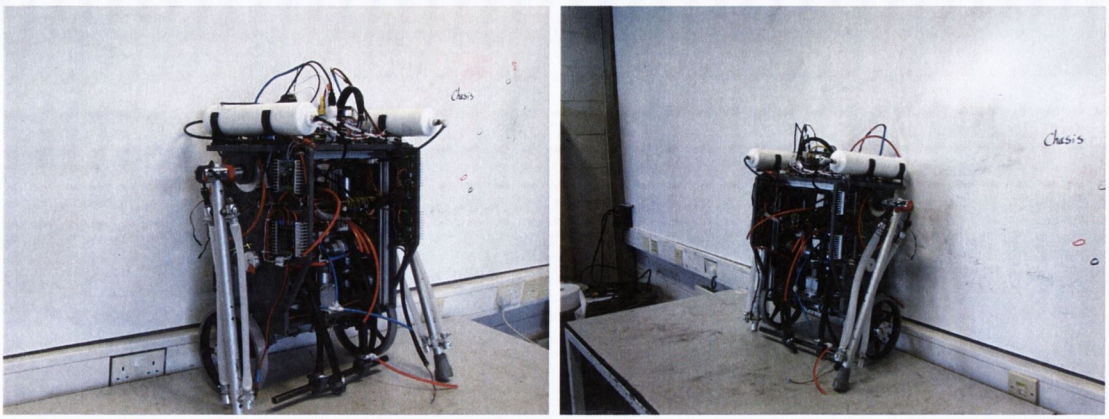


Figure B.5: Assembly of the torso, lower hip mechanism (LHM) and arm structures on the v2.0 embodiment

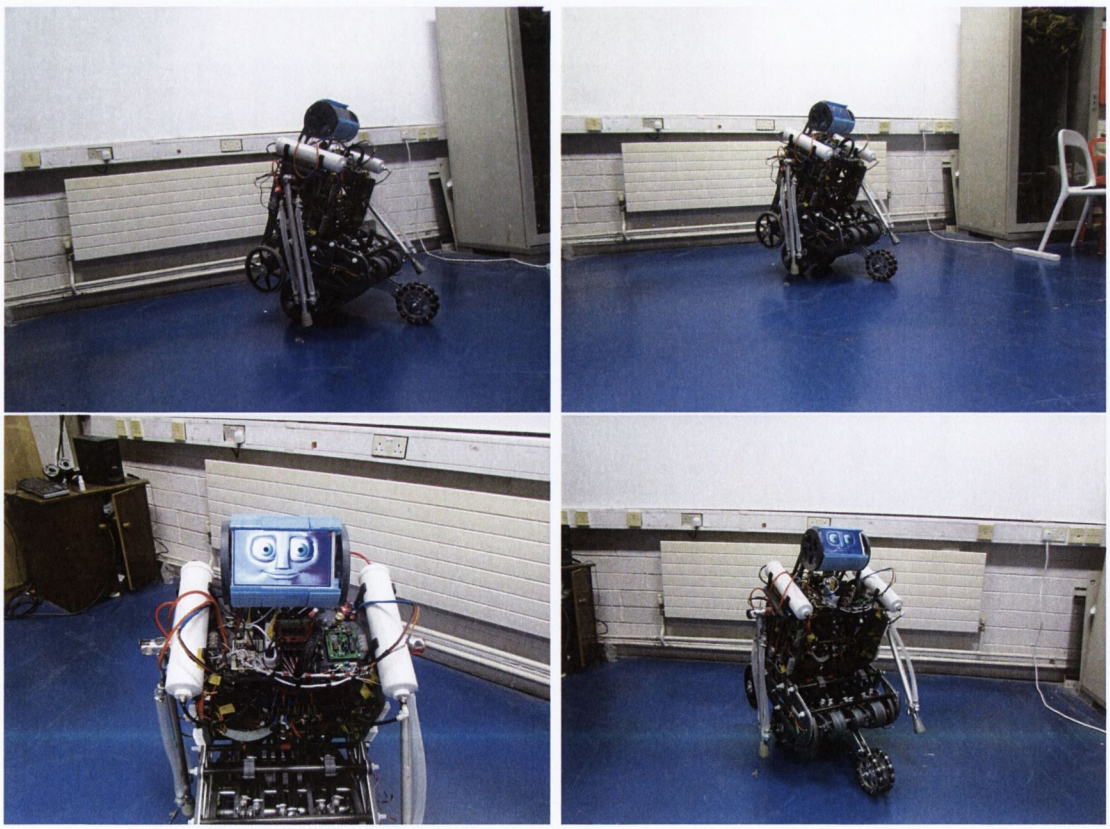
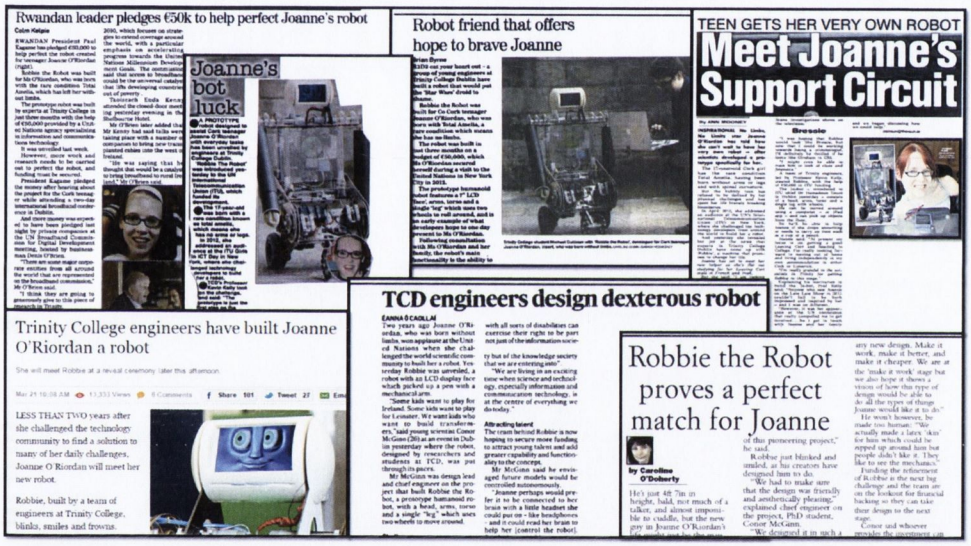


Figure B.6: Images of the v2.0 robot assembly with interactive social interface

Appendix C

Awards/Publicity



(a)



(b)



(c)

Figure C.1: Press coverage of the v1.0 embodiment (a) Miscellaneous press articles on the robot (b) headline on RTE main evening news (c) front page of the Irish Times weekend edition. March 2014

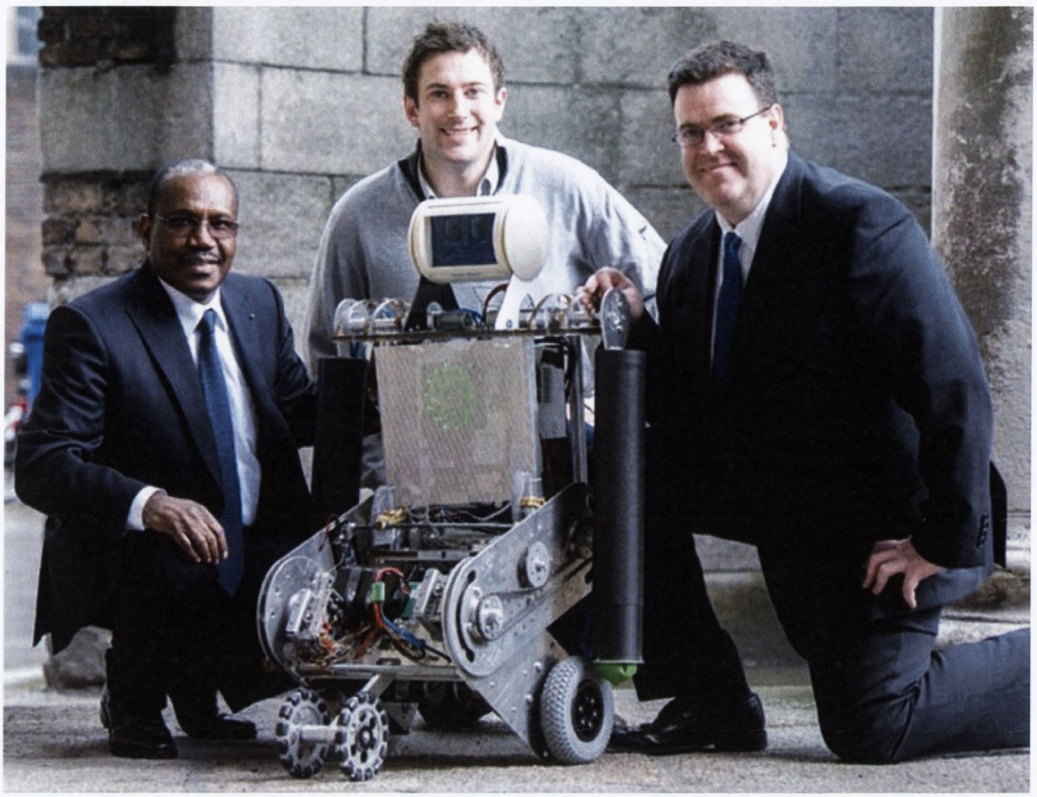


Figure C.2: At the press launch of Robbie v1.0 (l-r): Dr. Hamadoun Tour, Secretary General ITU; Conor McGinn, lead engineer; Prof. Kevin Kelly, project lead. March 2014



Figure C.3: Presenting the design of the robot morphology at the 'Universal Design Grand Challenge'(UDGC) finals. May 2014



Figure C.4: Conor McGinn accepting the 'Smart World, Full Life'award with Dean of Research, Prof. Vinnie Cahill, at the Discover Research Dublin event. September 2014



Figure C.5: The TCD Engineering team accepting the Engineers Ireland Excellence Award for Innovation. November 2014

Appendix D

Inverse Kinematics Matlab Code

Using Matlab and the 'Robotics Toolbox'[191], the forward kinematics are defined. A graphical description of the code is given in figure D.1a. The forward kinematics algorithm takes in input data for the number of degrees of freedom in the system, and the Denavit-Hartenberg (DH) parameters: θ, d, a, α. This loop will iterate until all of the links have been assigned the required DH parameters. With all the system parameters defined, the end-effector position is computed using the homogeneous transform matrix for the entire linked chain. In the Matlab code, this process utilises the functions *fkine*, *SerialLink* and *Link* which are each defined in the 'Robotics Toolboxrq.

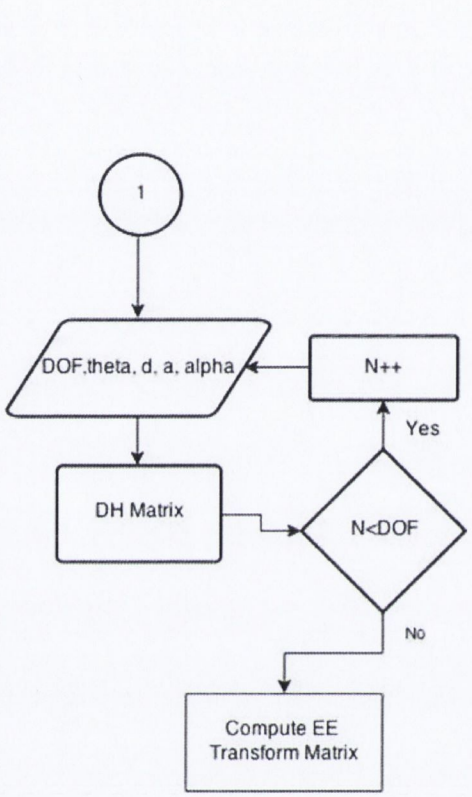
The general idea behind the inverse kinematics algorithm is that it takes in a desired end effector position in Cartesian coordinates (x,y,z) and iterates the joint angles until a solution converges. The inverse kinematics function used in the Matlab code, *ikine*, is a modified version of the one found in the 'Robotics Toolbox'.

With the desired end-effector position defined, the inverse kinematics loop starts by checking to make sure the iteration limit is not exceeded. It then proceeds to check the current position of the end effector by computing the forward kinematics as described above. The Jacobian matrix is then computed using the functions 'jacob0'and 'jacobn'. The pseudo-inverse of the Jacobian is then computed using the built-in Matlab function *pinv*. The error between the current position and desired position is calculated by subtracting the current position from the desired position. This solution is then multiplied by a scaling constant 'β'(less than one), to ensure that the step-size in the desired change in angles is small. The change in the joint angles are computed by:

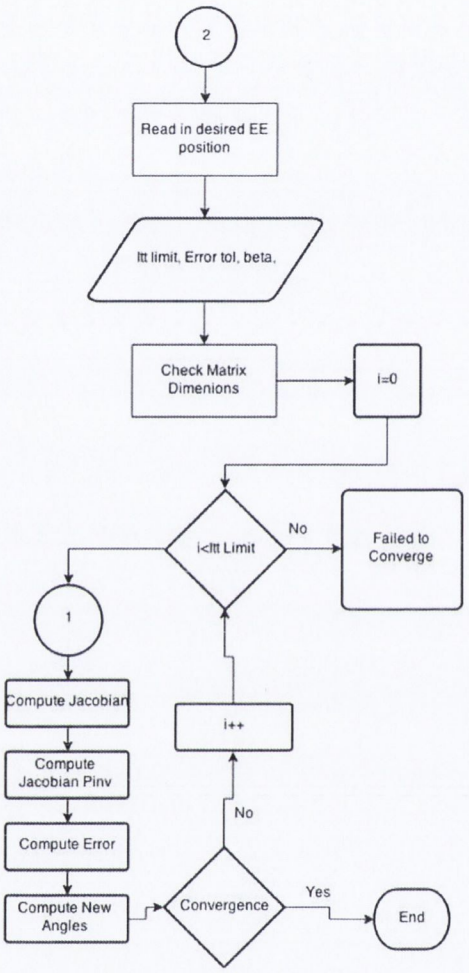
$$\Delta\theta = J^{+}\Delta e$$

The new joint angles are updated by adding the change in joint angles to the current joint angles. The error is checked against the tolerance specified in the code. If the error is less than or equal to the tolerance, the solution has converged. If the solution has not

converged the iteration count will increase and the solution will loop until convergence is found.



(a) forward kinematics



(b) inverse kinematics

Figure D.1: Flowchart describing the how (a) the forward kinematic model is implemented (b) the joint trajectories are generated for the inverse kinematic model

Robot_Main_Kinematics.m

```
clear;
clc;

%Robot Parameter Setup
Shank=4.5;
Stab_Length=7;
Knee= 5;
Torso= 6;
Shoulder=2;
arm=5;
theta(1)=0.29 ;
theta(2)=0.64;
theta(3)=1.6;
theta(4)=pi;
theta(5)=-6;
theta(6)=0;
theta(7)=0;

%   DH Parameters      th          d          a              alpha
links(1) = Link([     0           0       -Shank            pi    ], '
   standard');
links(2) = Link([     0           0         Knee            0     ], '
   standard');
links(3) = Link([     0           0         Torso           0     ], '
   standard');
links(4) = Link([     0         -arm         0              pi    ], '
   standard');
links(5) = Link([     0           0         arm             0     ], '
   standard');

robbie = SerialLink(links, 'name', 'leg'); %Creates Robot Object
    as a
                                            %Serial Link

qz=[theta(1) theta(2) theta(3) theta(4) theta(5)];% Sets initial
    position
                                                 %of joint
                                                    angles

%q=jtraj(qr,qr2,t); %generates trajectory for FKine plot
%Plots the robot serial link system
figure(1)
robbie.plot(qz,'nobase','noshadow','workspace', 20*[-1 1 -1 1 -1
    1 ]);
```

```
hold on;

%M is a mask vector which is used in the IKine code to
%Determine the DOF
M=[1 1 1 1 1 0];

%TS determines the time plot
TS=70;
T1 = transl(-1.357 , -3.598, 5); % define the start point of EE
T2 = transl(-5,-8, 5);  % and destination of EE
T = ctraj(T1, T2, TS);  % compute a Cartesian path

%The IKine function  is called and takes in the Cartesian Path,
%the initial joint angles and the Mask Vector
qi = robbie.ikine(T,qz,M);

%Plots of joint angles changing with time
figure(2)
subplot(3,1,1); plot(qi(:,1)*(180/pi)); xlabel('Time (s)');
   ylabel('Joint 1 (Deg)');
subplot(3,1,2); plot(qi(:,2)*(180/pi)); xlabel('Time (s)');
   ylabel('Joint 2 (Deg)');
subplot(3,1,3); plot(qi(:,3)*(180/pi)); xlabel('Time (s)');
   ylabel('Joint 3 (Deg)');

figure(3);
subplot(3,1,1); plot(qi(:,4)*(180/pi)); xlabel('Time (s)');
   ylabel('Joint 5 (Deg)');
subplot(3,1,2); plot(qi(:,5)*(180/pi)); xlabel('Time (s)');
   ylabel('Joint 5 (Deg)');

%Animation of Robot Inverse Kinematics
figure(4);
robbie.plot(qi,'workspace', 15*[-1 1 -1 1 -1 1 ]);
hold on;

theta1=qi(:,1)*(180/pi);
theta2=qi(:,2)*(180/pi);
theta3=qi(:,3)*(180/pi);
theta4=qi(:,4)*(180/pi);
theta5=qi(:,5)*(180/pi);

%Output angles changing over time
THETA=[ theta1 theta2 theta3 theta4 theta5]
```

Ikine.m

```
function [qt] = ikine(robot, tr, varargin)
    % set default parameters for solution
    ilimit = 1000;
    tol = 1e-4;
    alpha = 0.5;

    opt.varstep = false;
    [opt,args] = tb_optparse(opt, varargin);

    n = robot.n;

    %Checks to make sure default angles  have been taken in
    if ~isempty(args)
        q = args{1};
        if isempty(q)
            q = zeros(1, n);
        else
            q = q(:)';
        end
    else
        q = zeros(1, n);
    end

    %Mask matrix indicates joint DOF, the following code
    %checks to make sure correct Mask Matrix has been specified
    if length(args) > 1
        m = args{2}
        m = m(:)
        if numel(m) ~= 6
            error('Mask matrix should have 6 elements');
        end
        if numel(find(m)) ~= robot.n
            error('Mask matrix must have same number of 1s as
                robot DOF')
        end
    else
        if n < 6
            error('For a manipulator with fewer than 6DOF a mask
                matrix argument must be specified');
        end
        m = ones(6, 1);
    end

    % make this a logical array so we can index with it.
```

```
m = logical(m)

npoints = size(tr,3);     % number of points
qt = zeros(npoints, n);   % preallocate space for results
tcount = 0;               % total iteration count

%A check to make sure the matrix T is a homogenous matrix
 if ~ishomog(tr)
 error('T is not a homog xform');
 end

 %Computes the initial Jacobian matrix for default joint
    angles
J0 = jacob0(robot, q)
J0 = J0(m, m)
if cond(J0) > 100
    warning('Initial angles near singular, convergence may
       be slow');
end

for i=1:npoints
    T1 = tr(:,:,i)%Setup the desired EE position

    % initialize state for the ikine loop
    eprev = 0;
    count = 0;

    while true
        % update the count and test against iteration limit
        count = count + 1;

        if count > ilimit
            warning('ikine: iteration limit exceeded');
            break
        end

        % compute the error
        T0=robot.fkine(q')

        %Calculation of error, takes in forward kinematics
           of
        %current robot position and the desired position
        %(Current Position-Desired Position)
       e = [     T1(1:3,4)-T0(1:3,4);
      0.5*( cross(T0(1:3,1), T1(1:3,1)) + ...
       cross(T0(1:3,2), T1(1:3,2)) + ...
```

```
        cross(T0(1:3,3), T1(1:3,3)) ...
    )];

    % compute the current Jacobian
    J = jacob0(robot, q);
    %Using the Pseudo Inverse Method,
    %Compute the change in angles
    % equation: deltaq=alpha*transpose(J)*inv(J*transpose(
        J))*e

    dq = alpha * pinv( J(m,:) ) * e(m); %above equation
        but with
                                        %matrix indexing
    %Add change in angle to current angle configurations
    q = q + dq';
    nm = norm(e(m));

      if norm(e) > 1.5*norm(eprev)
          warning('Solution Diverging'); %Checks for
              Divergence
      end

      %The current error becomes the previous error for
          next loop
      eprev = e;

      %check to make sure the tolerence of error is not
          too small,
      %as this indicates convergence, which is the desired
          result
      if nm <= tol
          break
      end

  end  % end ikine solution for tr(:,:,i)
  qt(i,:) = q';
  tcount = tcount + count;
%
end
```

Jacob0.m

```
function J0 = jacob0(robot, q, varargin)


    opt.rot = false;
    opt = tb_optparse(opt, varargin);

    %
    %   dX_tn = Jn dq
    %
    Jn = jacobn(robot, q)   % Jacobian from joint to wrist space

    %
    %  convert to Jacobian in base coordinates
    %
    Tn = fkine(robot, q)% end-effector transformation
    R = t2r(Tn)
    T2= [R zeros(3,3)]

    J0 = [R zeros(3,3); zeros(3,3) R] * Jn
```

Ikine.m

```
function [qt] = ikine(robot, tr, varargin)
    % set default parameters for solution
    ilimit = 1000;
    tol = 1e-4;
    alpha = 0.5;

    opt.varstep = false;
    [opt,args] = tb_optparse(opt, varargin);

    n = robot.n;

    %Checks to make sure default angles  have been taken in
    if ~isempty(args)
        q = args{1};
        if isempty(q)
            q = zeros(1, n);
        else
            q = q(:)';
        end
    else
        q = zeros(1, n);
    end

    %Mask matrix indicates joint DOF, the following code
    %checks to make sure correct Mask Matrix has been specified
    if length(args) > 1
        m = args{2}
        m = m(:)
        if numel(m) ~= 6
            error('Mask matrix should have 6 elements');
        end
        if numel(find(m)) ~= robot.n
            error('Mask matrix must have same number of 1s as
                robot DOF')
        end
    else
        if n < 6
            error('For a manipulator with fewer than 6DOF a mask
                matrix argument must be specified');
        end
        m = ones(6, 1);
    end

    % make this a logical array so we can index with it.
```

```
m = logical(m)

npoints = size(tr,3);     % number of points
qt = zeros(npoints, n);   % preallocate space for results
tcount = 0;               % total iteration count

%A check to make sure the matrix T is a homogenous matrix
 if ~ishomog(tr)
 error('T is not a homog xform');
 end

 %Computes the initial Jacobian matrix for default joint
    angles
J0 = jacob0(robot, q)
J0 = J0(m, m)
if cond(J0) > 100
    warning('Initial angles near singular, convergence may
       be slow');
end

for i=1:npoints
    T1 = tr(:,:,i)%Setup the desired EE position

    % initialize state for the ikine loop
    eprev = 0;
    count = 0;

    while true
        % update the count and test against iteration limit
        count = count + 1;

        if count > ilimit
            warning('ikine: iteration limit exceeded');
            break
        end

        % compute the error
        T0=robot.fkine(q')

        %Calculation of error, takes in forward kinematics
           of
        %current robot position and the desired position
        %(Current Position-Desired Position)
       e = [     T1(1:3,4)-T0(1:3,4);
      0.5*( cross(T0(1:3,1), T1(1:3,1)) + ...
       cross(T0(1:3,2), T1(1:3,2)) + ...
```

```
        cross(T0(1:3,3), T1(1:3,3)) ...
    )];

    % compute the current Jacobian
    J = jacob0(robot, q);
    %Using the Pseudo Inverse Method,
    %Compute the change in angles
    % equation: deltaq=alpha*transpose(J)*inv(J*transpose(
        J))*e

    dq = alpha * pinv( J(m,:) ) * e(m); %above equation
        but with
                                        %matrix indexing
    %Add change in angle to current angle configurations
    q = q + dq';
    nm = norm(e(m));

      if norm(e) > 1.5*norm(eprev)
          warning('Solution Diverging'); %Checks for
              Divergence
      end

      %The current error becomes the previous error for
          next loop
      eprev = e;

      %check to make sure the tolerence of error is not
          too small,
      %as this indicates convergence, which is the desired
          result
      if nm <= tol
          break
      end

  end  % end ikine solution for tr(:,:,i)
  qt(i,:) = q';
  tcount = tcount + count;
%
end
```

Jacobn.m

```
function J = jacobn(robot, q, varargin)

    opt.trans = false;
    opt.rot = false;

    opt = tb_optparse(opt, varargin);

    n = robot.n;
    L = robot.links;          % get the links

    if isa(q, 'sym')
        tau(6, robot.n) = sym();
    else
        J = zeros(6, robot.n);
    end
    U = robot.tool;
    for j=n:-1:1
        j
        if robot.mdh == 0
            % standard DH convention
            U
            U = L(j).A(q(j)) * U
        end
        if L(j).RP == 'R'
            % revolute axis
            d = [   -U(1,1)*U(2,4)+U(2,1)*U(1,4)
                -U(1,2)*U(2,4)+U(2,2)*U(1,4);
                -U(1,3)*U(2,4)+U(2,3)*U(1,4)]
            delta = U(3,1:3)' % nz oz az
        else
            % prismatic axis
            d = U(3,1:3)';        % nz oz az
            delta = zeros(3,1); %  0  0  0
        end
        J(:,j) = [d; delta]

        if robot.mdh ~= 0
            % modified DH convention
            U = L(j).A(q(j)) * U;
        end
    end

    if opt.trans
        J = J(1:3,:);
```

```
    elseif opt.rot
        J = J(4:6,:);
    end

    if isa(J, 'sym')
        J = simplify(J);
    end
```

fkine.m

```
function [t allt] = fkine(robot, q)
%
% evaluate fkine for each point on a trajectory of
% theta_i or q_i data
%

n = robot.n;

if nargout > 1
    allt = zeros(4,4,n);
    if isa(q, 'sym')
        allt = sym(allt);
    end
end

L = robot.links;
if numel(q) == n
    t = robot.base;
    for i=1:n
        t = t * L(i).A(q(i));

        if nargout > 1
            allt(:,:,i) = t; % intermediate transformations
        end
    end
    t = t * robot.tool;
else
    if numcols(q) ~= n
        error('q must have %d columns', n)
    end
    t = zeros(4,4,0);
    for qv=q',      % for each trajectory point
        tt = robot.base;
        for i=1:n
            tt = tt * L(i).A(qv(i));
        end
        t = cat(3, t, tt * robot.tool);
    end
end

if isa(t, 'sym')
    t = simplify(t);
end
```

SerialLink.m

```
classdef SerialLink < handle

    properties
        name
        gravity
        base
        tool
        manuf
        comment

        plotopt
        lineopt
        shadowopt

        qteach

        fast_rne    % mex version of rne detected

    end

    events
        Moved
    end

    properties (SetAccess = private)
        n
        links
        mdh
        T
    end

    properties (Dependent = true, SetAccess = private)
        config
    end

    properties (Dependent = true)
        offset
        qlim
    end

    methods
        function r = SerialLink(L, varargin)
        %SerialLink Create a SerialLink robot object
```

```
r.name = 'noname';
r.manuf = '';
r.comment = '';
r.links = [];
r.n = 0;
r.mdh = 0;
r.gravity = [0; 0; 9.81];
r.base = eye(4,4);
r.tool = eye(4,4);

r.lineopt = {'Color', 'black', 'Linewidth', 4};
r.shadowopt = {'Color', 0.7*[1 1 1], 'Linewidth',
    3};
r.plotopt = {};

if exist('frne') == 3
    r.fast_rne = true;
end

if nargin == 0
    % zero argument constructor, sets default values
    return;
else
    % at least one argument, either a robot or link
        array

    if isa(L, 'SerialLink')
        if length(L) == 1
            % clone the passed robot
            for j=1:L.n
                newlinks(j) = copy(L.links(j));
            end
            r.links = newlinks;
        else
            % compound the robots in the vector
            r = L(1);
            for k=2:length(L)
                r = r * L(k);
            end
        end
    elseif isa(L, 'Link')
        r.links = L;    % attach the links
    elseif isa(L, 'double')
        % legacy matrix
        dh_dyn = L;
        clear L
```

```
            for j=1:numrows(dh_dyn)
                L(j) =          Link();
                L(j).theta =    dh_dyn(j,1);
                L(j).d =        dh_dyn(j,2);
                L(j).a =        dh_dyn(j,3);
                L(j).alpha =    dh_dyn(j,4);

                if numcols(dh_dyn) > 4
                    L(j).sigma = dh_dyn(j,5);
                end
            end
            r.links = L;
        else
            error('unknown type passed to robot');
        end
        r.n = length(r.links);
    end

    % process the rest of the arguments in key, value
       pairs
    opt.name = 'robot';
    opt.comment = [];
    opt.manufacturer = [];
    opt.base = [];
    opt.tool = [];
    opt.offset = [];
    opt.qlim = [];
    opt.plotopt = [];

    [opt,out] = tb_optparse(opt, varargin);
    if ~isempty(out)
        error('unknown option <%s>', out{1});
    end

    % copy the properties to robot object
    p = properties(r);
    for i=1:length(p)
        if isfield(opt, p{i}) && ~isempty(getfield(opt,
           p{i}))
            r.(p{i}) = getfield(opt, p{i});
        end
    end

    % set the robot object mdh status flag
    mdh = [r.links.mdh];
    if all(mdh == 0)
```

```
            r.mdh = mdh(1);
        elseif all (mdh == 1)
            r.mdh = mdh(1);
        else
            error('robot has mixed D&H links conventions');
        end
    end


    function r2 = mtimes(r, l)
    %SerialLink.mtimes Concatenate robots


        if isa(l, 'SerialLink')
            r2 = SerialLink(r);
            r2.links = [r2.links l.links];
            r2.base = r.base;
            r2.n = length(r2.links);
        elseif isa(l, 'Link')
            r2 = SerialLink(r);
            r2.links = [r2.links l];
            r2.n = length(r2.links);
        end
    end

    function display(r)


        loose = strcmp( get(0, 'FormatSpacing'), 'loose');
        if loose
            disp(' ');
        end
        disp([inputname(1), ' = '])
        if loose
            disp(' ');
        end
        disp(char(r))
        if loose
            disp(' ');
        end
    end

    function s = char(robot)
    %SerialLink.char Convert to string

        s = '';
```

```
            for j=1:length(robot)
                r = robot(j);

                % informational line
                if r.mdh
                    convention = 'modDH';
                else
                    convention = 'stdDH';
                end
s = sprintf('%s (%d axis, %s, %s)', r.name, r.n, r.config,
    convention);

                % comment and other info
                line = '';
                if ~isempty(r.manuf)
                    line = strcat(line, sprintf(' %s;', r.manuf)
                        );
                end
                if ~isempty(r.comment)
                    line = strcat(line, sprintf(' %s;', r.
                        comment));
                end
                s = char(s, line);

                % link parameters
                s = char(s, '
                    +---+-----------+-----------+-----------+-----------+
                    ');
                s = char(s, '| j |     theta |         d |
                            a |     alpha |');
                s = char(s, '
                    +---+-----------+-----------+-----------+-----------+
                    ');
                s = char(s, char(r.links, true));
                s = char(s, '
                    +---+-----------+-----------+-----------+-----------+
                    ');

                % gravity, base, tool
                s_grav = horzcat(char('grav = ', ' ', ' '),
                    mat2str(r.gravity));
                s_grav = char(s_grav, ' ');
                s_base = horzcat(char('  base = ',' ',' ', ' '),
                    mat2str(r.base));

                s_tool = horzcat(char('   tool =  ',' ',' ', ' '
```

```
            ), mat2str(r.tool));

            line = horzcat(s_grav, s_base, s_tool);

            s = char(s, ' ', line);
            if j ~= length(robot)
                s = char(s, ' ');
            end
        end
    end

    %
       %%%%
```

```
    for i=1:r.n
        L(i).offset = v(i);
    end
    r.links = L;
end

function v = get.offset(r)
    v = [r.links.offset];
end

function set.qlim(r, v)
    if numrows(v) ~= r.n
        error('insufficient rows in joint limit matrix')
            ;
    end
    L = r.links;
    for i=1:r.n
        L(i).qlim = v(i,:);
    end
    r.links = L;
end

function v = get.qlim(r)
    L = r.links;
    v = zeros(r.n, 2);
    for i=1:r.n
        if isempty(L(i).qlim)
            if L(i).isrevolute
                v(i,:) = [-pi pi];
            else
                v(i,:) = [-Inf Inf];
            end
        else
            v(i,:) = L(i).qlim;
        end
    end
end

function set.gravity(r, v)
    if isvec(v, 3)
        r.gravity = v;
    else
        error('gravity must be a 3-vector');
    end
end
```

```
        function v = get.config(r)
            v = '';
            for i=1:r.n
                v(i) = r.links(i).RP;
            end
        end

        % general methods
function s = mat2str(m)
    m(abs(m)<eps) = 0;
    s = num2str(m);
end
```